Open Cluster Groups and Complexes

Dissertation
zur Erlangung des akademischen Grades
"doctor rerum naturalium"
(Dr. rer. nat.)
in der Wissenschaftsdisziplin "Astrophysik"

Leibniz-Institut für
Astrophysik Potsdam

eingereicht an der
Mathematisch-Naturwissenschaftlichen Fakultät
der Universität Potsdam

angefertigt am
Leibnitz-Institut für Astrophysik Potsdam (AIP)

von
Dipl. Phys. Claudia Conrad

unter Betreuung von: Prof. Dr. Matthias Steinmetz,
Dr. Roelof S. de Jong,
Dr. Ralf-Dieter Scholz,
Dr. Olivier V. Schnurr

Potsdam, June 15, 2015

Published online at the
Institutional Repository of the University of Potsdam:
URN urn:nbn:de:kobv:517-opus4-77605
http://nbn-resolving.de/urn:nbn:de:kobv:517-opus4-77605

”Remember to look up at the stars and not down at your feet.
Try to make sense of what you see
and wonder about what makes the universe exist.
Be curious.
And however difficult life may seem,
there is always something you can do and succeed at.
It matters that you don’t just give up.“

Stephen Hawking (In an Interview with Diane Sawyer, for ABC News, June 2010)

Contents

List of Figures

List of Tables

Abstract

It is generally agreed upon that stars typically form in open clusters and stellar associations, but little is known about the structure of the open cluster system. Do open clusters and stellar associations form isolated or do they prefer to form in groups and complexes? Open cluster groups and complexes could verify star forming regions to be larger than expected, which would explain the chemical homogeneity over large areas in the Galactic disk. They would also define an additional level in the hierarchy of star formation and could be used as tracers for the scales of fragmentation in giant molecular clouds? Furthermore, open cluster groups and complexes could affect Galactic dynamics and should be considered in investigations and simulations on the dynamical processes, such as radial migration, disc heating, differential rotation, kinematic resonances, and spiral structure.

In the past decade there were a few studies on open cluster pairs (de La Fuente Marcos & de La Fuente Marcos 2009a,b,c) and on open cluster groups and complexes (Piskunov et al. 2006). The former only considered spatial proximity for the identification of the pairs, while the latter also required tangential velocities to be similar for the members. In this work I used the full set of 6D phase-space information to draw a more detailed picture on these structures. For this purpose I utilised the most homogeneous cluster catalogue available, namely the Catalogue of Open Cluster Data (COCD; Kharchenko et al. 2005a,b), which contains parameters for 650 open clusters and compact associations, as well as for their uniformly selected members. Additional radial velocity (RV) and metallicity ($[M/H]$) information on the members were obtained from the RAdial Velocity Experiment (RAVE; Steinmetz et al. 2006; Kordopatis et al. 2013) for 110 and 81 clusters, respectively. The RAVE sample was cleaned considering quality parameters and flags provided by RAVE (Matijevič et al. 2012; Kordopatis et al. 2013). To ensure that only real members were included for the mean values, also the cluster membership, as provided by Kharchenko et al. (2005a,b), was considered for the stars cross-matched in RAVE.

6D phase-space information could be derived for 432 out of the 650 COCD objects and I used an adaption of the Friends-of-Friends algorithm, as used in cosmology, to identify potential groupings. The vast majority of the 19 identified groupings were pairs, but I also found four groups of 4-5 members and one complex with 15 members. For the verification of the identified structures, I compared the results to a randomly selected subsample of the catalogue for the Milky Way global survey of Star Clusters (MWSC; Kharchenko et al. 2013), which became available recently, and was used as reference sample. Furthermore, I implemented Monte-Carlo simulations with randomised samples created from two distinguished input distributions for the spatial and velocity parameters. On the one hand, assuming a uniform distribution in the Galactic disc and, on the other hand, assuming the COCD data distributions to be representative for the whole open cluster population.

The results suggested that the majority of identified pairs are rather by chance alignments, but the groups and the complex seemed to be genuine. A comparison of my results to the pairs, groups and complexes proposed in the literature yielded a partial overlap, which was most likely because of selection effects and different parameters considered. This is another verification for the existence of such structures.

The characteristics of the found groupings favour that members of an open cluster grouping originate from a common giant molecular cloud and formed in a single, but possibly sequential, star formation event. Moreover, the fact that the young open cluster population showed smaller spatial separations between nearest neighbours than the old cluster population indicated that the lifetime of open cluster groupings is most likely comparable to that of the Galactic open cluster population itself. Still even among the old open clusters I could identify groupings, which suggested that the detected structure could be in some cases more long lived as one might think.

In this thesis I could only present a pilot study on structures in the Galactic open cluster population, since the data sample used was highly incomplete. For further investigations a far more complete sample would be required. One step in this direction would be to use data from large current surveys, like SDSS, RAVE, Gaia-ESO and VVV, as well as including results from studies on individual clusters. Later the sample can be completed by data from upcoming missions, like Gaia and 4MOST. Future studies using this more complete open cluster sample will reveal the effect of open cluster groupings on star formation theory and their significance for the kinematics, dynamics and evolution of the Milky Way, and thereby of spiral galaxies.

Zusammenfassung

Es ist weithin anerkannt, dass Sterne typischerweise in offenen Sternenhaufen und Sternassoziationen entstehen, dennoch ist wenig über Strukturen in diesem System der offenen Sternhaufen bekannt. Entstehen offenen Sternhaufen und Sternassoziationen isoliert oder entstehen sie bevorzugt in Gruppen und Komplexen? Gruppen und Komplexe von offenen Sternhaufen könnten bestätigen, dass Sternentstehungsregionen größer sind als erwartet, was die Homogenität der chemischen Zusammensetzung über weite Areale in der galaktischen Scheibe erklären würde. Sie würden auch eine weitere Stufe in der Hierarchie der Sternentstehung definieren und könnten als Indikatoren für die Skalen der Fragmentierung in Riesenmolekülwolken dienen. Des Weiteren könnten Gruppen und Komplexe von offenen Sternhaufen die Dynamik unserer Galaxis beeinflussen und sollten in Untersuchungen und Simulationen von dynamischen Prozessen, wie radiale Migration, kinematische Aufheizung der Scheibe, differentielle Rotation, kinematische Resonanzen und der Spiralstruktur, miteinbezogen werden.
In den vergangenen Jahrzehnten gab es einigen Studien zu Paaren von offenen Sternhaufen (de La Fuente Marcos & de La Fuente Marcos 2009a,b,c) sowie zu Gruppen und Komplexen von offenen Sternhaufen (Piskunov et al. 2006). Erstere betrachteten ausschließlich räumliche Nähe für die Identifizierung der Paare, während letztere auch ähnliche tangentiale Geschwindigkeiten für die Mitglieder verlangten. In dieser Arbeit nutzte ich den kompletten Satz an 6D-Phasenrauminformationen, um ein vollständigeres Bild dieser Strukturen zu erstellen. Aus diesem Grund habe ich den homogensten Sternhaufenkatalog verwendet, der zu dieser Zeit verfügbar war, nämlich den Catalogue of Open Cluster Data (COCD; Kharchenko et al. 2005a,b), welcher Parameter für 650 offene Sternhaufen und Sternassoziationen, sowie deren einheitlich ausgewählte Mitglieder, enthält. Weitere Radialgeschwindigkeits- (RV) und Metallizitätsinformationen ($[M/H]$) für die Sternhaufenmitglieder wurden mit Hilfe des RAdial Velocity Experiment (RAVE; Steinmetz et al. 2006; Kordopatis et al. 2013) für 110 beziehungsweise 81 Haufen bestimmt. Der RAVE-Datensatz wurde mit Hilfe von Qualitätsparametern aus RAVE (Matijevič et al. 2012; Kordopatis et al. 2013) gereinigt. Um sicherzustellen, dass nur echte Mitglieder für die Mittelwertbestimmung betrachtet wurden, wurde auch die Haufenmitgliedschaft, wie von Kharchenko et al. (2005a,b) bereitgestellt, für die in RAVE identifizierten Sterne miteinbezogen.
6D-Phasenrauminformationen konnten für 432 der 650 COCD Objekte bestimmt werden und ich habe eine angepasste Variante des Friends-of-Friends Algorithmus genutzt, der in der Kosmologie verwendet wird, um potenzielle Gruppierungen zu identifizieren. Der überwiegende Teil der 19 identifizierten Gruppierungen waren Paare, ich habe aber auch vier Gruppen mit 4-5 Mitgliedern und einen Komplex mit 15 Mitgliedern gefunden. Für die Bestätigung der identifizierten Strukturen, verglich ich die Ergebnisse mit einem zufällig ausgewählten Datensatz aus dem Milky Way global survey of Star Clusters (MWSC; Kharchenko et al. 2013), der kürzlich erst zur Verfügung gestellt wurde und hier als Vergleichsdatensatz verwendet wurde. Des Weiteren, habe ich Monte-Carlo Simulationen mit zufälligen Datensätzen implementiert, die anhand von zwei unterschiedlichen Varianten für die Ausgangsverteilungen der räumlichen und Geschwindigkeitsparameter generiert wurden. Zum Einen unter der Annahme einer gleichmäßigen Verteilung in der galaktischen Scheibe und zum Anderen unter der Annahme, dass die Datenverteilungen im COCD repräsentativ sind für die gesamte Population der offenen Sternhaufen.

Die Ergebnisse deuteten darauf hin, dass die Mehrheit der identifizierten Paare eher zufällige Anordnungen sind, aber die Gruppen und der Komplex schienen echt zu sein. Ein Vergleich meiner Ergebnisse mit den in der Literatur vorgeschlagenen Paaren, Gruppen und Komplexen ergab eine teilweise Überschneidung, die höchstwahrscheinlich durch Auswahleffekte und die Verwendung unterschiedlicher Parameter bedingt war. Dies ist eine weitere Bestätigung für die Existenz solcher Strukturen.
Die Eigenschaften der gefundenen Gruppierungen bevorzugen, dass die Mitglieder einer Gruppierung von offenen Sternhaufen aus einer gemeinsamen Riesenmolekülwolke stammen und in einem Sternentstehungsereignis geformt wurden, das möglicherweise auch sequenziell ablief. Außerdem zeigte die junge Population der offenen Sternhaufen kleinere räumliche Abstände zwischen den nächsten Nachbarn als die alte Haufenpopulation, was darauf hindeutet, dass die Lebenszeit von Gruppierungen von offenen Sternhaufen vergleichbar ist mit der für die Population galaktischer offener Sternhaufen selbst. Dennoch wurden auch unter den alten offenen Sternhaufen Gruppierungen identifiziert, was andeutete, dass die gefundenen Strukturen doch in einigen Fällen langlebiger ist als man denken könnte.
In dieser Doktorarbeit konnte ich nur eine Pilotstudie zu Strukturen in der Population der galaktischen offenen Sternhaufen präsentieren, da der verwendete Datensatz höchst unvollständig war. Für zukünftige Untersuchungen wäre ein deutlich vollständigerer Datensatz notwendig. Ein Schritt in diese Richtung wäre die Verwendung von Daten aus großen momentan verfügbaren Beobachtungskampagnen, wie dem SDSS, RAVE, Gaia-ESO und dem VVV, sowie das miteinbeziehen der Ergebnisse von Studien an einzelnen offenen Sternhaufen. Später könnte dieser Datensatz durch die Verwendung von Daten aus kommenden Missionen, wie Gaia und 4MOST, komplettiert werden. Zukünftige Studien mit einem vollständigeren Datensatz werden den Einfluss von Gruppierungen von offenen Sternhaufen für die Sternentstehungstheorie und ihre Bedeutung für die Kinematik, Dynamik und Entwicklung der Milchstraße, und damit auch für andere Spiralgalaxien, enträtseln.

Chapter 1

Introduction

Section 1.1

General aspects

The universe harbours about 10^{11} galaxies of different ages and morphology. Each of these galaxies contains about $10^9 - 10^{11}$ stars at different stages of their evolution. In spiral galaxies, like our Milky Way, the young stellar population concentrates in a relatively thin disc, while the older stellar population spreads out to higher latitudes and also defines the stellar halo of the host galaxy. It is widely agreed upon that the majority of these stars formed in a clustered mode (Lada & Lada 2003; Lada 2006). Hence, studying stellar clusters is the key to understand the formation and evolution of stars and galaxies, as well as the structures in galaxies. This was one reason for putting stellar clusters in the focus of the project presented in this thesis. In the following chapter I briefly summarise the current state of the art in the research of open cluster, stellar associations, as well as their connection to star formation, Galactic structure and dynamics.

1.1.1 Open clusters

Stellar cluster can basically be understood as accumulations of stars within galaxies that are gravitationally bound and, therefore, move with a common velocity vector. The challenge in reality is to separate these overdensities from the stellar field population. For example, if one only follows the assumption that stellar clusters occupy a confined area in the sky, one could be easily mislead, because in astronomy and astrophysics 2D-observations of objects distributed in 3D-space are performed, which induces projection effects. Thus, if one only considers spatial criteria, stars that are actually in the fore- or background of a stellar cluster could be misidentified as members. In consequence, velocities and distances of stars are usually considered as well for the identification of stellar clusters and their members.
In this work I primarily investigated open clusters in the Milky Way, which show different morphologies ranging from centrally concentrated systems to irregular shapes (see Fig. 1.2). However, the density profiles for the majority of open clusters can be approximately described by a so called King profile (King 1962; Leonard 1988). For the common motion criterion velocities in two basic directions are accessible: proper motions, describing the tangential motion in the celestial plane, and radial velocities, providing an estimate for velocities along the line of sight. The HIPPARCOS mission[1] (Perryman et al. 1997) was the first extensive survey for astrometric data of stars in the solar neighbourhood.

[1] HIPPARCOS - High Precision Parallax Collecting Satellite.

It provided accurate positions and trigonometric parallaxes with accuracies to the 10 – 20% level for about 100,000 stars down to magnitudes of $V \sim 12$ mag. The related TYCHO catalogues[2] (Høg et al. 2000) gave proper motions for about 2.5 million stars down to magnitudes of $V \sim 11$ mag. On 19. December 2013 the Gaia satellite (Vallenari 2014) was launched and will again significantly improve and extend the current sample of astrometric data, including positions, distances and proper motions, through providing measurements from the sub-mas down to the 10 μas level for about 10^9 stars in the Milky Way down to magnitudes of $G = 20$ mag. Besides accurate multi-epoch position measurements, providing proper motions an parallaxes, Gaia will also get radial velocities for the brightest stars through own spectroscopic observations.

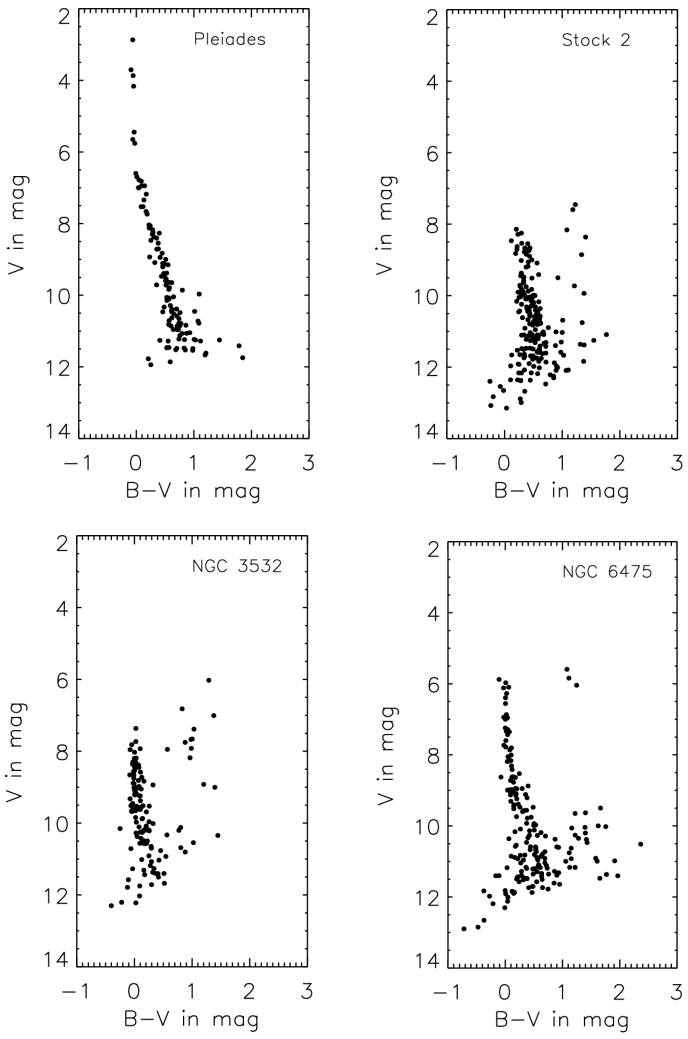

Figure 1.1: CMDs generated from most probable kinematic members ($P_{kin} \geq 61\%$) for four open clusters selected from the COCD.

Photometric and spectroscopic surveys have different magnitude limits, resulting in different sizes of the generated data sample. Current photometric surveys, such as the Sloan Digital Sky Survey (SDSS; Abazajian et al. 2003), have magnitude limits of $g' \sim 22$ mag[3]. Present spectroscopic surveys, such as the RAdial Velocity Experiment (RAVE; Steinmetz et al. 2006), have magnitude limits at about $V \sim 13$ mag. This shows that potential open cluster members are better accessible via proper motions than by radial velocities. Thus, for the majority of identified open clusters the kinematic membership is often based only on proper motions, simply due to the lack of radial velocity measurements of all stars in the area around an open cluster.

At present, there are more and more efforts to include radial velocity measurement for the open cluster membership selection (Geller et al. 2008, 2010; Hole et al. 2009; Carrera 2012; Hayes & Friel 2014; Tofflemire et al. 2014), in parts because for some clusters the proper motion values of the members are similar to those of the surrounding field stars. Regardless of whether only proper motions, or radial velocities, or both parameters are used for the kinematic membership selection, the criterion is rather simple. For real members, their differences in proper motion/radial velocity to the mean has to be within the error margins of the kinematic parameter considered.

Another interesting aspect of open clusters is the distributions of confirmed members in a colour-magnitude diagram (CMD), as illustrated in Fig. 1.1 for four open clusters selected from the Catalogue of Open Cluster Data (COCD; Kharchenko et al. 2005a,b) using kinematic members[4]. These diagrams provide a way to illustrate stellar evolution, since stars of different type, age, or mass occupy characteristic regions in the CMD. For the general stellar population with a variety of distances, clear features can only be identified when using absolute magnitudes.

[2]The TYCHO catalogues were supplementary to the main HIPPARCOS catalogue.
[3]The SDSS g' waveband roughly corresponds to the widely used V band.
[4]More details on the COCD, the membership selection, and corresponding stellar catalogues can be found in Sect. 2.1.2.

For open clusters, on the other hand, clear features are already present in the CMD when using apparent magnitudes, such as a main sequence, indicating that the members of open clusters are of similar age. The finding that cluster members have similar ages can be used as an additional requirement for the membership selection to further reduce contamination by field stars, since the latter should have different ages and differ from the characteristic features of an open cluster. The members for most of the known open clusters were identified using a combination of the criteria listed above and since they interlink, the entire membership selection procedure is usually an iterative process.
Images of three open clusters are displayed in Fig. 1.2, namely of the Pleiades, the Hyades, and Westerlund 2. The former two are very nearby open clusters and of intermediate age. The Pleiades are 120 Myrs old and located at a distance of 130 pc (Kharchenko et al. 2005a), while the Hyades are 625 Myrs old and located at about 46 pc (Perryman et al. 1998). Westerlund 2, on the other hand, is a very young and massive cluster, which is further away. Its age was derived to be no more than 2 Myrs and its distance was determined to be about 2.85 kpc (Carraro et al. 2013).

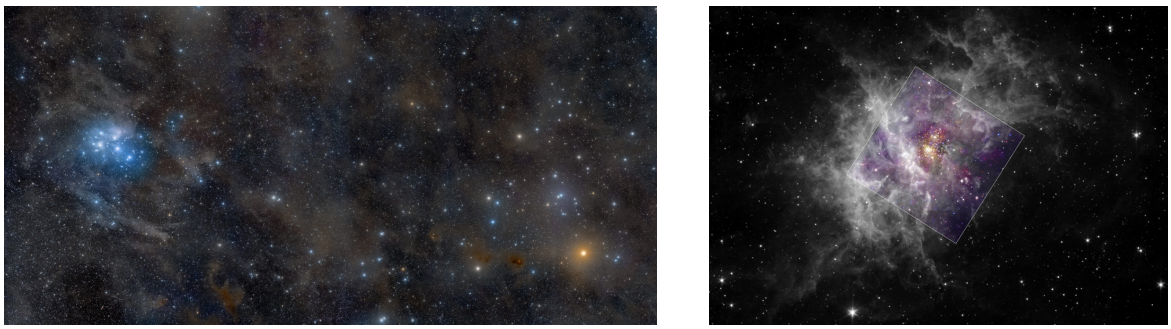

Figure 1.2: Images of Galactic open clusters, as copied from the NASA APOD website[5]. Left panel: The nearby Pleiades (left corner) and Hyades (right corner) clusters (posted on 17 Nov. 2011), spanning 20° on the sky. Right panel: The young and massive Westerlund 2 cluster (posted on 26 June 2010).

From confirmed open clusters in the Milky Way some general characteristics can be visualised. The core radii are typically a few pc and the tidal radii are of the order of 10 pc. The distribution for the apparent total radii, converted to pc, is illustrated in Fig. 1.3. When compared to the histogram of the tidal King-radii (Fig. 1 in Kharchenko et al. (2013)), the distribution presented here peaks at lower values. This is because the apparent total radii were accessed visually and did not take into account the faint members and therefore underestimated the actual tidal radii. Open clusters show a typical stellar density of about $10^2 - 10^4$ stars/pc^3 and the number of members reaches up to a few 1000 stars. However, not all these members are accessible through astrometry or spectroscopy, which is why the number of observed open cluster members in Fig. 1.3 is typically smaller than the expected number. Due to the large number of members, certain parameters for open clusters, such as ages, distances and velocities, can be derived more accurately than for isolated stars.
The ages of open clusters are often determined through isochrone fitting, as for example done by Kharchenko et al. (2005a,b, 2012). This required an understanding of the reddening effects in direction of the open cluster investigated, as well as ensured selection of potential cluster members. From a visual inspection of the cluster CMD one could get a first rough idea on which range of ages is covered and which set of isochrones is reasonable to be used. For very young cluster with ages of only a few Myrs, the members populate tracks leading up to the main sequence and Pre-Main sequence isochrones would have to be used (e.g. by Siess et al. 2000). For older open clusters with ages of several 100 Myrs would populate tracks leading away from the main sequence and post-main sequence isochrones have to be used (e.g. by Girardi et al. 2002). At the main sequence, isochrones for different stellar parameters are very close to each other. Hence, the more potential members are used the more accurate is the age determination. Currently, the best estimates for logarithmic ages of open clusters are accurate to about 0.2 dex.

[5]NASA Astronomy Picture of the Day (APOD) website: http://apod.nasa.gov/

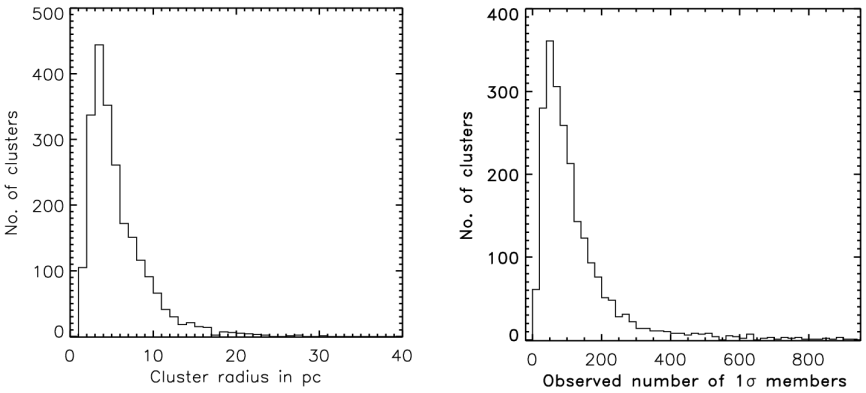

Figure 1.3: Left panel: Histogram for the cluster radii in pc, as derived from the apparent visual total radius r_2 (given in deg). Right panel: Histogram for the observed number of 1σ-members within the determined cluster radii (right). Both histograms were generated with data from the Milky Way global survey of Star Clusters (MWSC; Kharchenko et al. 2013).

For an accurate determination of the cluster radius, a reliable estimate on its distance is essential. For nearby clusters, within a few 100 pc, trigonometric parallaxes are used to determine the distance of the cluster. For more distant systems this method is challenging, since the parallaxes are of the order of their uncertainties. For these clusters one could use the CMD and compare the main sequence generated from apparent magnitudes to the expected main sequence generated from absolute magnitudes, referred to as distance modulus. To determine the absolute magnitudes one has to understand the reddening effects induced through interstellar extinction by gas and dust clouds. Furthermore, the location of the main sequence is usually identified by isochrone[6] fitting, which is highly dependent on the stellar evolution model chosen. Spectroscopic information on open cluster members, combined with assumptions on the Galactic potential and stellar populations can also be used for distance estimates (Binney et al. 2014). Considering the challenges for the different distance estimate methods, it is not surprising that the best distances values are typically accurate to the 10 %-level.

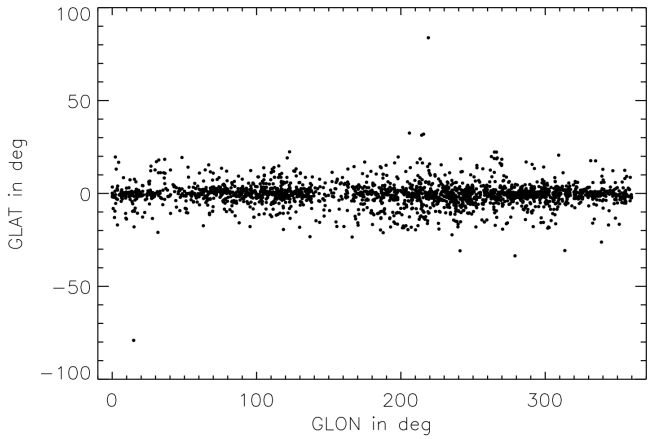

Figure 1.4: Spatial distribution of open clusters generated with data from the Milky Way global survey of Star Clusters (MWSC; Kharchenko et al. 2013) in Galactic coordinates (b vs. l).

The distribution of open clusters in the sky using Galactic coordinates showed another interesting characteristic (see Fig. 1.4). The vast majority of clusters are located either in or near the Galactic thin disc ($|b| \leq 30°$), where star formation is predominantly taking place. Hence, open clusters can be considered representative for the young stellar population in the Milky Way. The derived ages for the known open clusters confirm this, as the values range from a few Myrs to a few Gyrs. At optical wavelengths the gas and dust in star forming regions obscures the light from cluster members in the line of sight, which induces a volume limit and at larger distances only the very massive and bright clusters are detectable.

[6]Isochrones are tracks for stars of fixed age, derived using theoretical models for specific stellar parameters (e.g. mass, metallicity).

1.1.2 Stellar associations

Besides open clusters, stellar associations define a second type of accumulations with a more loose distribution. The density of typically 10 − 100 members is about ∼ 0.1 stars/pc^3. This stellar density is far lower than that for open clusters and just slightly higher than that of the field population. Therefore, stellar associations are not gravitationally bound and are expected to dissolve even faster than open clusters. This is reflected in the typical ages of just a few 10 Myrs. Thus, it is not surprising that stellar associations are often directly related to active star forming regions, such as Orion (Alves & Bouy 2012; Rivilla et al. 2013), Scorpius-Centaurus (Preibisch & Mamajek 2008; Ortega et al. 2009), Taurus-Auriga (D'Orazi et al. 2011; Mooley et al. 2013), or Cygnus (Wright et al. 2014). Two exemplary images for OB-associations are displayed in Fig. 1.5, namely Cepheus OB3 and Cygnus OB2.

Figure 1.5: Images of Galactic stellar associations, as copied from the NASA APOD website. Left panel: The Cepheus OB3 association (posted on 19 Oct. 2013). Right panel: The Cygnus OB2 association (posted on 4 March 2011).

The young age of stellar associations also implies that the majority of the low-mass stars (M≤ 1$M_\odot$) in these systems are still in the pre-main sequence stage of their evolution (Briceño et al. 2007). Moreover, it has been suggested that star formation in OB-associations is sequential and possibly triggered by effects like shock waves from supernova explosions (Blaauw 1964; Preibisch & Zinnecker 2007).
The identification of the members and determination of mean parameters is similar as for open clusters. Depending on the dominant stellar type detected in a stellar association, they can be divided into two groups. OB-associations show a large fraction of young O and B stars, which emit a lot of ionising radiation, while T-associations harbour a large fraction of T Tauri stars.

Section 1.2 The hierarchy of star formation

Open cluster are commonly believed to be the birth places for the vast majority of stars (Lada & Lada 2003; Lada 2006), which poses a direct link to star formation and provides a key to understand the origin of stars. The molecular clouds, where star formation takes place, show different levels of fragmented and clumpy structure (Elmegreen 2007, 2010). The detected substructures in the internal gas of very young open clusters (Carpenter & Hodapp 2008) typically dissolve after a few Myrs, before the gas expulsion (Cartwright & Whitworth 2004; Schmeja et al. 2008).

Interestingly within clusters stars preferably form in binary and triple systems (Goodwin & Kroupa 2005; Goodwin et al. 2007; Duchêne et al. 2007), providing an explanation for the larger binary fraction in open clusters compared to the field population. The binary and multiple systems in open clusters are expected to affect cluster parameters, such as velocity dispersion, and the clusters dynamical evolution (Kouwenhoven & de Grijs 2008; Geller et al. 2008, 2010; Gieles et al. 2010).
Another characteristic discovered in open clusters is mass segregation, describing that the massive stars in a cluster are typically observed in the centre, while in the periphery only lower mass members are detected (Hillenbrand & Hartmann 1998; de Grijs et al. 2002c,a,b; Gouliermis et al. 2004). In Fig. 1.6 this effect is illustrated for 15 clusters[7] of different age and at different distances.

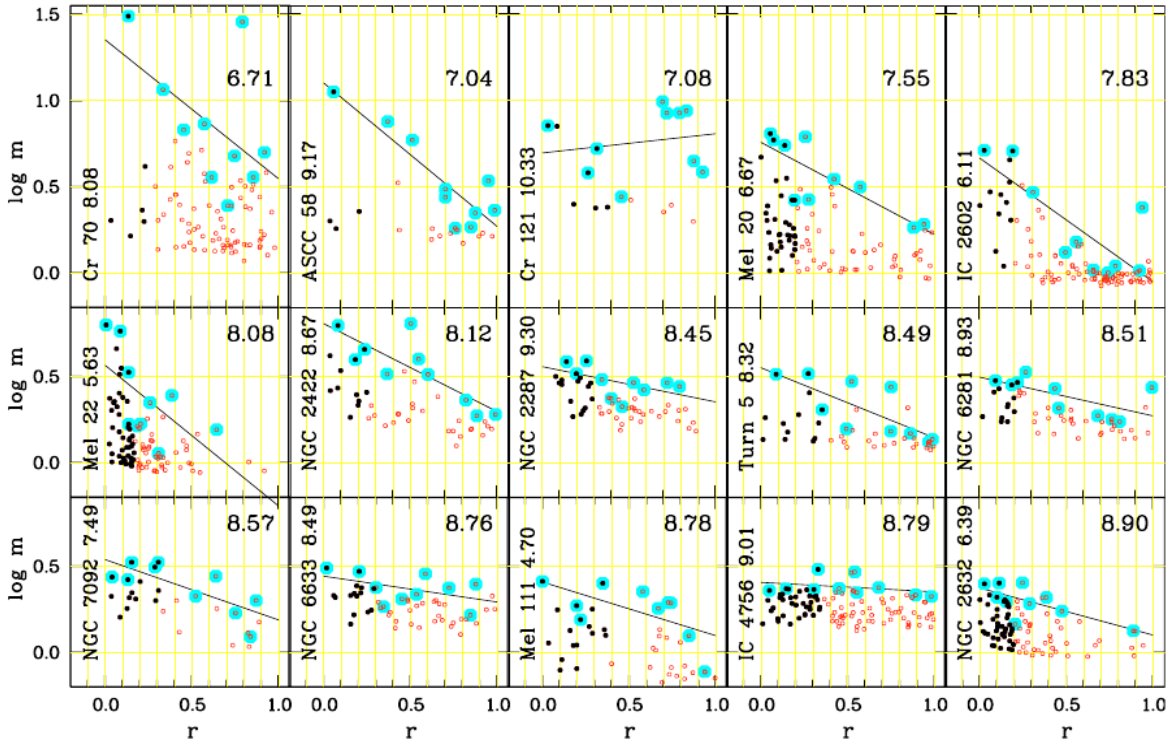

Figure 1.6: Mass of cluster members in relation with their distance from the centre in units of cluster radius for 15 open clusters, as copied from Schilbach et al. (2006). Their name and distance modulus are given on the left and their logarithmic ages on top of each panel. Black dots and red open circles show members in the core and coronal area, respectively. The cyan circles highlight the most massive members at a given distance from the cluster centre. These most massive members were then included for the regression (solid line).

The cause for this effect is not yet clearly established, but observational studies and theoretical simulations favour the scenario of primordial mass segregation, rather than dynamical segregation. Sagar & Bhatt (1989) conducted a proper motion study on eight open cluster and found that only for one cluster the brighter main sequence stars showed lower proper motion values, which would have indicated dynamical mass segregation. N-body simulations by Allison et al. (2009) on open clusters showed that the cool, substructured clusters mass segregate dynamically for masses down to a few solar masses on time scales of a few Myrs. One could conclude that dynamical mass segregation can only take place in the very early stages of star and cluster formation and mainly affects the gas, as well as the O and B stars in a cluster, but for the intermediate and older open clusters mass segregation can be considered to be primordial.

[7]The 15 clusters shown in Fig. 1.6 were selected from the Catalogue of Open Cluster Data (Kharchenko et al. 2005a,b) by Schilbach et al. (2006).

It is often said that members of the same cluster formed at the same time and thus have the same age, but already studies on NGC 2264 showed that there are discrepancies. Walker (1956) identified the turnoff for this cluster at the spectral type O7, which corresponds to an age of 3 Myrs, whereas Adams et al. (1983) used low-mass stars and derived an age of 10 Myrs. Such a discrepancy in ages when using different stellar types was also found for other open clusters and Herbig (1962) pointed out that this indicates that low-mass stars form earlier than high-mass stars. Otherwise, the formation of for example M stars would be interrupted by the supernova explosion of a B star in the same cluster after 10 Myr, because low-mass stars form over a longer time span than high-mass stars. Moreover, a supernova explosion within an open cluster would cause the expulsion of the remaining gas and consequently the sequential formation of the cluster members would have to take place within a few Myrs. This defines the maximum age spread within open clusters, which is typically within the error margins of cluster age determination. Hence, for general purposes it can be assumed that cluster members are of about the same age.
On the one hand, there are internal processes affecting the stability and evolution of open clusters, such as gas expulsion induced by supernova explosions or kinematic encounters that in some cases lead to ejection of members. On the other hand, also external forces influence the evolution of open clusters, like dynamical interactions with molecular clouds or tidal stripping through the Galactic gravitational field (Spitzer 1958). All these effects result in loss of members or gas from the gravitational field of an open cluster, and therefore in mass loss. Fig. 1.7 shows the results for a simulation of mass loss of open clusters over time for different assumptions on the star formation efficiency (SFE)[8], namely 10-60%, as conducted by Goodwin & Bastian (2006) and Goodwin (2009).

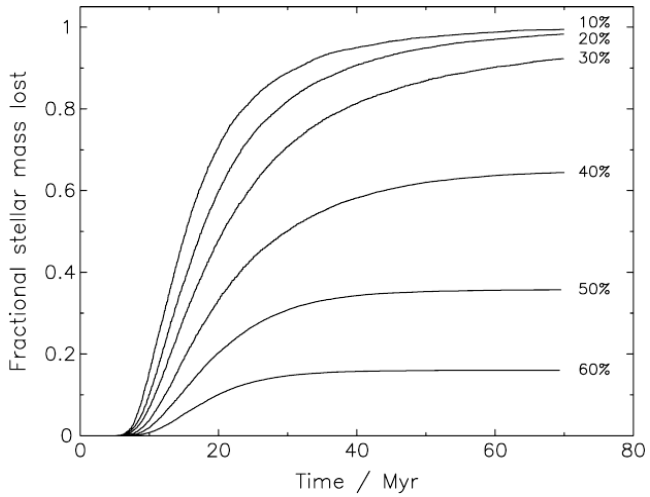

Figure 1.7: Time dependent fractional mass loss of open clusters, as copied from Goodwin (2009). The simulations were conducted within a distance of 20 pc from the cluster centre and for different assumptions on the star formation efficiency, illustrated by different lines (10 – 60%, see also Goodwin & Bastian 2006).

One can see that clusters with very low densities and/or mass (SFE of 10-30%), loose the majority of their mass within 20 or 30 Myrs, which is often referred to as infant mortality and mainly related to gas expulsion. Through internal and external kinematic interactions these low-SFE clusters get entirely disrupted within either 50 Myrs (SFE of 10-20%) or a few 100 Myrs (SFE of 30%). Clusters with higher density and/or mass have higher chances to survive the internal and external disruption processes, though they also undergo mass loss within the first 30-40 Myrs.
Former members of open clusters, which were either ejected or spread out after the host cluster dissolved, join the field population. These stars are typically of spectral type A and later, because the O and B stars, if present, typically end their life before the cluster dissolves. This aspect explains why the most massive stars can only be observed in a cluster environment and that the field population has a different mass function than, in particular, the young cluster population. Hence, the initial mass function, which describes the typical stellar composition of galaxies, should be better accessible from young open clusters than from the field population.

[8]The star formation efficiency describes how much gas is transformed into stars in a molecular cloud and is dependent, amongst others, on the density, mass, metallicity and environment of the molecular cloud, as well as the cores within.

SECTION 1.3

GALACTIC STRUCTURE AND DYNAMICS

Besides their direct link to star formation, open clusters can be used as tracers for Galactic structure and dynamics. In spiral galaxies, like our Milky Way, star formation primarily takes places in the vicinity of spiral arms (Bonnell & Dobbs 2007; Dobbs & Pettitt 2014). Thus, open cluster could be expected to trace the spiral structure of the Milky Way. This is in particular the case for the young population with ages of a few 10 Myrs, because clusters older than a few 100 Myrs should have migrated out of their birthplace due to dynamical interactions. The dynamical interaction between open clusters and the Galactic field, leads to larger eccentricities of their orbits and an increase for the height over the midplane (Z). This is also referred to as heating of the Galactic disc (Smith et al. 2012). Fig. 1.8 illustrates this aspect for Z, using open clusters from the Milky Way global survey of Star Clusters (MWSC; Kharchenko et al. 2013). The younger clusters (ages $\leq$ 60 Myr) are exclusively located within the thin disc ($|Z| \leq 400$ pc), while a considerable fraction of older clusters was detected at higher latitudes (van den Bergh & McClure 1980). In radial direction a relation of the location for open clusters with their age is not that clearly established as for the vertical direction.

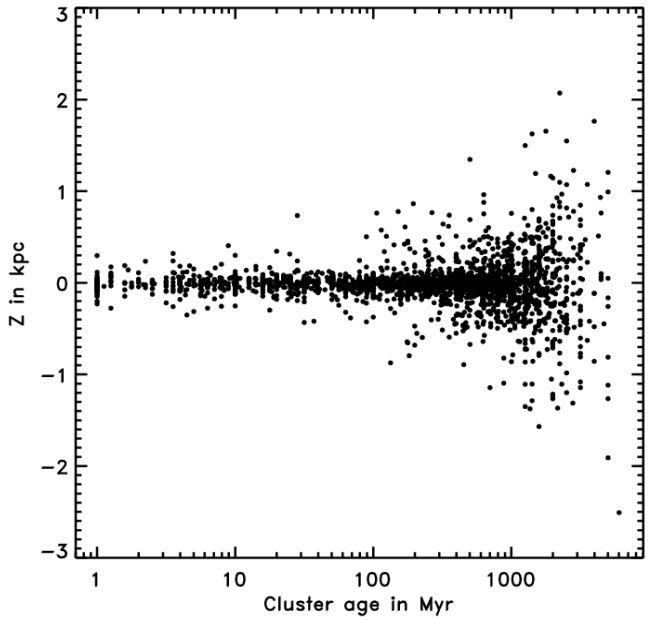

Figure 1.8: Distribution in height over and under the midplane (Z) with respect to cluster age for Galactic open clusters. This plot was generated with data from the Milky Way global survey of Star Clusters (MWSC; Kharchenko et al. 2013).

More than that, the general open cluster population enables a better determination of the orbital motion in the Milky Way, simply because their parameters, such as position, distance and velocity, can be determined to higher accuracy than for isolated stars. Hence, open clusters are essential to trace the kinematics and dynamics of the Galaxy, including heating and migration of Galactic objects. As a consequence a better determination of the Galactic potential is possible.

Furthermore, even the stellar population could be traced to former open clusters, following the assumption that the majority of stars form in a clustered mode. As open clusters dissolve, typically after a few 100 Myrs, their former members join the field population, but still share similar age and chemical composition, although moving on different velocity vectors. The identification of stellar population fulfilling these aspects are then traced through backwards orbit calculations to identify their birthplace (Mitschang et al. 2013, 2014). This is referred to as chemical tagging. Since this field of research is relatively young, future results will show how well stellar populations can be traced to their birthplace. In addition, this method could reveal how similar the age and chemical composition of members in open clusters really is.

All the aspects illustrate that open clusters are essential to understand the formation and evolution of stars and our Milky Way, as they can be used as laboratories and tracers. They are essential to obtain a detailed picture for the processes in spiral galaxies and to better understand the universe we live in.

SECTION 1.4

PAST INVESTIGATIONS ON OPEN CLUSTERS AND STELLAR ASSOCIATIONS[9]

Throughout the past decades several comprehensive studies, observational and literature compilations, were carried out to identify and characterise Galactic open clusters (OCs). One important study was conducted by Lyngå (1987), providing a catalogue of 1151 OCs partly equipped with distances, ages and even more sparsely with metallicities. It is often referred to as the Lund catalogue. Another set of catalogues was provided by Ruprecht et al. (1981), containing solely central coordinates and identifiers for 137 globular clusters, 1112 open clusters and 89 associations. The Two Micron All Sky Survey (2MASS; Cutri et al. 2003) provided a new source for cluster searches. Bica et al. (2003a,b) identified 276 infrared clusters and stellar groups as well as 167 embedded clusters related to nebulae. Besides the identifiers and coordinates, they listed angular sizes measured by eye. Dutra et al. (2003) extended these catalogues to the southern hemisphere by 123 clusters, providing the same type of information. Another extensive infrared OC catalogue in 2MASS was generated by Froebrich et al. (2007) near the Galactic disc ($|b| < 20°$). They provided coordinates, radii and stellar densities for 1788 open and globular clusters, including 1021 new objects. In the optical HIPPARCOS (Perryman et al. 1997) and TYCHO-2 (Høg et al. 2000) provided another opportunity for OC searches. Platais et al. (1998) published positions, distances, diameters, ages and proper motions for 102 clusters and associations in HIPPARCOS, including 82 known objects and 20 new discoveries. Alessi et al. (2003) detected 11 new OCs in the TYCHO-2 data and listed positions, diameters, distances, ages, proper motions and velocity dispersions.
Presently, most known OCs are summarised in two main online compilations. One is the collection of optically visible open clusters and candidates by Dias et al. (2002) (hereafter referred to as DAML). It contains positions for 2174 open clusters, including a few associations, while for other parameters, like radii, distances, ages, and proper motions, are provided in subsets for the majority of the entries. Radial velocities (RVs) were given for 543 listings (25%) and metallicities ($[M/H]$) or iron abundances ($[Fe/H]$) for 202 clusters (9%). The second is the WEBDA data base[10], created by Mermilliod (1988) and maintained by Netopil et al. (2012), collecting information on 970 Galactic OCs and 248 OCs in the Small Magellanic Cloud. For the Galactic OCs they listed positions, diameters, distances, ages, proper motions, RVs and colour excess, if available. The vast majority of WEBDA entries (910) is included in the DAML. These compilations are inevitable for comprehensive studies, being the most complete collections of open clusters and associations. However, the information therein are highly inhomogeneous, due to different data sources and algorithms used for the membership selection and parameter determination. Furthermore, the provided parameters were not transferred to a uniform reference system, possibly inducing additional systematic biases, which in turn could lead to false conclusions on the overall characteristics of the OC system.
Kharchenko et al. (2005a,b) presented the Catalogue of Open Cluster Data (COCD) comprising in total 650 Galactic open clusters and associations (OCs). The OCs were extracted from the DAML or newly discovered. They applied a uniform membership selection and provided a mostly homogeneous set of parameters for the clusters and their members. Kharchenko et al. (2007) extended the RV information in the COCD, based on the second edition of the Catalogue of Radial Velocities with Astrometric Data (CRVAD-2; Kharchenko et al. 2007) and literature values. The results were published in the Catalogue of Radial Velocities of Open Clusters and Associations (CRVOCA; Kharchenko et al. 2007).

[9]This section corresponds in most parts to the introduction from Conrad et al. (2014). For this publication I analysed and interpreted the data obtained from the COCD and RAVE and wrote the entire text, considering discussion on details with the co-authors.
[10]WEBDA - http://www.univie.ac.at/webda

SECTION 1.5
STUDIES ON STRUCTURES IN THE OPEN CLUSTER POPULATION

Up to the present open clusters were mainly investigated as isolated stellar systems, but are they really isolated? Groupings of open clusters could shed new light on the formation of stars and help to better understand the structure and dynamics of our Milky Way. Piskunov et al. (2006) found accumulations of COCD objects based on spatial distributions and proper motions, after they divided their sample into age bins. They proposed two groups, namely the Perseus-Auriga group with eight members of ages between 220 and 400 Myr and the Hyades moving group with nine members of ages between 0.4 and 1.4 Gyr. The open cluster complexes (OCC) proposed by Piskunov et al. (2006) are younger: OCC1 with 20 members covering an age range from 5 to 50 Myr and OCC2 harbouring 20 members of ages between 204 and 390 Myr.
de La Fuente Marcos & de La Fuente Marcos (2009a,b,c) provided a series of papers on smaller open cluster groupings based on the WEBDA online data base and DAML. In the first paper de La Fuente Marcos & de La Fuente Marcos (2009a) focused on the investigation of a kinematically coherent open cluster group spread over the Cassiopeia and Perseus constellations. This Cassiopeia-Perseus family is located at a distance of about 2 kpc with a diameter of 600 pc and the members cover an age range of $20-40$ Myr. In the second publication de La Fuente Marcos & de La Fuente Marcos (2009b) assumed that the separation of open cluster pairs should not exceed three times the typical cluster tidal radius ($\sim$ 30 pc) in the Milky Way. Due to incompleteness at higher distances they split up their sample. Within their volume limited sample (d < 850 pc) they identified 16 pairs, two triples, and one quadruple. At higher distances they found 18 additional open cluster pairs and one more triple with distances up to 2.3 kpc. In the third paper de La Fuente Marcos & de La Fuente Marcos (2009c) discussed the hierarchy of star formation in the Galactic disc based on open cluster pairs. They found evidence for highly hierarchical star formation in the Milky Way and stated that in neighbouring regions star formation is synchronised. This limits the time interval available for cluster formation and de La Fuente Marcos & de La Fuente Marcos (2009c) concluded that the vast majority of clusters should form in larger complexes.

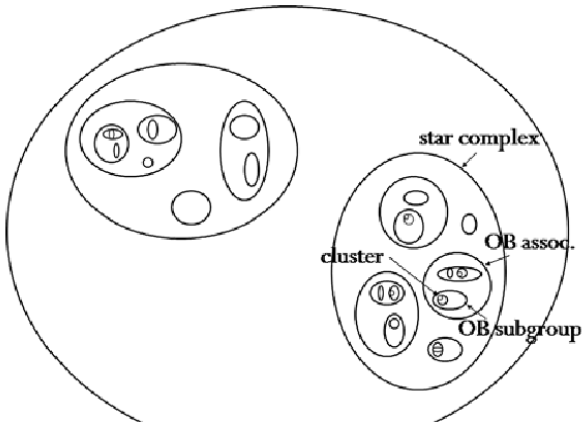

Figure 1.9: Schematic for the hierarchical star formation in the Milky Way, as copied from Elmegreen (2009).

In the Milky Way Piatti et al. (2010) verified another binary of open clusters with a separation of 3.6 pc. Both these clusters are rather small with individual total radii of about 1 pc. Elias et al. (2009) investigated the Gould belt open cluster population and found differences between the Orion and Sco-Cen regions. The former showed a very clumpy structure and can, therefore, be referred to as a cluster complex. The latter seemed to be dominated by isolated star formation and is more likely an OB association. Elmegreen (2009, 2011) supported the picture of hierarchical star formation in the Milky Way. They found that the fragmentation of giant molecular clouds is reflected in the distribution of young stars. On the largest scale they form cluster complexes, and on smaller scales OB associations and open clusters, down to isolated stars. A schematic for this hierarchical structure in Galactic star forming regions from Elmegreen (2009) is shown in Fig. 1.9.
There were a few studies on hierarchical star formation in nearby galaxies. Bonatto & Bica (2010) investigated the Magellanic Clouds and identified similar patterns as in the Milky Way. For example that the young stars followed the fragmentation of the gas. Moreover, the degree of grouping appeared to be higher for young clusters than for old ones, which they suggested to be most likely caused by dynamical interactions.

In M33 the fractal dimension of molecular gas was found to be significantly smaller than for the Milky Way (Sánchez et al. 2010) with a transition from fractal structures to uniform distributions at a scale of about 500-1000 pc. Efremov (2010) and Gusev & Efremov (2013) investigated star cluster complexes in the spiral arms of M31 and M74, respectively. For both galaxies the cluster complexes appeared to be almost equally spaced in a chain-like structure along the spiral arms. These findings suggest that grouping of open clusters is not only a Galactic phenomenon.

SECTION 1.6 OUTLINE OF THIS THESIS

The goal of the project presented in this thesis was to investigate potential groupings in the open cluster population, which would indicate an additional level of structure in the Galaxy and help gain a more detailed picture on the relation between the fragmentation of gas and star formation, as well as how stars and clusters built up to galaxies. All open cluster pairs, groups and complexes proposed so far were identified either solely using spatial information or by additionally including proper motions, but never the full set of 6D phase-space information. This could lead to contamination or misidentification of groupings and potential members through by chance alignment and projection effects. Genuine groupings of open clusters and/or stellar associations can be expected to move with a common velocity vector. For this reason I investigated potential structures in the galactic open cluster population using 6D phase-space information in the Cartesian system. Although the majority of known open clusters lack radial velocity information, which would be required for such an approach, I generated a working sample of sufficient size with mean parameters of sufficient accuracy. A detailed investigation of this cluster sample showed that even in an incomplete sample evidence for groupings in the Galactic open cluster population can be identified.

Chapter 2: In order to conduct such an investigation an appropriate data set is essential. One of the largest online compilations for Galactic open clusters currently available is the New Optically Visible Open Clusters and Candidates Catalog (DAML; Dias et al. 2002), providing rather inhomogeneous parameters for the objects listed. For the work presented in this thesis, on the other hand, I needed a homogeneous sample on open clusters, which is why the DAML was only used as a reference catalogue for the metallicities. When starting the project the most extensive homogeneous data set available was the Catalogue of Open Cluster Data (COCD; Kharchenko et al. 2005a,b), which became the main source for my investigations, complemented by data obtained from the second version of the Catalogue of Radial Velocities with Astrometric Data (CRVAD; Kharchenko et al. 2007), the Catalogue of Radial Velocities of Open Clusters and Associations (CRVOCA; Kharchenko et al. 2007), and the RAdial Velocity Experiment (RAVE; Kordopatis et al. 2013). In the second chapter of this thesis I briefly describe the catalogues and data sets employed throughout the thesis.

Chapter 3: For the identification of overdensities in the open cluster population I planned to use 6D phase-space information, but the COCD significantly lacked radial velocities, even when complemented with data from the CRVAD-2 and CRVOCA. Therefore, additional radial velocities were obtained from RAVE through cross-matching of cluster members with the catalogue for the fourth data release (DR4). These additional data enabled me to newly computed mean radial velocities and metallicities for a larger subset of COCD clusters, which then defined my final working sample. In the third chapter I show that the RAVE data are of sufficient quality for the intended investigation of the open cluster population, through evaluating the uncertainties of the data and comparing the results with reference samples.

Chapter 4: After ensuring that the derived mean parameters for my working sample, containing 432 clusters, were of sufficient accuracy, I determined the Cartesian XYZ-coordinates and UVW-velocities and used these 6D phase-space information to search for overdensities in the open cluster population through applying an adaption of the Friends-of-Friends (FoF) algorithm, as used in cosmology. Spheres in coordinate and velocity space had to be predefined to use the FoF-like algorithm, which were based on educated guess for the size of the expected structures. The values for these search radii are to a certain degree arbitrary, although derived by an educated guess, and further verification was necessary to ensure which of the identified groupings were genuine. I followed two approaches, namely a comparison to a randomised sample selected from a reference catalogue (Milky Way global survey of star clusters (MWSC; Kharchenko et al. 2013)) and Monte-Carlo simulations of randomised samples generated from parameter distributions that were representative for the open cluster population. Chapter 4 summarises the determination and characteristics of the 6D-Cartesian parameters, as well as the identification, verification, and characterisation of the identified open cluster groupings.

Chapter 5: In the final chapter I summarise the main findings of the project presented in this thesis and provide an outlook on what should be done to generate a more complete sample, as well as what open cluster groupings might tell us about our Galaxy and its evolution. The verification revealed that at least the large complex with its 15 members was most likely genuine, while for the majority of pairs a chance alignment is the more likely scenario. A closer look at the complex favoured the scenario that its members originate from a common giant molecular cloud and formed in a single, possibly sequential, formation event. However, the data set used for this project was highly incomplete and I could only provide a pilot study for the existence and detectability of open cluster groupings. A step towards a more complete sample would be to use the more extensive MWSC catalogue complemented by infrared data from the VISTA Variables in the Via Lactea survey (VVV), additional spectroscopic data from RAVE, SEGUE and APOGEE[11], as well as results from studies on individual clusters. With a more complete cluster sample it should be possible to identify further genuine groupings and to verify that also open clusters form in a clustered mode. This would provide further constraints on theoretical simulations on star formation as well as on the evolution and kinematics of the Milky Way.

Appendix: The tables for the newly computed mean RV values of 110 COCD clusters and mean $[M/H]$ data for 81 COCD clusters were too large to be included in the text flow. The same is true for the parameters of the final working sample, which comprised 432 open clusters, and therefore these information are presented in the appendix of this thesis. For the 19 potential OC groupings found with the lower limit of the radius for the search sphere in velocity space the distributions in coordinate and velocity space, as well as their age and metallicity spread, were also shifted to the appendix. As were the larger tables summarising the parameters of the resulting grouping from the upper limit of the radius for the search sphere in velocity space.

ADDITIONAL REMARKS

Chapter 3 was already published as Conrad et al. (2014) and parts of the introduction, as well as the majority of the catalogue description, were also taken from this paper. In the pre-process of generating this publication, I performed all steps of the selection, analysis and interpretation. That is I selected the COCD as being most suitable cluster sample for the project and cross-matched the most probable cluster members with the catalogue of the RAVE survey to obtain additional radial velocity and metallicity data. I performed the analysis of the RAVE data and the interpretation of the results, yielding the mean parameters derived from RAVE to be suitable for the purposes of the project presented in this thesis. In the final process of writing the manuscript for the publication (Conrad et al. 2014) I was in contact with the co-authors and discussed details, resulting in an even better understanding of the data and results. The writing of the paper was entirely done by myself under consideration of the discussions with the co-authors.

[11] SEGUE and APOGEE are part of the Sloan Digital Sky Survey (SDSS).

Chapter 2

The Catalogues[1]

Section 2.1

Catalogues on Galactic open clusters

2.1.1 DAML

The New Optically Visible Open Clusters and Candidates Catalog[2] (Dias et al. 2002) is the most extensive online compilation for Galactic open clusters in the optical and is hereafter referred to as the DAML. This compilation is updated continuously and for my study I used the Version 3.3 as provide on 10 Jan. 2013, which comprised almost 2200 objects. Position for the cluster centres in the equatorial and Galactic system and proper motions were listed for all objects, while radial velocities were provided for about 25% and overall metallicities or iron abundances for about 9% of the listed clusters. Almost no stellar associations are included in the DAML, because they are still embedded and better visible in the infrared.
The DAML compilation is not a homogeneous catalogue but merely a collection of literature values for known Galactic open clusters. Thus, the listed parameters for the included clusters originate from different projects, using different methods and reference systems to derive their values. The DAML provides a good overview on the number of Galactic clusters, but does not provide a homogeneous sample for detailed investigations on the cluster population. The study presented in this work required a homogenous cluster sample. Thus the DAML could not be used as working sample, but was could still sufficient to be utilised as reference sample.
For the study presented in this work mainly the $[M/H]$ information were of interest, which were not provided by the actual working sample compiled from the Catalogue of Open Cluster Data (COCD; Kharchenko et al. 2005a,b) and had to be taken from the DAML. As stated above the cluster parameters were inhomogeneous in the DAML, which is in particular true for the listed "metallicities", since different methods either provided overall metallicities ($[M/H]$) and actual iron abundance ($[Fe/H]$) and Dias et al. (2002) did not distinguish between those. In total the DAML listed $[M/H]$ or $[Fe/H]$ for 97 COCD objects and only 20 of those were based on more than five individual measurements. The uncertainties in these "metallicities" were below 0.3 dex for all objects were this parameter was available. However, the additional information, namely the source and method used to determine the "metallicities", helped to distinguish between $[M/H]$ and $[Fe/H]$.

[1] This chapter is an extended version of the catalogue description in Conrad et al. (2014). For this publication I analysed and interpreted the data obtained from the COCD and RAVE and wrote the entire text, considering discussion on details with the co-authors.
[2] DAML - http://www.astro.iag.usp.br/~wilton/

In cases where the listed "metallicity" was derived solely based on iron lines it rather corresponded to the iron abundance ($[Fe/H]$), while photometric methods most likely resulted in a value comparable to the overall metallicity ($[M/H]$). If no information on the technique or literature reference was given in the DAML, I assumed the value to refer to $[M/H]$. However, the $[M/H]$ data in the DAML originate from different studies using a variety of methods and therefore, the values have to be used and evaluated with a high amount of caution.

2.1.2 THE COCD AND CSOCA

This project was primarily based on the most homogeneous data set for open cluster currently available, that is the Catalogue of Open Cluster Data (COCD; Kharchenko et al. 2005a,b). The COCD was constructed from the All-Sky Compiled Catalogue of 2.5 million stars (ASCC-2.5; Kharchenko 2001), which contained relatively bright stars ($V_{Johnson}$ down to 12.5 mag) listed with proper motions. The photometric and astrometric parameters in the ASCC-2.5 were collected and combined from data given in the HIPPARCOS (Perryman et al. 1997), TYCHO (Høg et al. 1997, 2000), CMC[3] (Fabricius 1993), and PPM[4] (Röser & Bastian 1991; Bastian & Röser 1993) catalogues, and were provided in the Johnson photometric and HIPPARCOS proper motion reference systems.
In a first step, Kharchenko et al. (2005a) extracted a subsample of stars from the ASCC-2.5 that were located in regions around 520 known clusters and associations from the DAML. These areas were predefined as quadratic fields centred at the cluster centre coordinates with a side length of $2 \cdot (r_{cl} + 0.1°)$, where r_{cl} was the given radius of the cluster in DAML. This subsample of ASCC-2.5 stars were then summarised in the Catalogue of Stars in Open Cluster Areas (CSOCA; Kharchenko et al. 2004b), along with their parameters, such as equatorial and Galactic coordinates, ASCC-2.5 identifier, proper motions, trigonometric parallaxes, B and V magnitudes, as well as radial velocities and spectral type information, if available. Moreover, they provided angular distances to the cluster centre and three membership probabilities for each star in the CSOCA.

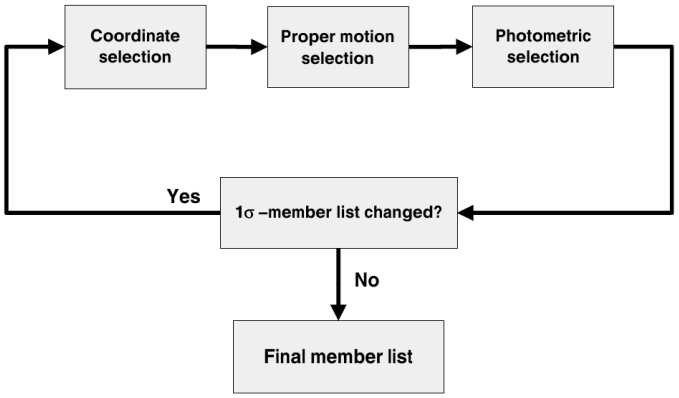

Figure 2.1: Schematic for the selection procedure used to identify open cluster members and to construct the COCD, as copied from Kharchenko et al. (2004b).

For the membership selection Kharchenko et al. (2004b) applied a uniform procedure considering radial stellar density distributions (P_{pos} - spatial membership probability), common kinematics (P_{kin} - kinematic membership probability) and isochrones in the colour-magnitude diagram (P_{phot} - photometric membership probability), which was ran repeatedly and typically converged after a few iterations (see Fig. 2.1). For P_{kin} and P_{phot} Kharchenko et al. (2004b) provided equations for the membership probability, which correspond to Eq. 2.1 and 2.2, respectively.

[3]CMC - The Carlsberg Meridian Catalogs
[4]PPM Star Catalogues - Positions and Proper Motions Star Catalogue for the northern and southern hemisphere

$$P_{kin} = \exp\left\{-\frac{1}{4}\cdot\left[\left(\frac{PM_X-\overline{PM_X}}{\epsilon_{PM,X}+\delta_\epsilon}\right)^2+\left(\frac{PM_Y-\overline{PM_Y}}{\epsilon_{PM,Y}+\delta_\epsilon}\right)^2\right]\right\} \quad (2.1)$$

$$P_{phot} = \exp\left\{-\frac{1}{2}\cdot\left[\frac{\Delta(B-V)}{\epsilon_{(B-V)}}\right]^2\right\} \quad (2.2)$$

with
$$\Delta(B-V) = (B-V)-(B-V)_b \quad \text{for} \quad (B-V)<(B-V)_b$$
$$\Delta(B-V) = (B-V)-(B-V)_r \quad \text{for} \quad (B-V)>(B-V)_r$$

The $PM_{X,Y}$ and $\epsilon_{PM,X,Y}$ in Eq. 2.1 are the proper motion components and standard errors of the individual star in the ASCC-2.5, $\overline{PM_{X,Y}}$ the averaged proper motions of the corresponding cluster, and δ_ϵ is the correction for external uncertainties in the proper motions. The $(B-V)_b$ and $(B-V)_r$ in Eq. 2.2 correspond to the colour indices of the blue and red limits in V-magnitude of the individual ASCC-2.5 star and $\epsilon_{(B-V)}$ to the uncertainty in the colour index for the individual star. Hence, all stars of the cluster region with $(B-V)_b \leq (B-V) \leq (B-V)_r$ have $P_{phot} = 100\%$ and are real members.

The P_{pos} values were set to unity for objects within the OC radius and zero otherwise. The P_{kin} and P_{phot} could take values of 0−100% and was larger for stars sharing the common motion of the corresponding cluster and for stars that were closer to the corresponding OC-isochrone in the colour-magnitude diagram, respectively. In this work, stars with P_{phot} and $P_{kin} \geq 61\%$ were called 1σ-members, those with P_{phot} and $P_{kin} \geq 14\%$ were referred to as 2σ-members and targets with P_{phot} and $P_{kin} \geq 1\%$ were considered as 3σ-members. In addition, the CSOCA listed variability and binarity flags mainly from TYCHO-1 and -2 (Høg et al. 1997, 2000), HIPPARCOS (Perryman et al. 1997), CMC(Fabricius 1993), GCVS[5] (Samus et al. 1997), NSV[6] (Kazarovets et al. 1998) and PPM (Röser & Bastian 1991; Bastian & Röser 1993).

The GCVS/NSV flags only indicated if a star was variable or not, but did not specify the variability type. Neither did the CMC variability flag, which in addition gave information on insufficient or missing magnitudes. The PPM binarity flag again only indicated binary candidates, but did not provide further information on the system. More detailed information on variability and binarity were provided by the TYCHO and HIPPARCOS flags. I found that about 10.4% of the CSOCA stars were provided with flags indicating variability and about 4.1% with flags indicating binarity. Among the flagged stars I found 3336 (1.7% of the CSOCA) indicated to be duplicity induced variables.

The first version of the COCD comprised 520 clusters and was extended by Kharchenko et al. (2005b) through an independent search for open clusters in the ASCC-2.5, which resulted in 109 previously unknown and 21 additional DAML clusters. The complete COCD provided center positions, core radii, tidal radii, distances, ages and mean proper motions (PMs) for in total 650 OCs[7], based primarily on the most probable members with P_{phot} and $P_{kin} \geq 61\%$. Mean radial velocities were provided for about 50% of the listed objects, but metallicities were not included at all. For the vast majority of the clusters the distances were derived from a photometric approach, since the majority of trigonometric parallaxes listed in the CSOCA were of insufficient quality. Basically, Kharchenko et al. (2005a,b) used 3-colour information and additional spectral type information, where available, for the most probable members ($P > 61\%$). Interstellar extinction was taken into account as well. In cases where 3-colour and spectral type information were not available, literature values for the distances were listed in the COCD.

[5]GCVS - The General Catalog of Variable Stars

[6]NSV - The New Suspected Variables catalog

[7]Since there are only 7 compact associations among the 650 entries in the COCD, I refer to all objects as OCs.

The ages for the COCD clusters were mainly derived using post-main sequence isochrones from the Padova grid (Girardi et al. 2002) and pre-main sequence isochrones from the Grenoble Pre-main sequence tracks Internet-server (Siess et al. 2000). First, Kharchenko et al. (2005a,b) determined ages for the most probable kinematic OC members through isochrone fitting and then averaged these individual ages to obtain the mean age of the corresponding cluster. For the clusters, where the isochrone method could not be applied, literature values were included in the COCD.
Uncertainties for individual clusters were provided for the proper motions and radial velocities, while for the distances and ages only general uncertainties were given. The distances were accurate to the 10% level and the uncertainties for the logarithmic ages were about 0.2-0.25 dex.

2.1.3 THE CRVAD AND CRVOCA

The radial velocity (RV) information in the CSOCA and COCD were obtained from the Catalogue of Radial Velocities with Astrometric Data (CRVAD; Kharchenko et al. 2004a), which was primarily based on the General Catalogue of mean Radial Velocities (Barbier-Brossat & Figon 2000). Kharchenko et al. (2007) updated the CRVAD to a second version (CRVAD-2) using additional stellar RVs from the Geneva-Copenhagen survey (Nordström et al. 2004), the Pulkovo Compilation of Radial Velocities (Gontcharov 2006), as well as CORAVEL and HIPPARCOS/TYCHO-2 kinematics on K and M giants (Famaey et al. 2005). Kharchenko et al. (2007) stated that only 71% of the CRVAD-2 entries were provided with RV uncertainties. Another 21.5% had RV quality indices from Dufolt et al. (1995), either indicating specific standard errors or insufficient data. Only nine stars in the CRVAD-2 showed flags indicating insufficient data, which was negligible compared to the 7.5% of CRVAD-2 entries with no uncertainties available.

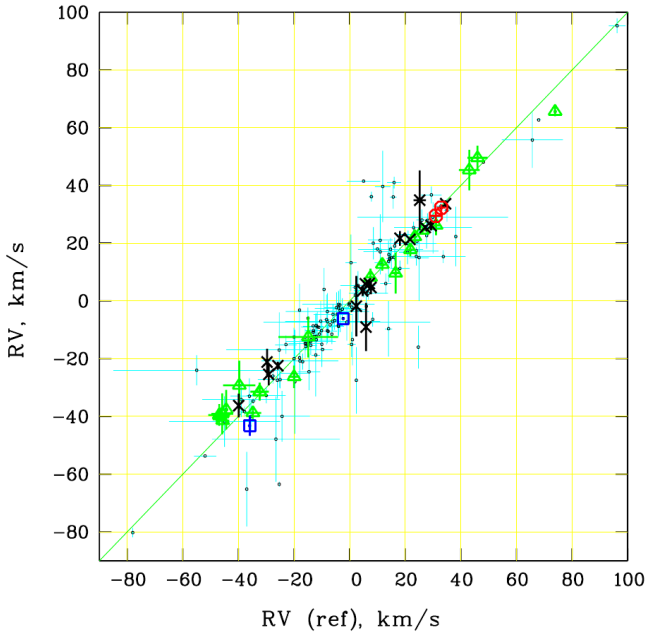

Figure 2.2: Comparison between the computed and literature RV data in the CRVOCA, as taken from Kharchenko et al. (2007, Fig. 2).

In addition, Kharchenko et al. (2007) presented the updated RV information for open clusters in the Catalogue of Radial Velocities of Open Clusters and Associations (CRVOCA), which is currently the most extensive and homogeneous RV catalogue for Galactic open clusters. It contains literature and newly computed $\overline{RV}$ for 516 open clusters and associations, including 395 COCD objects. The calculated $\overline{RV}$ were based on potential cluster members with P_{kin} and $P_{phot} \geq 1\%$. For 32 clusters they found no such potential member and took one star with P_{kin} >1% and its RV value as representative for the corresponding clusters. The literature values were obtained from the DAML for clusters and from Melnik & Efremov (1995)[8] for associations (for a detailed list of references see Kharchenko et al. 2007). For 177 objects in the CRVOCA computed and literature values were available. In Fig. 2.2 one can see that both values agree very well.
Among the 395 COCD clusters in the CRVOCA, 363 have calculated $\overline{RV}$. The remaining 32 OCs were provided with only literature values. The CRVOCA is currently the most homogeneous RV reference sample for Galactic open clusters.

[8]Melnik & Efremov (1995) provided the Catalog of Line-of-sight Velocities and Proper Motions of the OB Associations that is available via the following website. http://lnfm1.sai.msu.ru/~anna/page3.html

In this work I recomputed the mean RV values for the COCD clusters excluding the 3σ-members and only included values for the 2σ-members if not enough measurements on 1σ-members were available. These values were more representable for the clusters than the ones listed in the CRVOCA, which could have suffered from field contamination through including least probable members. A cross-match between the CSOCA and the CRVAD-2 revealed that 5% of the 3σ-members, 6% of the 2σ-members and 9% of the 1σ-members in the CSOCA were also listed in the CRVAD-2.

SECTION 2.2
THE RADIAL VELOCITY EXPERIMENT (RAVE)

The RAdial Velocity Experiment (RAVE) was a spectroscopic stellar survey in the southern hemisphere, observing preferably at high Galactic latitudes. The data were obtained with the six degree field (6dF) instrument at the Anglo Australian Observatory, providing mid-resolution (R=7500) spectra in the spectral range covering the CaII-triplet (8410 – 8795 Å). There were several data releases that not only used additional input catalogues and extended the provided catalogue, but also improved and extended the pipeline and stellar parameters. The input catalogues for the first data release (DR1; Steinmetz et al. 2006) were TYCHO-2 (Høg et al. 2000) and SSS[9] (Hambly et al. 2001) and the basic pipeline for the determination of the heliocentric radial velocities was based on a standard cross-correlation procedure (Tonry & Davis 1979) using Fourier transforms. For the RV determination the red and blue end of the spectra were excluded to avoid poor focus, defining the effective wavelength range to be 8460 – 8746 Å. Wavelength calibration as well as the normalisation of the continuum were performed prior to the RV determination.
In the first spectra a zero-point shift was detected, which resulted in an RV offset of the order of ~ 1.5 km/s and was believed to be most likely caused by temperature variations in the spectrograph room and was corrected in the pipeline. The RAVE DR1 pipeline yielded quality parameters for the derived RV data, such as χ^2 -values, signal-to-noise ratios, flags, correction parameters and a cross-correlation factor for the template matching. The respective template spectra were taken from the libraries by Zwitter et al. (2004) and Munari et al. (2005) for different spectral types. The typical RV uncertainties in DR1 were determined to be 2 km/s. The corresponding RAVE catalogue provided photometry from TYCHO-2, the DEep Near-Infrared southern sky Survey (DENIS; Epchtein et al. 1997), USNO-B (Monet et al. 2003), and 2MASS (Cutri et al. 2003). The proper motions were obtained and combined from TYCHO-2, SSS, 2MASS, GSC 1.2 (Morrison et al. 2001), and UCAC-2 (Zacharias et al. 2004), but no stellar parameters were provided for DR1, such as effective temperature (T_{eff}), surface gravity ($\log g$), and metallicity ($[M/H]$).
In the second data release of RAVE (DR2; Zwitter et al. 2008) the RV pipeline was improved, resulting in RV uncertainties of typically 1 km/s, and stellar parameters (T_{eff}, $\log g$, and $[M/H]$) were provided in the corresponding catalogue, derived in the process of fitting template spectra to observed spectra for the RV determination. The calibration for the metallicities in DR2 was derived following equation 2.3, where the $[M/H]$ and $[m/H]$ are the calibrated and uncalibrated metallicities, $[\alpha/Fe]$ the α-enhancement, and $\log g$ the surface gravity of a star observed by RAVE. The $[\alpha/Fe]$ values in RAVE DR2 could not be determined to high accuracy, but still reflect overall characteristics for the stellar population and the change from star to star was found to not be random.

$$[M/H] = 0.938[m/H] + 0.767[\alpha/Fe] - 0.064 \log g + 0.404 \tag{2.3}$$

For stars cooler than 9000 K and with signal-to-noise ratio (S/N) of 40 the uncertainties in T_{eff} were about 400 K. Hotter stars had higher uncertainties, and supergiants showed the smallest uncertainties in temperature. The uncertainties in surface gravity did not exceed 0.8 dex and were largest for cool stars and dwarfs.

[9] SSS is the abbreviation for the SuperCOSMOS Sky Survey.

The uncertainties in the calibrated metallicities were about 0.2 dex for stars cooler than 7000 K and increased significantly for hotter stars, while the α-enhancement showed recovery errors of up to 0.15 dex. In the third data release of RAVE (DR3; Siebert et al. 2011) several aspects of the pipeline were improved, such as the zero-point offset correction and the metallicity calibration. The new pipeline computed the zero-point offset correction using a third-order polynomial derived from sky lines in the spectral RAVE window with correlation to the fibre number and a constant correction, depending on the observational case. The metallicity calibration was now more detailed by using Eq. 2.4, where S/N was the signal-to-noise ratio in the DR3 data, and the c_0 to c_5 the coefficients for different stellar types and parameter ranges, as summarised in Tab. 2.1.

$$[M/H] = c_0 + c_1 \cdot [m/H] + c_2 \cdot [\alpha/Fe] + c_3 \cdot \frac{T_{eff}}{5040} + c_4 \cdot \log g + c_5 \cdot S/N \tag{2.4}$$

Table 2.1: Table for the coefficients in the metallicity calibration in RAVE DR3 (Eq. 2.4), as taken from Siebert et al. (2011). $N_{\rm tot}$ is the total number of data points used to derive the calibration. The first row includes the DR2 calibration results for comparison.

Calibration	$N_{\rm tot}$	c_0	c_1	c_2	c_3	c_4	c_5
				Full sample			
DR2	...	0.404	0.938	0.767	...	−0.064	...
DR3-0	223	0.578 ± 0.098	1.095 ± 0.022	1.246 ± 0.143	−0.520 ± 0.089	...	...
DR3-1	217	0.587 ± 0.091	1.106 ± 0.024	1.261 ± 0.140	−0.579 ± 0.078	...	0.001 ± 0.0004
DR3-2	223	0.518 ± 0.127	1.111 ± 0.031	1.252 ± 0.144	−0.399 ± 0.187	−0.019 ± 0.026	...
DR3-3	222	0.429 ± 0.132	1.101 ± 0.032	1.171 ± 0.147	−0.391 ± 0.186	−0.018 ± 0.026	0.001 ± 0.0004
				Dwarfs only			
DR3-0	89	0.612 ± 0.236	1.081 ± 0.045	1.215 ± 0.203	−0.546 ± 0.196	...	...
DR3-1	75	0.706 ± 0.199	1.250 ± 0.055	1.491 ± 0.184	−0.683 ± 0.165	...	0.001 ± 0.0004
DR3-2	82	−0.174 ± 0.222	1.061 ± 0.047	1.621 ± 0.158	−0.751 ± 0.160	0.232 ± 0.038	...
DR3-3	81	−0.170 ± 0.217	1.063 ± 0.047	1.586 ± 0.155	−0.751 ± 0.155	0.219 ± 0.037	0.001 ± 0.0003
				Giants only			
DR3-0	127	0.763 ± 0.197	1.094 ± 0.027	1.210 ± 0.193	−0.711 ± 0.207	...	...
DR3-1	119	0.399 ± 0.178	1.087 ± 0.027	1.300 ± 0.185	−0.383 ± 0.179	...	0.001 ± 0.0005
DR3-2	127	0.354 ± 0.287	1.162 ± 0.044	1.285 ± 0.194	−0.049 ± 0.398	−0.078 ± 0.040	...
DR3-3	127	0.239 ± 0.297	1.154 ± 0.045	1.217 ± 0.200	−0.006 ± 0.398	−0.080 ± 0.040	0.001 ± 0.0007

DR3-0: DR3 calibration with no S/N no log g available; **DR3-1:** DR3 calibration with only S/N, but no log g available; **DR3-2:** DR3 calibration with only log g , but no S/N available; **DR3-3:** DR3 calibration with S/N and log g available

For the fourth data release in RAVE (DR4; Kordopatis et al. 2013) new input catalogues were included, namely DENIS (Epchtein et al. 1997) and 2MASS (Cutri et al. 2003). Furthermore, additional stellar parameters for the RAVE stars were determined, such as distances, ages, and extinctions (Binney et al. 2014), as well as element abundances by Boeche et al. (2011). The observation footprint for the 482430 entries of 425561 stars in the RAVE DR4 is illustrated in Fig. 2.3. Moreover, a new pipeline for the determination of the stellar parameters was implemented based on the DEGAS[10] decision-tree method (Bijaoui et al. 2012) and the MATISSE[11] projection algorithm (Recio-Blanco et al. 2006). DEGAS was a decision-tree algorithm based on a grid of synthetic spectra with the parameters set (T_{eff}, $\log g$, $[M/H]$) and a subset of spectra at each node of the grid. It required a learning phase to establish the recognition rules, during which reference spectra were compared to the grid. After the learning process DEGAS determined the parameters of the observed spectra from computing weighted means of the differences to a subset of synthetic spectra at the corresponding node. The parameters from DEGAS were then used to renormalise the spectra, which usually converged after a few iterations. For spectra with S/N $\geq$ 30 pixel^{-1} MATISSE was run on the observed spectra with the DEGAS parameters as input, since it was shown by Kordopatis et al. (2011) that MATISSE managed to better interpolate between grid points. For spectra with lower S/N the DEGAS results were listed in the RAVE DR4 catalogue.

[10]DEGAS - DEcision tree alGorithm for AStrophysics
[11]MATISSE - MATrix Inversion for Spectral SynthEsis

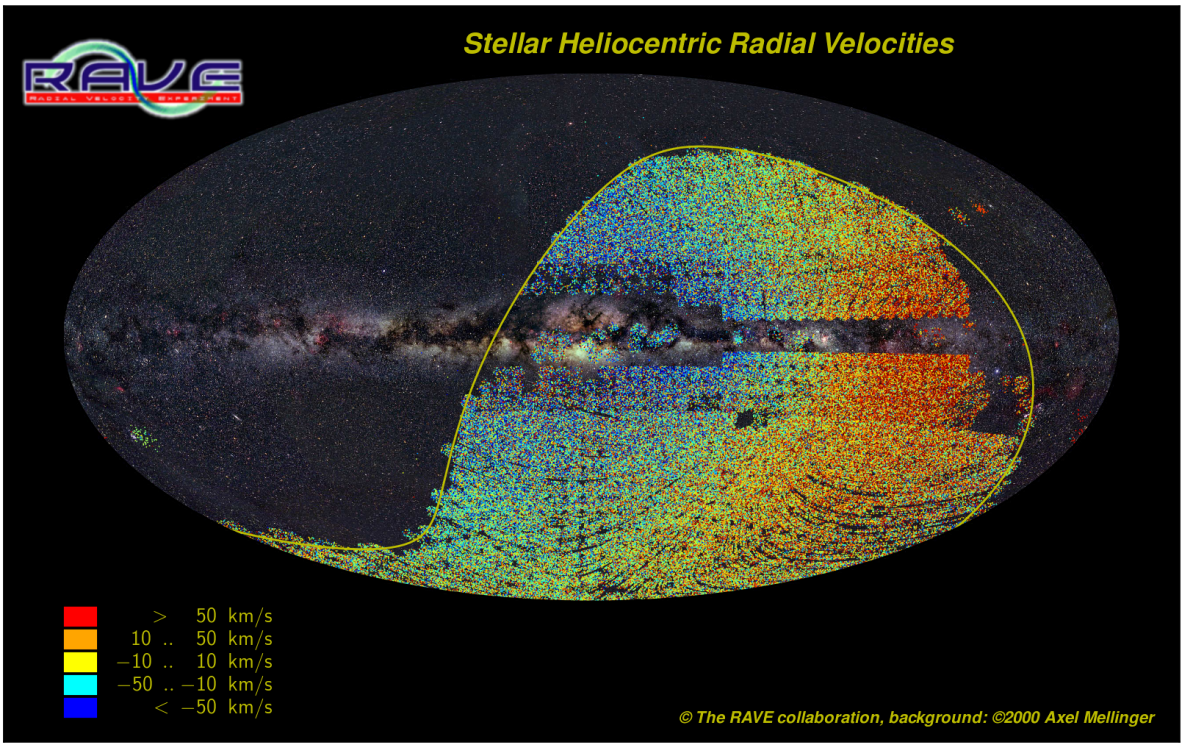

Figure 2.3: Observational footprint for the fourth data release of RAVE, as copied from the official RAVE website: http://www.rave-survey.aip.de/rave

2.2.1 BINARY STUDIES IN RAVE

Within the RAVE data base Matijevič et al. (2010, 2011) conducted studies on spectroscopic binaries. Matijevič et al. (2011) identified 1333 stars (6.6% of RAVE DR3) with significantly varying RV data, based on multiple measurements for about 8.7% of stars in the RAVE DR3, indicating those to be single-lined spectroscopic binaries (SB1). In addition, they stated that for larger numbers of repetitions (five or six measurements) the SB1 binary fraction could reach up to about 10-15% and refer to this as a lower limit for the binary fraction in RAVE. Matijevič et al. (2010) investigated the cross-correlation function of observed to template spectra (Munari et al. 2005) in DR2 and identified 123 double-lined spectroscopic binaries (SB2), indicated either by more than one peak or an asymmetric central peak in the spectrum. From simulations, Matijevič et al. (2010) concluded that RAVE could detect more than 2000 SB2 binaries, which would cover periods of about $0.8 - 2$ days, assuming a luminosity ratio of ≥ 0.3.
In their recent work, Matijevič et al. (2012) not only updated the SB2 list, but also provided quality flags on RAVE spectra, indicating peculiar features in the stellar spectra or verifying the provided stellar parameters to be reliable. These peculiar features might have been induced through binarity (SB2 binaries), problems with the spectra (in continuum, wavelength calibration, emission features), through stars being too close to the temperature limits of the pipeline (below 3500 K or above 7000 K) or stars being possible carbon stars. In some cases the spectra looked peculiar or had S/N below 20, but could not be classified into one of the above mentioned categories. These flags were included in the DR4 catalogue and stellar parameters derived from spectra with peculiar features had to be considered with care.

2.2.2 DEDICATED OPEN CLUSTER OBSERVATIONS IN RAVE

In 2004 members of the research team, that I was part of, proposed 12 observing fields to RAVE located in the Galactic plane (see Fig. 3.1). Each field contained at least 100 stars and fields with more than 150 targets were suggested to be observed repeatedly with different fibre configurations to avoid allocation problems due to crowding. In total the dedicated OC fields in RAVE covered about 1500 stars in areas around 85 known open clusters (OC areas[12]), including about 400 stars with known RVs from CRVAD-2 to ensure reliable $\overline{RV}$ determination for the observed OCs. The observation sample was compiled from stars being fainter than 9 mag in the SSS I-band with no bright object within a radius of 10" and no star brighter than I =16 mag within a radius of 8". The flux contamination of stars fainter than I =16 mag within a radius of 8" of the bright main target could be considered negligible. Hence, such objects were included in the observing sample. Up to the present, the overall number of OC areas covered by RAVE has increased by almost a factor of three with respect to the 85 proposed areas, due to additional by chance observations in OC areas.

[12]OC areas contained all stars located in regions around known OCs published by Kharchenko et al. (2005a,b), while the OCs in this work contained only actual members.

Chapter 3

Sample characteristics[1]

Section 3.1

Open cluster members

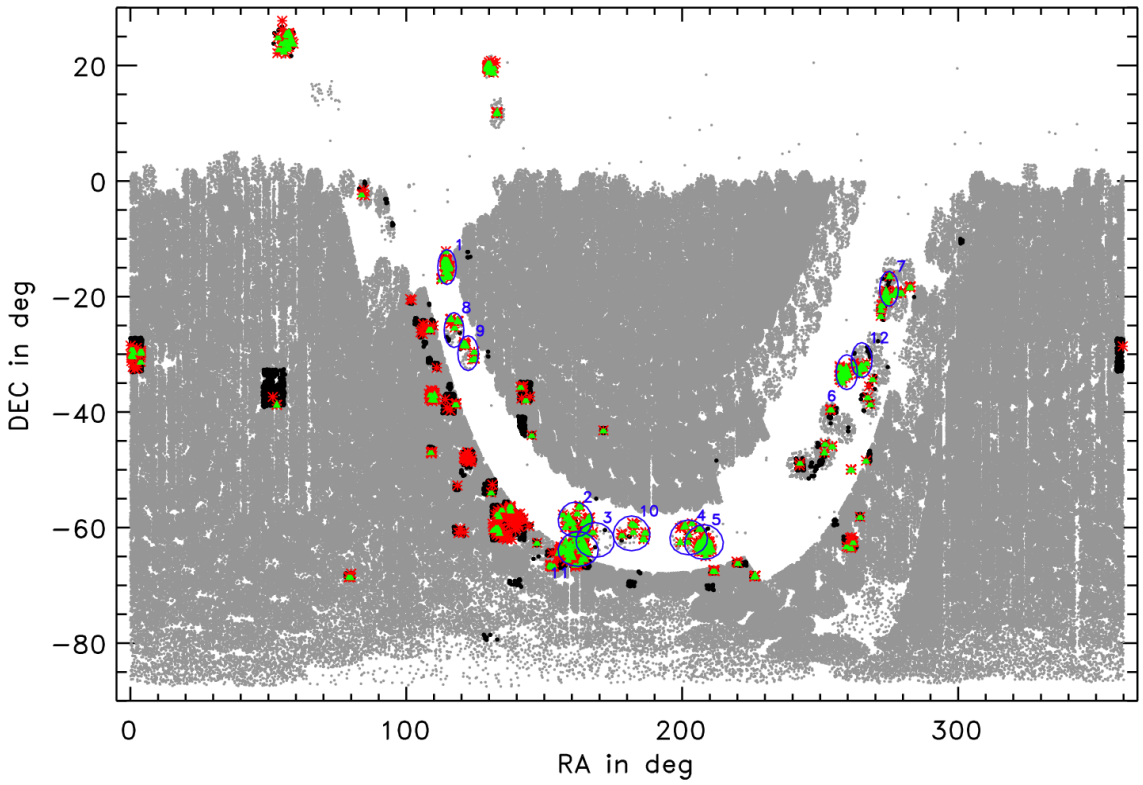

Figure 3.1: Spatial distribution of stars in OC areas covered by RAVE. Black dots represent my high-quality RV sample. The entire RAVE DR4 is underlayed in grey. The good and best RV members are overplotted as red asterisks and green triangles, respectively. The 12 dedicated OC fields are highlighted by blue circles. See the following text for details on the samples.

[1]This chapter, except for the last section, is consistent with the main part of the paper by Conrad et al. (2014) with minor changes to better include it in the read flow of this thesis. For this publication I analysed and interpreted the data obtained from the COCD and RAVE and wrote the entire text, considering discussion on details with the co-authors.

3.1.1 SAMPLE SELECTION AND DATA QUALITY

To set up my working sample, I first updated the RV information in CSOCA with values from CRVAD-2 and then cross-matched the RV-updated CSOCA with RAVE DR4 based on a coordinate comparison with a search radius of 3". The spatial distribution of all COCD objects identified in RAVE is displayed in Fig. 3.1, with the 12 dedicated OC fields highlighted. The majority of my OCs are located in or near the Galactic plane ($|b| \leq 20$ deg), usually avoided by RAVE. In addition to the 85 OC areas from the dedicated cluster observations, I found 159 more regions covered by RAVE. In total, I identified 6402 measurements of 4865 stars in 244 OC areas, all equipped with RV information in RAVE. I refer to this as my RV sample. Since $[M/H]$ determination required spectra of higher quality, my metallicity sample comprised 6209 measurements of 4785 stars in 244 OC areas. These two samples solely result from the cross-match between CSOCA and RAVE and still contain data of insufficient quality. To ensure good data quality in my working sample, I applied several constraints in RAVE quality parameters and spectral classification flags. As a final step I included OC membership probabilities in my list of requirements to clean the working sample from non-members.

QUALITY CUT IN SIGNAL-TO-NOISE

One obvious parameter to define quality constraints is the spectral signal-to-noise ratio. Throughout this work I used the listed SNR value in RAVE DR4 and show the distribution of RV uncertainties (eRV^*) with respect to the SNR in Fig. 3.2. To better identify the overall trend I computed the median in eRV^* (ϵRV) in bins along the SNR. For an SNR < 100 I chose a bin size of 4 and for an SNR ≥ 100 I changed it to 10, to include a sufficient number of data points. Typically, the overall trend is very flat and well below 5 km/s. Only for an SNR ≤ 10 a significant increase in ϵRV is present. Thus, I defined my first cut at SNR ≥ 10.

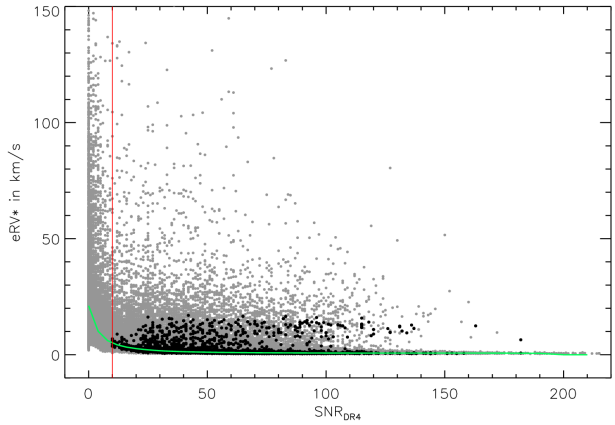

Figure 3.2: eRV^* vs. SNR distribution in RAVE DR4 (grey dots). Black dots show my high-quality RV sample. The solid green and red lines give the ϵRV trend and chosen cut at SNR ≥ 10, respectively.

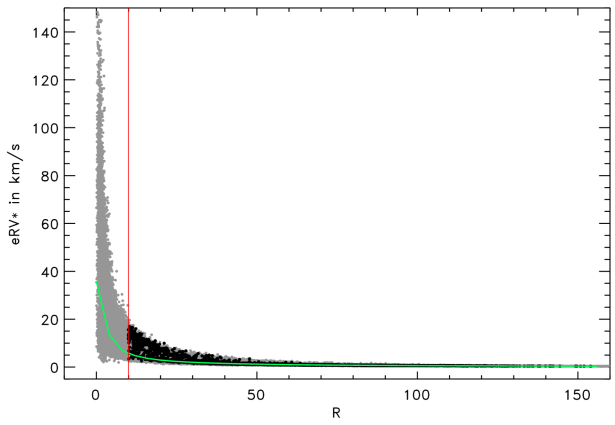

Figure 3.3: eRV^* vs. R distribution in RAVE DR4 (grey dots). Black dots show my high-quality RV sample. The solid green and red lines give the ϵRV trend and chosen cut at $R \geq 10$, respectively.

QUALITY CUT IN THE SPECTRAL CORRELATION COEFFICIENT

However, even at high SNR (≥ 50) a considerable fraction of RAVE entries show eRV^* of up to 40 km/s, making additional quality requirements necessary. Therefore, I checked the correlation coefficient (R), which characterised the goodness-of-match between the observed and the template spectrum.

The better the match, the higher is R, and the more reliable are the derived stellar parameters. The eRV^* vs. R distribution (Fig. 3.3) is much tighter and appears to be more suited to ensure well-measured RV data than the SNR. Again I computed the overall trend in DR4 as ϵRV in bins of 4 along R. At $R < 10$ the overall trend shows a significant increase, indicating poorly determined stellar parameters. My second cut at $R \geq 10$ cleaned my working sample from these unreliable targets and ensured $eRV^* \leq 20$ km/s.

QUALITY CUT IN THE RV CORRECTION PARAMETER

Moreover, RAVE provided RV corrections (*corr_RV*) based on systematic effects (for details see Steinmetz et al. 2006; Zwitter et al. 2008; Siebert et al. 2011). The effect of *corr_RV* on the data quality, especially regarding radial velocities, is shown as the eRV^* vs. *corr_RV* distribution in Fig. 3.4. Apparently, *corr_RV* can increase up to values of 50 km/s and the distribution becomes more clumpy for higher $|corr\_RV|$ values. This is seen even for stars that match the first two criteria (SNR ≥ 10 and $R \geq 10$). Thus, my third cut I defined as $|corr\_RV| \leq 9$ km/s, where the distribution is very smooth.

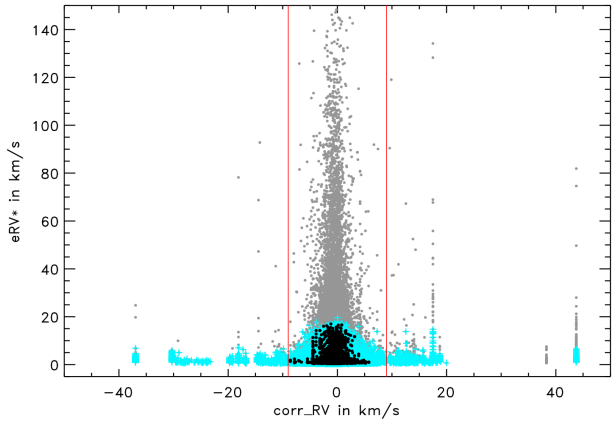

Figure 3.4: eRV^* vs. *corr_RV* distribution in RAVE DR4 (grey dots). Cyan crosses illustrate the subsample that matches SNR ≥ 10 and $R \geq 10$. Black dots show my high-quality RV sample and the red solid lines illustrate my cuts at $|corr\_RV| \leq 9$ km/s.

SPECTRAL FLAGS AND OC MEMBERSHIP

The study on the morphology of RAVE spectra by Matijevič et al. (2012) provided quality flags for the majority of RAVE spectra. The flags indicated SB2 binaries, too cool or too hot stars, problematic spectral features, and reliable spectra. If an object was flagged reliable, I considered it for my working sample. If the RAVE target was not classified at all, I only applied the quality constraints defined earlier (SNR ≥ 10, $R \geq 10$ and $|corr\_RV| \leq 9$ km/s). These four constraints defined my high quality RV sample in OC areas covered by RAVE. Since I aimed to investigate open clusters, I had to take into account the membership probabilities as well. Primarily, I used 1σ-members, and combined with the previous requirements, I refer to these as my best RV members. In certain cases I also included 2σ-members, which I call my good RV members.

Table 3.1: Numbers for the different RV samples in RAVE and in OC areas.

	RAVE DR4		OC sample			
Number of	entire RAVE	high-quality in RAVE	RV sample	high-quality RV sample	good RV members	best RV members
Measurements	483849	405944	6402	4768	764	520
Stars	426945	366922	4865	4064	664	443
Clusters	—	—	244	217	120	105

In Tab. 3.1 I summarise the samples considered in this work. Only about 1% of the RAVE DR4 stars were located in OC areas from COCD and only 37.5% of the COCD clusters were covered by RAVE. After applying all quality requirements, I can only use about 12% of the RAVE stars in OC areas to calculate $\overline{RV}$. The resulting OC sample is still larger than the sample covered by the dedicated RAVE cluster fields.

ADDITIONAL QUALITY CHECKS

To better characterise my working samples I checked the distribution of eRV^* for my different samples (Fig. 3.5). Since the size of each sample is different, I normalised each histogram by the corresponding total number of measurements to make them comparable. As expected, all histograms peak at about 1 km/s. However, eRV^* below 1 km/s are too optimistic, and thus I set all these very low eRV^* to 1 km/s when computing the $\overline{RV}$.

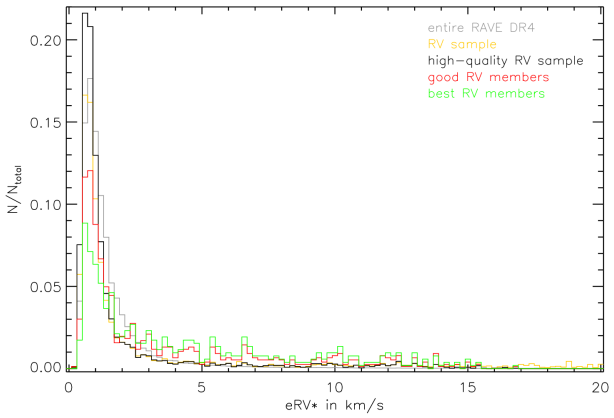

Figure 3.5: eRV^* histograms for RAVE DR4 (grey), my RV sample (yellow), high-quality RV sample (black), as well as my good (red) and best (green) RV members.

Table 3.2: Comparison of ϵRV in each observing year between my best RV members and RAVE.

	best RV members		entire RAVE	
Observing year	No. of entries	ϵRV in km/s	No. of entries	ϵRV in km/s
2003	0	—	19164	1.90
2004	109	4.51	28924	1.67
2005	104	4.20	30889	1.56
2006	9	1.64	78493	1.22
2007	18	0.88	53899	1.20
2008	18	1.13	60387	1.06
2009	15	1.11	75465	1.03
2010	181	4.47	59192	1.08
2011	20	0.87	50576	1.04
2012	46	1.66	25441	1.15
2013	0	—	1419	1.40
total	520	3.03	483849	1.18

My good and best RV members show a significant fraction of measurements with $eRV^* > 3$ km/s and therefore do not reflect the quality of the entire RAVE survey; yet I had to identify the reason for this finding. First, I checked for a possible relation between the eRV^* and RAVE observing date. In Tab. 3.2 I list the number of entries and ϵRV in each observing year for my best RV members and the entire RAVE DR4 for comparison. The majority of best RV members (394 out of 520 measurements) were observed in 2004, 2005, and 2010. The corresponding ϵRV are about a factor of 4 higher than the values of the remaining years. This is a specific feature of my OC member sample, since for the entire RAVE the ϵRV are almost equal for all observing years. Although I could now relate the less accurate RVs of my best RV members to certain RAVE observing years, I could not sufficiently explain the difference in data quality between RAVE and my good and best RV members. To check for the degree of magnitude dependence in eRV^*, I show the magnitude-separated eRV^* histograms for my high-quality RV sample in Fig. 3.6 and give the corresponding numbers of measurements and ϵRV in Tab. 3.3. For 8 – 12 mag the ϵRV are almost equal, only for the faintest magnitude interval the ϵRV value is about 0.5 km/s higher, as seen in Fig. 3.6 as well. Since the change in eRV^* is only 0.5 km/s, the magnitude dependence could be considered negligible in my working sample.

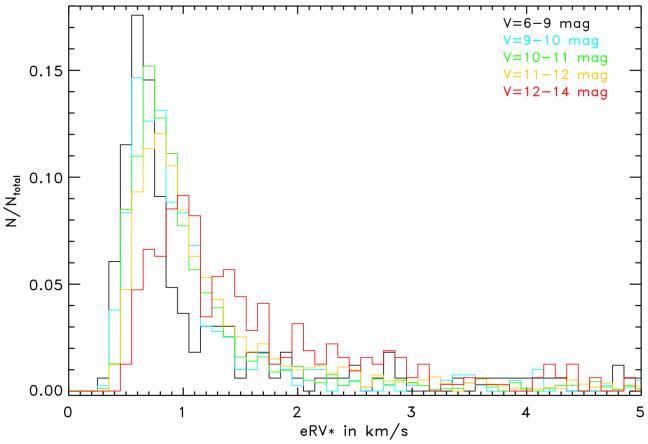

Figure 3.6: Magnitude dependent eRV^* histograms for my high-quality RV sample. The $V_{Johnson}$ intervals are 6-9 mag (black), 9-10 mag (blue), 10-11 mag (green), 11-12 mag (yellow), and 12-14 mag (red).

Open clusters are relatively young objects and are expected to be dominated by dwarfs. In my samples I separated dwarfs from giants based on $\log g$ in RAVE DR4. I considered giants to have $\log g < 3.75$ dex and dwarfs to show $\log g \geq 3.75$ dex. Objects with no $\log g$ were not included in this separation. The DR4 pipeline provided $\log g$, T_{eff} and $[M/H]$, as well as flags indicating potential problems in the convergence of the algorithm. Targets indicated to not converge or that had to be rerun were excluded from the $\log g$ separation. Thus, the number of dwarfs and giants in Tab. 3.3 does not necessarily add up to the total number of measurements in the corresponding magnitude bin.

Table 3.3: Number of entries, giant-to-dwarf ratios, and ϵRV in magnitude intervals as shown in Fig. 3.6 for my high-quality RV sample and good RV members.

$V_{Johnson}$	high-quality RV sample			good RV members		
in mag	No.	G/D[a]	ϵRV	No.	G/D[a]	ϵRV
6-9	193	110/ 78	0.95	34	10/ 23	3.79
9-10	472	261/ 186	1.01	49	18/ 29	1.83
10-11	1582	1231/ 243	0.92	136	51/ 74	1.50
11-12	2170	1505/ 477	1.03	419	224/150	1.45
12-14	350	175/ 123	1.48	126	50/ 52	2.63
total	4768	3282/1108	1.00	764	353/328	1.73

[a]G/D - giant-to-dwarf ratio.

Tab. 3.3 summarises the results for my high-quality RV sample and my good RV members. By total numbers the high-quality RV sample is dominated by giants with a giant-to-dwarf ratio of 2.96, while the good RV members contained an almost equal number of dwarfs and giants, showing a ratio of 1.08. These numbers confirmed my expectation that OCs contain a larger number of dwarfs and that RAVE preferably observed giants. Considering each magnitude interval, this becomes even more evident, because the number of good RV members that are dwarfs in $6 \leq V_{Johnson} < 11$ mag is higher than the number of giants, and for $11 \leq V_{Johnson} \leq 14$ mag the number of dwarfs and giants are almost equal for the good RV members. In all magnitude intervals the ϵRV of my good RV members are higher than the respective values in my high-quality RV sample, indicating a potential relation between stellar type and eRV^*.

To investigate this aspect in more detail, I display the eRV^* vs. $\log g$ diagram in Fig. 3.7. The pillar-like features in the $\log g$ distribution are due to the grid of synthetic spectra used to derive stellar parameters in RAVE DR4 (see Kordopatis et al. 2011, 2013). I found that higher values of $\log g$ also show higher eRV^*. Potential reasons for this dependence could be that dwarfs show fewer and weaker absorption lines, which were used to derive RV. For my good and best RV members the effect of higher eRV^* with higher $\log g$ appears to be stronger. Moreover, the location of my OCs in or near the Galactic disc might affect the quality of my working sample.

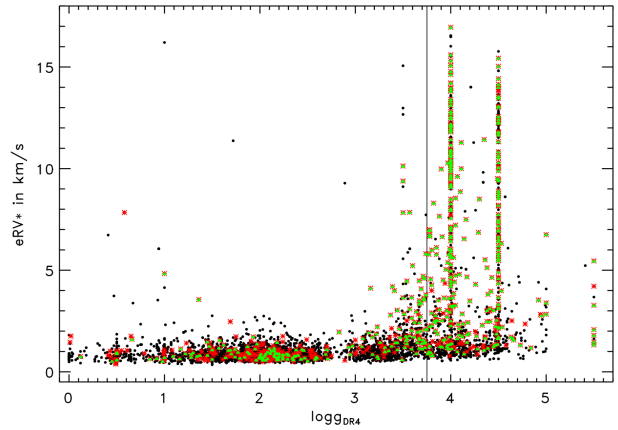

Figure 3.7: eRV^* distribution with respect to $\log g$. Symbol and colour coding is the same as in Fig. 3.1. The black solid line shows my giant-dwarf separation limit at $\log g = 3.75$.

Therefore, I present the eRV^* distribution with respect to the Galactic latitude (b) in the upper panel of Fig. 3.8. One can see that almost all good and best RV members with $eRV^* > 5$ km/s are located very close to the Galactic plane. In the lower panel I show the $\log g$ vs. b distribution and highlight all targets with $eRV^* > 5$ km/s, which appear to be predominantly dwarfs. This confirms that the higher eRV^* for my good and best RV members are mainly caused by the higher percentage of dwarfs in my OC sample. The possible effect of undetected binarity, extinction, or change in exposure time on eRV^* could not be study in detail with the data set used. Still, I could conclude that even though my OC sample in RAVE does not reflect the accuracy of the entire survey, the quality of my working sample is still sufficient for my purposes , which are determining the average radial velocities ($\overline{RV}$) for open clusters.

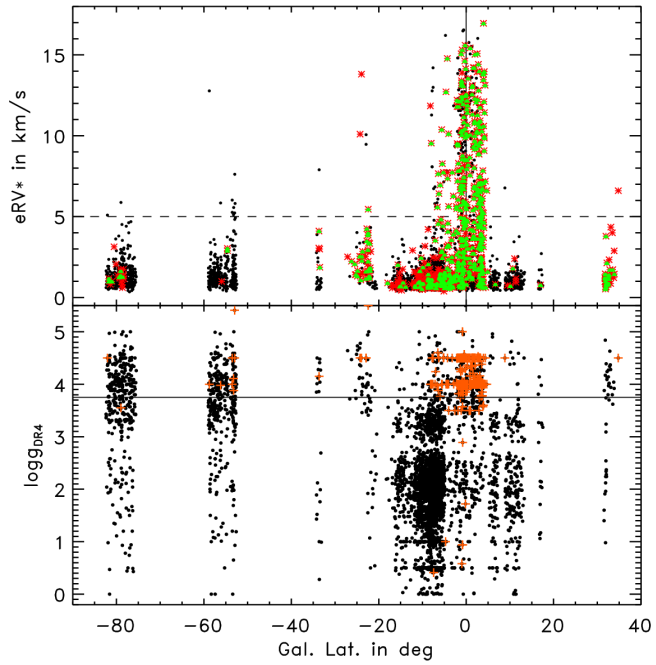

Figure 3.8: Distribution of eRV^* and $\log g$ with respect to b along with the mid-plane and $\log g$ limit (3.75) overplotted as black solid line in the upper and lower panel, respectively. The symbol colour-coding is the same as in Fig. 3.1, while dark orange crosses highlight targets with $eRV^* > 5$ km/s. This eRV^* limit is displayed as the black dashed line.

3.1.2 RADIAL VELOCITIES

To better evaluate the RVs collected from RAVE, I obtained reference values from CRVAD-2 and created a common sample for comparison via a cross-match based on coordinates with a matching radius of 3". The numbers and ϵRV for the two catalogues and the common sample are given in Tab. 3.4.

Table 3.4: Comparison of numbers and RV uncertainties between RAVE, CRVAD-2, and the resulting common sample. The ϵRV values are the median of the RV uncertainties and $\sigma\Delta RV$ correspond to the standard deviation of the difference distribution.

	Catalogues		OC sample			
	entire	high-quality	RV sample	high-quality RV sample	good RV members	best RV members
— RAVE —						
No. of entries	483849	405944	6402	4768	764	520
No. of clusters	—	—	244	217	120	105
ϵRV in km/s	1.18	1.11	1.23	1.00	1.73	3.03
— CRVAD-2 —						
No. of entries	54907	—	6782	—	1586	1092
No. of clusters	650	—	595	—	318	306
ϵRV in km/s	0.86	—	3.60	—	3.70	3.70
— common sample —						
No. of entries	2475	1774	531	262	51	32
No. of clusters	—	—	104	73	13	9
ϵRV_{RAVE} in km/s	1.23	1.02	6.06	1.45	2.04	2.28
$\epsilon RV_{CRVAD-2}$ in km/s	0.60	0.50	2.90	1.80	1.70	1.70
$\sigma\Delta RV$ in km/s	90.66	22.65	81.21	38.20	22.75	21.02

The increase of ϵRV after including membership probabilities, as stated above, is a RAVE-specific characteristic, since it is only present in the RAVE data, but not in CRVAD-2. For the good and best OC members with RV, on the other hand, the ϵRV are similar in the two catalogues. Interestingly, the common sample is very small (2500 listings) compared to the size of the two catalogues (RAVE: $\sim$ 460000 entries and CRVAD-2: $\sim$ 55000 stars) and only a very small fraction of objects in each catalogue is located within OC regions (about 1.3% in RAVE and about 12.3% in CRVAD-2). One reason for the small overlap between CRVAD-2 and RAVE is that each catalogue has different observing samples. RAVE is a southern-sky survey, while CRVAD-2 was an all-sky project. Another reason could be the slightly different magnitude range covered by the catalogues, as seen in Fig. 3.9.

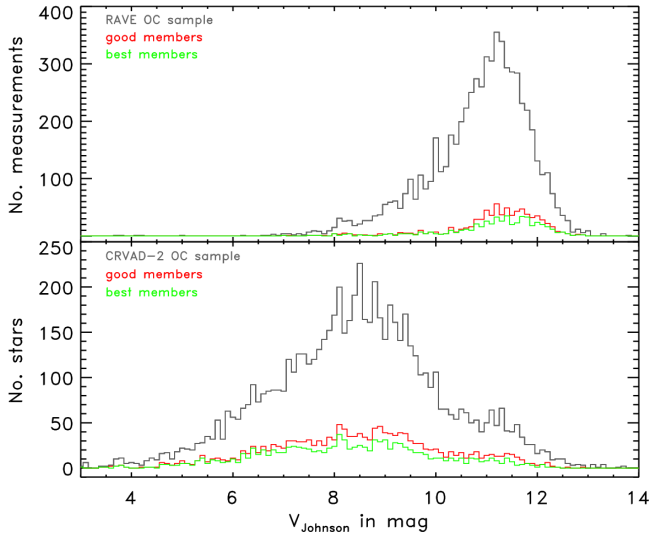

Figure 3.9: Histograms in $V_{Johnson}$ for RAVE (upper panel) and CRVAD-2 (lower panel) for objects in OC areas (grey), as well as my good (red) and best (green) RV members.

RAVE peaks at a magnitude of about 11.2 mag and CRVAD-2 at about 8.5 mag. Concluding from this, RAVE and CRVAD-2 covered different magnitude ranges shifted by almost 3 mag, as can be seen in Fig. 3.9 This also shows that RAVE covered fainter OC members than the CRVAD-2. Within OC areas the fraction of good and best members are comparably large. In RAVE 12.3% of objects in OC areas are good members and in CRVAD-2 the corresponding percentage is 23.4%. This indicated that the majority of objects in OC regions, included in each catalogue, were at least good members.
For the high-quality common sample I display the RV comparison between RAVE and CRVAD-2 in Fig. 3.10, along with the corresponding difference distribution. The RV differences were computed as $\Delta RV = RV_{CRVAD-2} - RV_{RAVE}$. Near $RV_{RAVE} = 0$ km/s I found several stars with intrinsically higher $RV_{CRVAD-2}$ than RV_{RAVE}. For my good and best RV members this feature entirely disappears. In the difference distribution a slight negative slope is visible in the high-quality sample. My good and best RV members do not show this slope distinctly, since only two stars show significant differences, which could be by chance. The remaining good and best members, except for the two deviating ones, show a spread in the difference distribution of 20 km/s. Hence, my selected good and best RV members agree well with the reference values and show a sufficiently good quality to derive $\overline{RV}$ for OCs in RAVE.

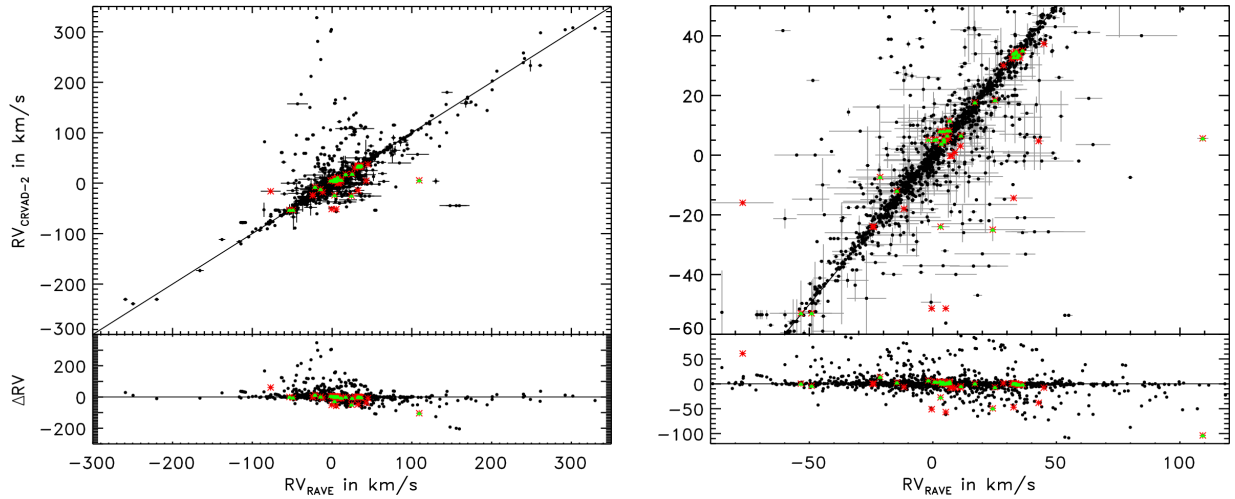

Figure 3.10: Upper panels: RV comparison between RAVE and CRVAD-2 for the high-quality common sample (black dots). Lower panels: Corresponding difference distribution. The black solid lines show the one-to-one relation and zero-difference line in the upper and lower panels, respectively. Red asterisks and green triangles highlight good and best RV members in the common sample, respectively. The right panels show the same diagrams enlarged to the RV range of my good and best RV members.

Still, I had to understand the identified systematics of my high-quality sample (see Fig. 3.10). Accordingly, I investigated the major CRVAD-2 source catalogues, namely Nordström et al. (2004), Gontcharov (2006), and Barbier-Brossat & Figon (2000). The results are presented visually in Fig. 3.11 and in numbers in Tab. 3.5. The vast majority of CRVAD-2 values were obtained from Barbier-Brossat & Figon (2000) and Nordström et al. (2004). The displayed difference distributions in Fig. 3.11 are relatively broad and might include several outliers. Therefore, I applied a 3σ-clipping algorithm to identify the actual distribution characteristics and also included the results for the clipped distributions in Tab. 3.5 and Fig. 3.11. In the difference distributions (clipped and unclipped) for the reference values from the source catalogues by Nordström et al. (2004) and Gontcharov (2006) the standard deviations in the high-quality sample are considerably lower than for the comparison with values from Barbier-Brossat & Figon (2000). Thus, the reference values from the first two catalogues seem to be more reliable.

Table 3.5: Numbers for the RV difference distributions comparing RAVE with the CRVAD-2 source catalogues for the high-quality sample, as well as my good and best RV members in the common sample.

	No.	ϵRV	$\overline{\Delta RV}$	$\sigma\Delta RV$
high-quality sample	before 3σ-clipping			
Nordström	825	0.40	-0.69	8.10
Gontcharov	93	0.60	-1.86	12.71
Barbier-Brossat	852	1.70	6.54	42.54
	after 3σ-clipping			
Nordström	743	0.30	-0.36	1.78
Gontcharov	89	0.60	-0.18	3.82
Barbier-Brossat	728	1.70	-0.57	11.27
good RV members	before 3σ-clipping			
Nordström	–	—	—	—
Gontcharov	5	0.40	-20.50	46.50
Barbier-Brossat	46	2.00	-4.77	18.93
	after 3σ-clipping			
Nordström	–	—	—	—
Gontcharov	4	1.30	0.29	0.90
Barbier-Brossat	38	1.80	-0.66	4.04
best RV members	before 3σ-clipping			
Nordström	–	—	—	—
Gontcharov	3	0.40	-34.42	59.96
Barbier-Brossat	29	1.80	-1.44	11.27
	after 3σ-clipping			
Nordström	–	—	—	—
Gontcharov	2	1.50	0.20	0.30
Barbier-Brossat	26	1.70	0.79	3.12

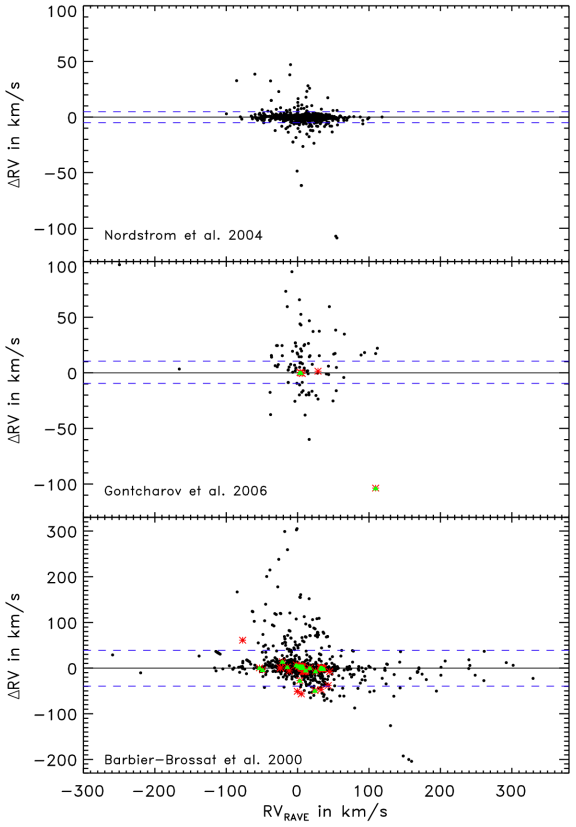

Figure 3.11: Radial velocity difference distributions comparing RAVE with the source catalogues for CRVAD-2 (Nordström et al. (2004), Gontcharov (2006), Barbier-Brossat & Figon (2000)). the colour-coding for the symbols is the same as in Fig. 3.10. The blue dashed lines show the limits for the applied 3σ-clipping.

Moreover, the systematic effect near $RV_{RAVE} = 0$ km/s is visible in all source catalogues, whereas the possible negative slope only appears in the comparison of my high-quality sample with values from Barbier-Brossat & Figon (2000). Thus, I concluded that the trend is not a feature induced by the RAVE data, but by the reference values from Barbier-Brossat & Figon (2000). Surprisingly, I found no good and best members in common with Nordström et al. (2004). Moreover, the number of common good and best RV members with Gontcharov (2006) is negligible, which in turn makes the questionable values by Barbier-Brossat & Figon (2000) the dominant source for RV references. Nevertheless, their values are the best RV references for OCs available, and since my good and best RV members in RAVE show a better agreement with these references than the high-quality data, it indicated that my cuts are suitable for deriving reliable $\overline{RV}$ for my OC sample.

3.1.3 METALLICITIES

I also aimed to provide mean metallicities ($\overline{[M/H]}$) for the clusters in RAVE. For the metallicity determination typically spectra of higher quality are needed and besides that different template spectra were used than for deriving RVs. In DR4 Kordopatis et al. (2013) applied several prior constraints, namely SNR ≥ 20, $v_{rot} < 100$ km/s, $eRV^* < 8$ km/s, $logg > 0.5$ and $T_{eff} > 3800$ K.

This resulted in a slightly smaller sample; 6209 out of the 6402 RAVE observations in OC regions were equipped with $[M/H]$ and I had to slightly adapt my quality constraints to conduct a reliable metallicity study. In addition, the DR4 pipeline provided quality flags for the convergence of the stellar parameter algorithm used to derive $\log g$, T_{eff}, and $[M/H]$. Since the RV values were derived by a different algorithm, I did not include them in my RV sample but had to do so now for my metallicity sample. Objects with no converging algorithm, or those which had to be rerun by the pipeline, were excluded from my metallicity study on open clusters.

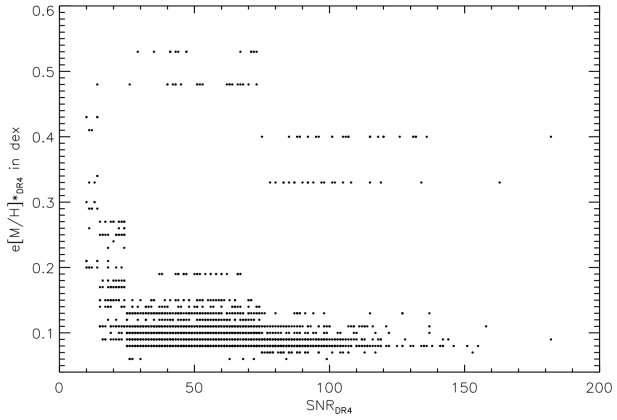

Figure 3.12: Distribution of $e[M/H]^*$ from RAVE DR4 with respect to SNR for my high-quality RV sample.

As noted by Kordopatis et al. (2013), the internal metallicity uncertainties ($e[M/H]^*$) in RAVE DR4 were derived from different sets of synthetic spectra, leading to a discrete distribution (see Fig. 3.12). These $e[M/H]^*$ might reflect model errors instead of realistic measurement uncertainties. Therefore, I preferred to evaluate the actual $[M/H]$ values and not the uncertainties to define the adapted cuts for my metallicity study in open clusters. In Fig. 3.13 I display the $[M/H]$ distribution with respect to SNR. To illustrate the overall trend in RAVE DR4, I calculated $\overline{[M/H]}$ in bins of 4 along SNR and changed the bin size to 10 for SNR $\geq$ 100, to gain enough data points in each bin. This overall trend is quite flat and shows no specific correlation, not even for low SNR. Therefore, I simply adapted the same cut as the RAVE DR4 pipeline at SNR $\geq$ 20.

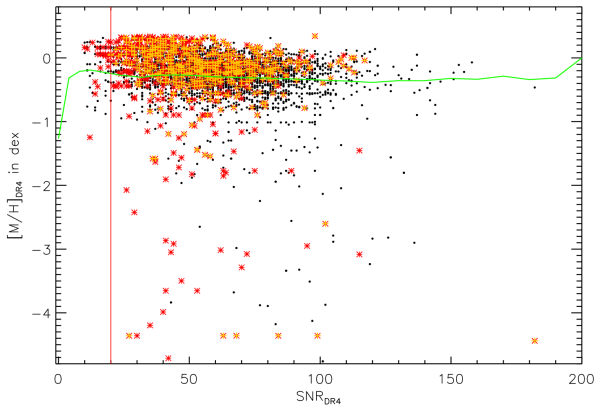

Figure 3.13: $[M/H]$ distribution with respect to SNR for my high-quality RV sample (black dots). Red asterisks and orange crosses illustrate my good RV and $[M/H]$ members, respectively. The red and green solid lines visualise my adapted cut at SNR $\geq$ 20 and the overall trend for the entire RAVE DR4, respectively.

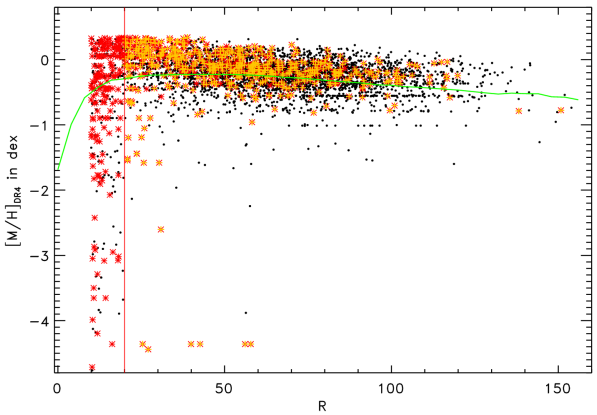

Figure 3.14: $[M/H]$ distribution with respect to R for my high-quality RV sample (black dots). Red asterisks and orange crosses illustrate my good RV and $[M/H]$ members, respectively. The red and green solid lines visualise my adapted cut at $R \geq 20$ and the overall trend for the entire RAVE DR4, respectively.

Moreover, I examined the $[M/H]$ distribution with respect to R (Fig. 3.14) and computed the overall trend in RAVE DR4 as $\overline{[M/H]}$ in bins of 4 along R. This overall trend indicates a slight correlation of $[M/H]$ with R, suggesting that the fewer lines in metal-poor stars lead to a better match of the observed to the template spectrum, at least for stars with $[M/H] \geq -1$ dex. Because of this slope I cannot use the overall trend to evaluate the cut refinement in R. However, for $R \leq 20$ a non-negligible number of good RV members show unexpectedly low $[M/H]$, and I chose the corresponding cut to $R \geq 20$ for my metallicity study in Galactic open clusters.
I was unable to identify any dependencies of $[M/H]$ on corr_RV and saw no need for additional changes of the constraints for my high-quality $[M/H]$ sample. Combined with the membership probabilities (P_{kin} and $P_{phot} \geq 14\%$ or P_{kin} and $P_{phot} \geq 61\%$), the new cuts define my good and best $[M/H]$ members, respectively. In Tab. 3.6 I summarise the corresponding numbers of measurements, stars, and clusters for my metallicity samples.

Table 3.6: Numbers for the different $[M/H]$ samples in RAVE and in OC areas.

	RAVE DR4		OC sample			
Number of	entire RAVE	high-quality in RAVE	$[M/H]$ sample	high-quality $[M/H]$ sample	good $[M/H]$ members	best $[M/H]$ members
Measurements	451474	354906	6209	3947	517	308
Stars	405176	322843	4785	3485	455	265
Clusters	—	—	244	192	94	77

Furthermore, I investigated a potential magnitude dependence of $[M/H]$, which might affect the reliability of my data (see Fig. 3.15). The few members at $[M/H] = -4.36$ dex show obviously unrealistic values and were therefore not considered any further in my metallicity study of OCs. To identify a possible dependence more clearly, I computed the unweighted $\overline{[M/H]}$ and $\sigma[M/H]$ for my high-quality $[M/H]$ sample in bins of 0.5 mag along the $V_{Johnson}$ magnitudes.

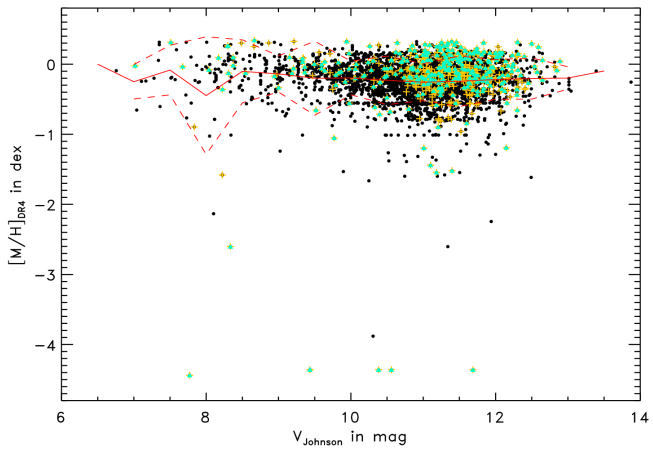

Figure 3.15: $[M/H]$ distribution with respect to the $V_{Johnson}$ magnitude for my high-quality $[M/H]$ sample (black dots). Orange crosses and turquoise triangles illustrate good and best $[M/H]$ members, respectively. Red solid and dashed lines visualise $\overline{[M/H]}$ and $\sigma[M/H]$ for my high-quality $[M/H]$ sample, respectively.

Both show a very flat behaviour and the variations at brighter magnitudes are most likely due to small number statistics and are not representative for the overall trend. Hence, I was unable to identify any considerable magnitude dependence of metallicities in RAVE, confirming my sample to provide reliable results. Since the CSOCA did not provide any metallicity data, no reference values for individual cluster members were available. For cluster mean metallicities, on the other hand, I found reference values in DAML, which I discuss in more detail in Sect. 3.2.3.

Section 3.2

Open cluster mean values

3.2.1 Radial velocities

First of all, I cleaned each OC from outliers by applying a 3σ-clipping algorithm to obtain the most representative $\overline{RV}$. Then I determined $\overline{RV}$ for in total 110 OCs and summarise the results in Tab. A.1 along with the identifiers COCD number (Seq) and cluster name. In addition, I provided two kinds of reference values. On the one hand, I computed $\overline{RV}$ from the CRVAD-2, and on the other hand I listed values from CRVOCA (Kharchenko et al. 2007). I preferred to use their computed $\overline{RV}$ and only where no calculated $\overline{RV}$ was available I gave the literature value. For 37 OCs I provided $\overline{RV}$ for the first time. The $\overline{RV}$ from RAVE and CRVAD-2 were primarily derived from best RV or 1σ-members, respectively. Only where just one or no most probable member was available I included good RV or 2σ-members as well to compute the $\overline{RV}$ in RAVE and CRVAD-2, respectively. The corresponding numbers are also included in Tab. A.1. CRVOCA included $\overline{RV}$ based on 3σ-members, while the $\overline{RV}$ references computed in this work considered at worst 2σ-members to reduce the field star contamination. A comparison between the reference catalogues yielded a very good agreement, as expected, indicating that in CRVOCA the field star contamination can be considered to be relatively low and the values as suitable references.
The provided $\overline{RV}$ in RAVE and CRVAD-2 were calculated as weighted mean considering individual eRV^* and membership probabilities P_{kin} and P_{phot} as weights (Eq. 3.1). As mentioned above, I considered all $eRV^* < 1$ km/s to be too optimistic and replaced them with 1 km/s, which is also reflected in Tab. A.1. I also give typical RV uncertainties in OCs ($\overline{eRV^*}$),computed as weighted mean from the individual eRV^* of the members (Eq. 3.4), including only OC membership probabilities as weights. The weighted standard deviation[2] ($\sigma\overline{RV}$; Eq. 3.2) and uncertainty of $\overline{RV}$ (e$\overline{RV}$; Eq. 3.3) could only be computed for OCs with at least two individual measurements. For clusters with only one representative RV value I did not provide $\sigma\overline{RV}$ and assumed $\overline{eRV^*} = eRV^*$.

$$\overline{RV} = \frac{\sum\limits_i RV_i \cdot g_i}{\sum\limits_i g_i} \tag{3.1}$$

$$\sigma\overline{RV} = \sqrt{\frac{n}{n-1} \cdot \frac{\sum\limits_i g_i \cdot (RV_i - \overline{RV})^2}{\sum\limits_i g_i}} \tag{3.2}$$

$$\mathrm{e}\overline{RV} = \frac{\sigma\overline{RV}}{\sqrt{n}} \tag{3.3}$$

$$\overline{eRV^*} = \frac{\sum\limits_i eRV_i^* \cdot (P_{kin,i} \cdot P_{phot,i})}{\sum\limits_i (P_{kin,i} \cdot P_{phot,i})}, \tag{3.4}$$

with the weights defined as

$$g_i = \frac{P_{kin,i} \cdot P_{phot,i}}{(eRV_i^*)^2}. \tag{3.5}$$

[2]The "n" in the nominator of "$n/(n-1)$" is a scaling factor, since the individual weights ($g_i = (P_{kin,i} \cdot P_{phot,i})/(eRV_i^*)^2$) never sum up to n, with $eRV^* \geq 1$ km/s and $(P_{kin}, P_{phot}) \leq 1$.

In Fig.3.16 I show the histograms for the total number of measurements and stars used to obtain the RAVE based and reference $\overline{RV}$, respectively. I only included OCs observed in RAVE. The vast majority of $\overline{RV}$ in all catalogues were based on fewer than six individual RV measurements and only a few OCs show $\overline{RV}$ derived from more than 20 individual RV measurements in either data set. CRVOCA shows the largest number of OCs with more than 20 individual RV values, since they used stars with lower membership probability than I did. Considering the different numbers of OCs covered by the catalogues, the distributions for the number of individual measurements show a very similar shape. This indicated that the resulting $\overline{RV}$ are of similar quality.

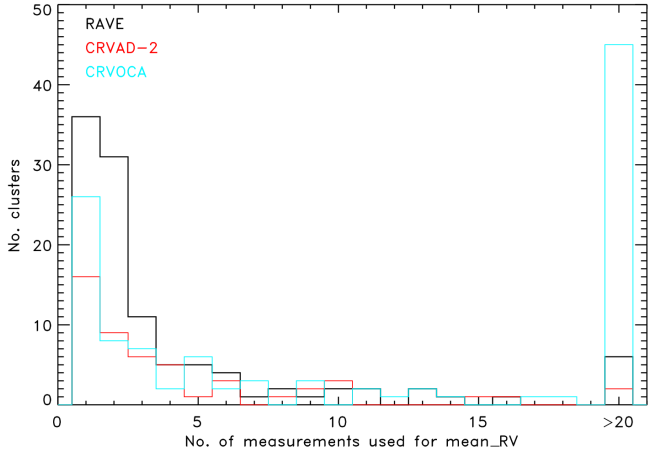

Figure 3.16: Histogram for the number of measurements or stars used to derive $\overline{RV}$ in RAVE (black) and CRVAD-2 (red), respectively. The cyan histogram shows the number of stars used for $\overline{RV}$ as given in the CRVOCA.

Fig. 3.17 illustrates a visual comparison between my RAVE results and the available references. The error bars represent the e$\overline{RV}$ in each catalogue. The RV difference ($\Delta\overline{RV}$) was defined as $\Delta\overline{RV} = \overline{RV_{Ref}} - \overline{RV_{RAVE}}$, where $\overline{RV_{Ref}}$ are the reference values obtained from CRVAD-2 or CRVOCA for the corresponding panel. The differences between RAVE results and reference values for my OCs (Fig. 3.17) appear to be larger than for the individual stars (Fig. 3.10).

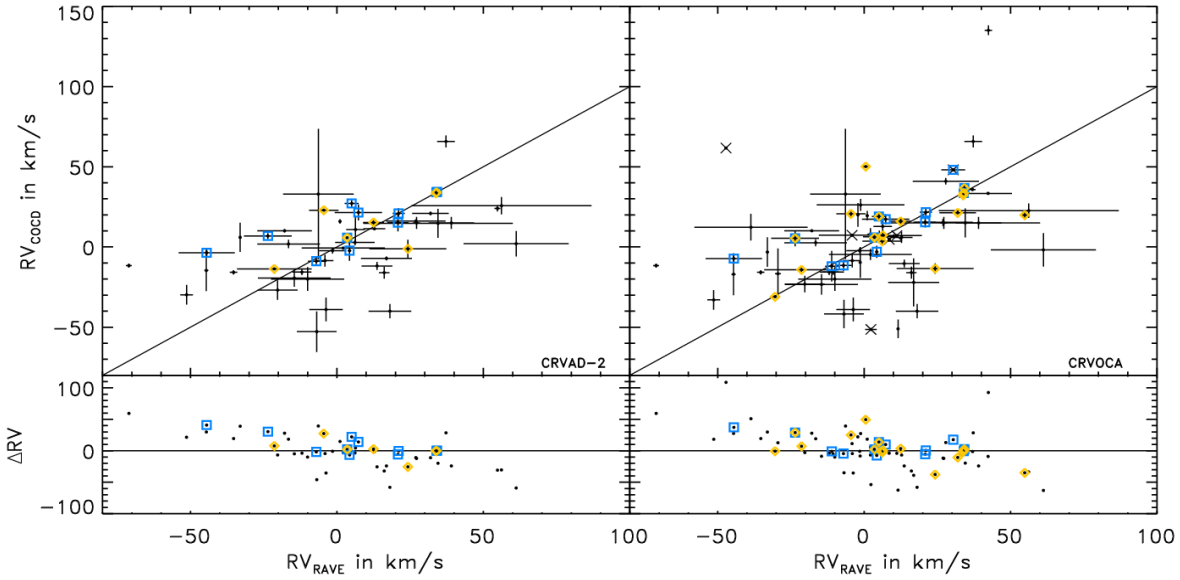

Figure 3.17: Upper panels: $\overline{RV}$ comparison between RAVE and reference values from CRVAD-2 (left) and CRVOCA (right). The black lines show the one-to-one relations. Lower panels: Corresponding difference distributions with the zero-difference lines included as black solid lines. Blue squares and yellow diamonds illustrate clusters with $\geq$ 10 individual RVs in RAVE and the reference catalogue, respectively. Black crosses indicate missing e$\overline{RV}$ information in CRVOCA.

One can see a negative slope in the difference distribution, which is mainly caused by two OCs with very large differences and cannot be verified to be statistically significant. Contributing factors to the apparently larger RV differences are the different OC members targeted by either survey and the potential systematics induced by the reference values from Barbier-Brossat & Figon (2000). In general, cluster $\overline{RVs}$ derived from only up to five individual measurements have to be considered with caution in all data sets used in the presented project (RAVE, CRVAD-2, and CRVOCA).
OCs with more than ten individual measurements in RAVE, on the other hand, show a very good agreement, except for three. The three exceptions (Platais 8, Sco OB4, and Sgr OB7; left panel of Fig. 3.17) are all stellar associations, which naturally show an intrinsically higher velocity dispersion, because they are not as tightly bound as open clusters. Since the membership selection is partly based on kinematics, it might be possible that for the stellar associations mistaken membership can contribute to the larger differences, in particular because different objects were targeted by RAVE and CRVAD-2.
CRVAD-2 references with more than ten individual RV measurements also show a good agreement, except for two actual open clusters: NGC 2516 and Collinder 228. In CRVOCA even better measured OCs show relatively large differences to the RAVE results. Thus, the field star contamination in CRVOCA is not negligible, though I stated it to be relatively low. Thus it could be concluded that RAVE apparently provided more reliable $\overline{RV}$ than CRVAD-2.

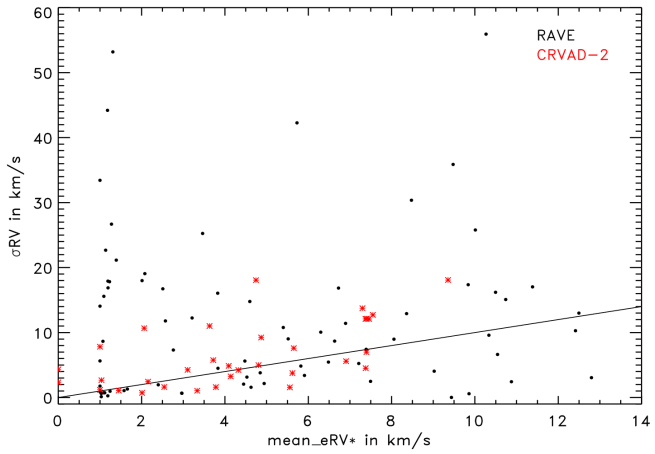

Figure 3.18: Comparison between the $\sigma\overline{RV}$ and $\overline{eRV^*}$ values in CRVAD-2 (red asterisks) and RAVE (black dots) for open clusters observed by RAVE. The black solid line represents the one-to-one relation.

In addition, I compared $\sigma\overline{RV}$ and $\overline{eRV^*}$ in RAVE and CRVAD-2 (Fig. 3.18). In both catalogues only very few OCs show $\sigma\overline{RV}$ similar to $\overline{eRV^*}$, the majority show higher $\sigma\overline{RV}$, and in certain cases they are about a factor of 5-10 higher than $\overline{eRV^*}$. There are several possible reasons, namely small number statistics, partly mistaken membership, or undetected binarity. Due to the first aspect, the $\sigma\overline{RV}$ have to be considered with care and cannot be regarded in any way representative for the internal cluster velocity dispersion. The aspect of binarity in my OCs is discussed in Sect. 3.2.2. Partly mistaken membership might be minimised when updated membership probabilities from the recently provided catalogue for the Milky Way Star Cluster (MWSC) survey (Kharchenko et al. 2013) are included.
Moreover, it would be a great improvement to also include RVs as criteria for OC membership, but this is only reasonable when RV data are available for all stars in OC areas. The CRVAD-2 $\sigma\overline{RV}$ are well below 20 km/s, whereas the RAVE values reach up to 60 km/s. Most likely, this is due to the different targets included to compute $\overline{RV}$ for the two catalogues (see Sect. 3.1.2).

3.2.2 BINARITY FRACTION

Above I pointed out that undetected binaries might have a significant influence on the accuracy of my $\overline{RV}$ results. For a detailed study multiple epochs for each member would be needed. I examined my best RV members in RAVE for multiple epochs and only identified 76 out of 443 stars, where each object is only provided with two measurements. This was by far not enough for a deep binary study based on RAVE data. Hence, I had to work with limited sources of information to give an approximate idea on the binary fraction in my sample.
In a first step I checked the duplicity flags in CSOCA and found 14 stars indicated as potential or confirmed binaries among my 443 best RV members. Secondly, I cross-matched my best RV members with the list of SB1 (Matijevič et al. 2011) and SB2 (Matijevič et al. 2010) binaries in RAVE and found no common object. This was not surprising, since I rejected objects with bad spectral flags from Matijevič et al. (2012). If I only considered the cuts SNR $\geq$ 10, $R \geq 10$, and $|corr\_RV| \leq 9$ km/s in RAVE along with P_{kin} and $P_{phot} \geq 61\%$, I found 11 SB2 binaries in 4 OCs. However, all these numbers were far below the 6% binary fraction suggested by Matijevič et al. (2011).
To provide a rough estimate on the binary fraction based on RAVE data I used a simple approach, namely that the large scatter in Fig. 3.17 and the high $\sigma\overline{RV}$ were mainly caused by undetected binarity. For each cluster I first computed the difference between individual RVs and $\overline{RV}$. Then I compared these differences with $3\overline{eRV^*}$, defining my assumed velocity dispersion. This analysis could only be done for OCs with at least two individual measurements, which reduced the number of clusters considered to 76. I assumed members exceeding the $3\overline{eRV^*}$ limit to be potential binaries and calculated the binary fraction with respect to the total number of RAVE measurements in the corresponding OC. The results are summarised in Tab. 3.7.

Table 3.7: Results for my rough binary fraction estimate in OCs with at least two RV measurements in RAVE.

binary fraction	0%	≤25%	25-50%	≥50%	total
No. of OCs	41	9	7	17	74
Proportion (%)	55.4	12.2	9.5	23.0	—

About half of my OCs with at least two RV measurements show no binarity and another 23% show a very high estimated binary fraction (≥50%). This effect is most likely due to small number statistics, where the binary fraction can change fast from 0% to more than 50% if just one more star is outside the defined $3\overline{eRV^*}$ limit. Therefore, the listed numbers can at most be considered as lower limits. In Tab. A.1 about 45.9% of OCs with at least two RV measurements show $\sigma\overline{RV} \geq 10$ km/s, which is similar to the 44.7% of OCs with non-zero binary fraction. This verified that undetected binaries were a dominant effect, inducing unexpectedly high $\sigma\overline{RV}$ for my OCs.

3.2.3 METALLICITIES

Because of the more stringent requirements for my $[M/H]$ sample, I was able to determine $\overline{[M/H]}$ for only 81 of my 110 OCs with $\overline{RV}$ in RAVE. Because I strictly distinguished between iron abundances and overall metallicities in DAML (see Sect. 2.1.1), I obtained reference $\overline{[M/H]}$ for only 12 OCs. Hence, for 69 clusters I presented $\overline{[M/H]}$ for the first time. The results are summarised in Tab. A.2 along with the cluster identifiers (COCD number and cluster name). My metallicity results were primarily obtained from best $[M/H]$ member measurements after cleaning each OC from outliers by applying a 3σ-clipping algorithm. Only where no or just one best $[M/H]$ member measurement was available I included good $[M/H]$ member measurements as well. The number of best and additional good $[M/H]$ member measurements are also included in Tab. A.2.

I computed the $\overline{[M/H]}$ as weighted mean, considering only the membership probabilities as weights (Eq. 3.6), since the listed $e[M/H]^*$ showed a very discrete distribution and might not reflect realistic measurement errors (see Sect. 3.1.3). For OCs with at least two individual $[M/H]$ measurements I computed weighted standard deviations[3] ($\sigma\overline{[M/H]}$; Eq. 3.7) and uncertainties of $\overline{[M/H]}$ (e$\overline{[M/H]}$; Eq. 3.8).

$$\overline{[M/H]} = \frac{\sum_i [M/H]_i \cdot w_i}{\sum_i w_i} \tag{3.6}$$

$$\sigma\overline{[M/H]} = \sqrt{\frac{n}{n-1} \cdot \frac{\sum_i w_i \cdot ([M/H]_i - \overline{[M/H]})^2}{\sum_i w_i}} \tag{3.7}$$

$$\mathrm{e}\overline{[M/H]} = \frac{\sigma\overline{[M/H]}}{\sqrt{n}}, \tag{3.8}$$

$$\text{with the weights defined as} \quad w_i = P_{kin,i} \cdot P_{phot,i}. \tag{3.9}$$

In Fig. 3.19 I display the histograms for the number of measurements and stars used to obtain $\overline{[M/H]}$ in RAVE and DAML, respectively. Again I only included OCs with $[M/H]$ data available in RAVE. As expected, the vast majority of OCs are covered by fewer than six individual $[M/H]$ measurements and small number statistics might affect my results. The number of references is too small to draw any conclusion on the shape of the number distribution.
From Fig. 3.20 one can see that the majority of OCs in RAVE, except for four, agree very well with the values from DAML within the uncertainties. I defined the differences between the catalogues as $\Delta\overline{[M/H]} = \overline{[M/H]_{DAML}} - \overline{[M/H]_{RAVE}}$ and they appeared to be similar to the uncertainties. Only the Pleiades (Melotte 22) were covered by more than ten individual measurements in RAVE and agree very well. In addition to the Pleiades, DAML listed two more clusters with $\overline{[M/H]}$ based on more than ten values, namely NGC 2422 and NGC 2354.

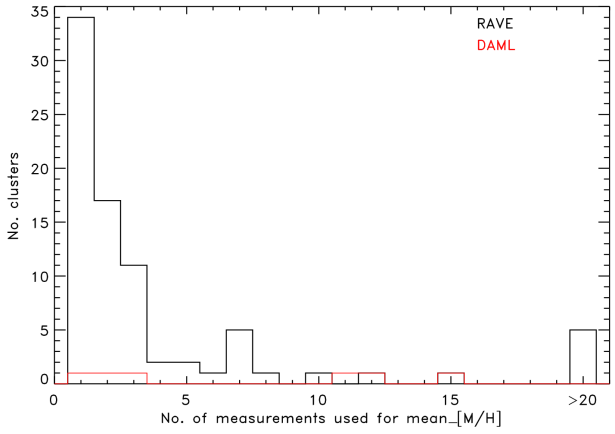

Figure 3.19: Number histogram of individual measurements or stars used to obtain $\overline{[M/H]}$ in RAVE (black) and DAML (red), respectively.

My metallicity study in RAVE could only give a rough idea on the $[M/H]$ behaviour of the Galactic OC system. The typical uncertainties of $\overline{[M/H]}$ for individual members, obtained from the pipeline, were about 0.1 dex and reflected only internal errors. When including external errors as well, the typical errors increased to values of about 0.3 dex (Boeche et al. 2011). The RAVE $[M/H]$ accuracy was apparently not high enough to carry out a detailed metallicity study within OCs.

[3]The "n" in the nominator of "$n/(n-1)$" is a scaling factor, since the individual weights ($w_i = P_{kin,i} \cdot P_{phot,i}$) never sum up to n, with $(P_{kin}, P_{phot}) \leq 1$.

A brief look at the difference distribution might suggest a negative slope with increasing metallicities. This apparent slope is primarily caused by four clusters, which are metal poor in RAVE. If I eliminate them, the distribution is consistent with not showing any trend and is centred around zero. In Tab. A.2 I found ten clusters and associations with $\overline{[M/H]}$ below −0.5 dex. This contradicts my expectation that open clusters and associations in the solar neighbourhood have about solar metallicity. Except for one OC with three best $[M/H]$ member measurements, the $\overline{[M/H]}$ values for all metal-poor OCs were based on either one best $[M/H]$ member and/or mainly on good $[M/H]$ members. Therefore, mistaken membership in combination with small number statistics could be one reason for very low $\overline{[M/H]}$.

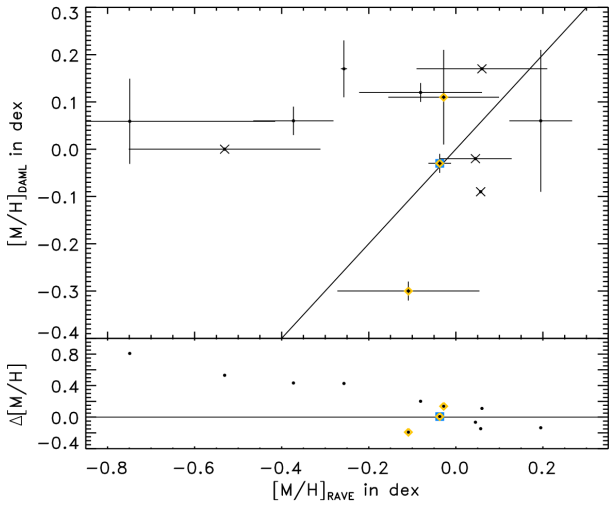

Figure 3.20: $\overline{[M/H]}$ comparison (upper) and difference distribution (lower) between RAVE DR4 and DAML, along with the one-to-one relation and zero-difference line (black solid lines). The blue squares and yellow diamonds highlight OCs with ≥10 individual $[M/H]$ measurements in RAVE DR4 and DAML, respectively. Black crosses indicate e$\overline{[M/H]}$ missing in one or both catalogues.

However, this would not explain the amount of very metal poor OCs I found in my sample, since my membership selection used a uniform algorithm on homogeneous spatial, photometric, and kinematic information. These unexpectedly metal-poor OCs could also indicate that the RAVE DR4 pipeline might underestimate the corresponding metallicities for certain spectra. This was supported by my finding that three out of the 23 individual $[M/H]$ measurements of Pleiades best members show values of −4.36 dex, which I excluded when I computed $\overline{[M/H]}$.

To verify this hypothesis I analysed the results of the chemical pipeline implemented for RAVE by Boeche et al. (2011). The authors employed slightly more stringent quality constraints (SNR ≥ 20, $v_{rot} < 50$ km/s and $4000 < T_{eff} < 7000$ K). It also has to be noted that the chemical pipeline did not cover the very metal-poor end, on contrary to the DR4 pipeline, since either the data quality was too low or the spectral characteristics were not covered by the data grid used in the chemical pipeline.

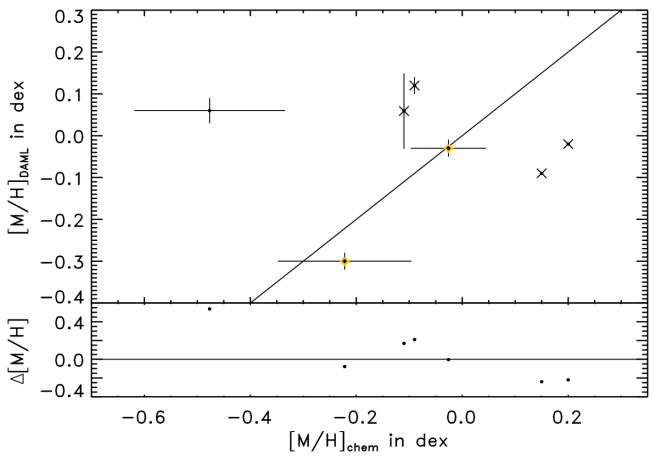

Figure 3.21: $\overline{[M/H]}$ comparison (upper) and difference distribution (lower) between the results from the RAVE chemical pipeline (Boeche et al. 2011) and the DAML, along with the one-to-one relation and zero-difference line (black solid lines). Yellow diamonds highlight OCs with ≥10 individual $[M/H]$ measurements in DAML. Black crosses indicate e$\overline{[M/H]}$ missing in one or both catalogues.

The chemical pipeline provided $\overline{[M/H]}$ for only 52 OCs with typically fewer individual measurements after applying my quality requirements on this data set. I included these additional results in Tab. A.2 along with the number of good and best member measurements in this data set and show a visual comparison to the reference $\overline{[M/H]}$ from DAML in Fig. 3.21.
The two RAVE metallicity sets, DR4 and the chemical pipeline, agree well with the references from DAML in the range $-0.5 < \overline{[M/H]} < 0.5$. However, the chemical pipeline did not provide any very metal-poor values for targets that match my quality requirements, and such stars were simply not listed in the resulting data table. This might indicate that the apparently very metal poor stars in DR4 suffer from lower data quality. Future investigation will show whether all these very metal-poor OCs simply arise from mistaken membership combined with low number statistics or if potentially underestimated metallicities in RAVE DR4 may also play a role.

3.2.4 SUMMARY ON THE RAVE DATA

Current compilations and catalogues of Galactic open clusters significantly lack spectroscopic information, such as RVs and metallicities. The RAVE survey allowed me to fill in some of the missing data. My project was based on the most homogeneous OC catalogue by Kharchenko et al. (2005a,b) (COCD) and the corresponding stellar catalogue (CSOCA). Via a cross-match I identified OC members in RAVE DR4, with a bias towards fainter stars. For the cleaned working sample I provided new RV and $[M/H]$ data. Interestingly, my OC members in RAVE did not represent the accuracy of the entire survey. I showed that this was most likely due to the larger fraction of dwarfs in my OC sample. Still, the data quality was sufficient enough for determining $\overline{RV}$ and $\overline{[M/H]}$ for Galactic open clusters, since the selected members showed a good agreement to previous RV and $[M/H]$ data in OCs. I derived $\overline{RV}$ for 110 OCs, including new data for 37 open clusters. $\overline{[M/H]}$ were derived for only 81 OCs, due to more stringent constraints for my metallicity sample. For 69 of these OCs I presented metallicities for the first time.
The $\overline{RV}$ sample from RAVE DR4 showed a better agreement to the reference values than the $\overline{[M/H]}$ sample. The relatively large spread in both comparison distributions was most likely caused by different stellar samples for each OC in RAVE and the reference catalogue, partly mistaken OC membership or undetected binarity. Partly mistaken membership might be minimised, when the updated membership probabilities from the Milky Way Star Cluster (MWSC) survey (Kharchenko et al. 2013) are included, which could not be done in the framework of this project. Furthermore, most my results were based on only a few individual measurements, which in general made them less robust against the effects mentioned. Thus, all these clusters in RAVE and the reference catalogues have to be considered with caution. Studies by Kouwenhoven & de Grijs (2008), Geller et al. (2008, 2010) and Gieles et al. (2010) supported the assumption that binarity may significantly affect the internal velocity dispersion of open clusters. Although I could not consider my $\sigma\overline{RV}$ to be representative for the internal cluster velocity dispersion, I came to the same conclusion based on a rough estimate on binarity for my OCs, yielding a comparable number of OCs with potential binaries present and OCs with unusually large $\sigma\overline{RV}$.
My $\sigma\overline{RV}$ results were of sufficient quality to derive reliable 3D-kinematics for the Galactic OC system. Combined with previous RV data on OCs this enabled me to re-evaluate the open cluster groups and complexes, proposed by Piskunov et al. (2006). The additional metallicity data obtained by RAVE might only give a rough idea on the $[M/H]$ behaviour of the Galactic OC system. I found 10 OCs with $\overline{[M/H]} < -0.5$ dex, which appeared to be too metal poor considering that those objects are located in the solar neighbourhood. Hence, the DR4 metallicities presented in this work have to be considered with care.

SECTION 3.3
FINAL SET OF PARAMETERS FOR MY OPEN CLUSTER WORKING SAMPLE

3.3.1 COMBINED RADIAL VELOCITIES

In Section 3.1.2 I showed that the CRVAD-2 and RAVE provided RV data of similar quality, which allowed me to combine the measurements from both catalogues and recompute the mean radial velocities ($\overline{RV}$) for the COCD clusters following Eq. 3.1-3.5 (see Sect. 3.2.1). CRVAD-2 and RAVE are complementary data sets and the combination of both catalogues provided more individual measurements per cluster, resulting in more accurate $\overline{RV}$. I primarily used best members, and only included good members, if no or just one best member for a cluster was available. The selection from the CRVAD-2 was solely based on membership probabilities, while for the RAVE selection additional quality constraints (SNR>10, $R \geq 10$ and $|corr\_RV| \leq 9$ km/s) and flag requirements (see Sect .3.1.2) were considered. If a star had multiple RV measurements in RAVE I took the value derived from the spectrum with the higher Signal-to-Noise ratio (SNR). If a cluster showed no individual RV measurements of sufficient quality in CRVAD-2 or RAVE, I used the RV value listed in CRVOCA. These values were either computed from stars in the OC regions with membership probability down to 1% or are collected literature values (for details see Kharchenko et al. (2007)) and I preferred to use the literature values. In total I extracted 432 clusters from the COCD with available RV data, defining my working sample.

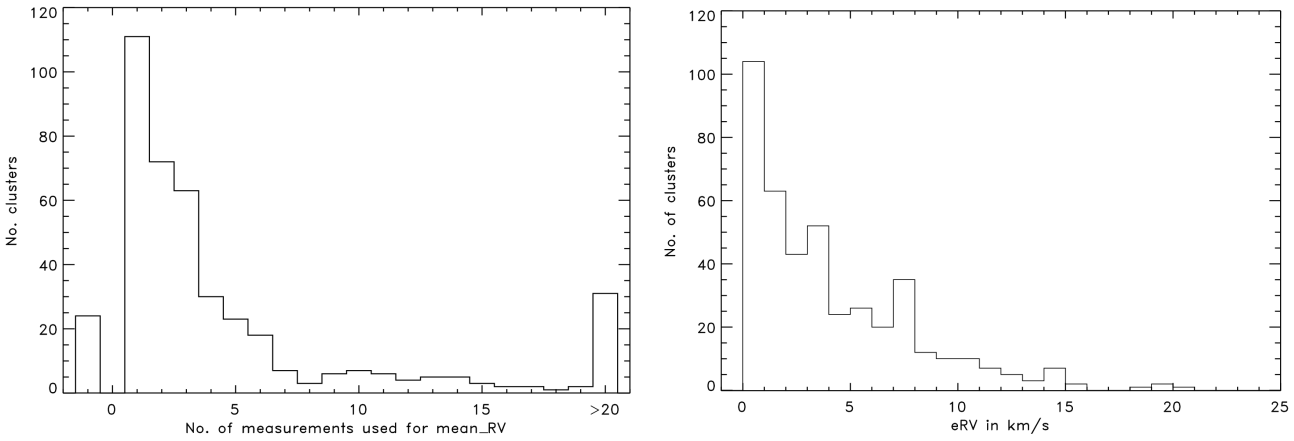

Figure 3.22: Left panel: Histogram for the number of individual measurements used to compute $\overline{RV}$ from RAVE and CRVAD-2 or the number of stars as given in the CRVOCA for my working sample. Right panel: Histogram for the $\overline{RV}$ uncertainties either as determined for the computed values or as taken from the CRVOCA.

The left panel of Fig. 3.22 shows the distribution for the number of individual measurement used to obtain $\overline{RV}$ for the OCs in my working sample. Clusters with number of stars equals "-1" were equipped with $\overline{RV}$ from CRVOCA based on only one member with $P_{kin} > 1\%$. One can see that, although the distribution was slightly shifted towards higher number of stars, because of the combined catalogues, the majority of clusters are still covered by less than seven individual RV measurements of good and best members. Thus, the $\overline{RV}$ values are still affected by small number statistics.
The right panel of Fig. 3.22 illustrates the distribution of the uncertainties in $\overline{RV}$ for the OCs in my working sample, which peaks at about 1-2 km/s, but show a tail out to 20 km/s. The shape of the e$\overline{RV}$ histogram is very similar to that for the individual RV measurements of OC members in RAVE (see Fig. 3.5).

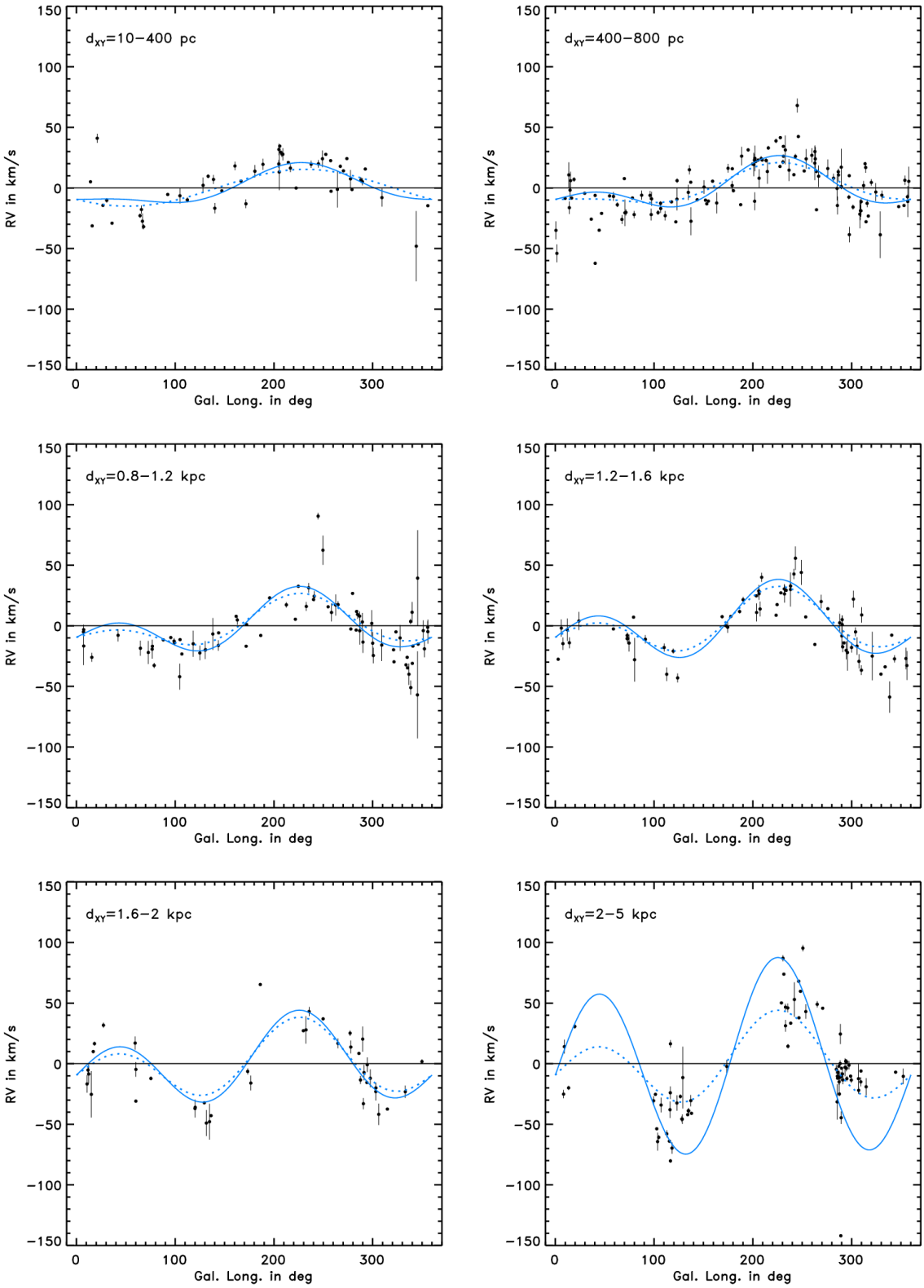

Figure 3.23: Dependency of the uncorrected radial velocities on Galactic longitude for different distance ranges from the sun in the XY-plane. The blue dashed and solid lines indicate the effects of the differential rotation and solar motion on the RV value for the lower and upper limit of the corresponding distance range.

The statistically computed uncertainties for the mean radial velocities were expected to be below the uncertainties of the individual RV measurements, but since typically only a few members for each cluster were equipped with RV measurements in RAVE or the CRVAD-2, the effect of small number statistics caused the e$\overline{RV}$ to be of the order of the individual eRV*. For the general discussion of the Galactic open cluster population this accuracy is sufficient, but for the discussion of individual clusters the values have to be considered with care.
The radial velocities presented here were not corrected for the solar motion with respect to the Galactic centre or the differential rotation within the Galactic disc. Thus, these catalogue RVs should show a sinusoidal variation, in particular, along the Galactic longitude, as displayed in Fig. 3.23 for different distance ranges from the sun in the Galactic plane. The d_{XY} in Fig. 3.23 correspond to the distance in the XY-plane from the sun, which is the description of the Galactic midplane in the Cartesian coordinate system.[4] The expected variation in RV with Galactic longitude (l) is clearly visible in the data. In theory, the differential rotation in the Galactic disc is defined through the Oort constants and the solar motion is basically the velocity vector of the sun with respect to the Galactic centre. For the radial velocities the resulting theoretical relation is given by:

$$RV = A \cdot d \cdot \sin 2l - (U_0 \cdot \cos l + V_0 \cdot \sin l) \tag{3.10}$$

where d is the distance of the cluster to the sun in kpc[5], $A = 14.5$ km s^{-1} kpc^{-1} is one of the Oort constants and $(U_0, V_0) = (9.44, 11.9)$ km/s are the (U, V) components of the solar motion, as given by Piskunov et al. (2006) for the Galactic OC system. In Fig. 3.23 the uncorrected RV data follow very nicely the theoretical lines, supporting the reliability of the derived $\overline{RV}$, even tough they suffer from small number statistics.

3.3.2 DISTANCES

The COCD provided distances for all 650 open clusters and stellar associations, derived from 3-colour information and spectral type information, where available or obtained from the literature (Kharchenko et al. 2005a,b). They stated that the distances were accurate to the 10% level. For this study I focused on the subsample of 432 clusters with available $\overline{RV}$ data.

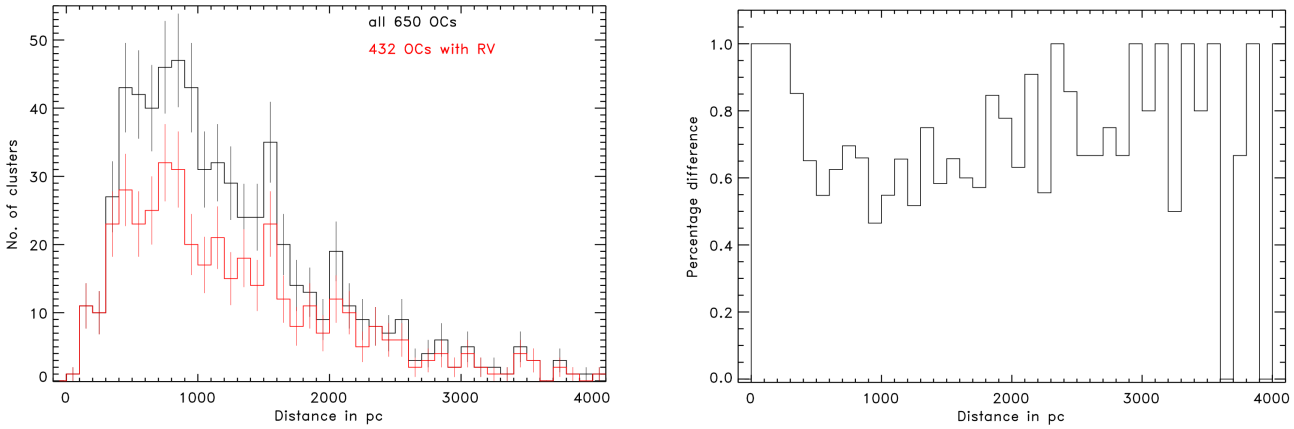

Figure 3.24: Left panel: Distance histogram in COCD for all 650 OCs (black) and my working sample of 432 OCs with RV available (red). The error bars were determined as $\sqrt{n}$, where n is the number of OCs in the corresponding bin. Right panel: Percentage difference between the distance histograms in the COCD computed as n_{432}/n_{650} for each interval.

[4]For a detailed description of the Cartesian coordinate system see Sect. 4.1.

[5]In general, Eq. 3.10 used 3D-distances, but for Fig. 3.23 I used the distance in the XY plane. The difference between both distances was small, since open clusters are predominantly located in the Galactic disc.

In Fig. 3.24 I compare the distance distribution for my working sample to the one for the entire COCD, with the corresponding percentage difference in the right panel. The distributions differ most in the distance range 400 pc and 1.8 kpc, where my working sample only covers about 50% of the entire COCD in the corresponding bins. Hence, in the immediate solar vicinity almost all OCs were equipped with RVs. Moreover, most of the very distant clusters ($d > 2.9$ kpc) have RV measurements, which might be because of very bright cluster members in these distant OCs. Only at the intermediate distance range a significant number of clusters lack RV information. Still, since the shape of both distributions is rather similar, my working sample could be considered representative for the COCD.

3.3.3 PROPER MOTIONS

The RAVE catalogue provided proper motions (PMs) from the PPMXL (Röser et al. 2010), TYCHO-2 (Høg et al. 2000), as well as UCAC-2, UCAC-3, and UCAC-4 (Zacharias et al. 2004, 2010, 2013) for the majority of the observed stars. The mean proper motions ($\overline{PM}$) for the clusters in the COCD, were based on ASCC-2.5 values (Kharchenko 2001), which were obtained from several source catalogues, such as the PPM catalogues (Röser & Bastian 1991; Bastian & Röser 1993), TYCHO-2 (Høg et al. 2000), and CMC (Fabricius 1993). In this work I used the homogeneous COCD proper motions, mainly because they were available for all clusters. Besides the $\overline{PM}$ in the equatorial system ($\overline{PM_{RA}}$ and $\overline{PM_{DEC}}$), Kharchenko et al. (2005a,b) also listed $\overline{PM}$ values in the Galactic coordinate system ($\overline{PM_l}$ and $\overline{PM_b}$).
The COCD only listed uncertainties for the proper motion components in the equatorial coordinate system (RA and DEC) and their distributions are displayed in Fig. 3.25 for the cluster mean values (e$\overline{PM}$, left panel) and the best OC members (ePM^*, right panel). The distributions for the e$\overline{PM}$ values appear to be narrower than the ePM^* distributions. This was expected, because all stars considered for the cluster identification and, therefore, all OC members were equipped with PM values, which resulted in larger statistics for the cluster proper motions. Furthermore, the e$\overline{PM}$ are statistical errors and are affected by the number of individual measurements. Both histograms illustrate that the proper motions are of sufficient accuracy for the purposes of the project presented in this thesis.

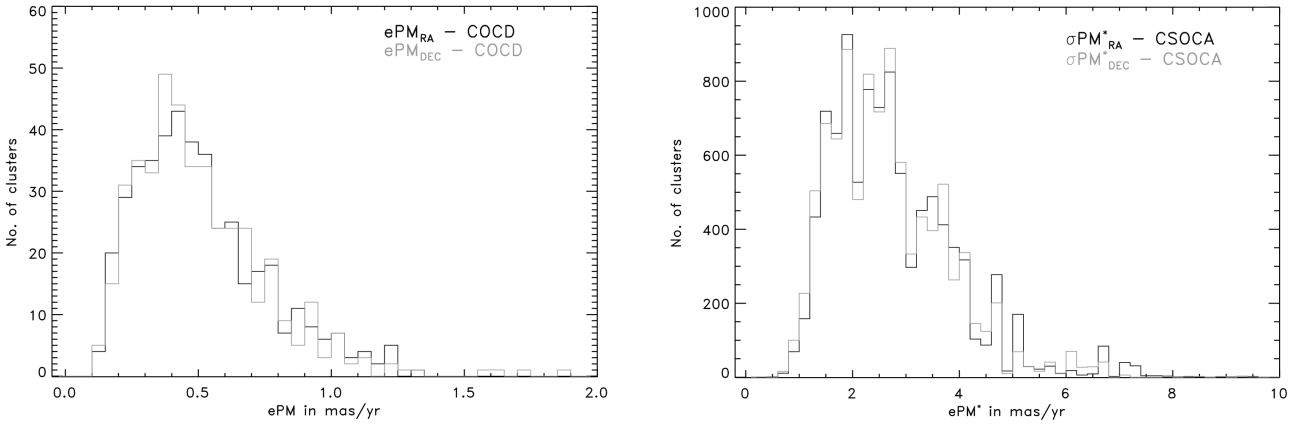

Figure 3.25: Histograms for the proper motion uncertainties in RA (black) and DEC (grey) for the clusters (left panel) and the best OC members (right panel) in the working sample.

As for the radial velocities, the provided proper motions were not corrected for solar motion and differential rotation and should show a variation with Galactic longitude. However, for more distant clusters the effect would be hard to detect, as proper motions decrease significantly with distance. But when converting the proper motions to tangential velocities (V_T), the mentioned effects should become more visible.

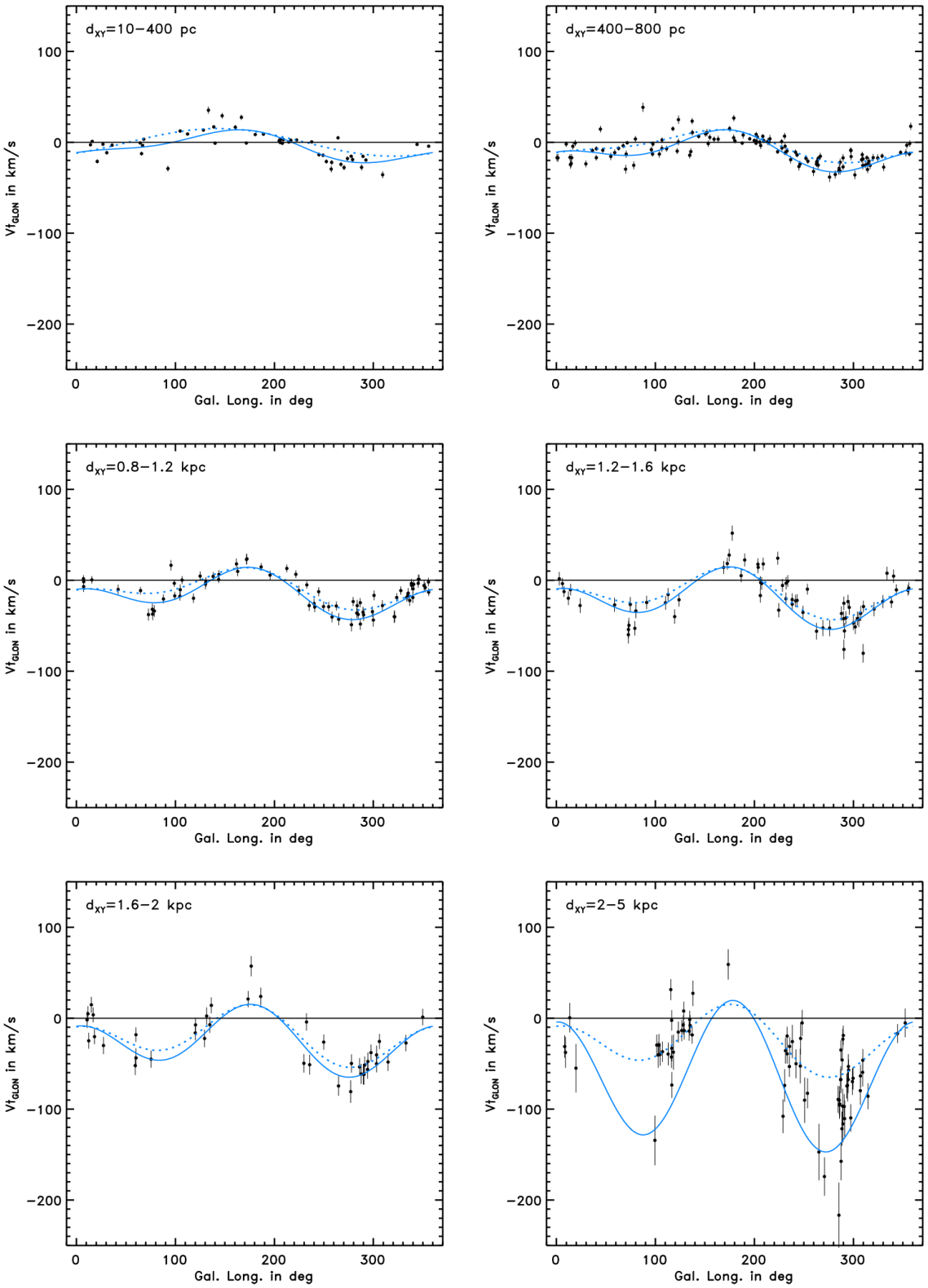

Figure 3.26: Dependency of the uncorrected tangential velocity in Galactic longitude ($V_{T,l}$) on the Galactic longitude for different distance ranges from the sun in the XY-plane. The blue dashed and solid lines indicate the effects of the differential rotation and solar motion for the lower and upper limits of the corresponding distance range.

This conversion is defined by Eq. 3.11 for the component of interest and the corresponding uncertainty can be determined by Eq. 3.13.

$$V_T = 4.74 \cdot PM \cdot d \tag{3.11}$$

where V_T is the tangential velocity component of interest in km/s, PM the proper motion component of interest in mas/yr, and d the distance of the cluster to the sun in kpc. Since open clusters are primarily located in the Galactic disc, the effect of solar motion and differential rotation should mainly affect the tangential velocity component in Galactic longitude ($V_{T,l}$). The theoretical description of the effect of solar motion and differential rotation in $V_{T,l}$ is defined by Eq. 3.12.

$$V_{T,l} = A \cdot d \cdot \cos 2l + B \cdot d + (U_0 \cdot \sin l - V_0 \cdot \cos l) \tag{3.12}$$

where d is the distance of the cluster to the sun and l its Galactic longitude, $(A, B) = (14.5, -13)$ km s^{-1} kpc^{-1} are the Oort constants, and $(U_0, V_0) = (9.44, 11.9)$ km/s are the U and V components of the solar motion, as provided by Piskunov et al. (2006) for the Galactic open cluster system. Fig. 3.26 illustrates the variation of $V_{T,l}$ with Galactic longitude for different distance ranges from the sun in the XY-plane. The data follow very nicely the theoretical curves and verify the reliability and sufficient quality of the tangential velocities and, therefore, of the proper motions used in this work.
Before calculating the uncertainties for the tangential velocities, I had to determine the uncertainties of the proper motions in Galactic longitude. The COCD only provide uncertainties for the proper motions in RA and DEC, but it could be assumed that the proper motion uncertainties in l and b are of the same order of magnitude. In RA and DEC the uncertainties were typically well below 1 mas/yr, which was very optimistic, and therefore I set the e$\overline{PM}$ in l and b to 1 mas/yr[6]. The uncertainties in tangential velocity for the component of interest is then defined by Eq. 3.13 following the Gaussian error propagation.

$$eV_T = \sqrt{4.74 \cdot [(ePM \cdot d)^2 + (PM \cdot ed)^2]} \tag{3.13}$$

Fig. 3.27 displays the distribution for the V_T uncertainties in the Galactic coordinate system. The $\overline{V_T}$ values seemed to be of comparable accuracy as the $\overline{RV}$ values. Both velocity uncertainty distributions are well below 20 km/s, but peak at slightly different values. The e$\overline{V_T}$ peak at about $3-4$ km/s, while the e$\overline{RV}$ values peak at about $1-2$ km/s. Hence, both velocity uncertainty contribute to comparable amounts to the uncertainties in the 3D Cartesian-velocities, that were used for the identification of OC groupings in the following chapter.

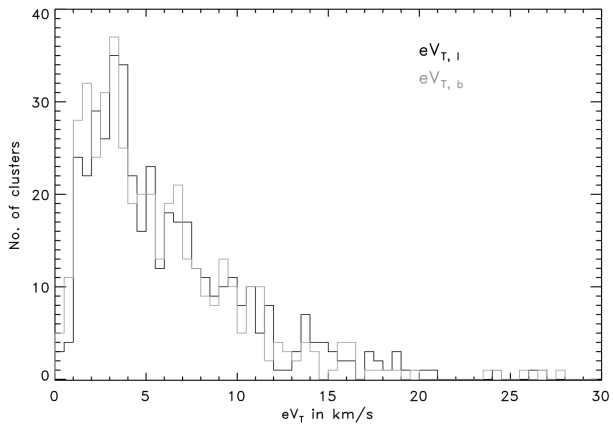

Figure 3.27: Histogram for uncertainties in V_T in Galactic longitude (black) and latitude (grey) for the clusters in the working sample.

[6]A more detailed discussion of the proper motion uncertainties can be found in the appendix Sect. B.

3.3.4 AGES

The COCD provided ages for all 650 objects in the COCD, either derived from isochrone fitting or obtained form the literature (Kharchenko et al. 2005a,b). They stated that the uncertainties for the ages in the COCD were of the order of $\sigma_{\log t} = 0.2 - 0.25$. Fig. 3.28 displays the age distribution for the entire COCD and my working sample along with the percentage difference between both samples.

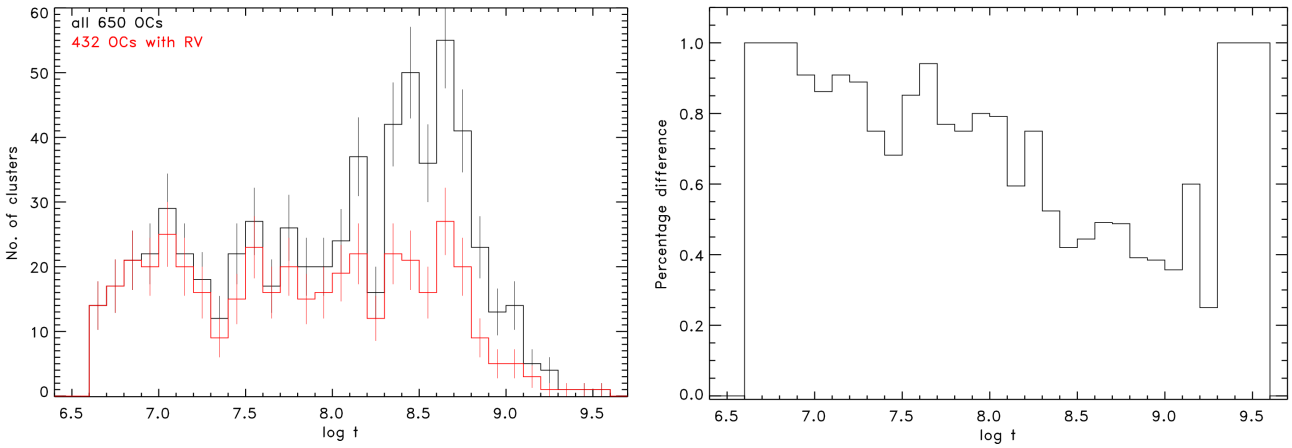

Figure 3.28: Left panel: Age histogram in the COCD for all 650 OCs (black) and the working sample of 432 OCs with available RV data (red). Right panel: Corresponding percentage difference (n_{432}/n_{650}).

For my working sample the number of older clusters ($8.3 < \log t < 9.3$) is significantly smaller than for the entire COCD, considering the percentage difference in the right panel. Also the overall distribution appeared to be flatter for my working sample than for the entire COCD, looking at the histogram in the left panel of Fig. 3.28. This indicated that, in particular, older open clusters lacked RV information.
One reason could be that the older clusters were on average too faint to determine accurate RV values for the members. Therefore, I checked whether the magnitude of the brightest most probable member of the clusters in the entire COCD, regardless of available RV data, and my working sample were related to the age of the corresponding cluster (Fig. 3.29).

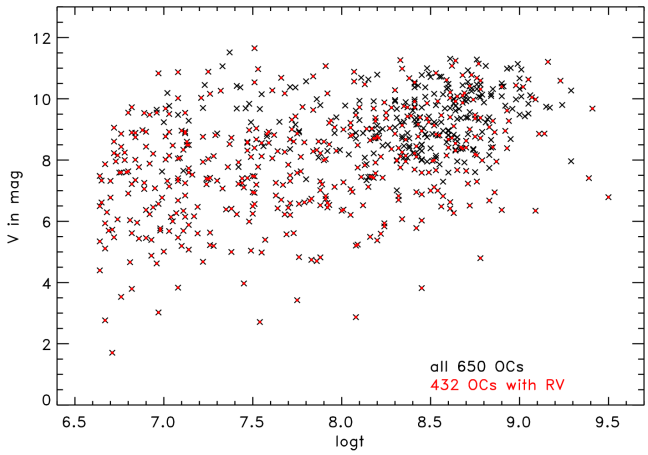

Figure 3.29: Dependency of cluster brightness on the age for the entire COCD (black), regardless of available RV data, and my working sample (red). The brightness of a cluster was defined by the brightest most probable member.

Almost all clusters with members brighter than 8 mag appeared to have radial velocity measurements, while for clusters with members fainter than about 9-11 mag more clusters with missing RV information were present. Moreover, the magnitudes of the brightest members show a slight positive slope with increasing cluster age in Fig. 3.29. The bright members for clusters with $\log t > 8.2$ dex showed magnitudes fainter than 9 mag and were more affected by the selection effect for RV information. This strengthens the statement made above that older clusters lack more RV data than younger OCs.

3.3.5 METALLICITIES

Since the COCD did not provide metallicity information, I combined the $\overline{[M/H]}$ data from RAVE with the literature values from DAML to obtain $[M/H]$ for my working sample. The RAVE based $\overline{[M/H]}$ were derived as described in Sect. 3.2.3, which have to be considered with care, due to small number statistics and potential limitation effects in the RAVE pipeline. The DAML metallicities are highly inhomogeneous and I could only include a subset of these values. The majority of spectroscopically derived values were based on iron lines only and are rather comparable to iron abundances than overall metallicities, while the photometric methods are more likely to result in overall metallicities, which I was interested in. If for a cluster RAVE and DAML provided $[M/H]$, I included the value based on more individual measurements.

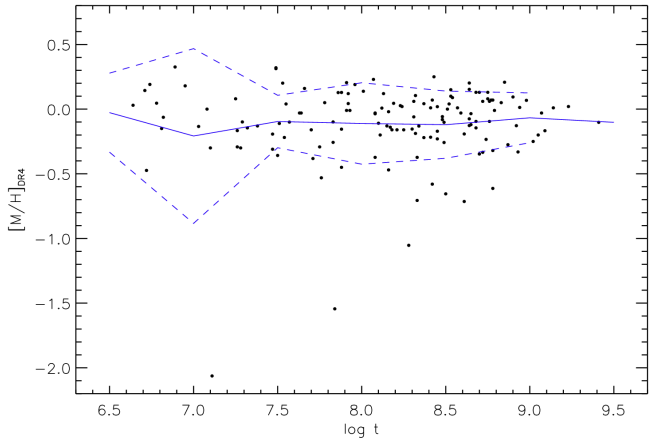

Figure 3.30: Age-metallicity relation for my open cluster working sample. The solid and dashed lines showed the mean $[M/H]$ and 1σ-limit, which were computed in bins of 0.5 dex along $\log t$.

Fig. 3.30 displays the age-metallicity relation for the clusters in my working sample with available $\overline{[M/H]}$. For the age range covered by my working sample no clear dependency or slope is visible. Hence, I conclude that the Galactic open cluster population in the solar neighbourhood, with ages ranging from a few Myr to a few Gyr, shows about similar overall metallicity. Apparently, a larger age range would be needed to detect the proposed age-metallicity relation for the Galactic cluster population.
Furthermore, I checked the metallicity gradient in my working sample within the Galactic plane and perpendicular to it. Fig. 3.31 illustrates these potential relations, where the Galactocentric radius (R_{XY} in kpc) was computed as

$$R_{XY} = \sqrt{(X + 8.5\text{kpc})^2 + Y^2}$$

with 8.5 kpc being the distance of the sun to the Galactic centre and the XY-coordinates given in kpc. In Fig. 3.31 no clear trend could be identified in either direction. Reasons for the rather constant $\overline{[M/H]}$ in my working sample could be the size of the sample, the sample not being diverse enough, and/or the population being too local.

Hence, for an investigation on the metallicity gradient, based on open clusters, a far more extensive sample of OCs equipped with homogeneous $\overline{[M/H]}$ data would be needed that reaches distances of at least 10 kpc from the sun.

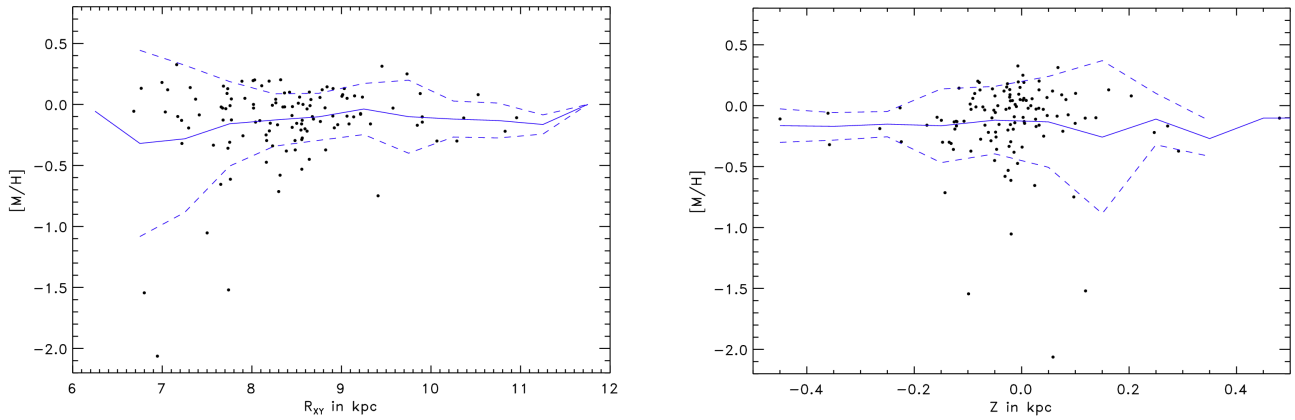

Figure 3.31: Metallicity gradients in radial (left) and vertical (right) direction. The solid lines show the mean metallicity computed in bins of 0.1 kpc along R_{XY} and the dashed lines the corresponding 1σ-limits.

Chapter 4

Open cluster groups and complexes

Section 4.1

6D phase-space information

In the previous chapter I discussed the characteristics of the COCD and RAVE data and defined a final working sample of 432 OCs with available RV. There I had to distinguish between member parameters and cluster parameter, but since hereafter only cluster parameters will be discussed I changed the nomination from $\overline{RV}$ to RV and equivalent for the other parameters. The aim of this project was to investigate open cluster groups and complexes and for their identification it was convenient to use positions and velocities in the Cartesian coordinate system with the sun as point of origin.
The XYZ-coordinates were obtained from a conversion of spherical Galactic coordinates to Cartesian coordinates following Eq. 4.1, where d is the distance of the cluster to the sun in kpc and l and b are the Galactic longitude and latitude. Here the positive X-axis points towards the Galactic anticentre, the Y-axis is positive in direction of Galactic rotation, and the positive Z-axis points towards the north Galactic pole.

$$\begin{pmatrix} X \\ Y \\ Z \end{pmatrix} = \begin{pmatrix} -d \cdot (\cos b \cdot \cos l) \\ d \cdot (\cos b \cdot \sin l) \\ d \cdot \sin b \end{pmatrix} \tag{4.1}$$

The UVW-velocities were computed from the spherical values in the Galactic coordinate system, but I had to correct the RV and PM_l values for differential rotation beforehand. The correction equations (Eq. 4.2 and 4.3) were taken from Binney & Merrifield (1998, p. 637-640). Since differential rotation is mainly a radial effect within the Galactic disc, a correction in the Galactic latitude component of the proper motion was negligible and therefore not included here.

$$RV_{corr} = RV - A \cdot d \cdot \sin 2l \tag{4.2}$$

$$PM_{l,corr} = PM_l - (A \cdot \cos 2l + B)/k \tag{4.3}$$

where k=4.74 is the factor ensuring unit consistency, d the distance of the cluster to the sun in kpc, RV the radial velocity of the cluster in km/s, PM_l and PM_b are the proper motion components in mas/yr, and $(A, B) = (14.5, -13)$ km s^{-1} kpc^{-1} are the Oort constants as determined by Piskunov et al. (2006) for the Galactic open cluster population in the COCD.

The Galactic UVW-velocities were then computed using Eq. 4.4[1], with U being positive towards the Galactic anticentre, V positive in direction of Galactic rotation and W being positive towards the north Galactic pole. The correction for the solar motion was applied in the final equation through simply adding the values provided by Piskunov et al. (2006) for the Galactic open cluster population[2]: $(U_0, V_0, W_0) = (-9.44, 11.9, 7.2)$ km/s.

$$\begin{pmatrix} U \\ V \\ W \end{pmatrix} = 4.74 \cdot d \cdot \left[PM_{l,corr} \cdot \begin{pmatrix} -\sin l \\ \cos l \\ 0 \end{pmatrix} + PM_b \cdot \begin{pmatrix} -\cos l \cdot \sin b \\ -\sin l \cdot \sin b \\ \cos b \end{pmatrix} \right] + RV_{corr} \cdot \begin{pmatrix} \cos l \cdot \cos b \\ \sin l \cdot \cos b \\ \sin b \end{pmatrix} + \begin{pmatrix} U_0 \\ V_0 \\ W_0 \end{pmatrix} \quad (4.4)$$

The UVW-velocities computed here were not the actual velocities of the clusters in the Galaxy with respect to the centre, but merely the velocity differences to the sun. Fig. 4.1 displays the velocity field in the Galactic plane and velocity component versus Galactic longitude diagrams for the computed UVW-velocities, corrected for differential rotation and solar motion. Since the field looks rather random and no systematic dependency on Galactic longitude is present, it was safe to conclude that the corrections were performed to a satisfying degree.

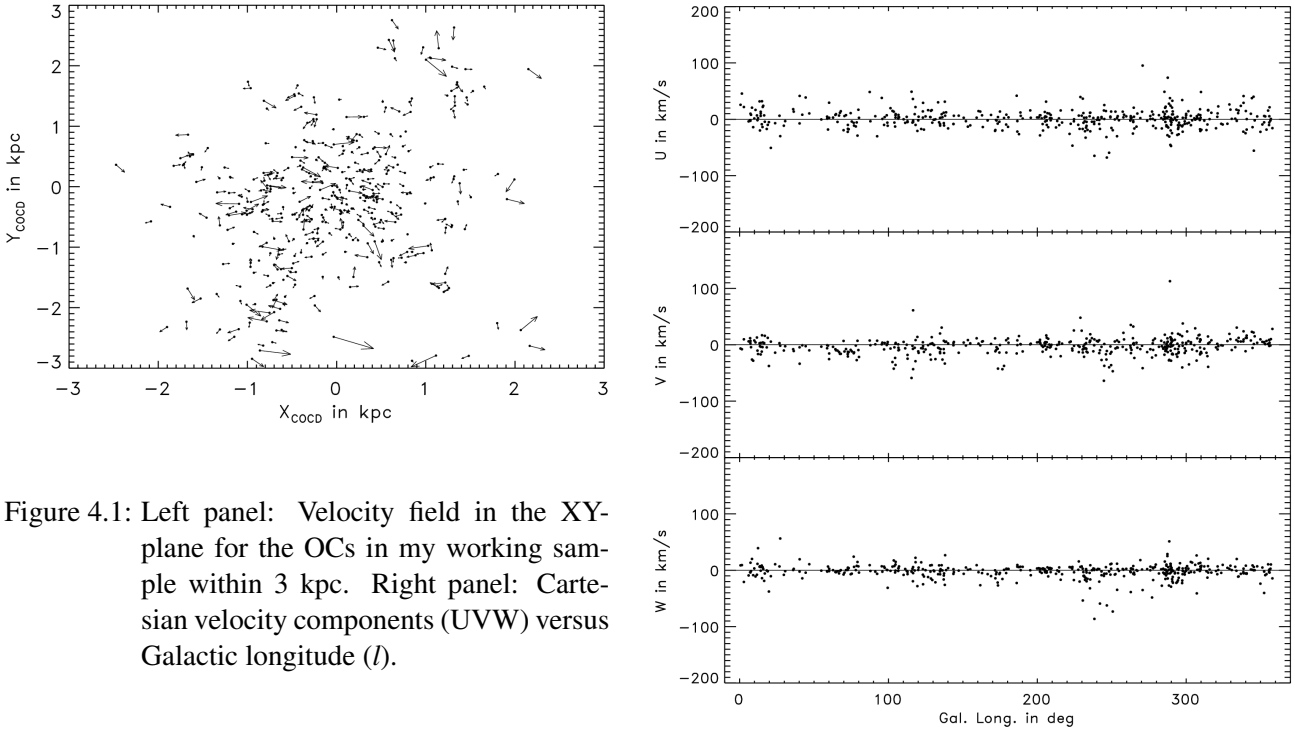

Figure 4.1: Left panel: Velocity field in the XY-plane for the OCs in my working sample within 3 kpc. Right panel: Cartesian velocity components (UVW) versus Galactic longitude (l).

The distributions for the UVW uncertainties[3] (Fig. 4.2) peak at about 3-4 km/s and the vast majority of values are well below 20 km/s. These uncertainties covered approximately the same range as the uncertainties for the input velocities (RV and V_T), which both contributed to equal amounts to the UVW-uncertainties. The contribution of the uncertainties in distance, used to calculate V_T, is not negligible, whereas the uncertainties in the Galactic coordinates (l and b) only play a minor role for the uncertainties in the Cartesian velocities. Thus, the resulting distribution for the uncertainties confirmed that the UVW-velocities were still of sufficient accuracy for the purpose of this project.

[1]Eq. 4.4 corresponds to a coordinate transformation in velocity space and was verified through private communication with Nina Kharchenko and Anatoly Piskunov.

[2]The change of sign in U_0 between Piskunov et al. (2006) and this work is because of the flipped direction of the X-axis.

[3]The equations for the velocity uncertainties in UVW are given in the Appendix of this thesis Sect. B.

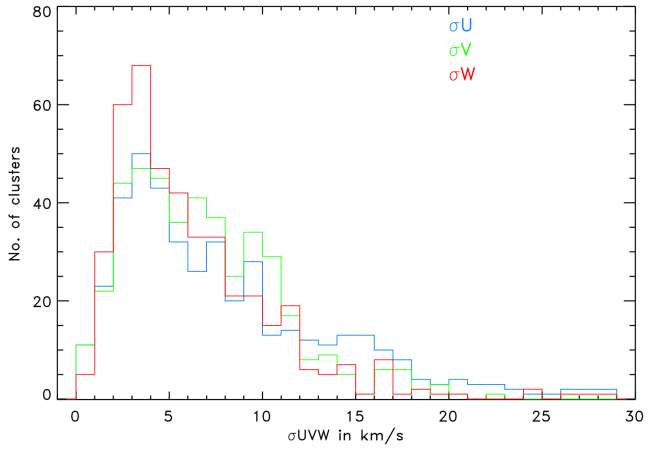

Figure 4.2: Histograms for the uncertainties in the computed and corrected Cartesian velocities (U - blue, V - green, W - red) in my open cluster working sample.

SECTION 4.2

IDENTIFICATION OF OPEN CLUSTER GROUPINGS

Members of an open cluster group or complex were expected to show spatial proximity. If the number of such groupings is large enough, they should appear as an additional peak in the separation distribution for the nearest neighbours (see Fig. 4.3). Furthermore, members of an open cluster group or complex should have similar velocity vectors. In general, objects in a restraint area of the Galactic disc could be expected to move with similar velocity vectors and a velocity dispersion indicating the amount of random motion in that region. For the purpose of this investigation I evaluated this random motion to gain insight on the importance of including velocities in the identification algorithm.

The upper right panel of Fig. 4.3 shows the minimal velocity difference between OC pairs, regardless of spatial proximity, and most likely reflects the velocity dispersion of the Galactic disc in the solar vicinity. The lower right panel of Fig. 4.3 illustrates the velocity difference between a cluster and its nearest spatial neighbour. It is interesting, that the latter distribution is much broader than the one for the minimal velocity difference, which verified the necessity for including the velocity as requirement for the group identification. Moreover, the difference between the distributions in the right panels of Fig. 4.3 showed that there is a non-negligible amount of random motion present in the Galactic OC population.

In this study no prior assumptions were made on the mean coordinates and/or velocities of the potential OC groupings, which were expected to be of irregular shape. A suitable tool to identify genuine OC groupings with a minimum of prior assumptions was the Friends-of-Friends (FoF) algorithm, as used in cosmology (Huchra & Geller 1982; Geller & Huchra 1983). The basic working principle is to identify intersecting spheres of defined radius, called the linking length. This linking lengths is equivalent to the expected typical separations within the groupings, but smaller than the separation between groupings. Here I adapted this working method in coordinate and velocity space and referred to it as FoF-like algorithm, which compared the 3D spatial separation and 3D velocity differences with the two defined linking lengths.

The spatial linking length should have a value between the typical size of open clusters ($\approx$ 10 pc) and the scale of the Galactic spiral arms ($\approx$ 1 kpc). The open cluster pairs identified by de La Fuente Marcos & de La Fuente Marcos (2009a,b,c) had predefined separations of in maximum 30 pc and the OC groups and complexes proposed by Piskunov et al. (2006) span regions of about 300 pc. The separation histogram for the nearest neighbours showed two peaks, one at about 50 pc and a second at about 100 pc (left panel of Fig. 4.3), which could be a signature for OC groupings. Hence, setting the spatial linking length in the FoF-like algorithm to 100 pc appeared to be a reasonable choice, although this held the possibility that the groups and complexes, proposed by Piskunov et al. (2006), may not be recovered to their entire size.

The velocity linking length should have a value comparable to a few multiples of the typical internal velocity dispersion of open clusters, which is of the order of a few km/s, to ensure similar velocity vectors of the group and complex members. The UVW-uncertainties were typically 3-4 km/s and mostly below 20 km/s (see Fig. 4.2), but show a rather broad distribution. Since the distribution for the UVW-uncertainties exceeded the expected values for the velocity dispersion of open clusters, I preferred to use the former to define the velocity linking length. The typical UVW-uncertainties were well below 10 km/s, but the distribution continued to values of 20 km/s. Thus, it seemed to be more reasonable to define a range of 10 – 20 km/s for the velocity linking lengths than a single value, which can be expected to include the most likely value.

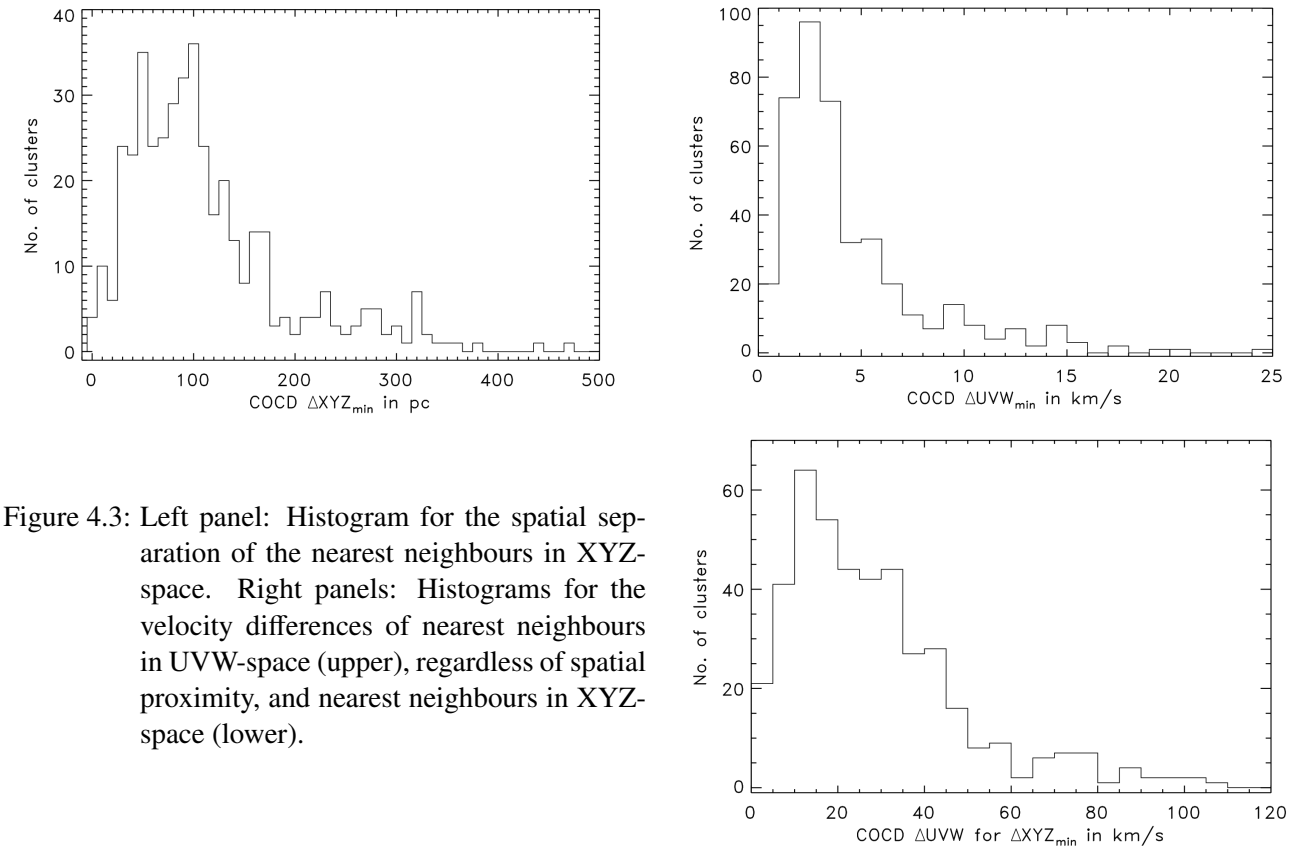

Figure 4.3: Left panel: Histogram for the spatial separation of the nearest neighbours in XYZ-space. Right panels: Histograms for the velocity differences of nearest neighbours in UVW-space (upper), regardless of spatial proximity, and nearest neighbours in XYZ-space (lower).

Because of the range in velocity linking length, I ran the FoF-like algorithm twice - first, with 100 pc and 10 km/s and, second, with 100 pc and 20 km/s. The resulting distributions in coordinate and velocity space of the identified groupings are displayed in the upper and lower panels of Fig. 4.4. In this study, I distinguished between pairs (two members), groups ($<$ 10 members), and complexes ($>$ 10 members) of open clusters. Interestingly, the majority of identified groupings were pairs for both sets of linking lengths. The identified OC groupings were detected preferably in the immediate solar neighbourhood at $\approx$ 1 kpc for a velocity linking length of 10 km/s and $\approx$ 2 kpc for 20 km/s, where apparently the coverage with 6D phase-space information is better. In velocity space the distribution of identified OC groupings appeared to be not as centralised as in coordinate space and the groupings did not separate as clearly at visual inspection.
As expected, the number and size of the identified OC groupings increased with larger velocity linking length. At a velocity linking length of 10 km/s, I found in total 19 groupings with 14 pairs, four groups with either three or four members, and one complex with 15 members (left panel of Fig. 4.5). At a velocity linking length of 20 km/s, I identified in total 42 groupings with 32 pairs, nine groups with either three, four, five, seven, or nine members, and one complex with 15 members (right panel of Fig. 4.5).

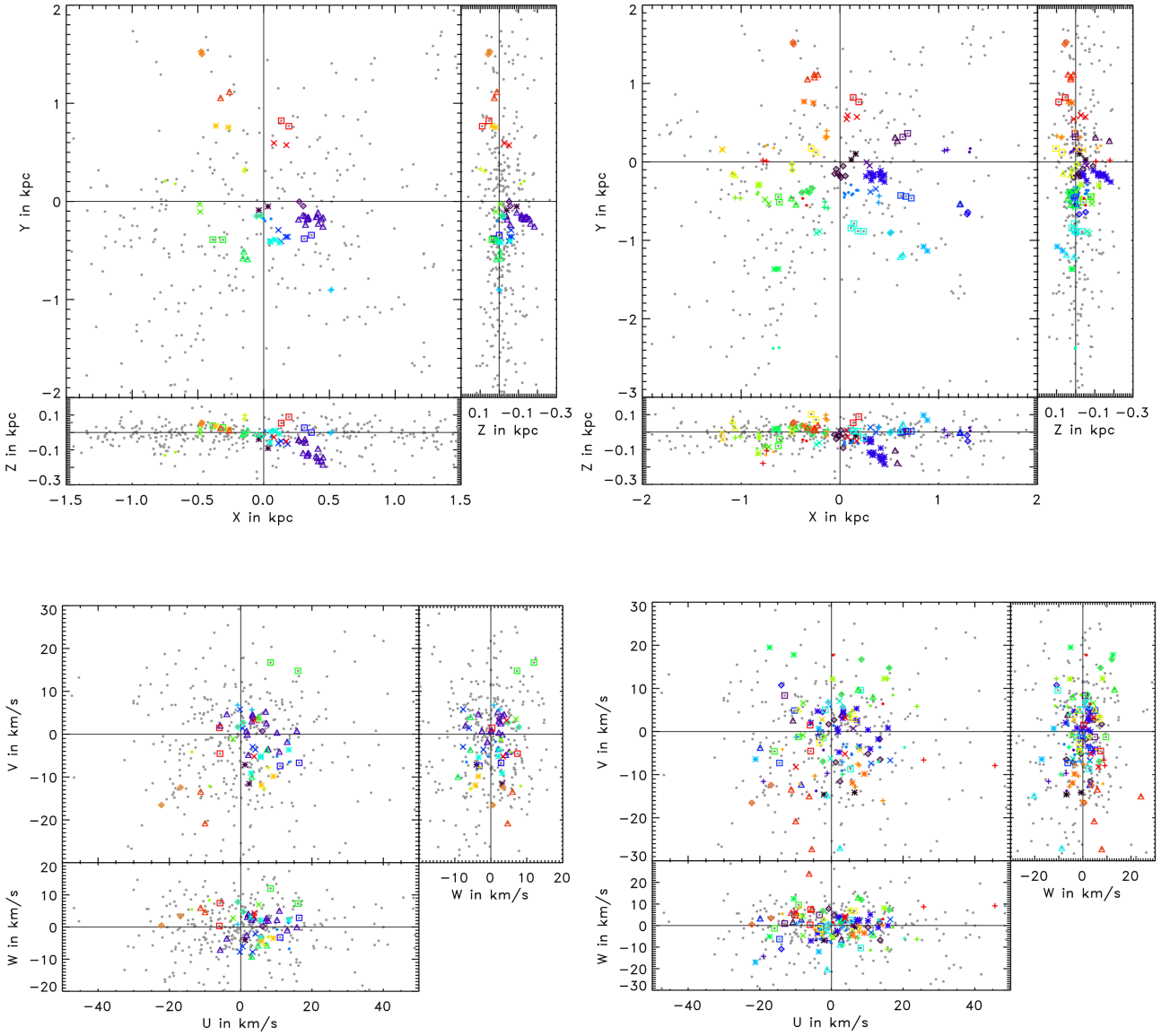

Figure 4.4: Distribution of the identified OC groupings in coordinate (upper panels) and velocity (lower panels) space for a spatial linking length of 100 pc and a velocity linking length of 10 km/s (left panels) or 20 km/s (right panels). The grey dots show the entire working sample, while the OC groupings are highlighted by different colours and symbols independently for both sets of linking lengths.

A closer look at the upper panels of Fig. 4.4 also showed that there are not only more and larger groupings, after increasing the velocity linking length, but that some smaller grouping seemed to merge. For example at $X \approx 0$ kpc and $Y \approx -0.1$ kpc or $X \approx 0.2$ kpc and $Y \approx -0.4$. Still, the number and size of the identified OC groupings stayed reasonable for the chosen range in velocity linking length.

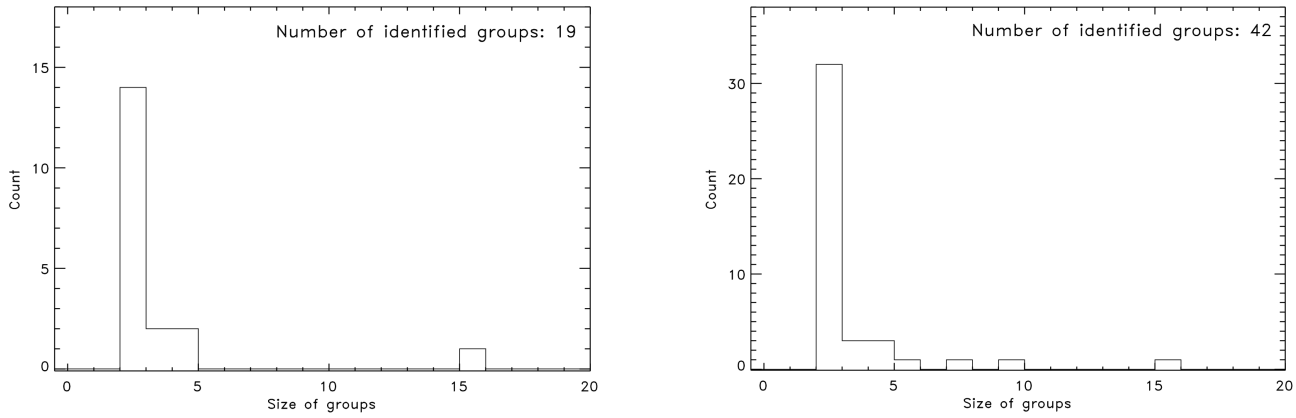

Figure 4.5: Histograms for the size of the identified OC groupings for both sets of linking lengths: 100 pc and 10 km/s (left); 100 pc and 20 km/s (right).

SECTION 4.3
VERIFICATION OF OPEN CLUSTER GROUPINGS

The previous section discussed the definition of the spatial and velocity linking lengths needed for the FoF-like algorithm and the identification of OC groupings. To a certain degree the definition of these linking lengths was arbitrary, but could be constrained. For the spatial linking length I showed that 100 pc was the most reasonable choice, but for the velocity linking length only a range of values could be defined. Although the defined linking length appeared to be reasonable, further verification of the linking lengths and identified structures was recommendable. In the following section I want to discuss two approaches for this verification. First, I compared my results from the COCD to a reference catalogue that became available recently. Second, I implemented Monte-Carlo simulations with two different input distributions for the randomised sample.

4.3.1 THE REFERENCE CATALOGUE

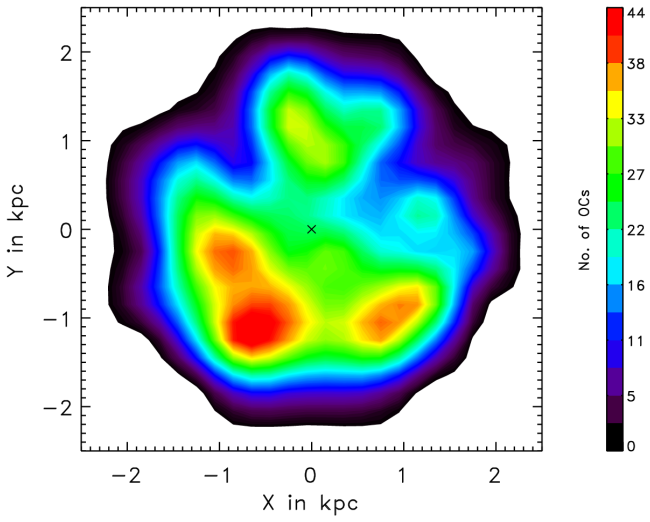

Figure 4.6: Smoothed density profile in the XY-plane for open clusters and associations in the MWSC within 1.8 kpc. The cross illustrates the position of the sun.

Kharchenko et al. (2013) provided a new and more extended cluster catalogue, namely the Milky Way global survey of star clusters (MWSC), comprising homogeneous data for about 3000 optical stellar associations, open, and globular clusters. It is complete to about 1.8 kpc and contained all COCD objects. The smoothed XY-surface density profile for the MWSC within its completeness limit (Fig. 4.6) showed voids and overdensities. The general open cluster population in the Milky Way was expected to be distributed almost homogeneously in the Galactic disc and the clearly distinct density differences present in Fig. 4.6 appeared to be larger than expected. Overdensities in the XY-surface density profile (Fig. 4.6) could be caused by the spiral structure in the Milky Way, because star formation is believed to primarily take place within spiral arms. Thus, young open clusters should follow this structure and might induce apparent overdensities. Voids in the XY-surface density profile (Fig. 4.6) could be caused by increased extinction induced by gas and dust clouds, which are more frequent in the Galactic disc. These clouds mainly obscure the light in the optical wavelengths and, since the MWSC is an optical catalogue, especially clusters that are only visible in the infrared would not be included by Kharchenko et al. (2013).

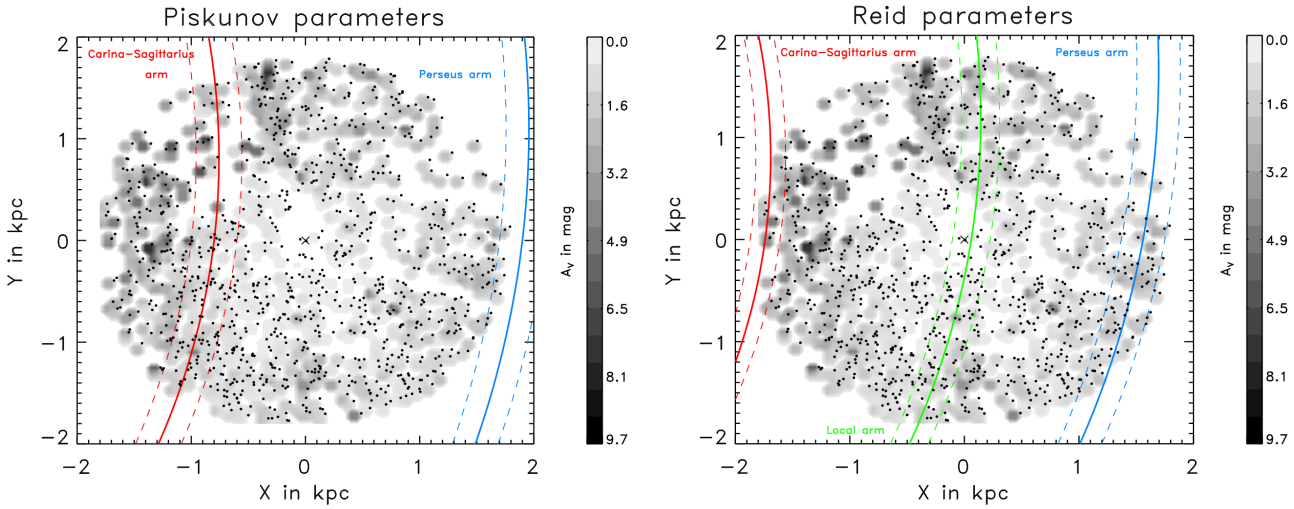

Figure 4.7: Effect of extinction and Galactic spiral arms on the spatial distribution of MWSC clusters. For the schematic spiral arms (Carina-Sagittarius arm - red, Perseus arm - blue, local arm - green) I applied parameters from Piskunov et al. (2006) (left panel) and Reid et al. (2014) (right panel). The grey scale illustrates the cluster extinction values as obtained from the MWSC. The cross shows the position of the sun.

To evaluate which aspect affected the distribution more, I compared the location of the MWSC clusters with the location of the Galactic spiral arms and an extinction map obtained from the MWSC in Fig. 4.7. The Galactic spiral arms should roughly follow logarithmic spirals and I used two sets of parameters for the nearby spiral arms. On the one hand, I applied the parameters provided by Piskunov et al. (2006), which were derived from a fit of logarithmic spirals to the location of young clusters in the Perseus and Carina-Sagittarius regions (left panel of Fig. 4.7). On the other hand, I used parameters determined by Reid et al. (2014) from trigonometric parallaxes and proper motions of masers (right panel of Fig. 4.7). For the Piskunov set the Carina-Sagittarius arm directly crosses one of the voids and the Perseus arm is outside the considered area, while for the Reid set all spirals were outside the voids and, in particular, the local arm is well associated with the central overdensity. The MWSC provided extinction values for all listed objects, which were used to create the contour map shown in Fig. 4.7. These contours were not equivalent to an extinction map, because no values were available for regions between the MWSC objects, they merely give a rough idea on the extinction distribution in the Galactic open cluster population. Towards the edges of the left apparent void the extinction values seem to increase, while towards the right apparent void a trend in extinction is not that clear. This indicated that at least the left apparent void is likely to be caused by obscuration though gas or dust clouds in the Galactic disc.

It can be concluded that both effects, the spiral structure and obscuring clouds, contributed to the apparent slightly inhomogeneous spatial distribution of the MWSC clusters and associations, but that in general the Galactic cluster population within the completeness limit could be assumed to be distributed homogeneously. For the construction of the MWSC additional input catalogues were considered to create a more extensive parameter set, namely 2MASS, PPMXL, and SDSS. The latter was mainly used to extend the RV information on OC members. Because of this difference in input catalogues between MWSC and COCD, I wanted to evaluate how representative the MWSC was for the COCD. First, I compared the spatial distribution in the XY-plane of clusters in both catalogues (left panel of Fig. 4.8). The majority of COCD clusters (red dots) showed an offset compared to the positions of MWSC clusters, which was more significant in the XY-plane than in the RA-DEC distribution (right panel in Fig. 4.8).

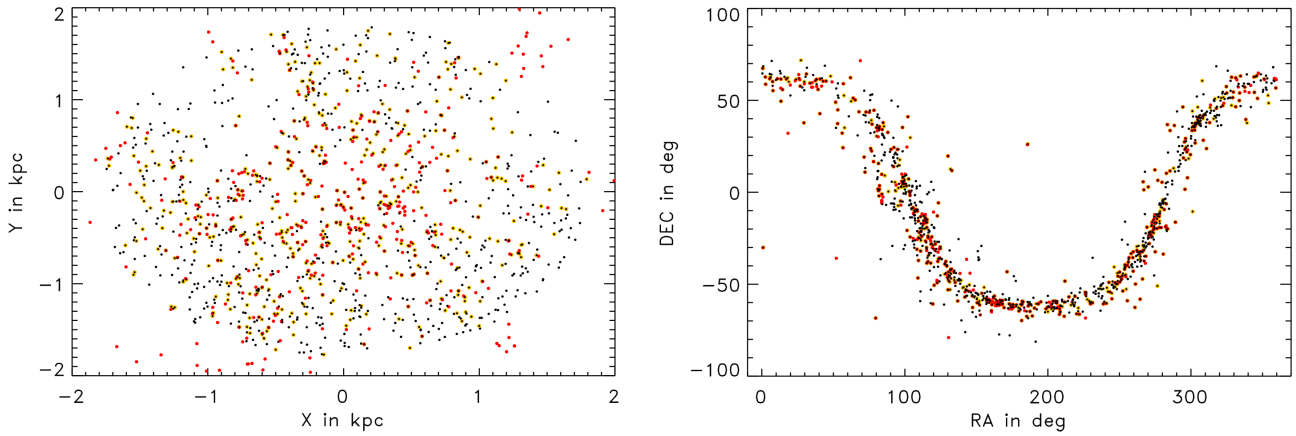

Figure 4.8: Distribution of open clusters in the XY-plane (left) and in RA-DEC coordinates (right). The black dots correspond to all MWSC clusters within the completeness limit of 1.8 kpc, yellow dots indicate MWSC clusters equipped with RVs and red dots show my COCD working sample.

A direct comparison in the Galactic coordinates (l and b) for a common sample in MWSC and COCD (see Fig. 4.9) verified that the shift in cluster centre position in the XY-plane between COCD and MWSC was not caused by changes of the input coordinates, but more likely by the revised cluster distances (see Fig. 4.14 panel a).

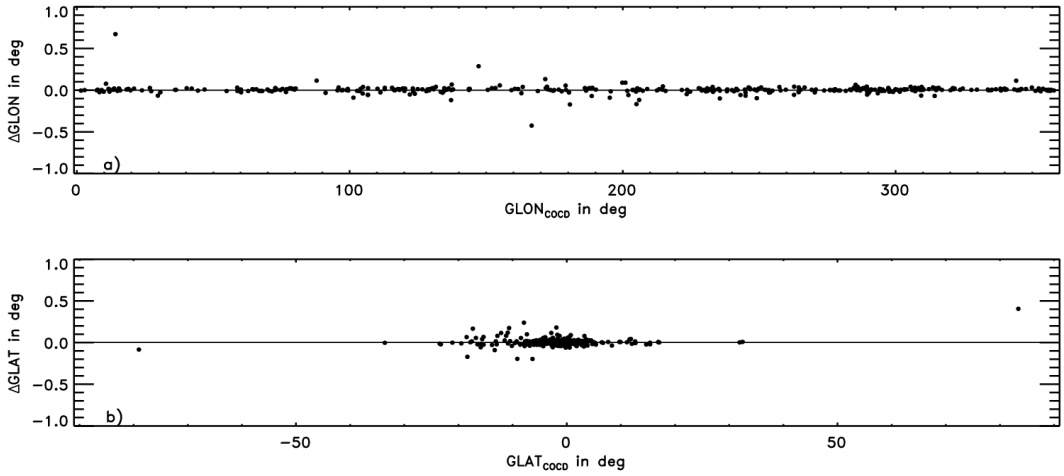

Figure 4.9: Comparison in the Galactic coordinates between COCD and MWSC: Galactic longitude (l; panel a) and Galactic latitude (b; panel b). The differences were computed as $\Delta(l, b) = (l, b)_{MWSC} - (l, b)_{COCD}$ and the black solid lines indicate zero-difference for reference.

Another aspect to evaluate was how the identified OC groupings were affected by the differences in the XY-plane between COCD and MWSC. Therefore, I extracted the members of the identified OC groupings in the MWSC and visualise the comparison for the position of the identified OC gropings in COCD and MWSC in the left and right panel of Fig. 4.10, respectively. The very local groupings (< 500 pc) appear to be of very similar position, but for the more distant groupings the members show larger separations in the XY plane. This illustrated very well the issue stated earlier, that the XY-positions changed noticeable between the COCD and the MWSC probably because of revised OC distances, which could result in different groupings identified in the MWSC than in the COCD.

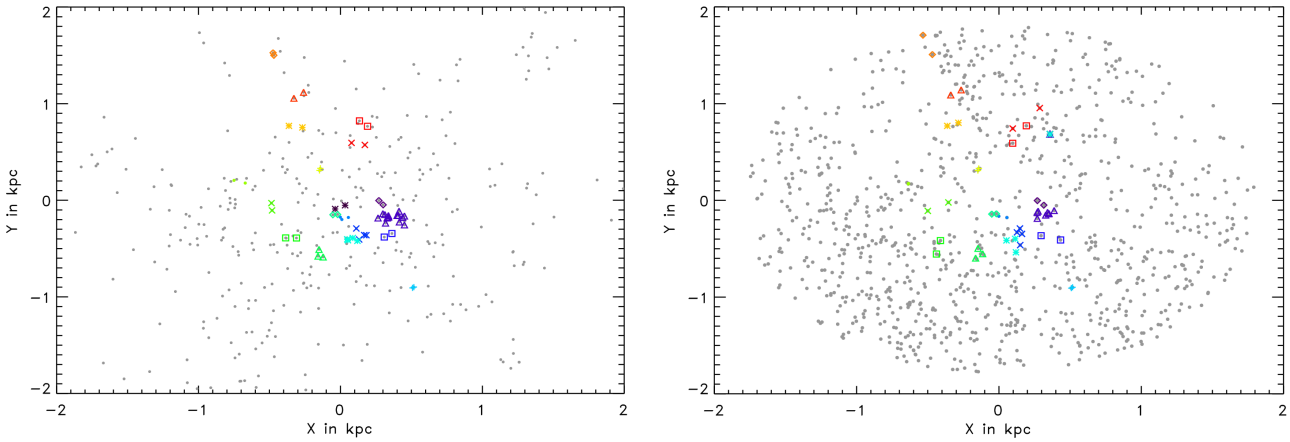

Figure 4.10: Comparison for the location of OC groupings between the COCD (left panel) and MWSC (right panel). The groupings were highlighted by different colours and symbols and refer to those detected in the COCD with linking lengths 100 pc and 10 km/s. The grey dots refer to the remaining COCD (left) and MWSC (right) clusters, which did not belong to a grouping.

To investigate the differences between MWSC and COCD in more detail, I compared the distributions for the Cartesian XYZ-coordinates and UVW-velocities for the selected common sample (Fig. 4.12). They agree very well and show very similar shape for both catalogues. Also the distributions for the separations between the nearest neighbours (Fig. 4.11) agree very well between both catalogues. Hence, for general studies of the Galactic open cluster population the MWSC is a good reference catalogue for the COCD.

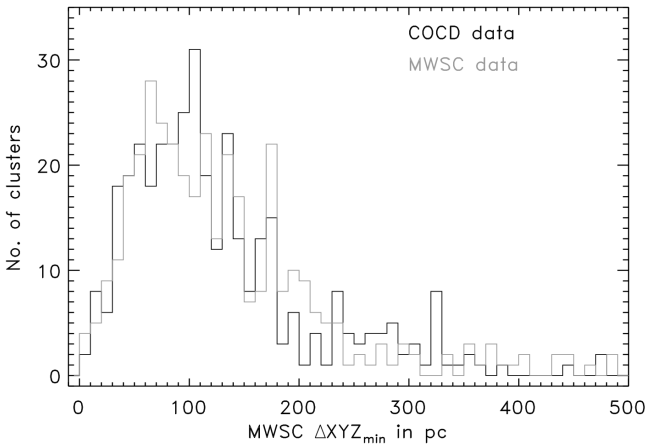

Figure 4.11: Histogram comparison for the spatial separation between nearest neighbours in the COCD (black) and the MWSC (grey) within the MWSC completeness limit of 1.8 kpc.

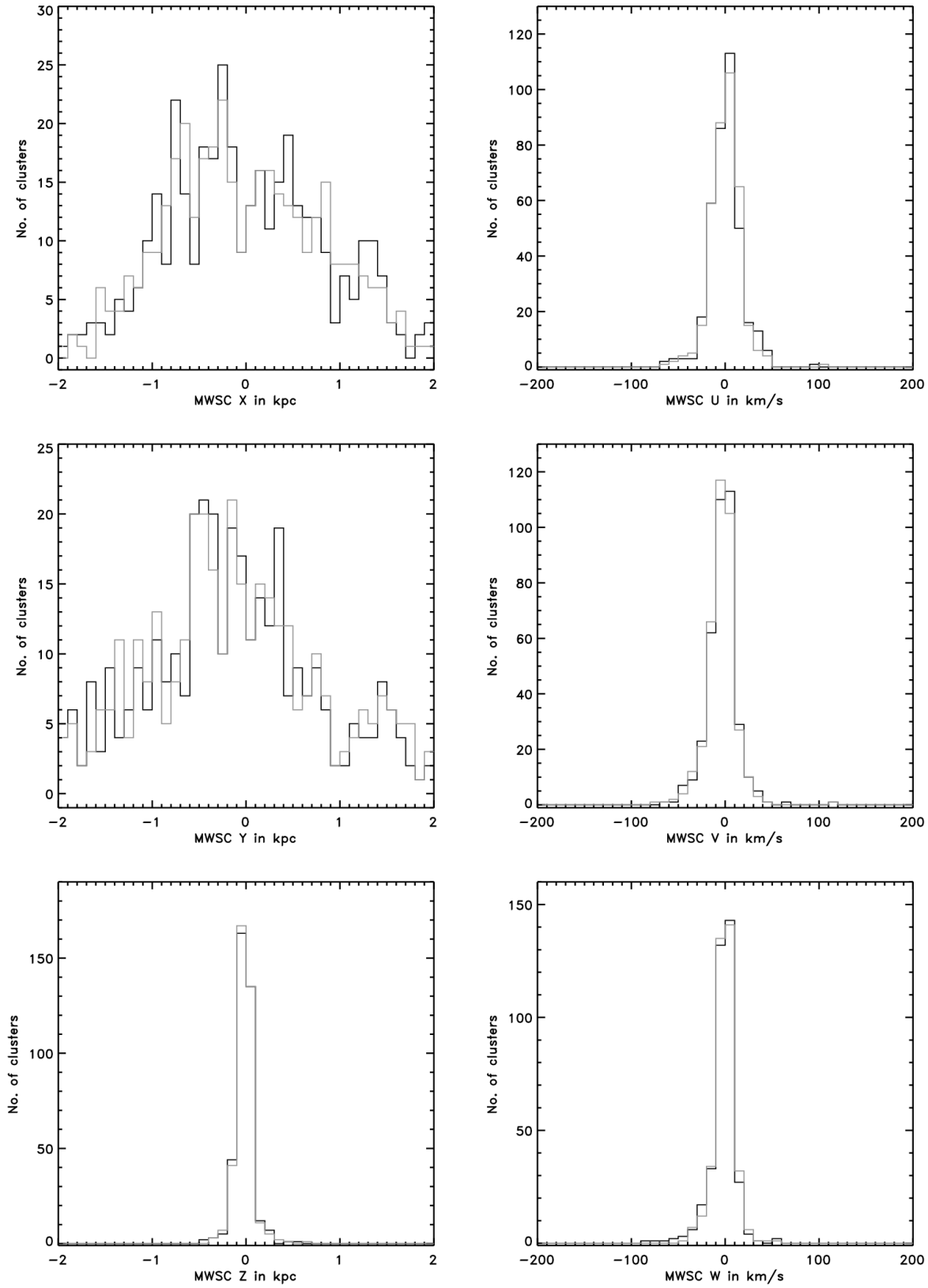

Figure 4.12: Comparison between the COCD and MWSC for the distributions of the Cartesian XYZ-coordinates (left panels) and UVW-velocities (right panels).

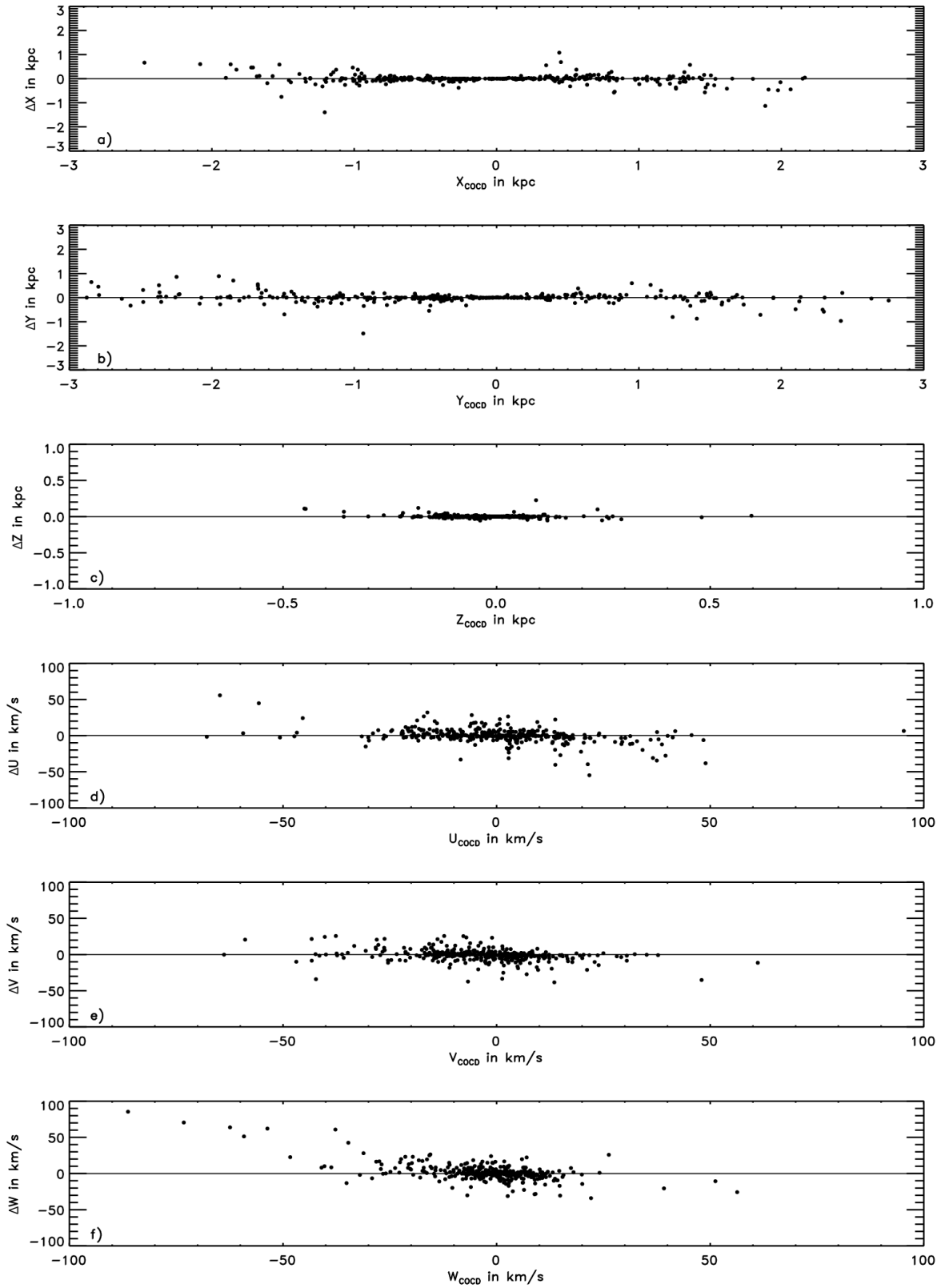

Figure 4.13: Comparison between the COCD and MWSC for the values of the Cartesian XYZ-coordinates (a-c) and UVW-velocities (d-f). The solid lines illustrate zero-difference between the catalogues.

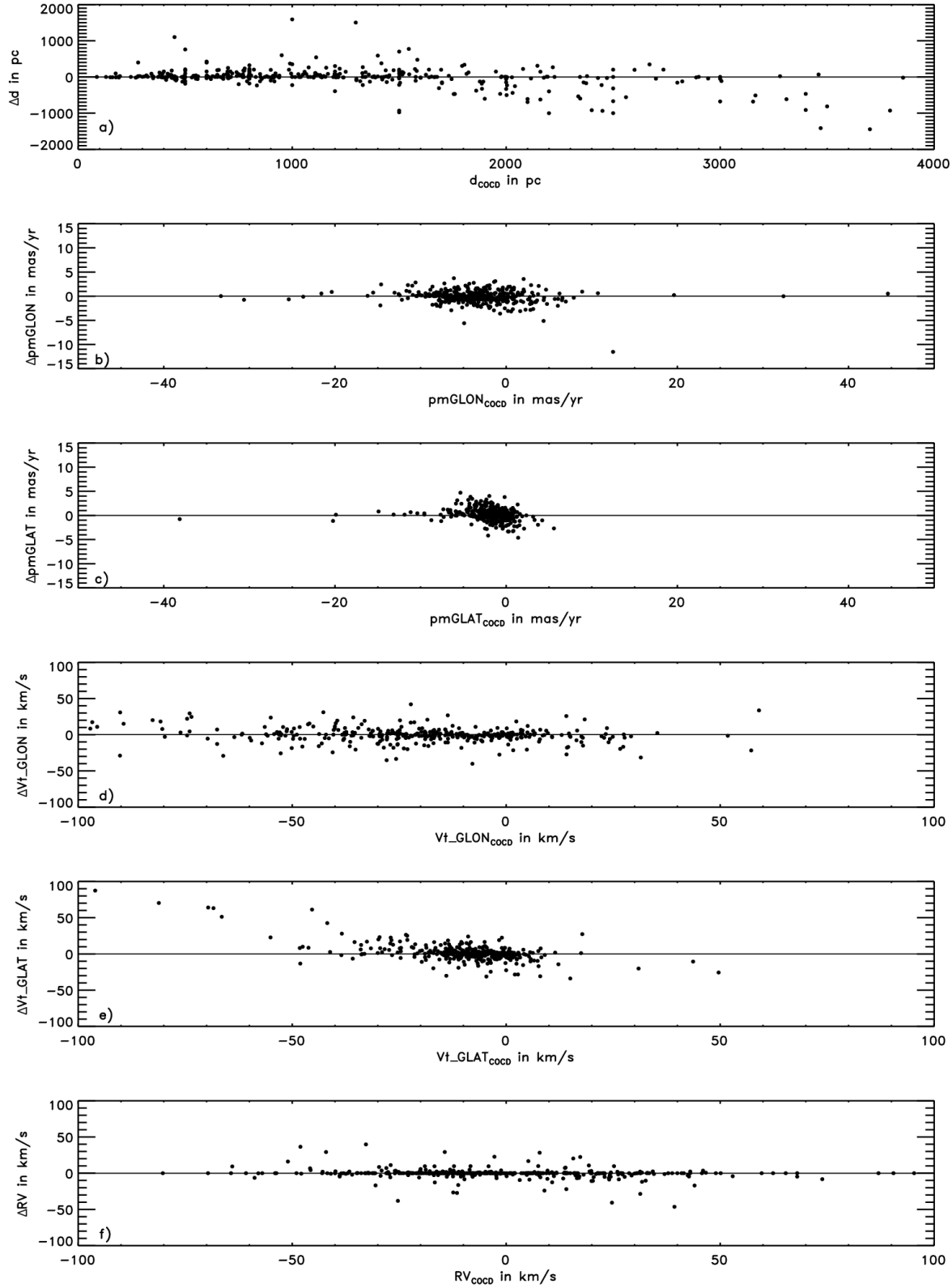

Figure 4.14: Comparison between the COCD and MWSC for the distance to the sun (panel a), proper motions in l and b (panel b and c), tangential velocities in l and b (panel d and e), and radial velocity (panel f). The solid lines illustrate zero difference between the catalogues.

Still, the question remained which input parameters caused the location offset in the XY-plane and how these differences affected the identification of OC groupings. Therefore, I compared the COCD and MWSC values for the individual clusters and the corresponding residuals were computed as $\Delta A = A_{MWSC} - A_{COCD}$, with A being the parameter of interest. Fig. 4.13 those for the output parameters (Cartesian coordinates and velocities) and Fig. 4.14 illustrates the comparison for the input parameters (distance, proper motion, tangential, and radial velocity).
First, I wanted to discuss the comparison for the output parameters, namely the XYZ-coordinates and the UVW-velocities (Fig. 4.13), to get a first hint on what is causing the shift in the cluster centre position between MWSC and COCD, as detected in Fig. 4.8. The X and Y coordinates (panel a and b of Fig. 4.13) show a very good agreement in the immediate solar vicinity (d≥ 1 kpc), but for more distant clusters larger differences of up to 1 kpc are present. The Z coordinates (panel c of Fig. 4.13), on the other hand, agree very well between both catalogues for all values. This indicated that with increasing distance the difference in XY-position is also increasing. This has no effect on the Z component, because open clusters are primarily located in the Galactic disc and their Z values are within a few 100 pc. The U and V velocities (panels d and e of Fig. 4.13) show no such clear tendency and agreed quite well, although they show a slight negative slope, which is most likely connected to the change in distance estimate. Only in W (panel f of Fig. 4.13) the differences between COCD and MWSC seem to increase with larger values, which could be due to the W velocity component being more affected by the radial velocity than the U and V components.
Second, I discussed the input parameters, namely distance, proper motions, tangential and radial velocities (Fig. 4.14), to strengthen the finding stated above. The distances (panel a) show increasing differences between the COCD and MWSC with larger distances. For clusters with $d > 2$ kpc even a negative slope is visible, implying that the distance estimates in the MWSC are systematically smaller than those in the COCD. The proper motions (panels b and c) agree very well, although in PM_b they show a slight negative slope. The radial velocities (panel f) show differences of typically below 20 km/s and reach in maximum up to 50 km/s, which is consistent with the uncertainty range found for the cluster population and for their members. When converting the proper motions to tangential velocities, to make them more comparable to the RV values, the differences in the comparison between COCD and MWSC became more noticeable. In each component they are spread further than in the RV comparison and even reached values of 100 km/s. They also reflect the negative slope seen in the distance comparison. The larger differences in the tangential velocities than in the RV indicated that the changes in distance estimate between COCD and MWSC played the dominant role for the shifts of position in the XY-plane.

MWSC SUBSAMPLE

In addition, I explored how the difference in the Cartesian parameters affected the statistics for the group identification and implemented Monte-Carlo simulations with a randomised sample created as a subsample of the MWSC with the same size as my working sample, hereafter abbreviated MC_{MWSC}. The MWSC listed 433 clusters with available RV information within its completeness limit, while only 333 COCD objects with RV data were located within a distance of 1.8 kpc. Therefore, I randomly selected 333 out of the 433 OCs in the MWSC completeness limit.
The mean spatial separation and velocity difference distributions for 1000 realisations of the MC_{MWSC}, as displayed in Fig. 4.16, look very similar to the corresponding histograms in the COCD working sample. Also the averaged parameter distributions (Fig. 4.15) for 1000 realisations of the MC_{MWSC} agree very well with those from the COCD working sample. Both aspects indicate that the statistics in the COCD and MWSC are in very good agreement for general investigations of Galactic open clusters.

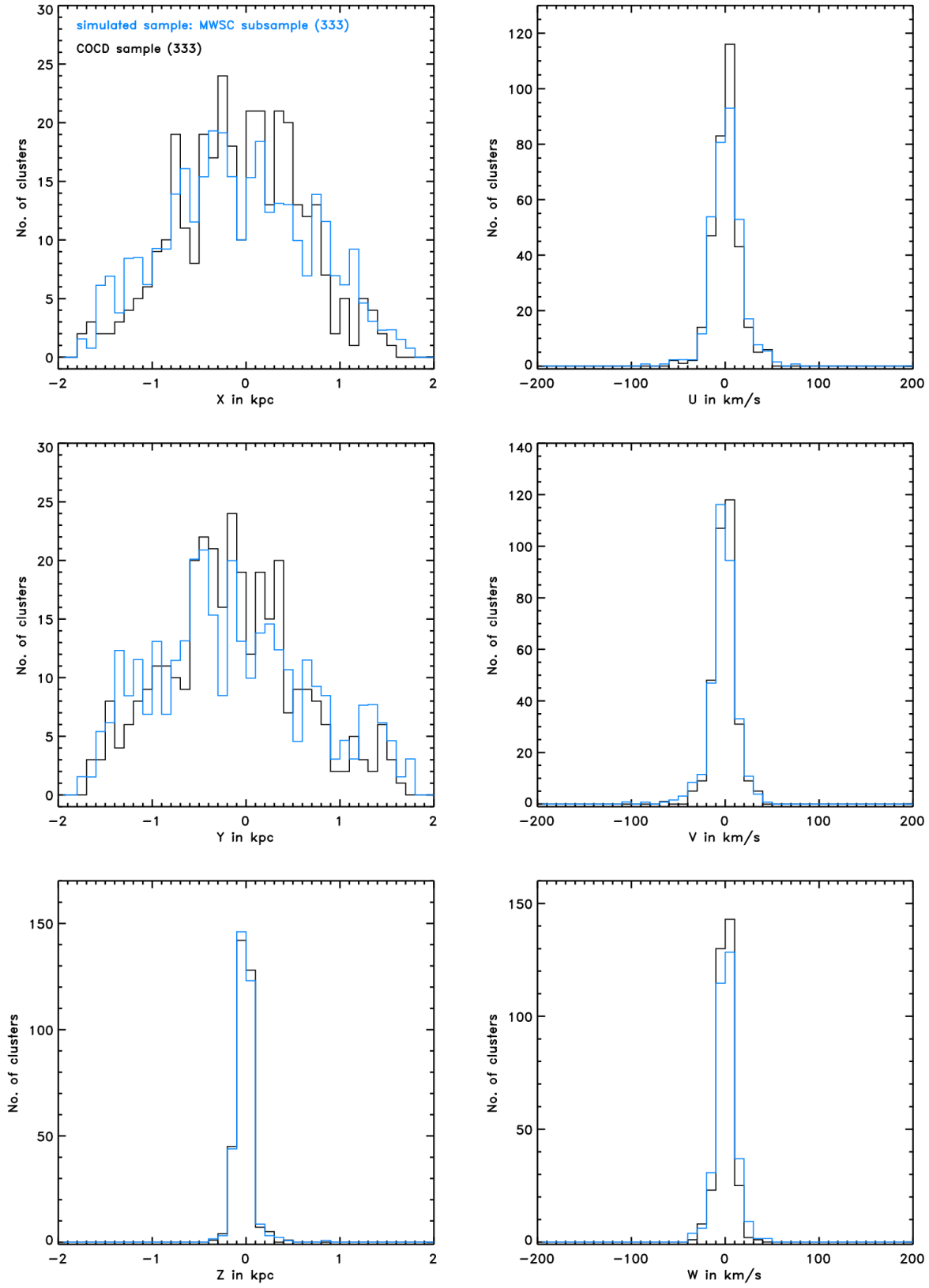

Figure 4.15: Distributions of the XYZ-coordinates (left panels) and UVW-velocities (right panels) for 1000 realisations of the MC_{MWSC} (blue) in comparison with the COCD working sample within 1.8 kpc (black) for comparison.

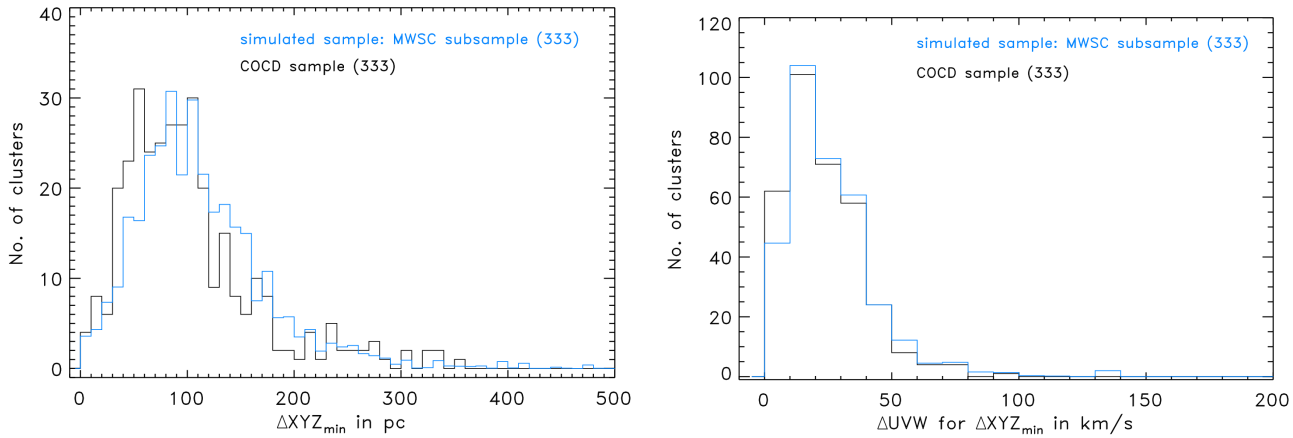

Figure 4.16: Histograms for the spatial separation (left panel) and velocity difference (right panel) for the nearest neighbours in coordinate space. The blue histograms show the averaged distributions for 1000 realisations of the MC_{MWSC}. The black histograms show the corresponding distributions in my working sample.

For the identification of the OC groupings, I applied the same FoF-like algorithm as for my COCD working sample with the first set of linking lengths (100 pc and 10 km/s). Fig. 4.17 illustrates the distributions for the number and size of the identified groupings in 1000 realisations of the MC_{MWSC} in comparison with the results from my working sample in the COCD. The MC_{MWSC} randomised sample recovered relatively well the number of identified OC groupings found in my working sample, since the value for my working sample is within the 1σ level of the distribution. However, in the simulated sample only pairs were detected, while in my working sample also groups and one complex were found.

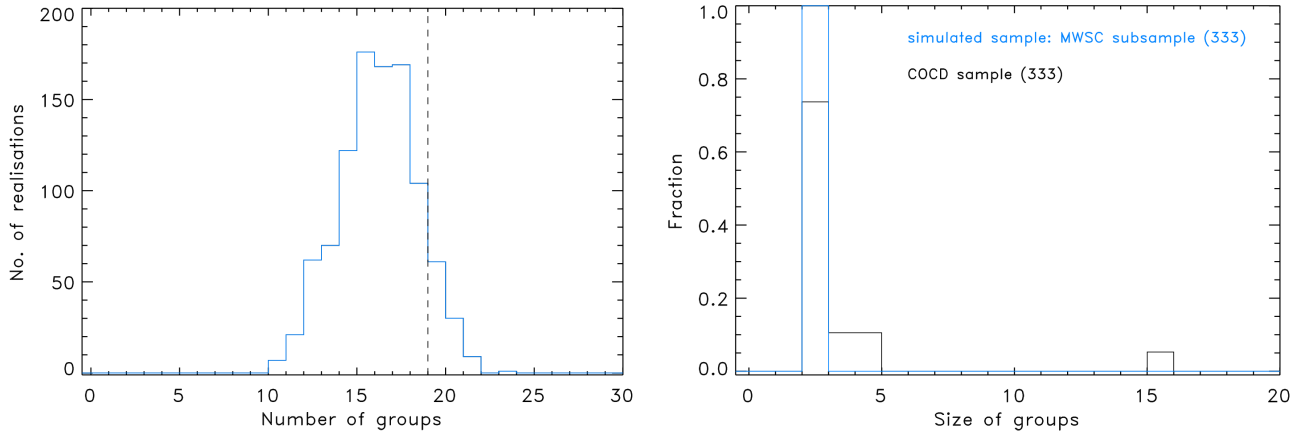

Figure 4.17: Histograms for the number (left panel) and size (right panel) of the identified OC groupings from 1000 realisations of the MC_{MWSC} (blue) for linking lengths 100 pc and 10 km/s. The black histogram and dashed line show the results for the COCD working sample.

In addition, I carried out the same Monte-Carlo simulations using the second set of linking lengths (100 pc and 20 km/s) for the group identification in the randomised sample. The results for the number and size of detected groupings are similar (Fig. 4.18), although the value for the number of groupings from the working sample is slightly outside the 1σ level of the simulated distribution and that not only pairs but also a fraction of triples (~ 0.01) was found. This was most likely because of the increased value for the velocity linking length, allowing larger 3D-velocity differences within the groupings.

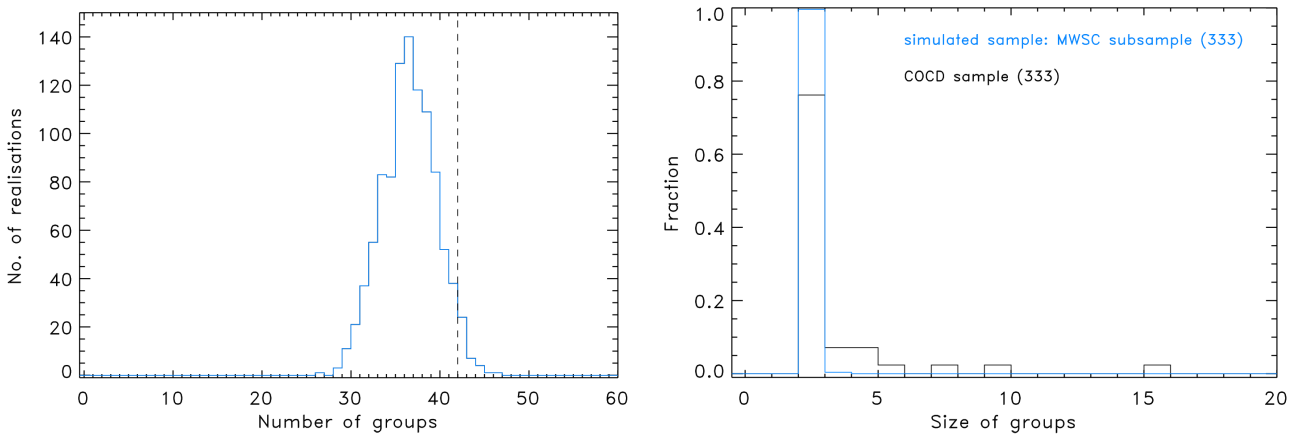

Figure 4.18: Histograms for the number (left panel) and size (right panel) of the identified OC groupings from 1000 realisations of the MC_{MWSC} (blue) for linking lengths 100 pc and 20 km/s. The black histogram and dashed line show the results from the COCD working sample.

All in all, the MWSC can safely be considered a good reference catalogue for the COCD when investigating general aspects. The relatively good agreement for the number of groupings detected in the MC_{MWSC} simulated sample with the results from the COCD working sample supported the suspicion of structure in the Galactic open cluster population. However, finding exclusively pairs in the randomised MWSC subsample suggested that not only the different distance estimates in the COCD and MWSC affect the identification of OC groupings, but also that the random selection of clusters in a highly incomplete sample significantly decreased the possibility to detect larger groups.

4.3.2 MONTE-CARLO SIMULATIONS

To evaluate the significance of the identified structure, I carried out Monte-Carlo simulations with randomised data sets. On contrary to the simulations described in the previous section, the input for the Monte-Carlo simulations presented in the following were based on general distributions and were not a random subset of actual data. All simulations were implemented within the completeness limit of the MWSC, which was ensured through the criterion $\sqrt{X^2 + Y^2 + Z^2} \leq 1.8$ kpc,. This was applicable because all groupings that were identified in the working sample were located within 2 kpc for both sets of linking lengths. Within this region my working sample decreased to 333 open clusters, defining the size of the simulated sample for a better comparison. As input distributions for the XYZ-coordinates and UVW-velocities I applied two different approaches. On the one hand, a uniform spatial distribution in the Galactic disc and Gaussian profiles in the velocities with the width defined by the typical velocity dispersion in the Galactic disc. On the other hand, I used the actual spatial and velocity distributions in my working sample as input.
For consistency purposes I applied the same FoF-like algorithm, as performed on my working sample, for the group identification in the simulated data with linking lengths of either 100 pc and 10 km/s or 100 pc and 20 km/s. To draw statistically robust conclusions on the significance of the identified structures, I compared the actual COCD results to averaged distributions for the parameters and resulting distributions for the number and size of detected groupings obtained from 1000 realisations of the Monte-Carlo simulations for both approaches of input distributions.

SIMULATION INPUT: UNIFORM DISTRIBUTION

In general, open clusters are expected to be distributed almost homogeneously in the Galactic disc. Thus, in a first step, I assumed a uniform distribution in the X and Y spatial components and a sech profile in Z, as expected for the vertical distribution in the Galactic disc. The width for the sech-profile was assumed to be equivalent to the estimated thickness of the thin disc in the solar neighbourhood of about 1 kpc in total and 500 pc from the midplane. Since the UVW-velocities were corrected for solar motion and differential rotation, it was safe to assume that the velocity components of the simulated sample would follow Gaussian profiles. The mean for these assumed Gaussian profiles were set to zero and the sigma was expected to be equivalent to the velocity dispersion in the solar neighbourhood of about 5 km/s in each component. Hereafter I abbreviate this set of simulations as MC_{Uni}.

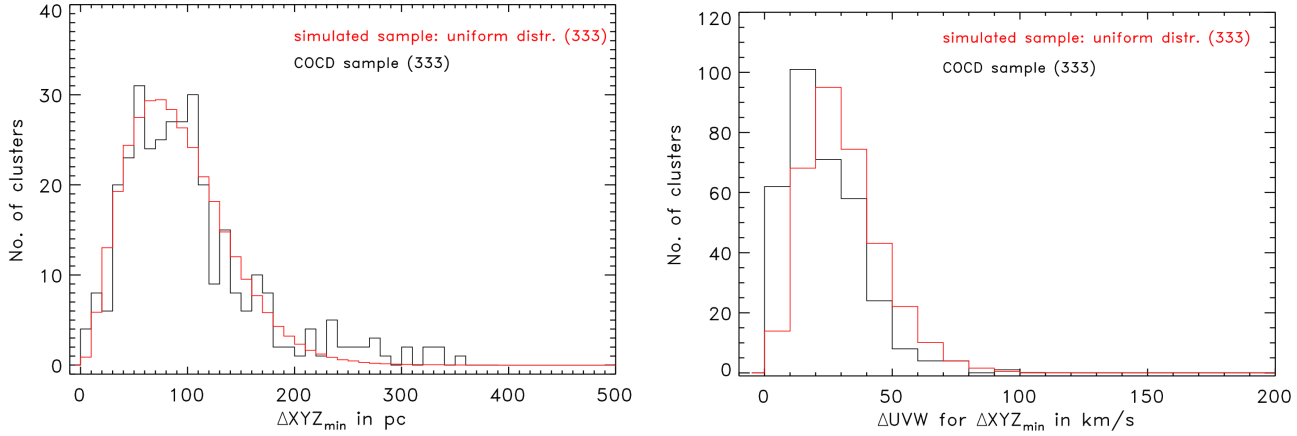

Figure 4.19: Histograms for the spatial separation (left panel) and velocity difference (right panel) for the nearest neighbours in coordinate space, averaged for 1000 realisations of the MC_{Uni} (red). The black histograms show the distributions for the COCD working sample.

The resulting averaged distributions for the spatial separation of the nearest neighbours in XYZ-space (left panel of Fig. 4.19) agree very well, while the corresponding velocity differences (right panel of Fig. 4.19) show a slight offset between the real and simulated data.

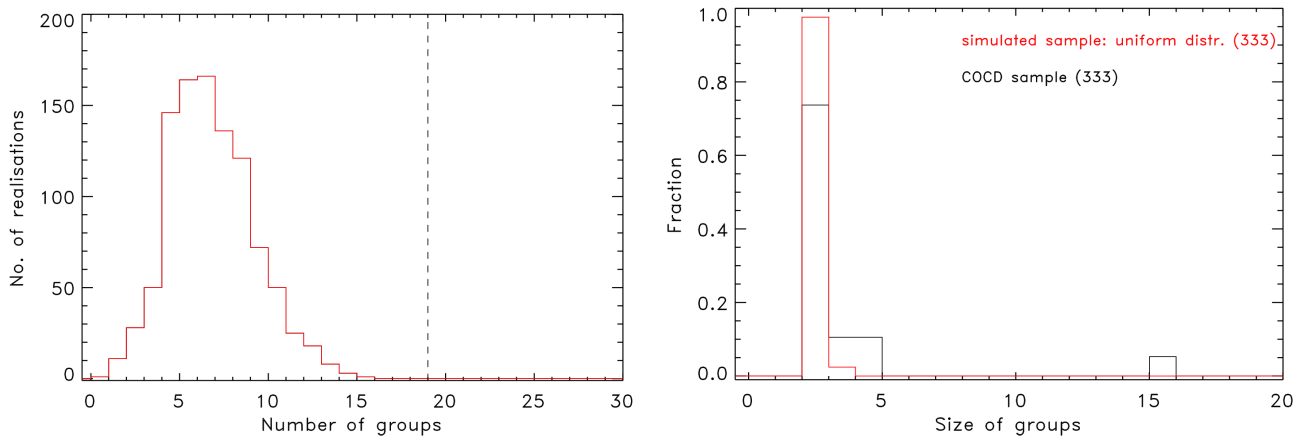

Figure 4.20: Histograms for the number (left panel) and size (right panel) of identified OC groupings from 1000 realisations of the MC_{Uni} (red) for linking lengths of 100 pc and 10 km/s. The black histogram and dashed line show the results for the COCD working sample.

The distribution for the number and size of the identified groupings in the simulated sample, using the first set of linking lengths (100 pc and 10km/s; see Fig. 4.20), also show discrepancies between the results for the simulated and real data. In the MC_{Uni} typically 5-6 groupings were found, while in the COCD working sample 19 groupings were identified. The vast majority of the groupings in the MC_{Uni} were pairs complemented by a few triples, while in the COCD working sample the fraction of groupings with three or four members is larger and even a complex with 15 members was identified. The discrepancies in the number and size of the found OC groupings in the simulated sample to the results from the COCD working sample suggested that the majority of the detected groupings could be real, but the discrepancies in the comparison for the parameters (see Fig. 4.22) put this finding in a relative perspective.
The Monte-Carlo simulations performed with the second set of linking lengths (100 pc and 20 km/s) yielded similar results (see Fig. 4.21), only the number of detected groupings showed a slightly smaller offset to the result for my working sample and the fraction of triples in 1000 realisations of the MC_{Uni} slightly increased, which could be expected when using a larger value for the velocity linking lengths.

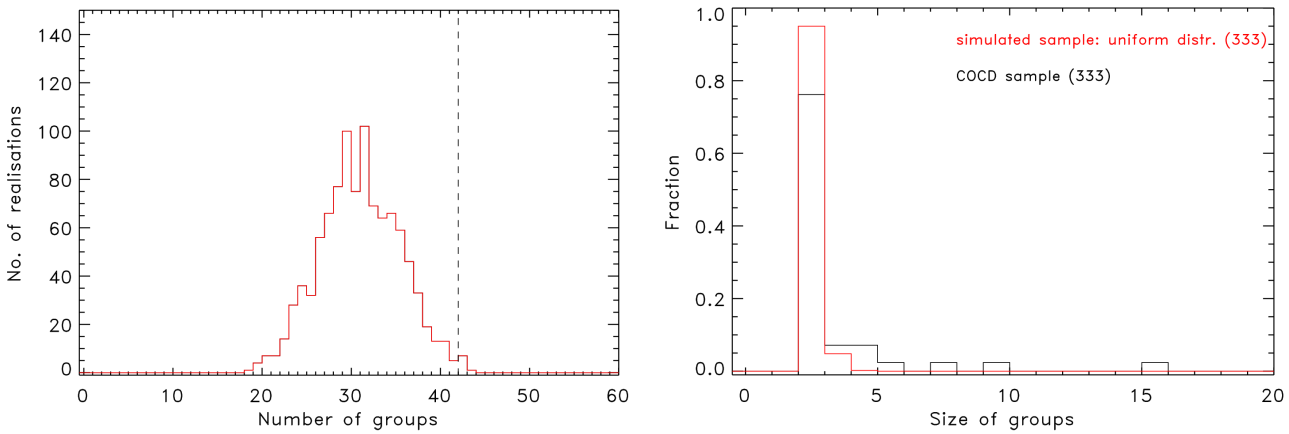

Figure 4.21: Histograms for the number (left panel) and size (right panel) of identified OC groupings from 1000 realisations of the MC_{Uni} (red) for linking lengths of 100 pc and 20 km/s. The black histogram and dashed line show the results for the COCD working sample.

In addition, I compared the averaged distributions of the Cartesian coordinates and velocities from 1000 realisations of the MC_{Uni} with the corresponding distributions for my working sample in the considered area (Fig. 4.22). The Z component, as well as the V and W velocities, show a good agreement, whereas the averaged distribution in U for the simulated sample is slightly broader than the one for the COCD working sample. In the X and Y coordinates a significant disagreement between the simulated and real sample is present.
This indicates that the chosen input distributions are not as suitable for describing the actual COCD data as expected. This might have been induced by the incompleteness of the working sample, especially regarding RV information. The disagreement in the X and Y coordinates between the MC_{Uni} and COCD data could also be responsible for the large discrepancy in the number and size distributions for the detected OC groupings in both samples. Thus, I checked if a different setup for the Monte-Carlo simulations would lead to a different result and a better agreement in the representation of the actual COCD working sample. These results are presented in the following section.
However, first I wanted to answer the question whether the general distribution of the open clusters can be considered to be homogeneous and created another randomised data set using Monte-Carlo simulations ($MC_{XYcheck}$). I assumed the same input distributions as for MC_{Uni}, but created a randomised sample of 1000 objects within a distance of 1.8 kpc, which corresponds to the size of the cluster sample within the MWSC completeness limit, regardless of available RV information.

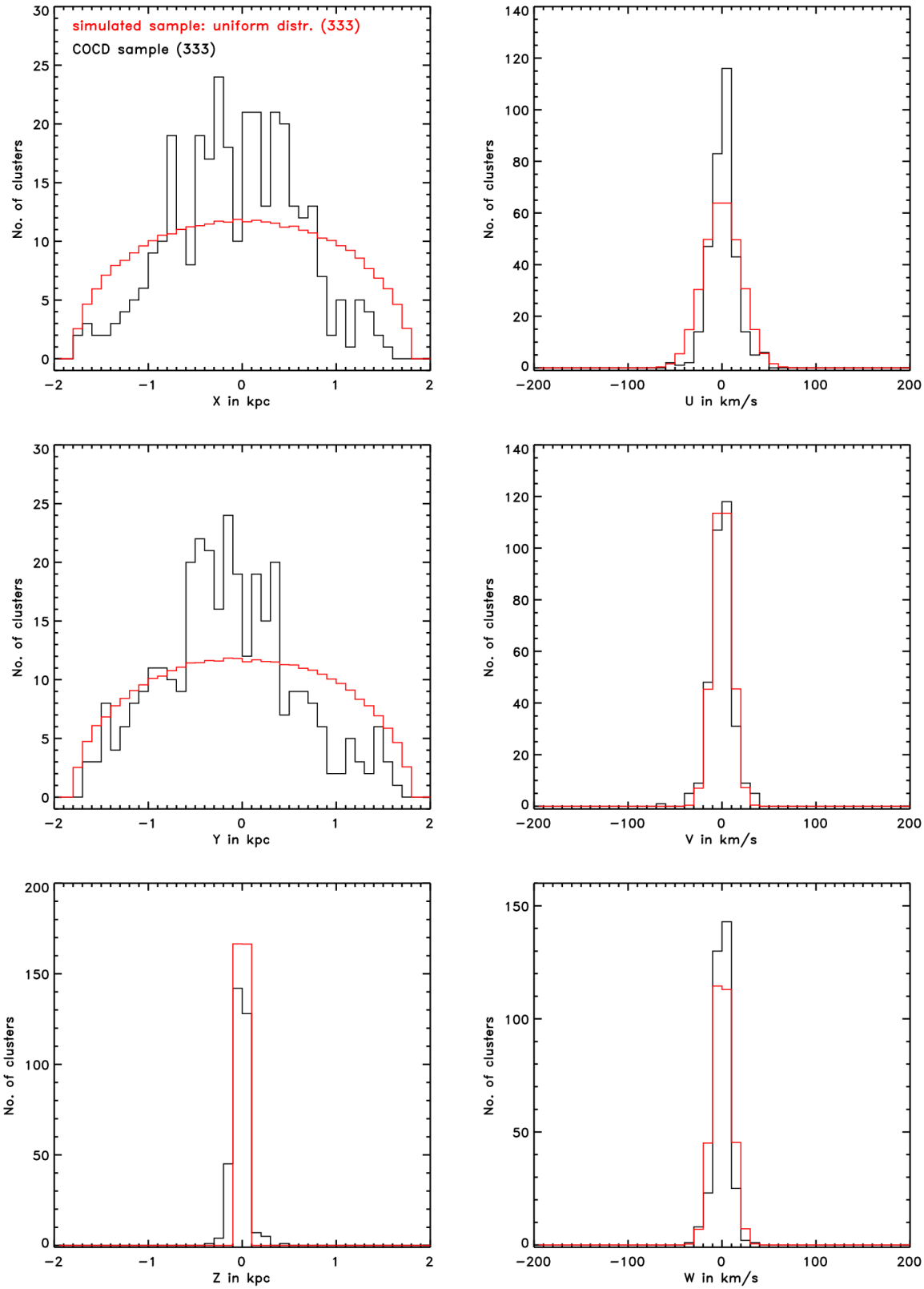

Figure 4.22: Distributions for the XYZ-coordinates (left panels) and UVW-velocities (right panels) averaged for 1000 realisations of the MC_{Uni} (red). The black histograms illustrate the distributions for the COCD working sample for comparison.

I compared the resulting distribution in the X and Y coordinates, averaged over 1000 realisations of the $MC_{XYcheck}$, to the X and Y distributions in the MWSC within the same area, as displayed in Fig. 4.23. One can see that the distributions for the simulated and real sample agree quite well, which confirmed that, in general, the Galactic open cluster population could be considered distributed almost homogeneously, but the subset of OCs with available RV data appeared to be not that uniformly distributed. This could be because of selection effects present for the spectroscopic observations, which could not be specified further in this work. Hence, the approach is reasonable, but not applicable for the working sample used in this work.

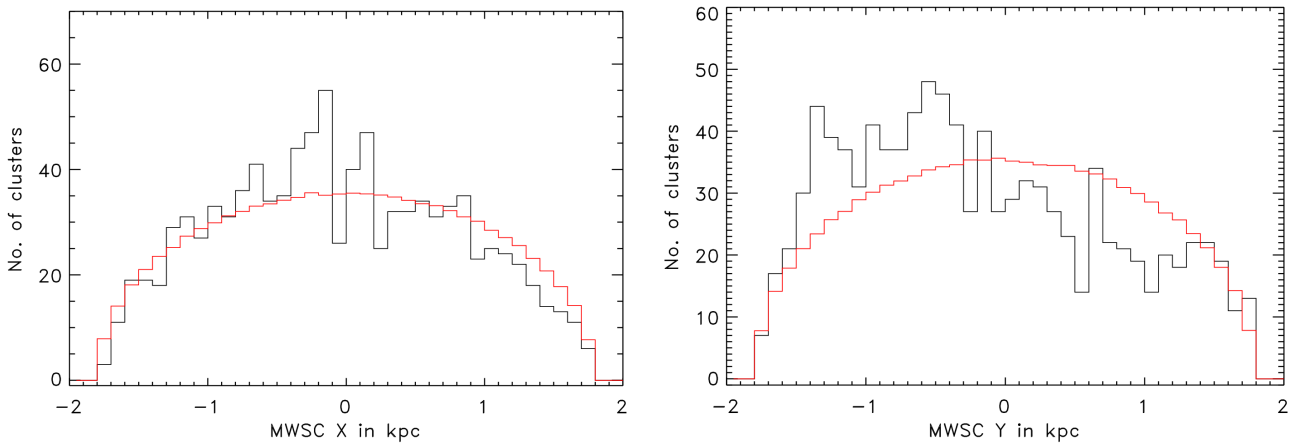

Figure 4.23: Averaged distributions in X (left) and Y (right) coordinates for 1000 realisations of the $MC_{XYcheck}$ (red). The black histograms show the distributions for the real MWSC data in the same volume.

SIMULATION INPUT: COCD DATA DISTRIBUTIONS

Since a uniform distribution is not suitable to describe my working sample, I followed a second approach, namely using the actual data distributions of the working sample as input for the Monte-Carlo simulations, hereafter abbreviated MC_{Data}.

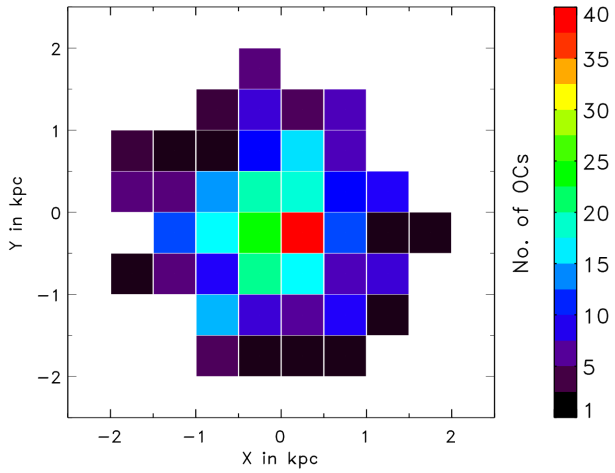

Figure 4.24: 2D-histogram illustrating the density distribution of COCD clusters in the XY-plane within the MWSC completeness limit of 1.8 kpc.

The COCD clusters were mainly located in or near the Galactic plane, which allowed me to consider the Z component of the 3D-position to be independent. In the XY-plane I used a 2D histogram to describe the density profile, as displayed in Fig. 4.24. The 2D-histogram was generated from my working sample with a bin size of 500 pc.

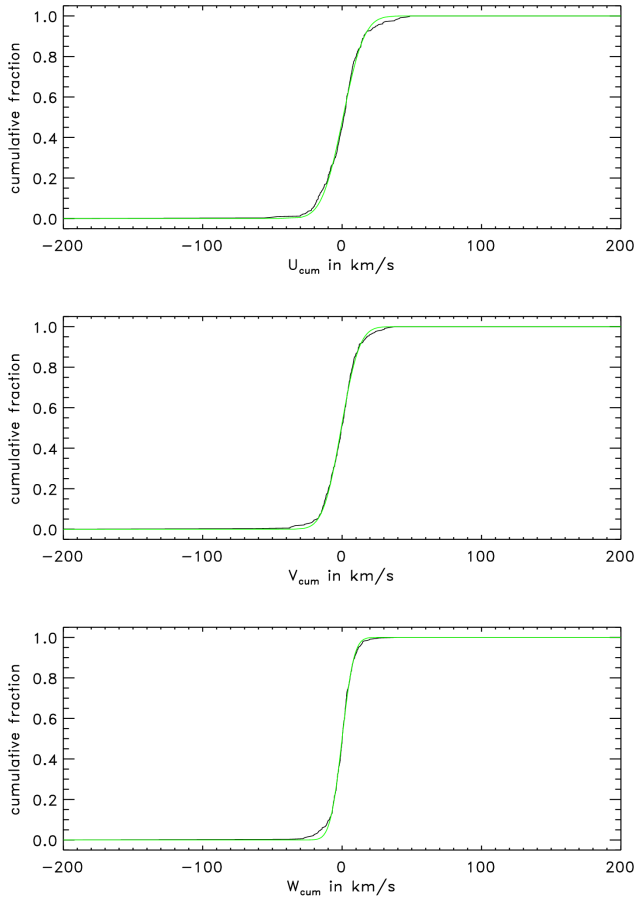

Figure 4.25: Cumulative distribution function for the UVW-velocities. The black lines show the distributions for the COCD working sample and the green lines are the corresponding fitted distributions.

In Z I fitted a sech-profile to the corresponding histogram in my working sample with a bin size of 100 pc. These bin sizes were chosen to include a reasonable number of clusters in each bin and to ensure that the structure investigated here was averaged out. For the velocity components I again assumed Gaussian profiles and fitted those to the cumulative distributions for my working sample, as shown in Fig. 4.25. This was done to gain a unique description of the distributions independent of bin size and to ensure that the structure in velocity space was also averaged out.

As for the MC_{Uni}, I compared the averaged distributions for 1000 realisations of the MC_{Data} of the spatial separations and velocity differences of the nearest neighbours in XYZ-space to those from my working sample, as shown in Fig. 4.26. On contrary to the MC_{Uni}, the spatial separation and velocity difference distributions from the MC_{Data} resulted in a better agreement with the COCD working sample. The comparison of the averaged distributions in the XYZ-coordinates and UVW-velocities for 1000 realisations of the MC_{Data}, as displayed in Fig. 4.27, also showed a better good agreement with the COCD working sample than the resulting averaged distributions for the MC_{Uni}. Both aspects verified that using the working sample distributions of the XYZ-coordinates and UVW-velocities as input for the Monte-Carlo simulations resulted in a more representative randomised sample of the actual data and would also make the results more reliable.

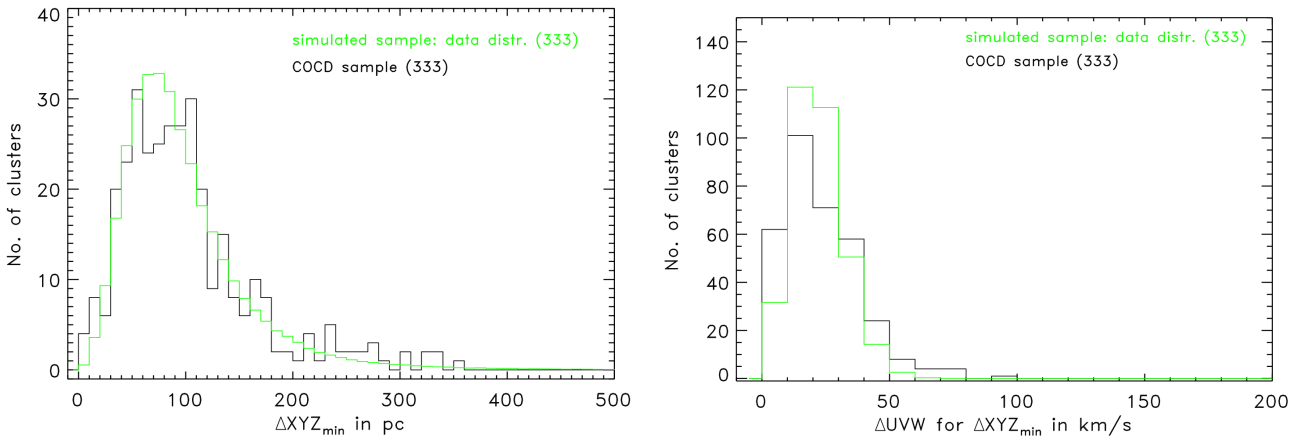

Figure 4.26: Distributions for the spatial separation (left panel) and velocity difference (right panel) of the nearest neighbours in XYZ-space for 1000 realisations of the MC_{Data} (green). The black histograms correspond to the results from my working sample.

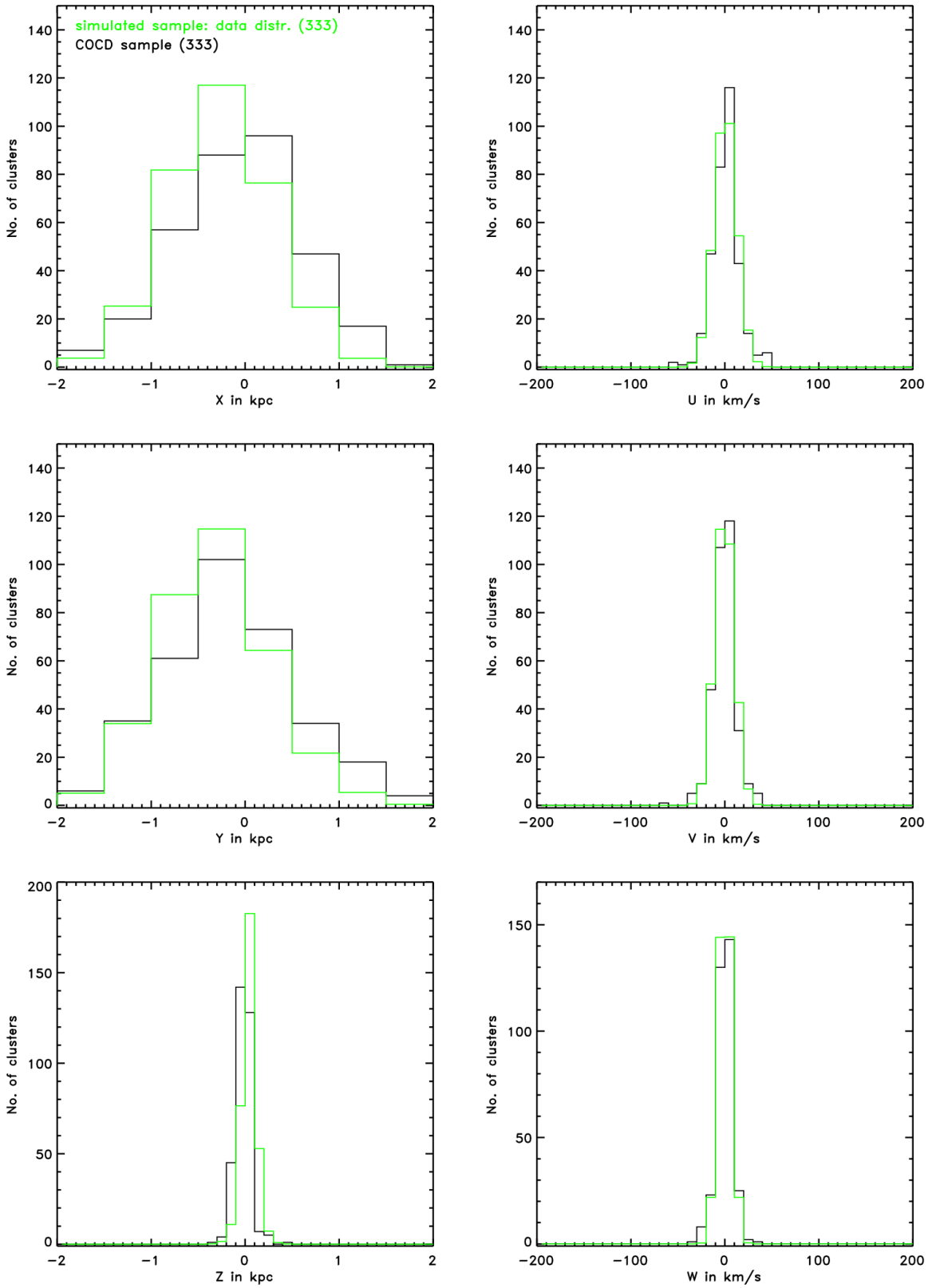

Figure 4.27: Distributions for the XYZ-coordinates (left panels) and UVW-velocities (right panels) averaged for 1000 realisations of the MC_{Data} (green). The black histograms illustrate the corresponding distributions for my COCD working sample for comparison.

Again I used the same FoF-like algorithm as for my working sample to identify OC groupings in the randomised sample with the first set of linking lengths (100 pc and 10 km/s) and illustrate the histograms for the number and size of the found groupings in 1000 realisations of the MC_{Data} in Fig. 4.28. The value for the number of identified groupings in my working sample is well covered by the distribution resulting from MC_{Data}, but again the found groupings in the randomised sample were heavily dominated by pairs, complemented by a few triples.

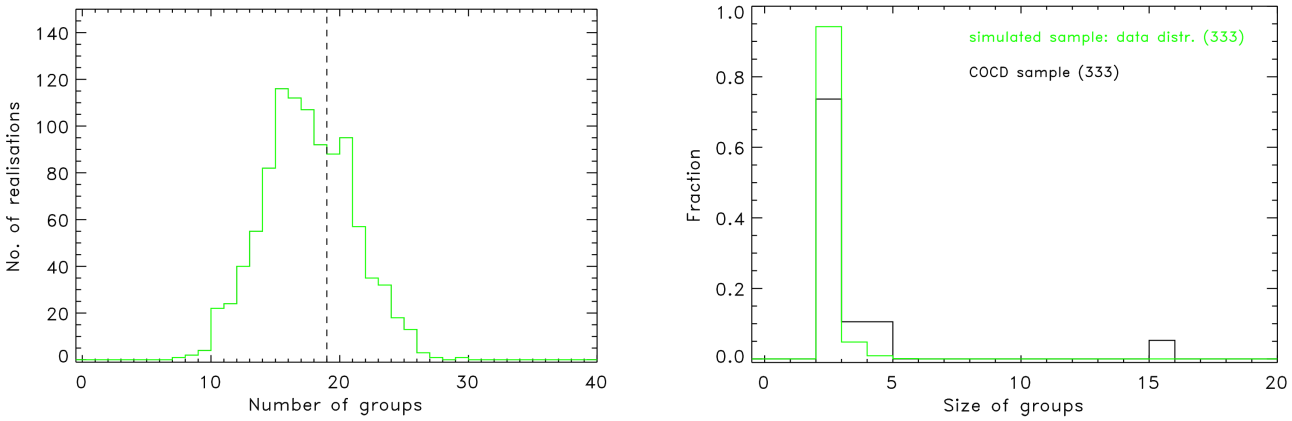

Figure 4.28: Histograms for the number (left panel) and size (right panel) of the identified OC groupings from 1000 realisations of the MC_{Data} (green) for linking lengths of 100 pc and 10 km/s. The black histogram and dashed line show the results from the COCD working sample.

For the MC_{Data} using the second set of linking lengths (100 pc and 20 km/s) I obtained similar results regarding the number and size of identified Galactic open cluster groupings in the simulated sample, compared to the results from the COCD working sample, as displayed in Fig. 4.29. Hence, I concluded that especially the detected OC pairs were statistically consistent with being random alignments and it would be challenging to verify the genuine pairs amongst them. The larger groups and the detected complex in the working sample, on the other hand, were more likely to be genuine. In particular the complex, because for both sets of linking lengths it had exactly the same members. Since for the MC_{Data} the distributions for the nearest neighbours and parameters agree better to the actual distribution in my working sample than for the MC_{Uni} simulations, the results for the former seem to be more reliable than the results for the latter.

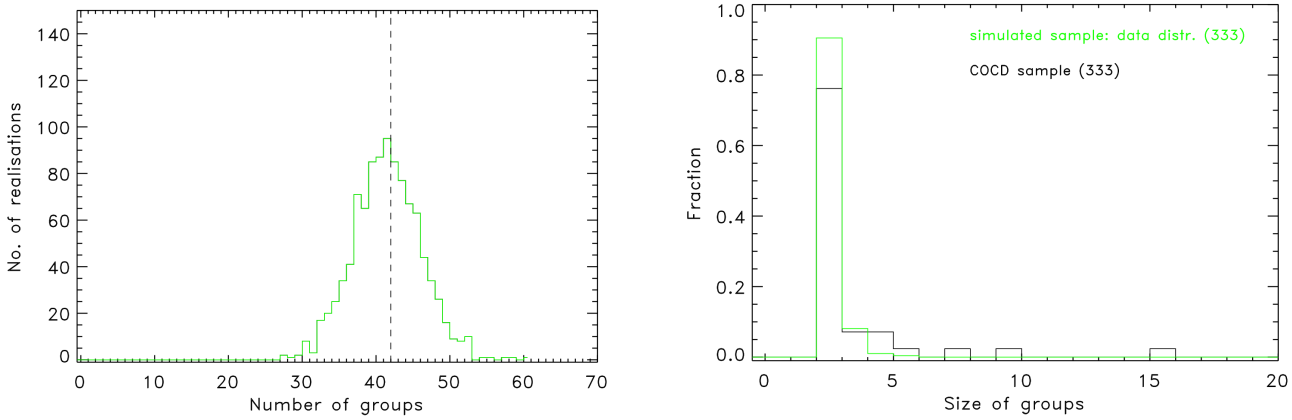

Figure 4.29: Histograms for the number (left panel) and size (right panel) of the identified OC groupings from 1000 realisations of the MC_{Data} (green) for linking lengths of 100 pc and 20 km/s. The black histogram and dashed line show the results from the COCD working sample.

In this work only a plausible range for the velocity linking length, namely 10 – 20 km/s, could be defined. The most probable value should lie within this range, but its definition would require a far more extensive OC sample with all 6D-phase space information available. A detailed investigation of the MWSC, complemented with OCs only visible in the infrared would be one step in this direction. Such an extended study could not be carried out in the framework of this project and remains an open question for future investigations.

SECTION 4.4

CHARACTERISATION OF THE FOUND OPEN CLUSTER GROUPINGS

In this section I want to discuss the characteristics for the identified groupings and, in a first step, I compared the position of the detected OC groupings with the spiral structure in the Galactic disc, as described by Reid et al. (2014) and visualised in Fig. 4.30. For the first set of linking lengths (100 pc and 10 km/s, left panel) the found groupings appear to roughly follow the spiral structure, but for the second set of linking lengths (100 pc and 20 km/s, right panel) the corresponding OC groupings also cover the areas in between. This indicates that the apparent correlation between the location of the found groupings and Galactic spiral structure could be simply a selection effect, because RV information were more accessible for nearby objects. It is more likely that the OC groupings are as homogeneously distributed in the Galactic disc as the cluster population itself.

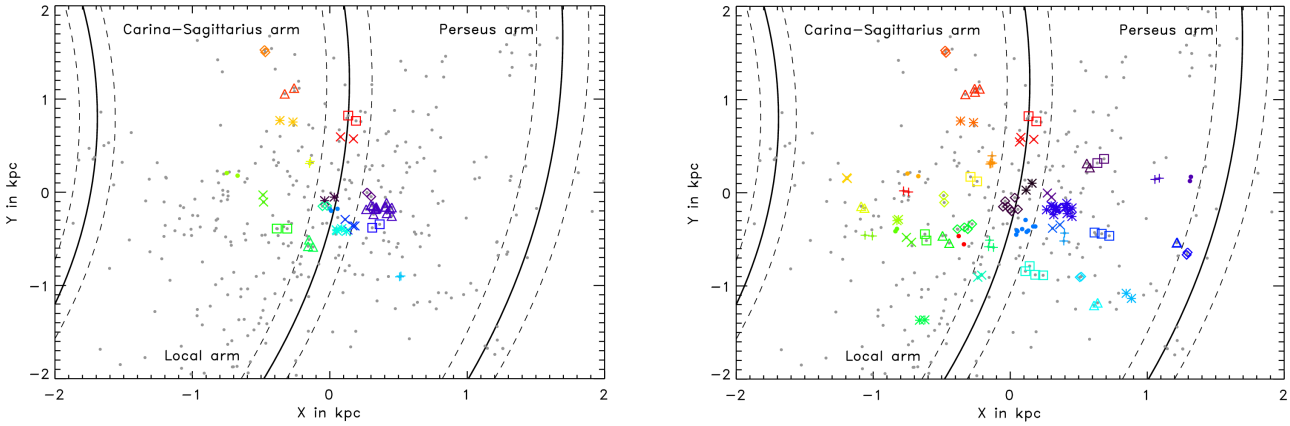

Figure 4.30: Comparison for the positions of the identified OC groupings with the Galactic spiral structure, using both sets of linking lengths (left panel - 100 pc and 10 km/s and right panel 100 pc and 10 km/s. The spiral arms are indicated by the black lines (solid - centre, dashed - width) and were determined using parameters provided by Reid et al. (2014). The groupings are highlighted by different colours and symbols and the grey dots indicate OCs in the working sample that did not belong to a grouping.

Another approach to evaluate the connection between OC groupings and star formation was to check the typical separations of the nearest neighbours in the young and old cluster population. Fig. 4.31 illustrates this comparison for the entire COCD (left), where the young clusters have ages below 20 Myr and the old clusters ages above 400 Myrs, and for the reference sample from the MWSC within 1.8 kpc (right), where the young clusters have ages below 50 Myr and the old clusters ages above 700 Myrs. There are two reasons for the choice of different interval margins used to extract the young and old cluster population in the COCD and the MWSC. First, because the MWSC is a far more extensive cluster catalogue than the COCD. Second, because I wanted a similar sample size for the young and old population in either catalogue and between the catalogues (145 OCs in COCD and about 195 OCs in the MWSC).

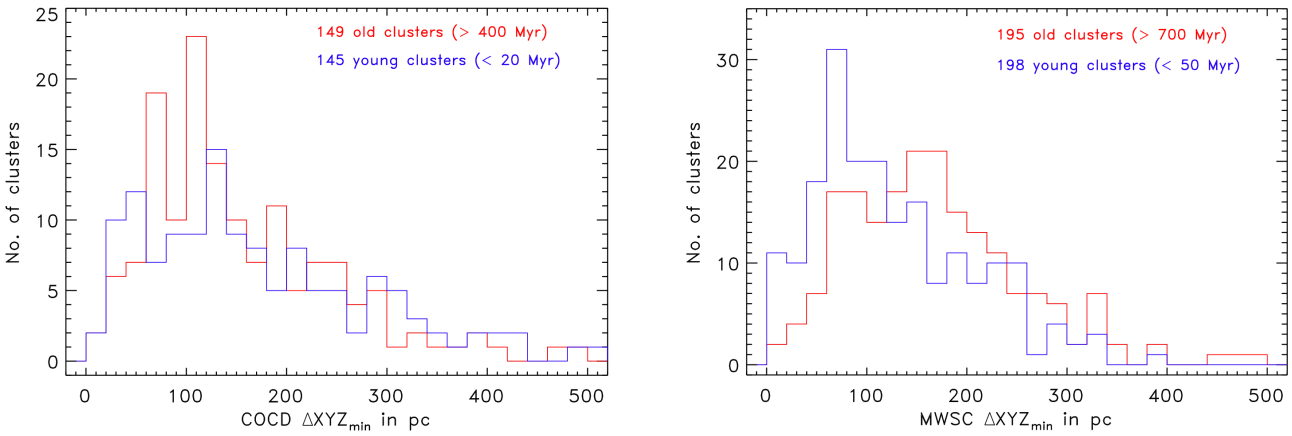

Figure 4.31: Comparison of the histograms for the spatial separations of the nearest neighbours in coordinate space between the young (blue) and old (red) Galactic open cluster population in the entire COCD (left; young < 20 Myr, old > 400 Myr) and the MWSC within the completeness limit of 1.8 kpc (right; young < 50 Myr, old > 700 Myr).

For the young cluster population in the COCD the distribution for the spatial separation of the nearest neighbours peaked at about 50 pc and 130 pc, while for the old clusters the distribution peaked at about 70 pc and 110 pc. In the MWSC the distribution for the spatial separation of the nearest neighbours peaked at about 70 pc for the young clusters and at about 170 for the old clusters. The double feature in the spatial separation distributions for the COCD sample could be because of the smaller sample size, which might affect the statistics. In both samples the young cluster population apparently showed a higher density than the old OC population, which supported the hypothesis that the OC groupings most likely originate from a common molecular cloud and that not only stars form in clusters, but that also clusters form in groups. Moreover, this difference indicated that the lifetime of these OC groupings might be comparable to the typical lifetime of open clusters and are most likely affected by the high infant mortality in the Galactic OC population.
Besides the general aspects discussed above, the mean parameters for the identified potential OC groupings are listed in Tab. 4.1 for the first set of linking lengths (100 pc and 10 km/s)[4], including XYZ-coordinates, UVW-velocities, distances and ages. Mean metallicities were not included, because for the majority of the clusters in groupings $[M/H]$ values were not available. The averaged values and the uncertainties in Tab. 4.1 were computed as simple mean and standard deviations based on the values for the members. The individual values for the members of the detected OC groupings are summarised in Tab. 4.2, also including metallicities.
In the identification, it was already indicated that all groupings were located within about 1 kpc and the numbers in Tab. 4.1 verify this finding. The vast majority of the detected OC groupings were actually located even within the stated completeness limit of the COCD (Piskunov et al. 2006, 850 pc;) and only three groupings were more distant than 1 kpc. Nevertheless, this aspects is more likely caused by the incompleteness of the working sample, and because of RV data being more accessible in the immediate solar vicinity, than reflecting an actual characteristic of OC groupings. When looking at the spatial coverage of the OC groupings identified using the second set of linking lengths (100 pc and 20 km/s) this became more clear, visually in the upper panels of Fig. 4.4 and in numbers when comparing Tab. 4.1 and Tab. C.2.
For the ages of the detected groupings, I found an age spread in the logarithmic ages of typically below 0.5 dex, but also values slightly beyond 1 dex. Compared to the typical uncertainties of the cluster ages in the COCD of 0.2 – 0.25 dex, this indicated a substantial age difference within the found potential OC groupings. In Fig. 4.32 I compare the maximum age difference with the age of the oldest cluster within a grouping for both sets of linking lengths (100 pc and 10 km/s - left, 100 pc and 20 km/s - right), and indicate pairs, groups and the complex by different symbols.

[4]The table for the mean parameters using the second set of linking lengths are provided in the Appendix Sect. C.2

Table 4.1: Parameters for the identified open cluster groupings using linking lengths of 100 pc and 10 km/s: Number of OC grouping and members, as well as mean parameters for the XYZ-coordinates, UVW-velocities, distances, and ages.

Number of OC grouping	No. of members	X_{mean} kpc	Y_{mean} kpc	Z_{mean} kpc	U_{mean} km/s	V_{mean} km/s	W_{mean} km/s	d_{mean} kpc	log t_{mean} dex
1	2	-0.002 (0.049)	-0.071 (0.027)	-0.065 (0.037)	1.8 (0.8)	-9.4 (3.1)	-0.4 (5.1)	0.107 (0.004)	7.81 (1.29)
2	2	0.286 (0.021)	-0.025 (0.031)	-0.055 (0.004)	4.8 (1.9)	2.2 (2.1)	1.3 (1.5)	0.293 (0.024)	7.82 (0.59)
3	15	0.367 (0.060)	-0.176 (0.038)	-0.118 (0.044)	5.2 (5.9)	1.0 (3.3)	1.1 (3.3)	0.427 (0.065)	7.18 (0.38)
4	2	0.336 (0.038)	-0.363 (0.026)	0.014 (0.019)	13.7 (3.8)	-7.1 (0.5)	-0.2 (4.3)	0.495 (0.006)	7.80 (0.46)
5	4	0.149 (0.033)	-0.355 (0.047)	-0.058 (0.007)	2.0 (2.1)	0.2 (4.4)	-5.9 (2.7)	0.391 (0.049)	7.62 (0.17)
6	3	0.022 (0.030)	-0.184 (0.013)	-0.012 (0.020)	12.4 (1.9)	-4.5 (2.4)	-2.1 (4.2)	0.188 (0.012)	7.91 (0.17)
7	2	0.513 (0.007)	-0.903 (0.006)	-0.001 (0.006)	1.1 (2.8)	6.3 (0.8)	1.6 (1.2)	1.038 (0.002)	7.98 (1.11)
8	4	0.077 (0.033)	-0.407 (0.013)	-0.012 (0.031)	6.9 (4.6)	-5.8 (2.3)	1.0 (3.0)	0.416 (0.016)	7.72 (0.92)
9	2	-0.036 (0.023)	-0.148 (0.002)	-0.017 (0.004)	-0.0 (1.1)	2.2 (0.7)	6.3 (2.2)	0.155 (0.007)	7.79 (0.06)
10	3	-0.144 (0.019)	-0.558 (0.043)	0.000 (0.012)	5.1 (2.1)	-3.2 (7.0)	-6.8 (2.0)	0.577 (0.040)	7.78 (0.71)
11	2	-0.348 (0.054)	-0.391 (0.001)	0.033 (0.007)	12.2 (5.4)	15.7 (1.4)	9.6 (3.3)	0.525 (0.035)	8.52 (0.11)
12	2	-0.484 (0.003)	-0.067 (0.054)	0.006 (0.016)	1.5 (5.1)	1.2 (3.3)	4.9 (3.0)	0.490 (0.005)	8.21 (0.42)
13	2	-0.711 (0.056)	0.192 (0.020)	-0.122 (0.013)	-11.2 (3.5)	-8.1 (5.6)	6.9 (2.1)	0.746 (0.061)	7.66 (0.28)
14	2	-0.145 (0.004)	0.319 (0.016)	0.088 (0.016)	7.2 (0.8)	-10.3 (3.5)	-4.3 (1.8)	0.361 (0.016)	7.85 (0.23)
15	2	-0.316 (0.067)	0.762 (0.011)	0.029 (0.012)	7.5 (2.4)	-10.9 (1.5)	-3.9 (0.6)	0.826 (0.037)	8.41 (0.49)
16	2	-0.472 (0.004)	1.514 (0.018)	0.053 (0.006)	-19.6 (3.8)	-14.5 (2.9)	2.0 (2.1)	1.587 (0.018)	7.12 (0.18)
17	2	-0.294 (0.048)	1.087 (0.044)	0.019 (0.010)	-10.6 (0.9)	-17.1 (5.2)	5.4 (0.9)	1.127 (0.030)	7.13 (0.01)
18	2	0.162 (0.040)	0.794 (0.040)	0.072 (0.025)	-5.9 (0.1)	-1.5 (4.3)	3.9 (5.0)	0.815 (0.029)	7.18 (0.69)
19	2	0.125 (0.066)	0.584 (0.015)	-0.039 (0.017)	3.8 (0.1)	-1.0 (5.9)	3.9 (0.7)	0.600 (0.000)	8.76 (0.24)

Note: Averaged metallicities could not be provided for the OC groupings in Tab. 4.1, because only about 30% of the clusters, which belong to a groupings, were equipped with $[M/H]$ information. This can be seen in seen in Tab. 4.2.

Table 4.2: Parameters for the members of the identified OC groupings, namely identifiers, XYZ-coordinates, UVW-velocities, distances, ages, and metallicities.

Group number	Seq	Name	X kpc	Y kpc	Z kpc	U km/s	V km/s	W km/s	d kpc	log t dex	$[M/H]$ dex
1	44	Alessi 13	0.033	-0.052	-0.091	2.4	-11.6	3.2	0.110	8.72	0.06
	204	Mamajek 1	-0.037	-0.090	-0.039	1.2	-7.1	-4.0	0.105	6.90	—
2	61	Platais 4	0.271	-0.003	-0.052	3.5	3.6	2.3	0.276	8.24	—
	68	Collinder 65	0.301	-0.047	-0.058	6.1	0.7	0.2	0.310	7.41	—
3	72	Collinder 69	0.413	-0.113	-0.092	15.8	0.8	-0.0	0.438	6.76	—
	73	NGC 1981	0.334	-0.178	-0.130	10.2	0.4	2.2	0.400	7.50	—
	74	NGC 1976	0.329	-0.183	-0.132	7.7	-3.4	2.1	0.399	7.71	—
	75	NGC 1977	0.415	-0.225	-0.164	2.1	-4.8	4.2	0.500	7.08	—
	76	NGC 1980	0.451	-0.255	-0.184	1.9	-0.1	3.2	0.550	6.67	—
	77	Collinder 70	0.338	-0.158	-0.117	13.0	-1.8	-1.0	0.391	6.71	0.14
	80	Sigma Ori	0.340	-0.172	-0.119	10.9	-4.1	5.1	0.399	6.82	—
	91	Platais 6	0.313	-0.148	-0.038	-3.9	4.7	-3.5	0.348	7.79	—
	95	NGC 2232	0.265	-0.183	-0.042	1.7	0.8	-2.5	0.325	7.49	—
	1016	ASCC 16	0.408	-0.156	-0.145	3.3	4.7	3.7	0.460	6.93	—
	1018	ASCC 18	0.439	-0.178	-0.159	7.2	2.6	2.8	0.500	7.12	—
	1019	ASCC 19	0.299	-0.139	-0.117	3.1	3.0	2.2	0.350	7.64	—
	1020	ASCC 20	0.399	-0.158	-0.136	7.0	5.3	2.0	0.450	7.35	—
	1021	ASCC 21	0.451	-0.163	-0.142	3.3	4.3	3.2	0.500	7.11	—
	1024	ASCC 24	0.318	-0.236	-0.057	-5.8	2.0	-7.0	0.400	6.96	—
4	125	Alessi 21	0.363	-0.344	0.000	16.4	-6.7	2.9	0.500	7.47	—
	147	NGC 2422	0.309	-0.381	0.027	11.1	-7.4	-3.2	0.491	8.12	-0.03
5	126	Collinder 132	0.183	-0.362	-0.066	4.1	-3.6	-2.1	0.411	7.51	—
	133	Collinder 135	0.112	-0.292	-0.062	3.3	-3.0	-7.8	0.319	7.54	-0.22
	136	Collinder 140	0.168	-0.361	-0.055	0.6	1.4	-6.0	0.402	7.57	-0.10
	162	NGC 2451B	0.132	-0.406	-0.050	-0.2	5.8	-7.7	0.430	7.88	-0.45
6	159	NGC 2451A	0.056	-0.178	-0.025	13.6	-6.5	-6.8	0.188	7.76	-0.53
	202	IC 2391	-0.001	-0.175	-0.021	13.4	-1.8	1.3	0.176	7.88	-0.15
	218	Platais 9	0.010	-0.199	0.011	10.2	-5.2	-0.8	0.200	8.09	—
7	163	NGC 2447	0.518	-0.899	0.003	-0.9	6.8	0.8	1.037	8.76	-0.10
	164	NGC 2448	0.508	-0.907	-0.005	3.2	5.7	2.5	1.040	7.19	—
8	182	Vel OB2	0.048	-0.404	-0.057	2.9	-9.1	3.2	0.411	7.26	-0.29
	190	vdBergh-Hagen 23	0.120	-0.420	-0.008	5.6	-5.2	2.1	0.437	7.14	—
	210	Trumpler 10	0.053	-0.414	0.005	5.7	-5.4	-3.4	0.417	7.38	-0.13
	1048	ASCC 48	0.087	-0.390	0.011	13.5	-3.6	2.2	0.400	9.09	—
9	216	Platais 8	-0.020	-0.147	-0.020	0.7	2.7	4.8	0.150	7.75	-0.30
	259	IC 2602	-0.053	-0.150	-0.014	-0.8	1.7	7.8	0.160	7.83	-0.09
10	245	Loden 143	-0.158	-0.579	-0.009	4.9	4.0	-5.7	0.600	8.45	—
	255	vdBergh-Hagen 99	-0.151	-0.509	-0.005	3.1	-9.9	-9.2	0.531	7.86	0.09
	1058	ASCC 58	-0.122	-0.587	0.014	7.4	-3.6	-5.7	0.600	7.04	—
11	333	Loden 915	-0.310	-0.391	0.028	8.4	16.7	12.0	0.500	8.44	—
	349	ESO 175-06	-0.386	-0.390	0.038	16.1	14.8	7.3	0.550	8.60	—
12	392	NGC 6281	-0.482	-0.105	0.017	5.1	3.5	7.0	0.494	8.51	0.00
	408	NGC 6405	-0.486	-0.029	-0.006	-2.1	-1.1	2.8	0.487	7.91	0.20
13	455	Collinder 394	-0.671	0.178	-0.113	-8.8	-12.1	8.3	0.703	7.86	—
	457	NGC 6716	-0.750	0.206	-0.131	-13.7	-4.1	5.4	0.789	7.47	-0.31
14	456	Stephenson 1	-0.142	0.331	0.099	6.7	-12.8	-5.6	0.373	7.69	—
	1100	ASCC 100	-0.148	0.308	0.077	7.8	-7.8	-3.1	0.350	8.01	—
15	466	Turner 9	-0.363	0.770	0.037	9.2	-9.8	-3.5	0.852	8.06	—
	1110	ASCC 110	-0.268	0.754	0.020	5.8	-11.9	-4.3	0.800	8.75	—

Table 4.2: continued

Group number	Seq	Name	X kpc	Y kpc	Z kpc	U km/s	V km/s	W km/s	d kpc	log t dex	$[M/H]$ dex
16	476	NGC 6871	-0.469	1.501	0.057	-22.2	-16.5	0.5	1.574	6.99	—
	477	Biurakan 1	-0.475	1.527	0.049	-16.9	-12.4	3.4	1.600	7.25	—
17	478	Biurakan 2	-0.328	1.056	0.026	-10.0	-20.8	4.7	1.106	7.14	—
	488	NGC 6913	-0.260	1.118	0.012	-11.2	-13.4	6.0	1.148	7.12	—
18	500	IC 1396	0.134	0.822	0.054	-6.0	1.5	0.3	0.835	6.69	—
	501	NGC 7160	0.191	0.766	0.089	-5.8	-4.5	7.4	0.794	7.66	—
19	509	NGC 7438	0.172	0.573	-0.051	3.8	-5.2	3.4	0.600	8.93	—
	1115	ASCC 115	0.078	0.594	-0.027	3.8	3.2	4.4	0.600	8.59	—

Fig. 4.32 suggests that the older the grouping the larger the internal age difference, but this might not be a genuine feature. In the COCD the ages were provided logarithmically with only overall uncertainties, which means that the older a cluster the larger would be the linear value for the uncertainty, which could affect the value for the age spread within the groupings. As stated above the majority of the pairs might not be real and also for the groups some potential members might be by chance alignments. This is another aspect that could explain the very large age differences, which were primarily present for the pairs and some of the groups, while the complex seemed to cover a pretty narrow age range.

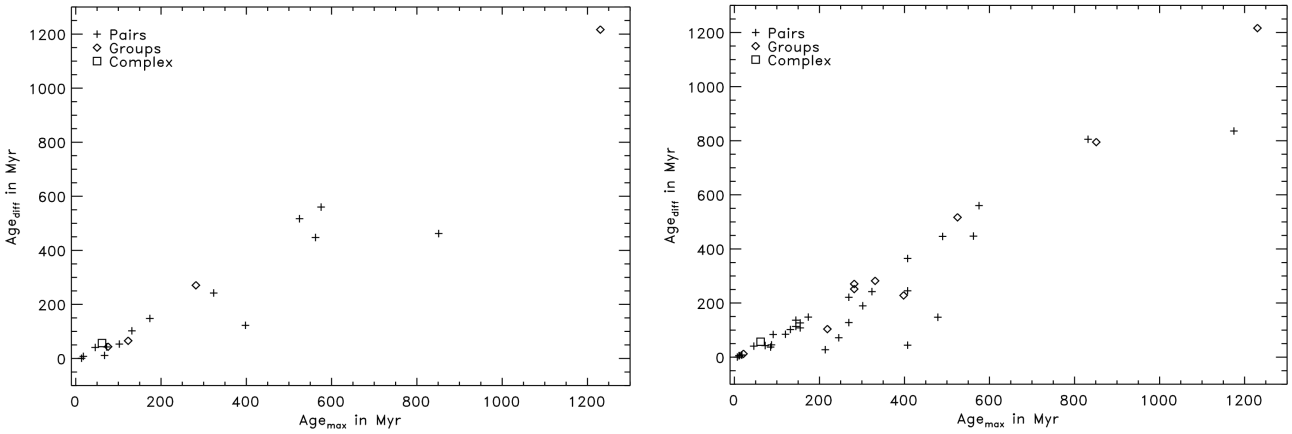

Figure 4.32: Relation between age of the oldest member and maximum age difference for the detected OC groupings using the first and second set of linking lengths in the left and right panel, respectively.

Although many of the OC pairs might not be real, some could be genuine and even show very large age differences. In this case it is unlikely that they formed in the same star forming region through one event. For such systems a formation scenario could be triggered star formation by an older cluster crossing a recent star forming region and basically catching the younger clusters through gravitational interaction. This is just a hypothesis and it is more likely that members of an OC grouping originate from the same molecular cloud, as indicated by the higher density of young compared to old clusters (see Fig. 4.31). For a detailed investigation of this question a far more extensive cluster sample with 6D-phase space information would be required and could not be discussed further in the framework of this study.
Since the found complex was likely to be genuine, it was only reasonable to take a closer look at its characteristics. The distributions in coordinate and velocity space along with the spread in age and metallicity are displayed in Fig. 4.33. For both sets of linking lengths (100 pc and either 10 km/s or 20 km/s) the complex was recovered with exactly the same members, which again verified the complex to be genuine.

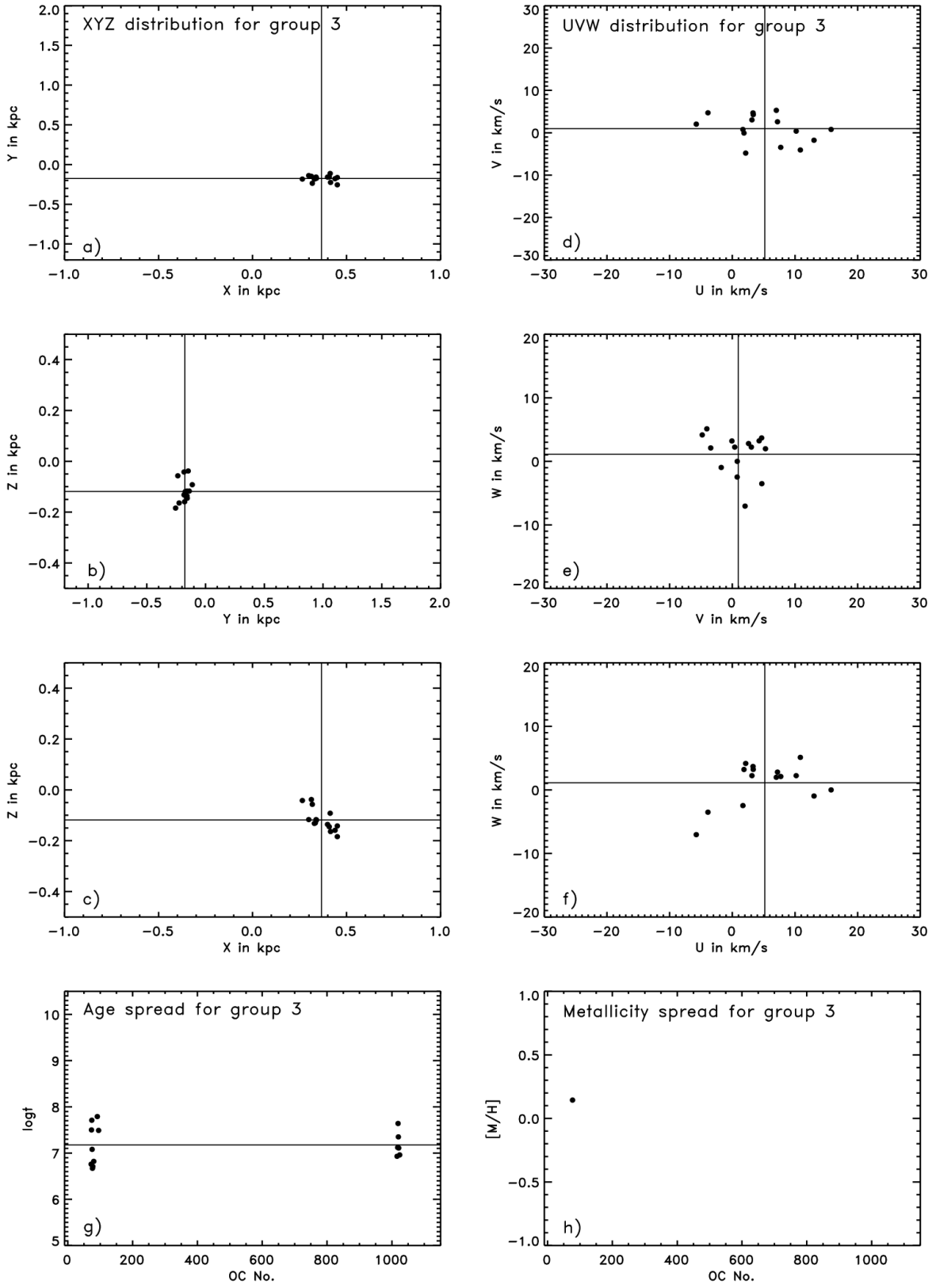

Figure 4.33: Parameter distributions for the members of the open cluster grouping No. 3. a-c) spatial distribution; d-f) velocity distribution; g) age spread; h) metallicity spread. The solid lines show the corresponding averaged values for the open cluster grouping No. 3.

In coordinate space the complex was very tight, covering about 200 pc in diameter, and in velocity space the total spread was about 20-30 km/s. The ages of the members covered a range of $\log t = 6.67 - 7.79$, which corresponds to linear ages of 4.7 – 61.7 Myr and could be comparable to the time scale of one sequential star forming event. Metallicity data were only available for one member and indicate a slightly metal rich environment, which was already suspected by the young age of the complex members.

4.4.1 COMPARISON TO THE LITERATURE

In addition to the characterisation of the identified OC groupings in this work, I compared my results to the pairs, groups, and complexes published in the literature (de La Fuente Marcos & de La Fuente Marcos 2009a,b,c; Piskunov et al. 2006). First, I considered the groups and complexes provided by Piskunov et al. (2006), which were identified based on spatial proximity and common tangential velocities. I compare their positions (grey squares) in the XY-plane to those for the OC groupings in this work (coloured symbols) in Fig. 4.34.

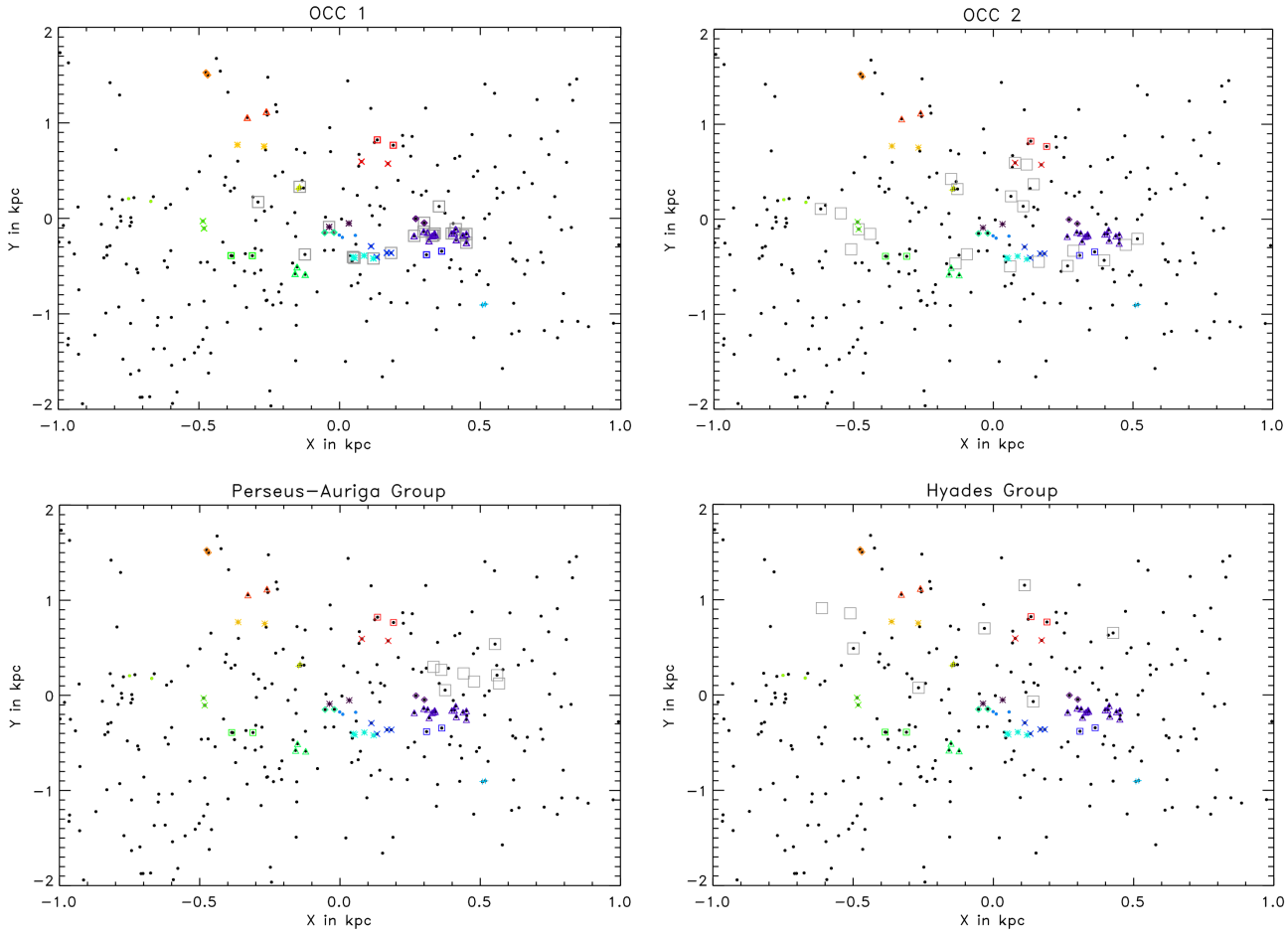

Figure 4.34: Spatial comparison in the XY-plane of the detected OC groupings in this work, highlighted by different colours and symbols, with the groups and complexes proposed by Piskunov et al. (2006). Black dots show COCD clusters with RV data, while grey squares indicate the OCC1 and OCC2 (upper left and right panels, respectively), as well as the Perseus-Auriga and Hyades group (lower left and right panels, respectively).

For the Gould-Belt complex (OCC1) from Piskunov et al. (2006) I found counterparts in my sample, namely the complex and a few pairs, which shows that the third dimension in velocity space held additional information and should not be neglected for the identification of structures in the open cluster population. For the OCC2, the Perseus-Auriga group, and the Hyades group, I did not find counterparts among my OC groupings. The main reason for this discrepancy was that the majority of the members in the OCC2 and the two groups were not equipped with RV data[5] and were therefore simply not included in my working sample, while for the OCC1 all members were provided with RV information. Still, the verification of the OCC1 indicated that also the other three proposed groupings may be real, although possibly split up into smaller groupings.
Second, I evaluated the pairs identified by de La Fuente Marcos & de La Fuente Marcos (2009a,b,c) solely considering spatial proximity. In particular, I concentrated on the sample and tables provided in de La Fuente Marcos & de La Fuente Marcos (2009b). In Tab. 4.3 I demonstrate the overlap between their sample[6], the COCD and my working sample. One can see that about 77% of the clusters, provided by de La Fuente Marcos & de La Fuente Marcos (2009b), were included in the COCD and only 49% of their clusters were included in my working sample. Only 15 clusters resided in some of my OC groupings, which corresponds to 39% of the common sample.

Table 4.3: Comparison between the cluster samples used by de La Fuente Marcos & de La Fuente Marcos (2009b) with the COCD, my working sample and the members of the identified OC groupings.

Cluster Name	COCD Number	in my work sample	in my OC groupings	Cluster Name	COCD Number	in my work sample	in my OC groupings
NGC 189	–	–	–	Ruprecht 91	266	yes	–
ASCC 1004	1004	yes	–	ESO 128-16	269	–	–
NGC 659	21	–	–	Markarian 38	–	–	–
NGC 663	22	yes	–	Feigelson 1	–	–	–
ASCC 1006	1006	yes	–	ASCC 1068	1068	–	–
Stock 4	24	–	–	Loden 565	305	yes	–
NGC 1746	60	yes	–	ESO 132-14	–	–	–
NGC 1758	–	–	–	NGC 5281	336	yes	–
Briceño 1	1016	yes	yes	Loden 1171	340	–	–
ASCC 1018	1018	yes	yes	Loden 1194	344	yes	–
ASCC 1020	1020	yes	yes	NGC 5617	353	–	–
ASCC 1021	1021	yes	yes	Pismis 19	–	–	–
NGC 1981	73	yes	yes	Trumpler 22	354	–	–
NGC 1976	–	–	–	Alessi 8	362	–	–
Collinder 70	77	yes	yes	Johansson 1	–	–	–
σ Orionis	80	yes	yes	NGC 6204	382	yes	–
Basel 8	100	yes	–	Hogg 22	383	yes	–
NGC 2251	102	yes	–	Lynga 14	–	–	–
NGC 2302	113	–	–	NGC 6242	387	yes	–
NGC 2306	114	–	–	Trumpler 24	–	–	–
ASCC 1034	1034	–	–	NGC 6250	390	yes	–
NGC 2421	146	–	–	ASCC 1090	1090	–	–
Czernik 31	–	–	–	NGC 6405	408	yes	yes
NGC 2428	152	yes	–	NGC 6425	413	yes	–
Ruprecht 151	158	yes	–	Basel 5	417	–	–

[5]The missing RV data for the OCCs in Piskunov et al. (2006) are indicated by the grey squares not associated by a black dot.
[6]The de La Fuente Marcos & de La Fuente Marcos (2009b) sample is summarised in Tab. 4.3 including all clusters listed in Tab. 1 and Tab. 2 of de La Fuente Marcos & de La Fuente Marcos (2009b).

Table 4.3: continued

Cluster Name	COCD Number	in my work sample	in my OC groupings	Cluster Name	COCD Number	in my work sample	in my OC groupings
NGC 2447	163	yes	yes	NGC 6469	419	–	–
NGC 2448	164	yes	yes	Ruprecht 139	424	–	–
Mamajek 1	204	yes	yes	Bochum 14	–	–	–
Collinder 197	–	–	–	Collinder 469	–	–	–
Alessi 43	1050	yes	–	NGC 6613	443	yes	–
BH 91	240	–	–	NGC 6618	444	yes	–
ASCC 1059	1059	–	–	ASCC 1100	1100	yes	yes
NGC 3228	241	–	–	ASCC 1101	1101	yes	–
Loden 46	242	–	–	NGC 6871	476	yes	yes
Ruprecht 89	244	–	–	Biurakan 1	477	yes	yes
NGC 3293	253	yes	–	Biurakan 2	478	yes	yes
Loden 165	–	–	–	Ruprecht 172	481	–	–
Carraro 1	–	–	–	Bica 1	–	–	–
NGC 3324	254	yes	–	Bica 2	–	–	–
			Total:	78	60	38	15

Table 4.4: Comparison to the OC pairs and groups proposed by de La Fuente Marcos & de La Fuente Marcos (2009b) with the members of the identified OC groupings in this work.

This work			de La Fuente Marcos & de La Fuente Marcos (2009b)			
			Table 1		Table 2	
Number of OC grouping	COCD Number	Cluster Name	Group Number	Cluster Name	Group Number	Cluster Name
1	44	Alessi 13			1	Mamajek 1
	204	Mamajek 1				Feigelson 1
2	61	Platais 4				
	68	Collinder 65				
3	72	Collinder 69	2	Collinder 70	3	Collinder 70
	73	NGC 1981		NGC 1981		σ Orionis
	74	NGC 1976	3	NGC 1976	4	σ Orionis
	75	NGC 1977		NGC 1981		NGC 1976
	76	NGC 1980	4	ASCC 20	5	ASCC 20
	77	Collinder 70		ASCC 16		Briceño
	80	σ Orionis	6	ASCC 21	7	ASCC 21
	91	Platais 6		ASCC 18		ASCC 18
	95	NGC 2232				
	1016	ASCC 16				
	1018	ASCC 18				
	1019	ASCC 19				
	1020	ASCC 20				
	1021	ASCC 21				
	1024	ASCC 24				

Table 4.4: continued

This work			de La Fuente Marcos & de La Fuente Marcos (2009b)			
			Table 1		Table 2	
Number of OC grouping	COCD Number	Cluster Name	Group Number	Cluster Name	Group Number	Cluster Name
4	125	Alessi 21				
	147	NGC 2422				
5	126	Collinder 132				
	133	Collinder 135				
	136	Collinder 140				
	162	NGC 2451B				
6	159	NGC 2451A				
	202	IC 2391				
	218	Platais 9				
7	163	NGC 2447	21	NGC 2447	15	NGC 2447
	164	NGC 2448		NGC 2448		NGC 2448
8	182	Vel OB2				
	190	vdBergh-Hagen 23				
	210	Trumpler 10				
	1048	ASCC 48				
9	216	Platais 8				
	259	IC 2602				
10	245	Loden 143				
	255	vdBergh-Hagen 99				
	1058	ASCC 58				
11	333	Loden 915				
	349	ESO 175-06				
12	392	NGC 6281	5	NGC 6405	6	NGC 6405
	408	NGC 6405		ASCC 90		ASCC 90
13	455	Collinder 394				
	457	NGC 6716				
14	456	Stephenson 1	1	ASCC 100	2	ASCC 100
	1100	ASCC 100		ASCC 101		ASCC 101
15	466	Turner 9				
	1110	ASCC 110				
16	476	NGC 6871	30	NGC 6871		
	477	Biurakan 1		Biurakan 1		
17	478	Biurakan 2	22	Ruprecht 172	17	Ruprecht 172
	488	NGC 6913		Biurakan 2		Biurakan 2
18	500	IC 1396				
	501	NGC 7160				
19	509	NGC 7438				
	1115	ASCC 115				

In their Tab. 1 de La Fuente Marcos & de La Fuente Marcos (2009b) listed 34 OC pairs extracted from the WEBDA online compilation and in their Tab. 2 they provided 27 pairs found in the DAML, with a significant overlap. Tab. 4.4 provides an overview on which pairs by de La Fuente Marcos & de La Fuente Marcos (2009b) were recovered in my working sample. For both their tables I found about one third of their pairs among my OC groupings and four of them being part of my complex. In some cases the pairs in common were identical, whereas in others there was only one mutual member. On the one hand, this is because only half of their clusters were included in my working sample. On the other hand, they based their identification solely on spatial proximity with a relatively stringent separation criterion of 30 pc, whereas in this study the spatial separation criterion was not that stringent (100 pc), which was compensated by also taking into account 3D-velocity information.

For both literature samples of open cluster pairs, groups, and complexes (de La Fuente Marcos & de La Fuente Marcos 2009a,b,c; Piskunov et al. 2006) structures could be verified through my working sample, though some only partly because of incompleteness of the available information and the cluster sample, along with that not all detected OC groupings might be genuine. However, the common pairs and complexes strengthened the statement that OC groups and complexes do exist. Future investigations will reveal further details on the structures in the open cluster population and the role they play in star formation and evolution processes in the Milky Way, as well as dynamics, structures and evolution of spiral galaxies.

Chapter 5

Discussion and Outlook

This work aimed at the identification and verification of an additional level of structure in the Galactic disc defined by accumulations of open clusters and stellar associations. A suitable data set for such a study was the Catalogue of Open Cluster Data (COCD), which was compiled by Kharchenko et al. (2005a,b) and provided homogeneous parameters and uniform membership selection for 650 open clusters and compact stellar associations. For this work 6D phase-space information were required, but the COCD lacked radial velocity information, which were complemented with data from the RAdial Velocity Experiment (RAVE; Steinmetz et al. 2006; Kordopatis et al. 2013) for 110 clusters in the COCD, including new values for 37 of these clusters. In addition, I obtained $[M/H]$ from RAVE for 81 COCD clusters. The final working sample selected from the COCD, that fulfilled the condition of being equipped with 6D phase-space information, comprised 432 clusters.
For the identification of groupings in the Galactic open cluster population I applied an adaption of the Friends-of-Friends (FoF) algorithm, as used in cosmology, in both coordinate and velocity space. The FoF-algorithm required predefined linking lengths, which were set by the limiting values in separation between a grouping and the field. In coordinate space I choose a value of 100 pc, which is expected to cover the typical separations of clusters belonging to a grouping, as deduced from the findings by Piskunov et al. (2006) and de La Fuente Marcos & de La Fuente Marcos (2009a,b,c). In velocity space I could only determine a range of $10 - 20$ km/s, which was derived from the UVW-uncertainty distribution and should cover the most likely value for the corresponding linking length. Therefore, I ran the FoF-algorithm twice. First for the set of linking lengths 100 pc and 10 km/s, which resulted in the identification of 19 potential OC groupings. Second, for the set of linking lengths 100 pc and 20 km/s, which resulted in the detection of 42 potential OC groupings.
Since the definition of the linking lengths was to a certain degree arbitrary, although based on an educated guess, further verification of the findings was recommendable. For this purpose I implemented Monte-Carlo simulations with randomised samples created from two distinguished input distributions for the spatial and velocity parameters. First, assuming a homogeneous distribution in the XY-plane, a sech-profile in Z and Gaussian profiles in the UVW-velocities. Second, using the actual parameter distributions of COCD objects in the XYZ-coordinates and UVW-velocities. These simulations revealed that the larger groups and the complex with 15 members appeared to be most likely genuine, although the majority of found groupings could be by chance alignments, which is the case in particular for the pairs. A similar finding resulted from a comparison with a random subsample from the Milky Way global survey of star clusters (MWSC; Kharchenko et al. 2013), making the finding more robust.
A characterisation of the identified OC complex, labelled as OC grouping No. 3, suggested that open cluster groupings originate from a common molecular cloud and form in one possibly sequential star formation event, because its mean age is $\log t = 7.176$ with a spread of 0.379 dex, which is just slightly larger than the overall uncertainty in the cluster ages. For both sets of linking lengths the same members were identified for this complex and it showed a very narrow distribution in coordinate and velocity space. This not only verified the complex to be genuine, but also proved that the chosen spatial linking length and range for the velocity linking length cover the most probable values for the dimensions of the investigated structure.

A comparison of the density between the young and old cluster population suggested that the found groupings have similar life times as the open cluster population itself. A comparison of my findings with pairs, groups and complexes proposed by Piskunov et al. (2006) and de La Fuente Marcos & de La Fuente Marcos (2009a,b,c), resulted in partial overlap. For example, the complex detected in my working sample partly recovered the OCC1 discovered by Piskunov et al. (2006). There may be several reasons for not recovering all proposed groupings from the literature, such as that the spatial linking length might have been chosen slightly too small to recover the entire OCC1 complex, which spans about 300 pc in diameter. Another reason could be that the literature studies neglected RV information, resulting in a different working sample than in this work. A third reason could be that some of proposed groupings in the literature, in particular the pairs, are rather by chance alignments than real OC groupings.

Requirements and opportunities for a more complete cluster sample

The cluster sample utilised in this work was homogeneous but highly incomplete, which allowed to only take a first step towards investigating the existence and characterisation of overdensities in the open cluster population. Hence, for a more detailed investigation of these structures a far more extensive data set would be required, covering a larger spatial volume and range in mass and age of clusters. Recently, a more extensive cluster catalogue became available with homogeneous parameters for about 3000 stellar associations, open and globular clusters in the Milky Way, namely the Milky Way global survey of star clusters (MWSC; Kharchenko et al. 2013). About 1000 of these clusters were equipped with RV data and the MWSC is complete to about 1.8 kpc, which would significantly extend the number of clusters with 6D phase-space information and the volume covered.
Both, the COCD and the MWSC, are optical catalogues, which posed a limitation for the completeness of the working sample. In particular, young clusters with ages of at most a few 10 Myrs are still embedded in the gas from the molecular cloud they formed in, absorbing most of the optical radiation form the stars. The emission of the older open clusters at larger distances is also affected by dust and gas clouds located in the line of sight, obscuring these objects at optical wavelengths. However, at infrared wavelength the dust and gas clouds become more transparent, allowing observations of younger and more distant clusters. Hence, including infrared observations would severely extend the working sample regarding covered volume, mass and age range. Several studies on open clusters in the infrared were performed using data from the VISTA[1] Variables in the Via Lactea survey (VVV; Borissova et al. 2011; Chené et al. 2012, 2013; Ramírez Alegría et al. 2014), mostly on massive clusters. Combining the large optical catalogue with infrared data from, for example, the VVV in a homogeneous way would enable compiling a far more complete working sample to investigate the Galactic open cluster population in more detail.
In the VVV radial velocities are included for most, if not all, of the investigated clusters, while in the MWSC there is still a significant lack of RV information. For the latter the radial velocities were obtained similar as for the COCD, complemented by my findings in RAVE (see Sect. 3.1.2, Tab. A.1 of this work and Conrad et al. 2014) and data retrieved from the ninth data release of the Sloan Digital Sky Survey (SDSS DR9; Ahn et al. 2012). The RAVE values presented by Conrad et al. (2014) only cover a small fraction of MWSC clusters and another cross-match of MWSC cluster members with the most recent data release of RAVE would provide further RV data for OCs. There have also been dedicated RV studies on individual open clusters, for example by Geller et al. (2008, 2010), Hole et al. (2009), Carrera (2012), Hayes & Friel (2014) or Tofflemire et al. (2014). Often these data are not included in larger OC catalogues, though they provide useful information. The Gaia-ESO survey (Gilmore et al. 2012; Friel et al. 2014; Cantat-Gaudin et al. 2014) also has a dedicated program on open clusters, providing RV data. Also the STELLar Activity (STELLA; Weber et al. 2013) robotic telescope could provide RV data for OCs in the northern hemisphere and could be used complementary.

[1] VISTA is the abbreviation for the Visible and Infrared Survey Telescope for Astronomy (Sutherland et al. 2014).

Moreover, the upcoming data from Gaia (Vallenari 2014) and the planned complementary spectroscopic instrument 4MOST[2] (Depagne & 4MOST consortium 2014), will further extend the RV data available for open cluster members. Besides additional RV data, Gaia will significantly improve the proper motion and distance information for open clusters, since it is expected to reach astrometric accuracies down to the 10 μas level. The planned multiple epochs for objects observed by Gaia, would also help to improve binary studies in open clusters and binaries would not have to be excluded from the membership selection and mean parameter determination, resulting in even more accurate cluster values. A better estimate on the fraction and characteristics of binaries in open clusters dependent on age would also put further constraints on the initial binary fraction and the evolution of the binary population in open clusters used in current and future simulations of open clusters (Parker et al. 2011; Geller 2013).
The RV data from the SDSS should be more or less complete for the MWSC objects, but the metallicities and chemical abundances from SDSS and related surveys (SEGUE[3] (Yanny et al. 2009) and APOGEE[4] (Allende Prieto et al. 2008)) could be used to extend the metallicity data on open clusters in a homogeneous way. These data could be complemented by information form RAVE, the Gaia-ESO survey and/or results from dedicated metallicity and abundance studies on open clusters (Jacobson et al. 2011a,b; Bragaglia 2012; Frinchaboy et al. 2013; Netopil & Paunzen 2013). The latter are summarised in the continuously updated DAML online compilation by Dias et al. (2002), but would have to be converted to a homogeneous system, as pointed out in Sect. 2.1.1. The inhomogeneity of the methods for the metallicity determination, in particular for the DAML listings, makes metallicity studies on open clusters to the least challenging. Nevertheless, it would be very interesting to conduct a detailed and global abundance comparison study on the Galactic open cluster population to identify possible signatures of their birthplace, which could directly relate to OC groupings.
As pointed out above, the combination of RV or $[M/H]$ data can be challenging. First of all, the membership selection has to be as uniform as possible, because different methods might identify different members and/or potential contamination by field stars. Second, all velocity or metallicity values have to be converted to a common frame of reference. For the velocities it is of advantage if the values are of comparable and best possible accuracy to not add additional noise or uncertainty. For the metallicities one has to be sure to only use either overall metallicities or iron abundances, because there could be significant differences between these values depending on the stellar type, though often the nomenclature is used interchangeable. Hence, each metallicity value provided for an open cluster would have to be evaluated individually and carefully and then potentially converted to a common system.

What can be learned from investigating open cluster groupings

Above I provided an overview on what remains to be done to compile a more complete sample of open clusters with a maximum of information to conduct most detailed investigations on the characteristics of and structures in the Galactic open cluster population. Since the work presented in this thesis was merely a pilot study to evaluate the existence and detectability of structures in the Galactic open cluster population based on a highly incomplete sample, the data were too sparse to investigate how such groupings would affect our understanding of star formation and the Milky Way. Still, in the following I want to give an outlook on how OC groupings can help to better understand star formation and evolution, as well as evolution, structure, kinematics and dynamics of the Milky Way, and thereby for other spiral galaxies.
Hierarchical structures in star forming regions were already proposed by Elmegreen (2009), who found similar structures as the open cluster groupings described in this work, just named them star complexes, and discussed the dependence of the boundedness of stellar accumulations on the density, star formation rate and efficiency.

[2] 4MOST is the abbreviation for the 4m Multi Object Spectroscopic Telescope.
[3] SEGUE is the Sloan Extension for Galactic Understanding and Exploration within SDSS.
[4] APOGEE is the Apache Point Observatory Galactic Evolution Experiment within SDSS.

In the past decade there have been more and more papers providing evidence for hierarchical structures in star forming regions and clumping in the open cluster population, as for example the mentioned studies by Piskunov et al. (2006), de La Fuente Marcos & de La Fuente Marcos (2009a,b,c) or Elmegreen (2009, 2011). This work showed a new approach on the identification of features in the open cluster population and a final proof of these structures would pose the question if open clusters also prefer to form in a cluster mode rather than isolated. A more complete open cluster sample, as for example created following the suggestions above, could reveal how common open cluster groupings are in the Milky Way.

Theoretical star formation simulations could be used as complementary sources for information on the relation between star formation and open cluster groupings. However, current N-body simulations often consider isolated clusters and neglect potential interaction or feedback from another cluster forming nearby, as would be the case in an OC grouping. Examples are the cluster simulations investigating the binary fraction by Parker et al. (2011) or Geller (2013). Another example would be the simulation by Urban et al. (2010), who evaluated the mass dependency of newly formed stars in a cluster, that is considered isolated, on the heating of dust in a molecular clouds and found that the stellar initial mass function is highly dependent on the amount of dust heating included in the simulation. Such simulations require the inclusion of fragmentation of the molecular cloud to form stars, which is usually implemented on the kpc scale as well as on the cluster size scale and below. But the results from this work suggest that OC groupings indicate a level of fragmentation on the 100 pc scale and could provide additional parameters and constraints to better understand and implement the fragmentation of giant molecular clouds in star formation simulations.

The complex identified in this work showed an age spread slightly larger than the typical uncertainties in logarithmic age obtained from the COCD. Since I could identify only one such system, there is no telling how significant this difference is and I could not distinguish between coeval or sequential formation of this structure, but the relatively small spread suggested that its members originated from the same giant molecular cloud. This raised the question, if OC groupings could help understanding triggered star formation as proposed by Preibisch & Zinnecker (2007) or Li et al. (2014), most likely induced by shock waves from supernova explosions of O and B members of open clusters. Assuming that multiple clusters are born in one molecular cloud, some might form uncorrelated at about the similar time, but others could be triggered through processes in another young open cluster nearby. More accurate age estimates, along with high resolution spectroscopy and accurate abundances, for a large number of chemical elements for as many members and clusters as possible in an OC grouping would be needed to resolve which is the dominant process for star and cluster formation or whether both scenarios play equal roles.

Open cluster groupings could not only be of importance for gaining better understanding of star formation, but could also provide further insight on Galactic structure, interaction and evolution. These structures store a significant amount of mass, simply because they combine the mass of several open clusters, and therefore they might induce a local gravitational potential, which might be strong enough to slightly perturb the kinematics of Galactic objects in their vicinity. The amount of this perturbation would highly depend on the lifetime and the strengths of the binding of these cluster accumulates. The longer the lifetime, the stronger they are typically bound and the stronger should be the local dynamical perturbation.

At present, no studies on the gravitational perturbation through groupings of open clusters are conducted. Reasons for this could be that open cluster groupings are not yet verified and understood in detail, or that these perturbations might be within the uncertainty margins of currently available velocity measurements of stars and clusters in the Milky Way. To investigate such potential perturbations, one would need to compare the kinematics of non members in the immediate neighbourhood of OC groupings to the kinematics of regions free from OC groupings at similar Galactocentric distance and height above the midplane. As it can be expected that these perturbations might be within the uncertainty margins of currently available velocity data, one would need far more accurate kinematic parameters, which will become available from the upcoming observation by the Gaia satellite and complementary instruments.

Another aspect where open cluster groupings might be of interest is the formation of globular clusters. It is currently believed that globular clusters[5] are either remnants of extremely massive open clusters with secondary star formation in their surrounding (Bastian et al. 2013; Bastian & Strader 2014a; Bastian et al. 2014b; Cabrera-Ziri et al. 2014) or stripped dwarf galaxies after close encounters with the Milky Way (Pfeffer et al. 2014). Open cluster groupings might hold a third formation possibility. It can be expected that within an OC grouping random motion is present, which might lead to interaction and/or collision of its members and in some cases to mergers. If the formation of OC groupings is sequential or if OC groupings result from capture of one cluster by another, this would also explain the multiple stellar populations detected in globular clusters. At the present, there is hardly any way to prove such a hypothesis. First, because the final existence of OC groupings remains yet to proven beyond any doubt, and second, the current sample are too incomplete to investigate the internal kinematics and interactions of OC groupings in detail. However, it is still an interesting idea, which could be included in simulations on globular cluster formation.

In conclusion, open cluster groupings hold a great potential to provide a new observational approach on star formation and Galactic kinematics. They indicate that stellar clusters also form in a clustered mode, which induces additional effects triggering and influencing the formation of stars, as well as additional parameters and constraints for the simulations related to the formation and evolution of stars. Another interesting idea is whether OC groupings are even related to the formation of globular clusters. Moreover, OC groupings might be of significance for studies on the Milky Way as a whole, because they accumulate a significant amount of mass, which might be enough to slightly perturb the Galactic gravitational potential. Including this aspect into simulations on Galactic kinematics and dynamics, could provide a better understanding of the processes in the Milky Way. Hence, the open cluster population and structures therein are a link between stellar astrophysics and investigations of the Milky Way as a whole.

[5]Globular clusters are typically $\sim$ 10 Gyrs old and located in the bulge/halo of the Milky Way. Since they are typically more massive than the vast majority of open clusters, they are of spherical shape.

Acknowledgment

The German-Russian open cluster research group, where this work was embedded, was supported by DFG grant RO 528/10-1, and RFBR grant 10-02-91338, and by Sonderforschungsbereich SFB 881 "The MilkyWay System" (subproject B5) of the German Research Foundation (DFG). Funding for RAVE has been provided by: the Australian Astronomical Observatory; the Leibniz-Institut für Astrophysik Potsdam (AIP); the Australian National University; the Australian Research Council; the French National Research Agency; the German Research Foundation; the European Research Council (ERC-StG 240271 Galactica); the Istituto Nazionale di Astrofisica at Padova; The Johns Hopkins University; the National Science Foundation of the USA (AST-0908326); the W. M. Keck foundation; the Macquarie University; the Netherlands Research School for Astronomy; the Natural Sciences and Engineering Research Council of Canada; the Slovenian Research Agency; the Swiss National Science Foundation; the Science & Technology Facilities Council of the UK; Opticon; Strasbourg Observatory; and the Universities of Groningen, Heidelberg and Sydney. The RAVE web site is at http://www.rave-survey.org

Moreover, I would like to thank the Leibniz-Institut für Astrophysik and its director Matthias Steinmetz for giving me the opportunity to conduct my PhD studies here, as well as Ralf-Dieter Scholz, Roelof S. de Jong and Olivier V. Schnurr for their supervision and helpful comments throughout the data analysis and writing of this thesis. For their insight and helpful discussions on the open cluster data and characteristics, I want to thank my collaborators on the open cluster project, namely Nina V. Kharchenko, Anatoly E. Piskunov, Elena Schilbach and Siegfried Röser. Furthermore, I want to thank the RAVE collaboration for helping me to better understand the RAVE data I was using, and in particular I want to thank Arnaud Siebert, Mary Williams, Corrado Boeche and Georges Kordopatis, who provided me with a better insight on the RAVE pipeline. In addition, I want to thank the STELLA collaboration, in particular Klaus G. Strassmeier, Thomas Granzer and Michael Weber, for an interesting discussion on the opportunities for open cluster studies using STELLA and providing me with observations of selected open cluster members, though the data could not yet be included in my study. For his help on understanding the working principle of the Friends-of-Friends algorithm and implementing my own version, I also want to thank Noam Liebeskind.

Finally, I want to thank my family, friends and, in particular, my partner for their emotional and moral support, as well as their patience.

Bibliography

Abazajian, K., Adelman-McCarthy, J. K., Agüeros, M. A., et al. 2003, *Astron. J.*, 126, 2081

Adams, M. T., Strom, K. M., & Strom, S. E. 1983, *Astrophys. J. Suppl.*, 53, 893

Ahn, C. P., Alexandroff, R., Allende Prieto, C., et al. 2012, *Astrophys. J. Suppl.*, 203, 21

Alessi, B. S., Moitinho, A., & Dias, W. S. 2003, *Astron. Astrophys.*, 410, 565

Allende Prieto, C., Majewski, S. R., Schiavon, R., et al. 2008, Astronomische Nachrichten, 329, 1018

Allison, R. J., Goodwin, S. P., Parker, R. J., et al. 2009, *Astrophys. J. Letters*, 700, L99

Alves, J. & Bouy, H. 2012, *Astron. Astrophys.*, 547, A97

Barbier-Brossat, M. & Figon, P. 2000, *Astron Astrophys. Suppl.*, 142, 217

Bastian, U. & Röser, S. 1993, PPM Star Catalogue. Positions and proper motions of 197179 stars south of -2.5 degrees declination for equinox and epoch J2000.0. Vol. III: Zones -00° to -20°. Vol. IV: Zones -30° to -80°.

Bastian, N., Cabrera-Ziri, I., Davies, B., & Larsen, S. S. 2013, *Monthly Notices Roy. Astron. Soc.*, 436, 2852

Bastian, N. & Strader, J. 2014a, *Monthly Notices Roy. Astron. Soc.*, 443, 3594

Bastian, N., Hollyhead, K., & Cabrera-Ziri, I. 2014b, *Monthly Notices Roy. Astron. Soc.*, 445, 378

Bica, E., Dutra, C. M., & Barbuy, B. 2003a, *Astron. Astrophys.*, 397, 177

Bica, E., Dutra, C. M., Soares, J., & Barbuy, B. 2003b, *Astron. Astrophys.*, 404, 223

Bijaoui, A., Recio-Blanco, A., de Laverny, P., & Ordenovic, C. 2012, StMet, 9, 55

Binney, J. & Merrifield, M. 1998, Galactic Astronomy

Binney, J., Burnett, B., Kordopatis, G., et al. 2014, *Monthly Notices Roy. Astron. Soc.*, 437, 351

Blaauw, A. 1964, *Anual Rev. Astron. Astrophys.*, 2, 213

Boeche, C., Siebert, A., Williams, M., et al. 2011, *Astron. J.*, 142, 193

Bonatto, C. & Bica, E. 2010, *Monthly Notices Roy. Astron. Soc.*, 403, 996

Bonnell, I. A. & Dobbs, C. L. 2007, in IAU Symposium, Vol. 237, IAU Symposium, ed. B. G. Elmegreen & J. Palous, 344–350

Borissova, J., Kurtev, R., Peñaloza, F., et al. 2011, in Revista Mexicana de Astronomia y Astrofisica Conference Series, Vol. 40, Revista Mexicana de Astronomia y Astrofisica Conference Series, 267–267

Bragaglia, A. 2012, in Science from the Next Generation Imaging and Spectroscopic Surveys, 3P

Briceño, C., Preibisch, T., Sherry, W. H., et al. 2007, Protostars and Planets V, 345

Cabrera-Ziri, I., Bastian, N., Davies, B., et al. 2014, *Monthly Notices Roy. Astron. Soc.*, 441, 2754

Cantat-Gaudin, T., Vallenari, A., Zaggia, S., et al. 2014, *Astron. Astrophys.*, 569, A17

Carpenter, J. M. & Hodapp, K. W. 2008, The Monoceros R2 Molecular Cloud, ed. B. Reipurth, 899

Carraro, G., Turner, D., Majaess, D., & Baume, G. 2013, *Astron. Astrophys.*, 555, A50

Carrera, R. 2012, *Astron. Astrophys.*, 544, A109

Cartwright, A. & Whitworth, A. P. 2004, *Monthly Notices Roy. Astron. Soc.*, 348, 589

Chené, A.-N., Borissova, J., Clarke, J. R. A., et al. 2012, *Astron. Astrophys.*, 545, A54

Chené, A.-N., Borissova, J., Bonatto, C., et al. 2013, *Astron. Astrophys.*, 549, A98

Conrad, C., Scholz, R.-D., Kharchenko, N. V., et al. 2014, *Astron. Astrophys.*, 562, A54

Cutri, R. M., Skrutskie, M. F., van Dyk, S., et al. 2003, VizieR Online Data Catalog, 2246, 0

de Grijs, R., Gilmore, G. F., Johnson, R. A., & Mackey, A. D. 2002a, *Monthly Notices Roy. Astron. Soc.*, 331, 245

de Grijs, R., Gilmore, G. F., Mackey, A. D., et al. 2002b, *Monthly Notices Roy. Astron. Soc.*, 337, 597

de Grijs, R., Johnson, R. A., Gilmore, G. F., & Frayn, C. M. 2002c, *Monthly Notices Roy. Astron. Soc.*, 331, 228

de La Fuente Marcos, R. & de La Fuente Marcos, C. 2009a, *New Astronomy*, 14, 180

de La Fuente Marcos, R. & de La Fuente Marcos, C. 2009b, *Astron. Astrophys.*, 500, L13

de La Fuente Marcos, R. & de La Fuente Marcos, C. 2009c, *Astrophys. J.*, 700, 436

Depagne, E. & 4MOST consortium, t. 2014, ArXiv e-prints, arXiv No.: 1409.2279

Dias, W. S., Alessi, B. S., Moitinho, A., & Lépine, J. R. D. 2002, *Astron. Astrophys.*, 389, 871

Dobbs, C. & Pettitt, A. 2014, ArXiv e-prints, arXiv No.: 1407.0250

D'Orazi, V., Biazzo, K., & Randich, S. 2011, *Astron. Astrophys.*, 526, A103

Duchêne, G., Delgado-Donate, E., Haisch, Jr., K. E., Loinard, L., & Rodríguez, L. F. 2007, Protostars and Planets V, 379

Dufolt, M., Figon, P., & Meyssonier, N. 1995, *Astron. Astrophys.*Suppl., 114

Dutra, C. M., Bica, E., Soares, J., & Barbuy, B. 2003, *Astron. Astrophys.*, 400, 533

Efremov, Y. N. 2010, *Monthly Notices Roy. Astron. Soc.*, 405, 1531

Elias, F., Alfaro, E. J., & Cabrera-Caño, J. 2009, *Monthly Notices Roy. Astron. Soc.*, 397, 2

Elmegreen, B. G. 2007, *Astrophys. J.*, 668, 1064

Elmegreen, B. G. 2009, *Astrophys. Sp. Sc.*, 324, 83

Elmegreen, B. G. 2010, in IAU Symposium, Vol. 266, IAU Symposium, ed. R. de Grijs & J. R. D. Lépine, 3–13

Elmegreen, B. G. 2011, in EAS Publications Series, Vol. 51, EAS Publications Series, ed. C. Charbonnel & T. Montmerle, 31–44

Epchtein, N., de Batz, B., Capoani, L., et al. 1997, The Messenger, 87, 27

Fabricius, C. 1993, Bulletin d'Information du Centre de Donnees Stellaires, 42, 5

Famaey, B., Jorissen, A., Luri, X., et al. 2005, *Astron. Astrophys.*, 430, 165

Friel, E. D., Donati, P., Bragaglia, A., et al. 2014, *Astron. Astrophys.*, 563, A117

Frinchaboy, P. M., Thompson, B., Jackson, K. M., et al. 2013, *Astrophys. J. Letters*, 777, L1

Froebrich, D., Scholz, A., & Raftery, C. L. 2007, *Monthly Notices Roy. Astron. Soc.*, 374, 399

Geller, M. J. & Huchra, J. P. 1983, *Astrophys. J. Suppl.*, 52, 61

Geller, A. M., Mathieu, R. D., Harris, H. C., & McClure, R. D. 2008, *Astron. J.*, 135, 2264

Geller, A. M., Mathieu, R. D., Braden, E. K., et al. 2010, *Astron. J.*, 139, 1383

Geller, A. M. 2013, in EAS Publications Series, Vol. 64, EAS Publications Series, 317–320

Gieles, M., Sana, H., & Portegies Zwart, S. F. 2010, *Monthly Notices Roy. Astron. Soc.*, 402, 1750

Gilmore, G., Randich, S., Asplund, M., et al. 2012, The Messenger, 147, 25

Girardi, L., Bertelli, G., Bressan, A., et al. 2002, *Astron. Astrophys.*, 391, 195

Gontcharov, G. A. 2006, Astronomy Letters, 32, 759

Goodwin, S. P. & Kroupa, P. 2005, *Astron. Astrophys.*, 439, 565

Goodwin, S. P. & Bastian, N. 2006, *Monthly Notices Roy. Astron. Soc.*, 373, 752

Goodwin, S. P., Kroupa, P., Goodman, A., & Burkert, A. 2007, Protostars and Planets V, 133

Goodwin, S. P. 2009, *Astrophys. Sp. Sc.*, 324, 259

Gouliermis, D., Keller, S. C., Kontizas, M., Kontizas, E., & Bellas-Velidis, I. 2004, *Astron. Astrophys.*, 416, 137

Gusev, A. S. & Efremov, Y. N. 2013, *Monthly Notices Roy. Astron. Soc.*, 434, 313

Hambly, N. C., MacGillivray, H. T., Read, M. A., et al. 2001, *Monthly Notices Roy. Astron. Soc.*, 326, 1279

Hayes, C. R. & Friel, E. D. 2014, *Astron. J.*, 147, 69

Herbig, G. H. 1962, *Astrophys. J.*, 135, 736

Hillenbrand, L. A. & Hartmann, L. W. 1998, *Astrophys. J.*, 492, 540

Høg, E., Bässgen, G., Bastian, U., et al. 1997, *Astron. Astrophys.*, 323, L57

Høg, E., Fabricius, C., Makarov, V. V., et al. 2000, *Astron. Astrophys.*, 355, L27

Hole, K. T., Geller, A. M., Mathieu, R. D., et al. 2009, *Astron. J.*, 138, 159

Huchra, J. P. & Geller, M. J. 1982, *Astrophys. J.*, 257, 423

Jacobson, H. R., Friel, E. D., & Pilachowski, C. A. 2011a, *Astron. J.*, 141, 58

Jacobson, H. R., Pilachowski, C. A., & Friel, E. D. 2011b, *Astron. J.*, 142, 59

Kazarovets, E. V., Samus, N. N., & Durlevich, O. V. 1998, Information Bulletin on Variable Stars, 4655, 1

Kharchenko, N. V. 2001, Kinematika i Fizika Nebesnykh Tel, 17, 409

Kharchenko, N. V., Piskunov, A. E., & Scholz, R.-D. 2004a, Astronomische Nachrichten, 325, 439

Kharchenko, N. V., Piskunov, A. E., Röser, S., Schilbach, E., & Scholz, R.-D. 2004b, Astronomische Nachrichten, 325, 740

Kharchenko, N. V., Piskunov, A. E., Röser, S., Schilbach, E., & Scholz, R.-D. 2005a, *Astron. Astrophys.*, 438, 1163

Kharchenko, N. V., Piskunov, A. E., Röser, S., Schilbach, E., & Scholz, R.-D. 2005b, *Astron. Astrophys.*, 440, 403

Kharchenko, N. V., Scholz, R.-D., Piskunov, A. E., Röser, S., & Schilbach, E. 2007, Astronomische Nachrichten, 328, 889

Kharchenko, N. V., Piskunov, A. E., Schilbach, E., Röser, S., & Scholz, R.-D. 2012, *Astron. Astrophys.*, 543, A156

Kharchenko, N. V., Piskunov, A. E., Schilbach, E., Röser, S., & Scholz, R.-D. 2013, *Astron. Astrophys.*, 558, A53

King, I. 1962, *Astron. J.*, 67, 471

Kordopatis, G., Recio-Blanco, A., de Laverny, P., et al. 2011, *Astron. Astrophys.*, 535, A106

Kordopatis, G., Gilmore, G., Steinmetz, M., et al. 2013, *Astron. J.*, 146, 134

Kouwenhoven, M. B. N. & de Grijs, R. 2008, *Astron. Astrophys.*, 480, 103

Lada, C. J. & Lada, E. A. 2003, *Anual Rev. Astron. Astrophys.*, 41, 57

Lada, C. J. 2006, *Astrophys. J. Letters*, 640, L63

Leonard, P. J. T. 1988, *Astron. J.*, 95, 108

Li, S., Frank, A., & Blackman, E. G. 2014, *Monthly Notices Roy. Astron. Soc.*, 444, 2884

Lyngå, G. 1987, Catalogue of open cluster data, Fifth edition

Matijevič, G., Zwitter, T., Munari, U., et al. 2010, *Astron. J.*, 140, 184

Matijevič, G., Zwitter, T., Bienaymé, O., et al. 2011, *Astron. J.*, 141, 200

Matijevič, G., Zwitter, T., Bienaymé, O., et al. 2012, *Astrophys. J. Suppl.*, 200, 14

Melnik, A. M. & Efremov, Y. N. 1995, Astronomy Letters, 21, 10

Mermilliod, J. C. 1988, Bulletin d'Information du Centre de Donnees Stellaires, 35, 77

Mitschang, A. W., De Silva, G., Sharma, S., & Zucker, D. B. 2013, *Monthly Notices Roy. Astron. Soc.*, 428, 2321

Mitschang, A. W., De Silva, G., Zucker, D. B., et al. 2014, *Monthly Notices Roy. Astron. Soc.*, 438, 2753

Monet, D. G., Levine, S. E., Canzian, B., et al. 2003, *Astron. J.*, 125, 984

Mooley, K., Hillenbrand, L., Rebull, L., Padgett, D., & Knapp, G. 2013, *Astrophys. J.*, 771, 110

Morrison, J. E., Röser, S., McLean, B., Bucciarelli, B., & Lasker, B. 2001, *Astron. J.*, 121, 1752

Munari, U., Sordo, R., Castelli, F., & Zwitter, T. 2005, *Astron. Astrophys.*, 442, 1127

Netopil, M., Paunzen, E., & Stütz, C. 2012, in: Developments of the Open Cluster Database WEBDA, ed. A. Moitinho & J. Alves, 53

Netopil, M. & Paunzen, E. 2013, *Astron. Astrophys.*, 557, A10

Nordström, B., Mayor, M., Andersen, J., et al. 2004, *Astron. Astrophys.*, 419

Ortega, V. G., Jilinski, E., de la Reza, R., & Bazzanella, B. 2009, *Astron. J.*, 137, 3922

Parker, R. J., Goodwin, S. P., & Allison, R. J. 2011, *Monthly Notices Roy. Astron. Soc.*, 418, 2565

Perryman, M. A. C., Lindegren, L., Kovalevsky, J., et al. 1997, *Astron. Astrophys.*, 323, L49

Perryman, M. A. C., Brown, A. G. A., Lebreton, Y., et al. 1998, *Astron. Astrophys.*, 331, 81

Pfeffer, J., Griffen, B. F., Baumgardt, H., & Hilker, M. 2014, *Monthly Notices Roy. Astron. Soc.*, 444, 3670

Piatti, A. E., Clariá, J. J., & Ahumada, A. V. 2010, *Publ. Astron. Soc. Pacific*, 122, 516

Piskunov, A. E., Kharchenko, N. V., Röser, S., Schilbach, E., & Scholz, R.-D. 2006, *Astron. Astrophys.*, 445, 545

Platais, I., Kozhurina-Platais, V., & van Leeuwen, F. 1998, *Astron. J.*, 116, 2423

Preibisch, T. & Zinnecker, H. 2007, in IAU Symposium, Vol. 237, IAU Symposium, ed. B. G. Elmegreen & J. Palous, 270–277

Preibisch, T. & Mamajek, E. 2008, The Nearest OB Association: Scorpius-Centaurus (Sco OB2), ed. B. Reipurth, 235

Ramírez Alegría, S., Borissova, J., Chené, A. N., et al. 2014, *Astron. Astrophys.*, 564, L9

Recio-Blanco, A., Bijaoui, A., & de Laverny, P. 2006, *Monthly Notices Roy. Astron. Soc.*, 370, 141

Reid, M. J., Menten, K. M., Brunthaler, A., et al. 2014, *Astrophys. J.*, 783, 130

Rivilla, V. M., Martín-Pintado, J., Jiménez-Serra, I., & Rodríguez-Franco, A. 2013, *Astron. Astrophys.*, 554, A48

Röser, S. & Bastian, U. 1991, PPM Star Catalogue. Positions and proper motions of 181731 stars north of -2.5 degrees declination for equinox and epoch J2000.0. Vol. I: Zones +80° to +30°. Vol. II: Zones +20° to -0°.

Röser, S., Demleitner, M., & Schilbach, E. 2010, *Astron. J.*, 139, 2440

Ruprecht, J., Balazs, B. A., & White, R. E. 1981, "Catalogue of star clusters and associations"

Sagar, R. & Bhatt, H. C. 1989, *Monthly Notices Roy. Astron. Soc.*, 236, 865

Samus, N. N., Durlevich, O. V., & Kazarovets, R. V. 1997, Baltic Astronomy, 6, 296

Sánchez, N., Añez, N., Alfaro, E. J., & Crone Odekon, M. 2010, *Astrophys. J.*, 720, 541

Schilbach, E., Kharchenko, N. V., Piskunov, A. E., Röser, S., & Scholz, R.-D. 2006, *Astron. Astrophys.*, 456, 523

Schmeja, S., Kumar, M. S. N., & Ferreira, B. 2008, *Monthly Notices Roy. Astron. Soc.*, 389, 1209

Siebert, A., Williams, M. E. K., Siviero, A., et al. 2011, *Astron. J.*, 141, 187

Siess, L., Dufour, E., & Forestini, M. 2000, *Astron. Astrophys.*, 358, 593

Smith, M. C., Whiteoak, S. H., & Evans, N. W. 2012, *Astrophys. J.*, 746, 181

Spitzer, Jr., L. 1958, *Astrophys. J.*, 127, 17

Steinmetz, M., Zwitter, T., Siebert, A., et al. 2006, *Astron. J.*, 132, 1645

Sutherland, W., Emerson, J., Dalton, G., et al. 2014, ArXiv e-prints, arXiv No.: 1409.4780

Tofflemire, B. M., Gosnell, N. M., Mathieu, R. D., & Platais, I. 2014, *Astron. J.*, 148, 61

Tonry, J. & Davis, M. 1979, *Astron. J.*, 84, 1511

Urban, A., Martel, H., & Evans, II, N. J. 2010, *Astrophys. J.*, 710, 1343

Vallenari, A. 2014, in IAU Symposium, Vol. 298, IAU Symposium, ed. S. Feltzing, G. Zhao, N. A. Walton, & P. Whitelock, 253–264

van den Bergh, S. & McClure, R. D. 1980, *Astron. Astrophys.*, 88, 360

Walker, M. F. 1956, *Astrophys. J. Suppl.*, 2, 365

Weber, M., Strassmeier, K. G., & Granzer, T. 2013, Publications de l'Observatoire Astronomique de Beograd, 92, 21

Wright, N. J., Parker, R. J., Goodwin, S. P., & Drake, J. J. 2014, *Monthly Notices Roy. Astron. Soc.*, 438, 639

Yanny, B., Rockosi, C., Newberg, H. J., et al. 2009, *Astron. J.*, 137, 4377

Zacharias, N., Urban, S. E., Zacharias, M. I., et al. 2004, *Astron. J.*, 127, 3043

Zacharias, N., Finch, C., Girard, T., et al. 2010, *Astron. J.*, 139, 2184

Zacharias, N., Finch, C. T., Girard, T. M., et al. 2013, *Astron. J.*, 145, 44

Zwitter, T., Castelli, F., & Munari, U. 2004, *Astron. Astrophys.*, 417, 1055

Zwitter, T., Siebert, A., Munari, U., et al. 2008, *Astron. J.*, 136, 421

Appendix A

Tables for the results from RAVE

Section A.1

Radial Velocities

The first of the following tables (Tab. A.1) summarises the mean radial velocities ($\overline{RV}$) for 110 OCs identified in the RAVE data. The first two columns give the identifiers, namely COCD number (Seq) and Name. Columns $3-7$ give the results for the obtained RAVE data, along with uncertainties and number of measurements available. Columns $8-12$ provide newly computed reference values obtained from the CRVAD-2, along with uncertainties and number of measurements available. The final three columns list reference values from the CRVOCA (Kharchenko et al. 2007), along with the uncertainties and number of stars given therein. For the latter, I preferred to use their computed $\overline{RV}$ and only give literature values, if no calculated $\overline{RV}$ was available. As stated in Sect. 3.2.1, the $\overline{RV}$ from RAVE and CRVAD-2 were primarily derived from best RV or 1σ-members, respectively. Only where just one or no most probable member was available I included good RV or 2σ-members as well to compute the $\overline{RV}$ in RAVE and CRVAD-2, respectively. The Eq. A.1-A.5 are the same as given in Sect. 3.2.1 and are given here for overview purposes to illustrate the calculations used to generate Tab. A.1. The provided $\overline{RV}$ (Eq. A.1) in RAVE and CRVAD-2 were calculated as weighted mean, with the weights defined by Eq. A.1.

$$\overline{RV} = \frac{\sum_i RV_i \cdot g_i}{\sum_i g_i} \tag{A.1}$$

$$\sigma\overline{RV} = \sqrt{\frac{n}{n-1} \cdot \frac{\sum_i g_i \cdot (RV_i - \overline{RV})^2}{\sum_i g_i}} \tag{A.2}$$

$$\mathrm{e}\overline{RV} = \frac{\sigma\overline{RV}}{\sqrt{n}} \tag{A.3}$$

$$\overline{eRV^*} = \frac{\sum_i eRV_i^* \cdot (P_{kin,i} \cdot P_{phot,i})}{\sum_i (P_{kin,i} \cdot P_{phot,i})}, \tag{A.4}$$

with the weights defined as $$g_i = \frac{P_{kin,i} \cdot P_{phot,i}}{(eRV_i^*)^2}.$$

I considered all $eRV^* < 1$ km/s to be too optimistic and replaced them with 1 km/s. The weighted standard deviation is defined by Eq. A.2, where the "n" in the nominator of "$n/(n-1)$" is a scaling factor, since the individual weights ($g_i = (P_{kin,i} \cdot P_{phot,i})/(eRV_i^*)^2$) never sum up to n, with $(P_{kin}, P_{phot}) \leq 1$ and $eRV^* \geq 1$ km/s. The uncertainties of the mean RV were obtained through Eq. A.3, while the typical RV uncertainties in OCs ($\overline{eRV^*}$) are computed by Eq. A.4 as weighted mean from the individual eRV^* of the members, with the weight defined only by the membership probabilities. The standard deviation and e$\overline{RV}$ could only be computed for OCs with at least two individual measurements and for clusters with only one representative I did not provide $\sigma\overline{RV}$ and assumed $\overline{eRV^*} = eRV^*$.

Section A.2

Metallicities

The second of the following tables (Tab. A.2) summarises the mean metallicities ($\overline{[M/H]}$) for 81 out of the 110 OCs identified in RAVE, because of the more stringent requirements for my $[M/H]$ sample. The first two columns provide the cluster identifiers, namely COCD number (Seq) and cluster name. The columns $3-7$ provide the results from RAVE DR4, along with uncertainties and number of individual measurements. Columns $8-10$ give the $\overline{[M/H]}$, uncertainty, and number of measurements obtained from the RAVE chemical pipeline (Boeche et al. 2011). The final five columns list the reference values from DAML (Dias et al. 2002), along with the uncertainties and number of stars, as well as the technique used and literature reference for the given values.
As stated in Sect. 3.2.3, the $\overline{[M/H]}$ from RAVE DR4 and the chemical pipeline were obtained using primarily best $[M/H]$ member measurements. Only where no or just one best $[M/H]$ member measurement was available, I included good $[M/H]$ member measurements as well. The Eq. A.5-A.8 are the same as given in Sect. 3.2.3 and are given here for overview purposes to illustrate the calculations used to generate Tab. A.2.

$$\overline{[M/H]} = \frac{\sum_i [M/H]_i \cdot w_i}{\sum_i w_i} \tag{A.5}$$

$$\sigma\overline{[M/H]} = \sqrt{\frac{n}{n-1} \cdot \frac{\sum_i w_i \cdot ([M/H]_i - \overline{[M/H]})^2}{\sum_i w_i}} \tag{A.6}$$

$$\mathrm{e}\overline{[M/H]} = \frac{\sigma\overline{[M/H]}}{\sqrt{n}}, \tag{A.7}$$

$$\text{with the weights defined as} \quad w_i = P_{kin,i} \cdot P_{phot,i}. \tag{A.8}$$

I compute the $\overline{[M/H]}$ (Eq. A.5) as weighted mean, with the weights defined by Eq. A.5. The weights were defined excluding the uncertainties in the individual $[M/H]$ measurements, because the listed $e[M/H]^*$ show a very discrete distribution and might not reflect realistic measurements errors (see Sect. 3.1.3). The weighted standard deviation is defined by Eq. A.6, where the "n" in the nominator of "$n/(n-1)$" is a scaling factor, since the individual weights ($w_i = P_{kin,i} \cdot P_{phot,i}$) never sum up to n, with $(P_{kin}, P_{phot}) \leq 1$. The uncertainties of the $\overline{[M/H]}$ are then obtained through Eq. A.3. The $\sigma\overline{[M/H]}$ and e$\overline{[M/H]}$ could only be calculated for clusters with at least two individual measurements, while for OCs with either none or just one individual $[M/H]$ measurement no standard deviation or uncertainty of the mean is listed, since the individual $e[M/H]^*$ might not reflect realistic measurements errors. For the same reason no typical $[M/H]$ uncertainties for the clusters in RAVE were provided.

Table A.1: $\overline{RV}$ for the OCs in RAVE, along with uncertainties, number of individual RV measurements, as well as reference values from CRVAD-2 and CRVOCA. As published in Conrad et al. (2014).

		RAVE					CRVAD-2					CRVOCA		
Seq	Name	$\overline{RV}$ km/s	e$\overline{RV}$ km/s	$\sigma\overline{RV}$ km/s	$\overline{eRV^*}$ km/s	No. of entries[a]	$\overline{RV}$ km/s	e$\overline{RV}$ km/s	$\sigma\overline{RV}$ km/s	$\overline{eRV^*}$ km/s	No. of entries[a]	$\overline{RV}$ km/s	e$\overline{RV}$ km/s	Star no.[b]
44	Alessi 13	1.1	0.5	0.6	3.0	2 (–)	15.9	1.4	2.3	0.0	1 (2)	19.5	3.0	3
47	Melotte 22	3.5	0.4	2.0	2.4	25 (–)	5.8	0.2	1.6	2.5	45 (–)	5.7	0.6	67
65	NGC 1901	-1.4	0.5	0.7	3.0	2 (–)	—	—	—	—	– (–)	14.0	1.3	1
77	Collinder 70	54.8	1.0	—	1.0	1 (–)	24.0	1.9	5.8	3.7	9 (–)	20.2	11.0	5
127	NGC 2354	42.3	8.1	14.1	1.0	3 (–)	—	—	—	—	– (–)	33.4	0.3	6
129	Alessi 3	-2.1	0.5	1.3	1.7	1 (5)	—	—	—	—	– (–)	20.0	7.4	-1
133	Collinder 135	27.0	10.1	22.7	1.1	5 (–)	16.2	0.8	1.6	5.6	4 (–)	15.3	2.2	4
142	Bochum 5	27.9	11.3	25.3	3.5	5 (–)	—	—	—	—	– (–)	16.0	2.5	1
147	NGC 2422	34.2	0.9	3.1	4.5	13 (–)	34.4	1.9	5.6	6.9	9 (–)	29.4	3.7	4
148	NGC 2423	21.1	2.0	12.2	3.2	36 (–)	20.9	3.2	7.8	1.0	6 (–)	18.1	0.2	7
149	Ruprecht 26	39.1	7.8	17.4	9.8	5 (–)	15.0	3.7	—	3.7	1 (–)	15.0	3.7	1
150	Melotte 71	0.5	1.0	—	1.0	1 (–)	—	—	—	—	– (–)	50.1	0.1	11
152	NGC 2428	46.7	2.7	5.5	6.5	4 (–)	—	—	—	—	– (–)	—	—	–
153	NGC 2430	31.3	11.8	16.7	2.5	2 (–)	—	—	—	—	– (–)	—	—	–
158	Ruprecht 151	31.3	4.8	16.1	3.8	11 (–)	—	—	—	—	– (–)	—	—	–
159	NGC 2451A	56.2	30.7	53.2	1.3	– (3)	25.7	5.3	10.7	2.1	4 (–)	27.7	0.5	21
160	NGC 2437	30.4	4.0	16.2	10.5	16 (–)	—	—	—	—	– (–)	48.1	0.1	1
163	NGC 2447	32.0	6.2	10.8	5.4	3 (–)	20.9	1.1	2.7	1.0	6 (–)	21.7	0.2	11
164	NGC 2448	27.2	1.2	2.2	4.9	– (3)	15.0	3.7	—	3.7	1 (–)	15.0	3.7	1
166	Haffner 16	37.2	3.0	—	3.0	1 (–)	65.8	3.7	—	3.7	1 (–)	65.8	3.7	1
167	NGC 2477	6.4	0.2	0.3	1.2	2 (–)	—	—	—	—	– (–)	7.3	0.1	49
171	NGC 2482	42.2	0.9	1.6	4.6	3 (–)	—	—	—	—	– (–)	—	—	–
175	NGC 2516	-4.5	5.0	8.6	1.1	– (3)	22.9	0.3	1.0	3.3	10 (–)	24.2	0.2	57
180	NGC 2527	42.4	1.3	3.8	4.8	9 (–)	—	—	—	—	– (–)	135.1	3.0	-1
182	Vel OB2	20.8	3.6	16.9	1.2	– (22)	15.2	5.4	7.6	5.7	2 (–)	24.0	9.7	13
191	Haffner 26	62.4	12.1	—	12.1	1 (–)	—	—	—	—	– (–)	—	—	–
192	NGC 2567	37.0	1.0	—	1.0	1 (–)	—	—	—	—	– (–)	35.8	0.1	1
193	NGC 2571	44.0	10.3	—	10.3	1 (–)	—	—	—	—	– (–)	—	—	–
201	NGC 2632	34.0	0.3	1.1	1.6	14 (–)	34.1	0.4	2.4	2.2	33 (–)	34.5	0.1	46

Table A.1: continued

		RAVE					CRVAD-2					CRVOCA		
Seq	Name	$\overline{RV}$ km/s	e$\overline{RV}$ km/s	$\sigma\overline{RV}$ km/s	$\overline{eRV^*}$ km/s	No. of entries[a]	$\overline{RV}$ km/s	e$\overline{RV}$ km/s	$\sigma\overline{RV}$ km/s	$\overline{eRV^*}$ km/s	No. of entries[a]	$\overline{RV}$ km/s	e$\overline{RV}$ km/s	Star no.[b]
202	IC 2391	12.5	3.5	—	3.5	1 (–)	15.3	1.3	4.2	4.3	10 (–)	14.1	0.2	15
212	NGC 2682	33.8	0.3	0.9	1.0	8 (–)	33.6	0.3	1.2	1.0	15 (–)	33.0	1.6	25
216	Platais 8	7.3	8.0	26.7	1.3	11 (–)	21.5	4.9	7.0	7.4	2 (–)	17.3	3.1	5
223	Turner 5	-1.2	15.0	21.1	1.4	2 (–)	—	—	—	—	– (–)	26.2	3.7	-1
226	Ruprecht 80	45.7	1.0	—	1.0	1 (–)	—	—	—	—	– (–)	—	—	–
230	NGC 3036	11.8	1.0	—	1.0	1 (–)	—	—	—	—	– (–)	—	—	–
243	IC 2581	2.2	14.1	—	14.1	1 (–)	-0.7	0.5	0.7	2.0	2 (–)	-4.6	3.5	5
248	Collinder 223	8.6	0.1	0.1	1.0	2 (–)	—	—	—	—	– (–)	4.7	0.0	1
249	Ruprecht 90	18.1	7.3	10.3	12.4	2 (–)	-40.0	4.4	—	4.4	1 (–)	-40.0	4.4	1
251	Loden 153	13.7	5.2	7.4	7.4	2 (–)	-11.8	2.5	4.3	0.0	1 (2)	-10.3	2.4	3
254	NGC 3324	-4.0	2.9	4.1	9.0	2 (–)	-8.5	3.7	—	3.7	1 (–)	-8.5	4.2	1
255	vdBergh-Hagen 99	12.8	3.7	9.0	5.5	6 (–)	11.3	0.8	1.1	1.4	2 (–)	13.0	2.0	1
258	Melotte 101	20.3	10.4	—	10.4	1 (–)	—	—	—	—	– (–)	—	—	–
259	IC 2602	5.0	2.4	19.1	2.1	65 (–)	27.2	2.1	4.3	3.1	4 (–)	16.2	0.3	18
260	Bochum 10	-1.5	4.6	—	4.6	1 (–)	-2.3	1.8	—	1.8	1 (–)	-2.3	1.8	1
261	Alessi 5	6.3	3.2	4.5	3.8	2 (–)	10.9	8.6	12.1	7.4	2 (–)	12.8	8.8	2
262	Collinder 228	24.2	13.1	—	13.1	1 (–)	-1.2	5.7	18.1	4.7	10 (–)	-13.5	3.3	24
266	Ruprecht 91	-4.1	11.3	—	11.3	1 (–)	—	—	—	—	– (–)	7.3	0.0	1
267	Loden 189	10.5	4.5	10.1	6.3	5 (–)	—	—	—	—	– (–)	—	—	–
268	Ruprecht 92	-10.6	3.7	5.2	7.2	2 (–)	—	—	—	—	– (–)	-15.6	1.8	-1
270	Trumpler 17	25.5	1.7	2.4	10.9	2 (–)	—	—	—	—	– (–)	—	—	–
271	Collinder 236	14.1	11.5	25.8	10.0	5 (–)	—	—	—	—	– (–)	—	—	–
273	NGC 3496	2.3	2.0	3.4	5.9	1 (2)	—	—	—	—	– (–)	-51.4	0.0	1
274	Pismis 17	-47.1	0.5	0.7	1.1	2 (–)	—	—	—	—	– (–)	61.7	0.0	1
275	Ruprecht 93	5.1	3.5	—	3.5	1 (–)	—	—	—	—	– (–)	—	—	–
276	NGC 3532	4.3	0.6	2.1	4.4	13 (–)	-2.3	6.4	11.0	3.6	3 (–)	3.1	2.5	3
283	Trumpler 18	-10.0	12.5	—	12.5	1 (–)	-20.0	7.4	—	7.4	1 (–)	-20.0	—	1
287	NGC 3680	2.2	1.0	—	1.0	1 (–)	—	—	—	—	– (–)	8.0	3.7	7
298	Loden 481	16.9	8.7	—	8.7	1 (–)	-7.1	1.2	—	1.2	1 (–)	-22.1	14.9	2
304	ESO 130-06	-1.2	3.4	4.8	5.8	2 (–)	—	—	—	—	– (–)	—	—	–

Table A.1: continued

		RAVE					CRVAD-2					CRVOCA		
Seq	Name	$\overline{RV}$ km/s	e$\overline{RV}$ km/s	$\sigma\overline{RV}$ km/s	$\overline{eRV^*}$ km/s	No. of entries[a]	$\overline{RV}$ km/s	e$\overline{RV}$ km/s	$\sigma\overline{RV}$ km/s	$\overline{eRV^*}$ km/s	No. of entries[a]	$\overline{RV}$ km/s	e$\overline{RV}$ km/s	Star no.[b]
305	Loden 565	-17.9	9.3	—	9.3	1 (–)	10.1	1.0	—	1.0	1 (–)	10.1	0.2	1
306	ESO 130-08	-38.5	6.3	9.0	8.1	2 (–)	—	—	—	—	– (–)	—	—	–
309	NGC 4349	-11.9	3.2	5.6	4.5	3 (–)	-15.7	1.8	—	1.8	1 (–)	-15.7	1.8	1
310	Collinder 258	-14.3	9.2	13.0	12.5	2 (–)	—	—	—	—	– (–)	—	—	–
322	Stock 16	-6.9	6.8	9.6	10.3	2 (–)	-52.8	12.6	21.9	37.0	3 (–)	-41.8	8.8	5
324	Loden 821	-3.7	5.7	11.4	6.9	4 (–)	-39.0	7.4	—	7.4	1 (–)	-39.0	7.4	1
327	Basel 18	-22.0	3.0	—	3.0	1 (–)	—	—	—	—	– (–)	—	—	–
328	Hogg 16	-51.3	2.2	3.1	12.8	2 (–)	-29.8	6.0	12.1	7.5	4 (–)	-36.0	6.8	4
333	Loden 915	-21.6	11.8	—	11.8	1 (–)	—	—	—	—	– (–)	—	—	–
335	Loden 1010	-18.2	3.3	6.6	10.5	4 (–)	—	—	—	—	– (–)	—	—	–
336	NGC 5281	-15.9	13.1	—	13.1	1 (–)	—	—	—	—	– (–)	—	—	–
337	Platais 12	-11.0	2.2	14.8	4.6	44 (–)	—	—	—	—	– (–)	-12.0	9.5	2
338	NGC 5316	10.0	5.3	12.9	8.4	6 (–)	—	—	—	—	– (–)	—	—	–
339	Loden 995	-6.1	1.2	—	1.2	1 (–)	—	—	—	—	– (–)	—	—	–
343	Ruprecht 110	-36.6	4.0	5.6	1.0	2 (–)	—	—	—	—	– (–)	—	—	–
356	Alessi 6	20.0	1.0	—	1.0	1 (–)	—	—	—	—	– (–)	—	—	–
367	Nor OB5	-20.2	6.8	11.8	2.6	1 (2)	-26.9	6.0	12.1	7.4	4 (–)	-23.1	5.1	7
382	NGC 6204	11.6	0.4	0.6	9.9	2 (–)	—	—	—	—	– (–)	-51.0	5.8	5
387	NGC 6242	39.3	39.5	55.9	10.3	2 (–)	—	—	—	—	– (–)	—	—	–
390	NGC 6250	-16.8	0.0	0.0	9.4	2 (–)	—	—	—	—	– (–)	—	—	–
393	Sco OB4	-23.6	8.1	42.3	5.7	27 (–)	6.9	1.8	4.5	7.4	6 (–)	3.0	6.3	7
396	vdBergh-Hahen 221	5.2	5.6	—	5.6	1 (–)	—	—	—	—	– (–)	6.3	3.8	3
397	IC 4651	-30.4	0.3	0.6	1.0	4 (–)	—	—	—	—	– (–)	-31.0	0.2	14
399	Antalova 1	-6.3	12.0	17.0	11.4	2 (–)	33.0	40.6	—	40.6	1 (–)	33.0	40.6	1
402	NGC 6383	-16.5	10.7	15.1	10.7	2 (–)	1.9	2.7	3.8	5.6	2 (–)	2.7	2.2	3
403	Trumpler 27	-35.3	1.2	1.8	1.0	2 (–)	-15.8	1.3	—	1.3	1 (–)	-15.8	—	1
404	Trumpler 28	-32.8	11.9	16.8	6.7	2 (–)	—	—	—	—	– (–)	—	—	–
405	ESO 139-13	-33.9	1.0	—	1.0	1 (–)	—	—	—	—	– (–)	—	—	–
408	NGC 6405	-7.0	2.7	8.7	6.6	10 (–)	-8.9	2.3	3.2	4.1	2 (–)	-6.4	—	1
410	Alessi 9	-71.0	1.0	—	1.0	1 (–)	-11.6	1.2	—	1.2	1 (–)	-11.6	1.2	1

Table A.1: continued

		RAVE					CRVAD-2					CRVOCA		
Seq	Name	$\overline{RV}$ km/s	e$\overline{RV}$ km/s	$\sigma\overline{RV}$ km/s	$\overline{eRV^*}$ km/s	No. of entries[a]	$\overline{RV}$ km/s	e$\overline{RV}$ km/s	$\sigma\overline{RV}$ km/s	$\overline{eRV^*}$ km/s	No. of entries[a]	$\overline{RV}$ km/s	e$\overline{RV}$ km/s	Star no.[b]
411	NGC 6416	-11.2	12.7	18.0	2.0	2 (–)	—	—	—	—	– (–)	—	—	–
413	NGC 6425	5.4	12.1	—	12.1	1 (–)	—	—	—	—	– (–)	—	—	–
418	Sco OB5	-10.5	6.4	—	6.4	1 (–)	—	—	—	—	– (–)	—	—	–
420	NGC 6475	-21.4	12.7	—	12.7	1 (–)	-13.7	0.4	1.6	3.8	16 (–)	-14.7	0.2	40
429	NGC 6546	-29.4	1.0	—	1.0	1 (–)	—	—	—	—	– (–)	-16.7	15.8	3
430	vdBergh 113	16.1	1.8	2.5	7.5	2 (–)	-16.0	3.7	—	3.7	1 (–)	-16.0	3.7	1
435	Sgr OB7	-44.5	9.6	30.4	8.5	10 (–)	-3.6	2.2	4.9	4.1	5 (–)	-6.1	17.1	3
436	Markarian 38	-33.0	0.5	0.7	1.1	2 (–)	6.0	9.1	—	9.1	1 (–)	-3.2	9.2	2
444	NGC 6618	-44.6	0.7	1.0	1.2	2 (–)	-14.7	12.8	18.1	9.4	2 (–)	-25.3	19.1	3
445	Trumpler 33	-8.5	7.7	—	7.7	1 (–)	—	—	—	—	– (–)	—	—	–
449	IC 4725	61.2	17.9	35.9	9.5	4 (–)	2.1	7.9	13.7	7.3	3 (–)	2.4	0.2	2
452	Ruprecht 145	-8.4	1.0	—	1.0	1 (–)	—	—	—	—	– (–)	—	—	–
1033	ASCC 33	34.5	25.5	44.2	1.2	– (3)	14.7	9.0	12.7	7.6	2 (–)	15.0	9.0	2
1057	ASCC 57	2.5	7.3	17.9	1.2	6 (–)	—	—	—	—	– (–)	—	—	–
1078	ASCC 78	-14.6	5.5	15.6	1.1	8 (–)	—	—	—	—	– (–)	—	—	–
1085	ASCC 85	11.2	8.5	—	8.5	1 (–)	—	—	—	—	– (–)	7.1	0.0	1
1089	Alessi 24	-38.6	19.3	33.4	1.0	3 (–)	—	—	—	—	– (–)	12.3	8.3	2
1091	ASCC 91	-14.5	1.0	—	1.0	1 (–)	—	—	—	—	– (–)	—	—	–
1093	ASCC 93	-14.5	12.4	—	12.4	1 (–)	-19.4	5.3	9.2	4.9	3 (–)	-23.3	6.4	3
1097	Alessi 40	-16.3	5.2	7.3	2.8	2 (–)	—	—	—	—	– (–)	—	—	–

[a]The number in brackets are the number of additional good member measurements used to compute $\overline{RV}$.

[b] "−1" indicates clusters were only one star was used considering only $P_{kin} > 1\%$.

Table A.2: $\overline{[M/H]}$ for the OCs in RAVE, along with uncertainties, number of individual $[M/H]$ measurements and reference values from DAML. As published in Conrad et al. (2014).

		RAVE DR4					RAVE chem. pipeline			DAML				
Seq	Name	$\overline{[M/H]}$ dex	e$\overline{[M/H]}$ dex	$\sigma\overline{[M/H]}$ dex	$e\overline{[M/H]}^*$ dex	No. of entries[a]	$\overline{[M/H]}$ dex	e$\overline{[M/H]}$ dex	No. of entries[a]	$\overline{[M/H]}$ dex	e$\overline{[M/H]}$ dex	No. stars	Tech.	Ref.
44	Alessi 13	0.06	0.15	—	0.15	1 (–)	—	—	– (–)	0.17	—	–	CMD	Po10
47	Melotte 22	-0.04	0.03	0.12	0.12	20 (–)	-0.03	0.07	6 (–)	-0.03	0.02	15	REC	G00
65	NGC 1901	-0.02	0.09	0.16	0.11	1 (2)	—	—	– (–)	—	—	–	—	—
77	Collinder 70	0.14	0.08	—	0.08	1 (–)	0.15	—	1 (–)	—	—	–	—	—
127	NGC 2354	-0.11	0.16	0.28	0.09	3 (–)	-0.22	0.13	3 (–)	-0.30	0.02	12	DDO	Cl99
129	Alessi 3	-0.28	0.07	0.16	0.11	1 (5)	-0.39	0.10	– (5)	—	—	–	—	—
133	Collinder 135	-0.22	0.09	0.21	0.10	5 (–)	-0.25	0.13	5 (–)	—	—	–	—	—
142	Bochum 5	-0.17	0.10	0.19	0.10	4 (–)	-0.20	0.06	3 (–)	—	—	–	—	—
147	NGC 2422	-0.03	0.13	0.34	0.12	7 (–)	—	—	– (–)	0.11	0.10	11	STO	N88
148	NGC 2423	0.07	0.04	0.19	0.10	27 (–)	-0.08	0.04	9 (–)	—	—	–	—	—
149	Ruprecht 26	0.31	0.11	—	0.11	1 (–)	—	—	– (–)	—	—	–	—	—
150	Melotte 71	-0.22	0.10	—	0.10	1 (–)	-0.20	—	1 (–)	—	—	–	—	—
152	NGC 2428	-0.14	0.10	0.14	0.10	2 (–)	-0.15	0.07	2 (–)	—	—	–	—	—
153	NGC 2430	0.13	0.15	0.21	0.11	2 (–)	-0.08	—	1 (–)	—	—	–	—	—
158	Ruprecht 151	-0.10	0.08	0.20	0.10	7 (–)	-0.21	0.01	3 (–)	—	—	–	—	—
159	NGC 2451A	-0.53	0.22	0.38	0.10	– (3)	—	—	– (–)	0.00	—	–	—	Ma00
160	NGC 2437	-0.75	0.33	0.58	0.14	3 (–)	-0.11	—	1 (–)	0.06	0.09	1	DTR	T97
163	NGC 2447	-0.10	0.15	0.21	0.11	2 (–)	—	—	– (–)	—	—	–	—	—
166	Haffner 16	-0.11	0.09	—	0.09	1 (–)	—	—	– (–)	—	—	–	—	—
167	NGC 2477	-0.19	0.00	0.00	0.07	2 (–)	-0.15	0.11	2 (–)	—	—	–	—	—
171	NGC 2482	-0.08	0.14	0.20	0.10	2 (–)	-0.09	—	1 (–)	0.12	0.02	3	DDO	T97
175	NGC 2516	-0.37	0.09	0.16	0.10	– (3)	-0.48	0.14	– (3)	0.06	0.03	2	DDO	T97
180	NGC 2527	0.06	0.00	0.00	0.11	2 (–)	0.15	—	1 (–)	-0.09	—	–	DDO	Pi95
182	Vel OB2	-0.29	0.04	0.21	0.09	– (21)	-0.28	0.06	– (18)	—	—	–	—	—
192	NGC 2567	-0.07	0.09	—	0.09	1 (–)	-0.04	—	1 (–)	—	—	–	—	—
201	NGC 2632	0.10	0.03	0.10	0.11	12 (–)	0.09	0.03	9 (–)	—	—	–	—	—
202	IC 2391	-0.15	0.10	—	0.10	1 (–)	—	—	– (–)	—	—	–	—	—
212	NGC 2682	-0.10	0.04	0.10	0.08	8 (–)	-0.16	0.06	8 (–)	—	—	–	—	—
216	Platais 8	-0.30	0.08	0.26	0.10	10 (–)	-0.21	0.08	8 (–)	—	—	–	—	—
223	Turner 5	-0.21	0.06	0.11	0.10	– (3)	-0.05	0.26	– (3)	—	—	–	—	—
226	Ruprecht 80	-0.37	0.10	—	0.10	1 (–)	-0.46	—	1 (–)	—	—	–	—	—
230	NGC 3036	-0.71	0.09	—	0.09	1 (–)	—	—	– (–)	—	—	–	—	—
248	Collinder 223	-0.22	0.00	0.00	0.10	2 (–)	-0.21	0.01	2 (–)	—	—	–	—	—

Table A.2: continued

		RAVE DR4					RAVE chem. pipeline			DAML				
Seq	Name	$\overline{[M/H]}$ dex	e$\overline{[M/H]}$ dex	$\sigma\overline{[M/H]}$ dex	$\overline{e[M/H]^*}$ dex	No. of entries[a]	$\overline{[M/H]}$ dex	e$\overline{[M/H]}$ dex	No. of entries[a]	$\overline{[M/H]}$ dex	e$\overline{[M/H]}$ dex	No. stars	Tech.	Ref.
251	Loden 153	0.19	0.13	—	0.13	1 (–)	—	—	– (–)	—	—	–	—	—
254	NGC 3324	-0.47	0.14	—	0.14	1 (–)	—	—	– (–)	—	—	–	—	—
255	vdBergh-Hagen 99	0.09	0.12	0.20	0.11	3 (–)	-0.29	—	1 (–)	—	—	–	—	—
259	IC 2602	-0.09	0.03	0.19	0.10	50 (–)	-0.10	0.03	37 (–)	—	—	–	—	—
261	Alessi 5	-0.38	0.10	—	0.10	1 (–)	-0.49	—	1 (–)	—	—	–	—	—
267	Loden 189	0.20	0.07	0.10	0.11	2 (–)	0.10	—	1 (–)	—	—	–	—	—
268	Ruprecht 92	0.20	0.13	—	0.13	1 (–)	—	—	– (–)	—	—	–	—	—
271	Collinder 236	0.04	0.13	—	0.13	1 (–)	—	—	– (–)	—	—	–	—	—
274	Pismis 17	-0.14	0.13	0.28	0.11	5 (–)	-0.33	0.00	2 (–)	—	—	–	—	—
275	Ruprecht 93	0.15	0.13	—	0.13	1 (–)	—	—	– (–)	—	—	–	—	—
276	NGC 3532	-0.02	0.06	0.15	0.11	7 (–)	-0.00	—	1 (–)	—	—	–	—	—
287	NGC 3680	-0.17	0.08	—	0.08	1 (–)	-0.23	—	1 (–)	—	—	–	—	—
304	ESO 130-06	-1.52	0.19	—	0.19	1 (–)	—	—	– (–)	—	—	–	—	—
306	ESO 130-08	-0.25	0.14	—	0.14	1 (–)	—	—	– (–)	—	—	–	—	—
309	NGC 4349	-0.02	0.09	—	0.09	1 (–)	—	—	– (–)	—	—	–	—	—
324	Loden 821	-0.10	0.13	—	0.13	1 (–)	—	—	– (–)	—	—	–	—	—
327	Basel 18	0.04	0.27	—	0.27	1 (–)	—	—	– (–)	—	—	–	—	—
337	Platais 12	-0.01	0.05	0.24	0.13	20 (–)	0.03	0.12	4 (–)	—	—	–	—	—
338	NGC 5316	0.04	0.08	0.12	0.13	2 (–)	0.20	—	1 (–)	-0.02	—	–	DDO	Pi95
339	Loden 995	-0.13	0.09	—	0.09	1 (–)	-0.20	—	1 (–)	—	—	–	—	—
343	Ruprecht 110	-0.36	0.19	0.27	0.09	2 (–)	-0.12	—	1 (–)	—	—	–	—	—
356	Alessi 6	-0.15	0.08	—	0.08	1 (–)	-0.16	—	1 (–)	—	—	–	—	—
367	Nor OB5	-2.06	0.36	0.62	0.10	1 (2)	—	—	– (–)	—	—	–	—	—
382	NGC 6204	-1.05	0.15	—	0.15	1 (–)	—	—	– (–)	—	—	–	—	—
393	Sco OB4	-0.09	0.07	0.26	0.13	15 (–)	-0.18	0.13	4 (–)	—	—	–	—	—
397	IC 4651	-0.13	0.03	0.06	0.08	4 (–)	-0.10	0.04	4 (–)	—	—	–	—	—
399	Antalova 1	-0.66	0.19	—	0.19	1 (–)	—	—	– (–)	—	—	–	—	—
403	Trumpler 27	-0.19	0.01	0.02	0.09	2 (–)	-0.08	0.17	2 (–)	—	—	–	—	—
404	Trumpler 28	0.33	0.11	—	0.11	1 (–)	—	—	– (–)	—	—	–	—	—
405	ESO 139-13	-0.32	0.08	—	0.08	1 (–)	-0.38	—	1 (–)	—	—	–	—	—
408	NGC 6405	0.20	0.07	0.12	0.11	3 (–)	—	—	– (–)	0.06	0.15	–	UBV	G00
410	Alessi 9	-0.58	0.09	—	0.09	1 (–)	—	—	– (–)	—	—	–	—	—
411	NGC 6416	-0.61	0.56	0.79	0.10	2 (–)	-0.08	—	1 (–)	—	—	–	—	—
429	NGC 6546	-0.33	0.08	—	0.08	1 (–)	-0.44	—	1 (–)	—	—	–	—	—
430	vdBergh 113	-0.36	0.09	—	0.09	1 (–)	—	—	– (–)	—	—	–	—	—

Table A.2: continued

		RAVE DR4					RAVE chem. pipeline			DAML				
Seq	Name	$\overline{[M/H]}$ dex	e$\overline{[M/H]}$ dex	$\sigma\overline{[M/H]}$ dex	$\overline{e[M/H]^*}$ dex	No. of entries[a]	$\overline{[M/H]}$ dex	e$\overline{[M/H]}$ dex	No. of entries[a]	$\overline{[M/H]}$ dex	e$\overline{[M/H]}$ dex	No. stars	Tech.	Ref.
435	Sgr OB7	-0.06	0.38	0.54	0.12	2 (–)	—	—	– (–)	—	—	–	—	—
436	Markarian 38	0.18	0.00	0.00	0.10	2 (–)	0.45	0.03	2 (–)	—	—	–	—	—
444	NGC 6618	0.13	0.11	—	0.11	1 (–)	0.02	—	1 (–)	—	—	–	—	—
445	Trumpler 33	-1.54	0.19	—	0.19	1 (–)	—	—	– (–)	—	—	–	—	—
449	IC 4725	-0.26	0.01	0.01	0.14	2 (–)	—	—	– (–)	0.17	0.06	–	HRS	G00
452	Ruprecht 145	-0.13	0.08	—	0.08	1 (–)	-0.39	—	1 (–)	—	—	–	—	—
1033	ASCC 33	-0.17	0.08	0.14	0.09	– (3)	-0.14	0.13	– (3)	—	—	–	—	—
1057	ASCC 57	-0.30	0.08	0.13	0.10	3 (–)	-0.18	0.11	3 (–)	—	—	–	—	—
1078	ASCC 78	-0.06	0.04	0.11	0.08	7 (–)	-0.04	0.04	7 (–)	—	—	–	—	—
1089	Alessi 24	-0.13	0.08	0.11	0.09	2 (–)	-0.11	0.09	2 (–)	—	—	–	—	—
1091	ASCC 91	-0.04	0.08	—	0.08	1 (–)	-0.25	—	1 (–)	—	—	–	—	—
1097	Alessi 40	0.13	0.17	0.23	0.08	2 (–)	-0.16	—	1 (–)	—	—	–	—	—

[a]The number in brackets are the number of additional good member measurements used to compute $\overline{[M/H]}$.

Technique abbreviations: DDO: DDO photometry; DTR: Piatti et al. (1995) recalibrated; REC: Gratton (2000) recalibrated; UBV: UBV photometry; SPE: spectroscopy

Reference abbreviations: Fr02: Friel et al. (2002); G00: Gratton (2000); Ma00: Margheim et al. (2000); Pi95: Piatti et al. (1995); T97: Twarog et al. (1997)

Appendix B

Tables for the final working sample from the COCD

In the final working sample, I combined RV data from RAVE and the CRVAD-2 and used coordinates, distances, proper motions, and ages as provided in the COCD, while the metallicities were primarily obtained from RAVE complemented by listings in the DAML. The coordinates, proper motions (each in RA-DEC and *l*-*b*), distances and radial velocities were the input parameters to determine the Cartesian XYZ-coordinates and UVW-velocities and are summarised in Tab. B.1, along with the cluster identifiers, namely COCD number (Seq) and cluster name. The resulting XYZ-coordinates and UVW-velocities are provided in Tab. B.2, along with the identifiers, ages, and metallicities, where available.
The Cartesian XYZ-coordinates were obtained from a conversion of spherical coordinates to Cartesian coordinates following Eq. B.1, which is the same equation as provided in Sect. 4.1 and is provided here for overview purposes. The positive X-axis points towards the Galactic anticentre, the positive Y-axis points in direction of Galactic rotation, and the positive Z-axis points towards the north Galactic pole.

$$\begin{pmatrix} X \\ Y \\ Z \end{pmatrix} = \begin{pmatrix} -d \cdot (\cos b \cdot \cos l) \\ d \cdot (\cos b \cdot \sin l) \\ d \cdot \sin b \end{pmatrix} \tag{B.1}$$

where l and b are the Galactic longitude and latitude given in degrees, and d the distance of the cluster to the sun in kpc, which results in Cartesian coordinates given in kpc. The corresponding uncertainties in the XYZ-coordinates were then computed using Eq.B.2[1], where the uncertainties in the Galactic coordinates (σ_l and σ_b) were assumed to be 1", while the uncertainties in the distances (σ_d) correspond to the 10 % level.

$$\begin{pmatrix} \sigma_X^2 \\ \sigma_Y^2 \\ \sigma_Z^2 \end{pmatrix} = \sigma_d^2 \cdot \begin{pmatrix} (\cos b \cdot \cos l)^2 \\ (\cos b \cdot \sin l)^2 \\ (\sin b)^2 \end{pmatrix} + d^2 \cdot \left[\sigma_b^2 \cdot \begin{pmatrix} (\cos b \cdot \sin l)^2 \\ (\sin b \cdot \sin l)^2 \\ (\cos b)^2 \end{pmatrix} + \sigma_l^2 \cdot \begin{pmatrix} (\sin b \cdot \cos l)^2 \\ (\cos b \cdot \cos l)^2 \\ 0 \end{pmatrix} \right] \tag{B.2}$$

The UVW-velocities could be derived through converting the spherical values to the Cartesian system, but beforehand the RV and PM_l values had to be corrected for differential rotation. These correction equations (Eq. B.3 and B.4) were taken from Binney & Merrifield (1998, p. 637-640)[2]. Since differential rotation is mainly a radial effect within the Galactic disc, a correction in the Galactic latitude component of the proper motion was negligible and therefore not included here.

$$RV_{corr} = RV - A \cdot d \cdot \sin 2l \tag{B.3}$$

$$PM_{l,corr} = PM_l - (A \cdot \cos 2l + B)/k \tag{B.4}$$

[1] The equation for the XYZ-uncertainties were not provided in Sect. 4.1, because the main focus was on the values and not the error propagation.
[2] Eq. B.3 and B.4 were already given in Sect. 4.1 and are provided here for completeness and overview purposes.

where $k = 4.74$ is the factor ensuring unit consistency, d the distance of the cluster to the sun in kpc, PM_l and PM_b the proper motion components in the Galactic system in mas/yr, RV the radial velocity of the cluster in km/s, and $(A, B) = (14.5, -13)$ km s^{-1} kpc^{-1} are the Oort constants as determined by Piskunov et al. (2006) for the Galactic open cluster population. The Galactic UVW-velocities were then computed using Eq. B.5[3], with U being positive towards the Galactic anticentre, V positive in direction of Galactic rotation and W being positive towards the north Galactic pole.

$$\begin{pmatrix} U \\ V \\ W \end{pmatrix} = Vt_{l,corr} \cdot \begin{pmatrix} -\sin l \\ \cos l \\ 0 \end{pmatrix} + Vt_b \cdot \begin{pmatrix} -\cos l \cdot \sin b \\ -\sin l \cdot \sin b \\ \cos b \end{pmatrix} + RV_{corr} \cdot \begin{pmatrix} \cos l \cdot \cos b \\ \sin l \cdot \cos b \\ \sin b \end{pmatrix} + \begin{pmatrix} U_0 \\ V_0 \\ W_0 \end{pmatrix} \tag{B.5}$$

The tangential velocities (V_T), as used in Eq. B.5, are determined through

$$V_{T,l,corr} = kd \cdot PM_{l,corr} \qquad \& \qquad V_{T,b} = kd \cdot PM_b$$

where $k = 4.74$ is the factor ensuring unit consistency, d the distance of the cluster to the sun in kpc, PM_l and PM_b the proper motion components in the Galactic system in mas/yr. The l and b in Eq. B.5 are again the Galactic longitude and latitude of the considered cluster in degrees, and RV the radial velocity of the cluster in km/s.The correction for solar motion could be applied in the final equation (Eq. B.5) through simply adding the values provided by Piskunov et al. (2006) for the Galactic open cluster population[4]: $(U_0, V_0, W_0) = (-9.44, 11.9, 7.2)$ km/s.
Here I also provide equations for the uncertainties in the UVW-velocities following Gaussian error propagation (see Eq. B.6 - B.8), where the uncertainties in l and b were set to 1", as already stated above.

$$\begin{aligned} e_U^2 &= (eV_{T,l} \cdot \sin l)^2 + (V_{T,l} \cdot \sigma_l \cdot \cos l)^2 \\ &+ (eV_{T,b} \cdot \cos l \cdot \sin b)^2 + (V_{T,b} \cdot \sigma_l \cdot \sin l \cdot \sin b)^2 + (V_{T,b} \cdot \sigma_b \cdot \cos l \cdot \cos b)^2 \\ &+ (eRV \cdot \cos l \cdot \cos b)^2 + (RV \cdot \sigma_l \cdot \sin l \cdot \cos b)^2 + (RV \cdot \sigma_b \cdot \cos l \cdot \sin b)^2 \end{aligned} \tag{B.6}$$

$$\begin{aligned} e_V^2 &= (eV_{T,l} \cdot \cos l)^2 + (V_{T,l} \cdot \sigma_l \cdot \sin l)^2 \\ &+ (eV_{T,b} \cdot \sin l \cdot \sin b)^2 + (V_{T,b} \cdot \sigma_l \cdot \cos l \cdot \sin b)^2 + (V_{T,b} \cdot \sigma_b \cdot \sin l \cdot \cos b)^2 \\ &+ (eRV \cdot \sin l \cdot \cos b)^2 + (RV \cdot \sigma_l \cdot \cos l \cdot \cos b)^2 + (RV \cdot \sigma_b \cdot \sin l \cdot \sin b)^2 \end{aligned} \tag{B.7}$$

$$\begin{aligned} e_W^2 &= (eVT, b \cdot \cos b)^2 + (V_{T,b} \cdot \sigma_b \cdot \sin b)^2 \\ &+ (eRV \cdot \sin b)^2 + (RV \cdot \sigma_b \cdot \cos b)^2 \end{aligned} \tag{B.8}$$

The uncertainties for the radial velocities (eRV) could be determined from the catalogues, but those for the tangential velocities ($eV_{T,l}$ and $eV_{T,b}$) need further discussion. Since the tangential velocities are calculated from the proper motions and distances, the corresponding uncertainties were computed following Eq. B.9[5].

$$eV_T = \sqrt{4.74 \cdot [(ePM \cdot d)^2 + (PM \cdot ed)^2]} \tag{B.9}$$

Thus, it is possible to reduce the discussion on the uncertainties to those in PM$_l$ and PM$_b$. The COCD only provided proper motion uncertainties in the equatorial system (ePM_{RA} and ePM_{DEC}), but not in l and b. Nevertheless, an approximate value defining the order of magnitude for the ePM_l and ePM_b values could be inferred from the ePM_{RA} and ePM_{DEC} values.

[3]Eq. B.5 corresponds to a coordinate transformation in velocity space and was verified through private communication with Nina Kharchenko. This equation was already provide in Sect. 4.1.
[4]The change of sign in U_0 between Piskunov et al. (2006) and this work is because of the flipped direction of the X-axis.
[5]Eq. B.9 was already given in Sect. 3.3.1 and is listed here for overview and completeness purposes.

To get an idea for the PM_l and PM_b uncertainties, I took a closer look at the uncertainty distributions for PM_{RA} and PM_{DEC} (Fig. B.1), which were expected to be of the same order of magnitude. The majority of the values were well below 1 mas/yr. This might be induced by the listed uncertainties corresponding to statistical uncertainties for the $\overline{PM}$ rather than actual measurement uncertainties. Based on these distributions and following a conservative approach, I set the uncertainties in the PM_l and PM_b for all clusters to a fixed value of 1 mas/yr.

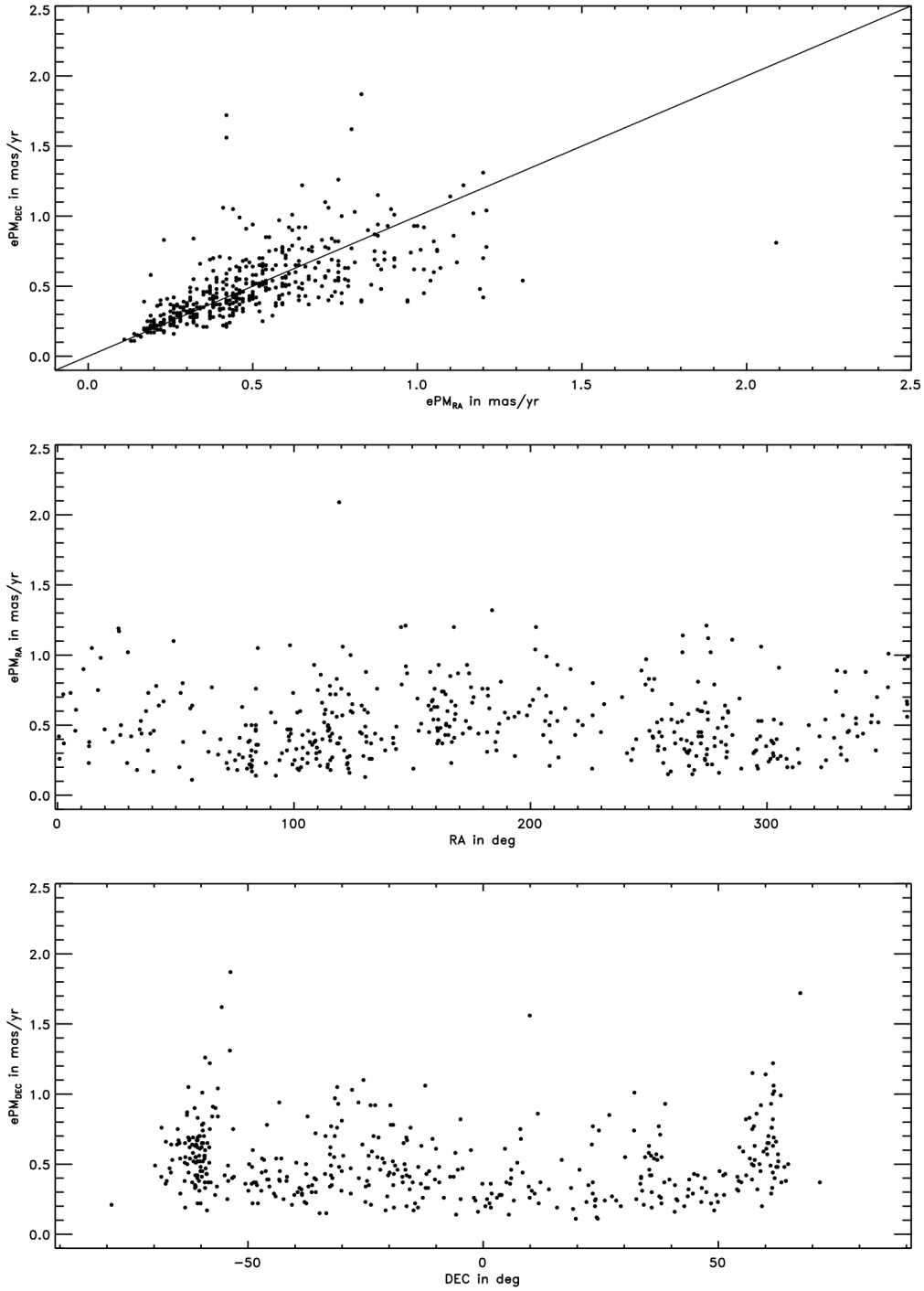

Figure B.1: Distributions for the proper motion uncertainties in RA and DEC. Upper panel: Comparison between ePM_{RA} and ePM_{DEC} with the one-to-one relation indicated by the solid line. Middle panel: Check for potential systematics of ePM_{RA} with respect to RA. Lower panel: Same as middle panel, but for DEC components.

Table B.1: Input Parameters for the final working sample: Coordinates and proper motions in RA-DEC and GLON-GLAT, along with radial velocities and distances.

Seq	Name	RA	DEC	PM_{RA} (ePM_{RA})	PM_{DEC} (ePM_{DEC})	GLON	GLAT	PM_{GLON}	PM_{GLAT}	RV (eRV)	d
		deg	deg	mas/yr	mas/yr	deg	deg	mas/yr	mas/yr	km/s	pc
2	Berkeley 59	0.55	67.42	-4.40 (0.42)	0.73 (1.72)	118.22	5.00	-4.18	1.55	-14.9 (10.7)	1000
3	Blanco 1	0.82	-30.14	19.86 (0.26)	2.37 (0.31)	14.17	-79.02	-2.15	-19.89	5.1 (0.0)	269
4	Alessi 20	2.64	58.76	7.48 (0.37)	-2.61 (0.50)	117.64	-3.69	6.97	-3.76	-11.5 (0.0)	450
5	Mayer 1	5.47	61.74	-5.27 (0.73)	-5.87 (1.06)	119.44	-0.93	-5.91	-5.23	-20.9 (2.0)	1429
8	NGC 129	7.50	60.22	-0.92 (0.46)	-0.48 (0.61)	120.27	-2.54	-0.96	-0.40	-36.0 (0.5)	1625
10	NGC 225	10.92	61.78	-3.18 (0.90)	1.99 (0.69)	122.01	-1.08	-3.12	2.09	-28.0 (0.0)	657
12	IC 1590	13.20	56.63	-1.36 (0.23)	-1.34 (0.83)	123.12	-6.24	-1.35	-1.35	-32.5 (6.4)	2384
13	Alessi 1	13.36	49.57	6.51 (0.38)	-7.70 (0.28)	123.26	-13.30	6.57	-7.65	6.0 (1.8)	800
14	NGC 381	17.08	61.60	0.81 (0.75)	-1.51 (0.82)	124.94	-1.21	0.91	-1.45	-22.4 (6.0)	1058
15	Platais 2	18.25	32.08	13.21 (0.98)	-9.98 (0.74)	128.23	-30.57	14.12	-8.65	2.2 (6.3)	201
17	NGC 457	19.89	58.30	-1.35 (0.47)	-1.49 (0.32)	126.63	-4.37	-1.18	-1.63	-27.1 (1.7)	2429
18	NGC 581	23.34	60.65	-0.69 (0.38)	0.20 (0.70)	128.05	-1.81	-0.71	0.09	-45.7 (2.4)	2194
19	NGC 637	25.77	64.04	0.34 (1.19)	-2.20 (0.48)	128.54	1.73	0.77	-2.09	-45.8 (3.9)	2160
20	NGC 654	25.99	61.88	-1.34 (1.17)	0.49 (1.02)	129.08	-0.37	-1.41	0.21	-11.5 (25.5)	2041
22	NGC 663	26.53	61.24	-2.91 (0.43)	-2.09 (0.29)	129.46	-0.94	-2.41	-2.66	-32.3 (1.2)	1952
25	NGC 752	29.41	37.78	7.66 (0.23)	-12.15 (0.26)	137.12	-23.26	10.72	-9.56	4.7 (0.1)	458
27	Stock 5	31.12	64.36	-0.85 (0.42)	-1.51 (0.38)	130.73	2.60	-0.39	-1.69	-19.8 (0.5)	1100
28	Stock 2	33.60	59.27	16.22 (0.18)	-13.39 (0.20)	133.36	-1.92	19.61	-7.59	9.6 (1.6)	380
29	NGC 869	34.77	57.15	-0.49 (0.47)	-0.90 (0.39)	134.63	-3.72	-0.16	-1.01	-38.9 (1.9)	2079
30	NGC 884	35.50	57.14	-0.84 (0.44)	-0.23 (0.50)	135.01	-3.60	-0.71	-0.50	-38.9 (2.2)	2345
32	Stock 7	37.41	60.71	-4.89 (0.60)	-0.62 (0.65)	134.66	0.09	-4.31	-2.38	-3.7 (6.3)	698
33	IC 1805	38.17	61.45	-1.34 (0.32)	-1.15 (0.33)	134.72	0.91	-0.80	-1.57	-47.9 (14.8)	1886
34	NGC 957	38.34	57.56	1.15 (0.73)	-1.52 (0.77)	136.28	-2.65	1.64	-0.96	-42.9 (0.7)	1815
35	Trumpler 2	39.22	55.92	1.40 (0.44)	-5.57 (0.42)	137.37	-3.97	3.49	-4.56	-27.5 (11.5)	649
36	NGC 1039	40.51	42.76	-0.22 (0.17)	-6.93 (0.20)	143.65	-15.62	2.77	-6.35	-9.8 (0.5)	499
37	NGC 1027	40.66	61.63	-2.42 (0.46)	1.41 (0.63)	135.74	1.55	-2.79	0.28	15.0 (3.8)	772
38	IC 1848	42.79	60.43	-2.51 (0.64)	-0.70 (0.65)	137.19	0.91	-1.94	-1.74	-30.5 (4.7)	2002
39	Collinder 33	44.82	60.40	2.70 (0.67)	3.17 (0.57)	138.09	1.34	0.89	4.07	-6.8 (13.1)	1000
41	Stock 23	49.05	60.05	-1.34 (1.10)	-1.11 (1.14)	140.08	2.09	-0.56	-1.65	-16.8 (4.2)	380
42	Melotte 20	51.49	49.12	21.98 (0.20)	-25.36 (0.17)	147.20	-6.33	32.40	-8.74	-2.4 (1.0)	190
44	Alessi 13	52.05	-35.90	36.97 (0.73)	-3.18 (0.40)	237.65	-55.71	0.87	37.10	19.5 (3.0)	110
45	NGC 1342	52.90	37.34	0.13 (0.80)	-2.72 (0.77)	154.97	-15.38	1.72	-2.11	-10.9 (0.1)	665
46	IC 348	56.14	32.16	5.37 (0.62)	-7.43 (1.01)	160.49	-17.81	8.88	-2.26	18.1 (3.5)	394
47	Melotte 22	56.83	24.12	19.33 (0.11)	-45.00 (0.12)	166.63	-23.47	44.60	-20.23	5.7 (0.6)	130
48	Tombaugh 5	56.95	59.05	-0.39 (0.64)	-2.64 (0.92)	143.94	3.57	1.33	-2.31	-5.8 (0.3)	1000
49	NGC 1502	61.96	62.33	-0.69 (0.45)	-1.03 (0.48)	143.67	7.65	0.19	-1.22	-16.3 (4.4)	821

Table B.1: continued

Seq	Name	RA deg	DEC deg	PM_{RA} (ePM_{RA}) mas/yr	PM_{DEC} (ePM_{DEC}) mas/yr	GLON deg	GLAT deg	PM_{GLON} mas/yr	PM_{GLAT} mas/yr	RV (eRV) km/s	d pc
50	NGC 1528	63.84	51.22	1.67 (0.31)	-2.46 (0.28)	152.05	0.25	2.91	-0.62	-10.1 (0.2)	776
51	NGC 1545	65.23	50.25	-1.63 (0.77)	-1.00 (0.45)	153.36	0.18	-0.45	-1.86	-13.1 (0.8)	711
52	NGC 1582	67.89	43.80	1.44 (0.29)	-0.30 (0.39)	159.25	-3.02	1.20	0.85	5.5 (1.0)	600
53	Platais 3	68.85	71.58	3.30 (0.40)	-20.50 (0.37)	138.74	15.98	17.85	-10.61	7.0 (3.7)	200
54	NGC 1647	71.47	19.11	-1.43 (0.23)	-1.83 (0.18)	180.33	-16.78	0.58	-2.25	-2.3 (0.4)	539
56	NGC 1662	72.10	10.94	-3.28 (0.19)	-1.78 (0.29)	187.68	-21.12	-0.42	-3.71	-13.8 (0.3)	437
57	NGC 1664	72.79	43.66	-2.54 (0.31)	-6.21 (0.32)	161.69	-0.45	3.16	-5.92	7.8 (0.8)	1199
58	Berkeley 14A	75.10	43.48	-0.73 (0.25)	-2.94 (0.27)	162.88	0.74	1.87	-2.39	4.8 (3.7)	1100
60	NGC 1746	75.96	23.77	-1.87 (0.18)	-3.07 (0.20)	179.07	-10.65	1.38	-3.32	2.0 (3.7)	760
61	Platais 4	76.72	22.37	2.36 (0.29)	-6.33 (0.35)	180.65	-10.90	6.52	-1.76	13.8 (5.1)	276
62	NGC 1778	77.01	37.02	-0.76 (0.41)	-3.11 (0.53)	168.90	-2.03	2.04	-2.47	7.5 (1.4)	1454
64	NGC 1817	78.06	16.69	-0.06 (0.63)	-3.13 (0.53)	186.15	-13.10	2.56	-1.80	65.3 (0.1)	1972
65	NGC 1901	79.56	-68.44	1.16 (0.50)	9.80 (0.41)	279.03	-33.60	-9.84	-0.74	-1.4 (0.5)	409
66	NGC 1893	80.68	33.41	0.35 (0.38)	-4.37 (0.36)	173.58	-1.69	3.80	-2.18	-2.2 (5.2)	3280
68	Collinder 65	81.52	15.70	1.16 (0.22)	-6.46 (0.19)	188.86	-10.86	6.07	-2.48	19.5 (4.6)	310
69	NGC 1907	82.02	35.33	0.15 (0.50)	-3.40 (0.46)	172.61	0.30	2.91	-1.76	0.1 (0.9)	1330
70	Stock 8	82.03	34.42	-1.44 (0.32)	-3.90 (0.55)	173.37	-0.19	2.44	-3.36	-6.4 (2.5)	1821
71	NGC 1912	82.18	35.83	0.23 (0.17)	-5.44 (0.19)	172.27	0.69	4.66	-2.82	1.0 (0.6)	1066
72	Collinder 69	83.79	9.70	0.40 (0.47)	-1.93 (0.34)	195.26	-12.12	1.86	-0.64	31.4 (1.4)	438
73	NGC 1981	83.79	-4.40	1.01 (0.46)	1.14 (0.47)	208.06	-18.96	-0.55	1.42	27.9 (2.4)	400
74	NGC 1976	83.82	-5.39	1.96 (0.31)	-0.77 (0.46)	209.01	-19.39	1.57	1.40	27.8 (5.0)	399
75	NGC 1977	83.85	-4.82	2.42 (0.76)	-1.90 (0.82)	208.48	-19.10	2.79	1.29	24.2 (2.0)	500
76	NGC 1980	83.85	-5.91	0.83 (0.50)	-0.36 (0.58)	209.51	-19.60	0.69	0.58	23.0 (0.2)	550
77	Collinder 70	83.88	-1.10	0.36 (0.14)	-0.68 (0.16)	205.03	-17.35	0.77	0.00	31.7 (4.7)	391
78	NGC 1960	84.07	34.14	0.50 (0.36)	-4.94 (0.21)	174.53	1.07	4.43	-2.24	-1.2 (4.6)	1318
80	Sigma Ori	84.67	-2.61	3.42 (1.05)	-0.20 (0.60)	206.82	-17.36	1.76	2.94	29.5 (0.5)	399
81	Stock 10	84.75	37.93	-3.34 (0.36)	-1.57 (0.55)	171.62	3.55	-0.44	-3.66	-13.1 (3.6)	380
82	NGC 2099	88.08	32.55	3.09 (0.23)	-7.35 (0.25)	177.64	3.09	7.90	-1.07	7.7 (0.0)	1383
84	NGC 2129	90.27	23.32	0.23 (0.59)	-0.68 (0.77)	186.59	0.13	0.70	-0.14	11.8 (1.4)	1515
86	NGC 2169	92.10	13.97	-2.17 (0.52)	-2.52 (0.32)	195.60	-2.94	1.16	-3.12	23.0 (1.5)	1032
87	NGC 2168	92.28	24.35	2.38 (0.14)	-2.95 (0.11)	186.60	2.24	3.73	0.66	-8.0 (0.3)	830
91	Platais 6	93.85	3.92	-4.45 (0.25)	-4.27 (0.28)	205.30	-6.19	1.70	-5.93	13.1 (14.9)	348
93	Collinder 89	94.87	23.30	0.42 (0.30)	-2.15 (0.37)	188.65	3.83	2.10	-0.64	26.2 (7.6)	800
95	NGC 2232	96.97	-4.80	-4.31 (0.32)	-2.40 (0.25)	214.54	-7.42	0.20	-4.93	21.0 (0.6)	325
96	Collinder 95	97.77	9.90	-1.81 (0.42)	-4.62 (1.56)	201.81	0.03	3.26	-3.74	-11.0 (7.4)	556
97	Collinder 97	97.83	5.95	-3.78 (0.47)	-2.03 (0.46)	205.34	-1.74	0.06	-4.29	23.0 (0.0)	500

Table B.1: continued

Seq	Name	RA	DEC	PM_{RA} (ePM_{RA})	PM_{DEC} (ePM_{DEC})	GLON	GLAT	PM_{GLON}	PM_{GLAT}	RV (eRV)	d
		deg	deg	mas/yr	mas/yr	deg	deg	mas/yr	mas/yr	km/s	pc
98	NGC 2244	97.98	4.94	-1.42 (0.39)	-0.32 (0.37)	206.30	-2.08	-0.37	-1.41	26.5 (5.1)	1445
99	NGC 2240	98.29	35.25	1.92 (1.07)	-12.88 (0.63)	179.21	11.84	12.49	-3.70	15.8 (1.0)	450
100	Basel 8	98.55	8.01	0.50 (0.47)	-2.29 (0.68)	203.84	-0.16	2.26	-0.61	11.0 (7.4)	1328
102	NGC 2251	98.65	8.37	0.67 (0.44)	-2.79 (0.44)	203.57	0.10	2.79	-0.69	24.7 (0.2)	1329
104	Collinder 106	99.34	5.95	-1.98 (0.22)	1.47 (0.40)	206.03	-0.41	-2.22	-1.08	28.7 (5.0)	1600
105	Collinder 107	99.63	4.63	-2.58 (0.73)	-0.75 (0.61)	207.34	-0.76	-0.52	-2.64	13.9 (6.2)	1450
107	NGC 2264	100.24	9.88	-2.70 (0.25)	-3.50 (0.26)	202.95	2.19	1.88	-4.00	21.8 (1.3)	660
109	NGC 2270	100.99	3.48	-0.17 (0.33)	-3.12 (0.28)	208.98	-0.07	2.70	-1.58	40.0 (3.7)	1400
110	NGC 2287	101.50	-20.76	-4.57 (0.19)	-0.67 (0.17)	231.02	-10.45	-1.34	-4.42	26.2 (1.0)	693
111	NGC 2281	102.07	41.08	-4.13 (0.18)	-7.74 (0.25)	174.90	16.88	5.68	-6.69	16.2 (3.6)	558
112	NGC 2301	102.94	0.46	-1.50 (0.20)	-4.35 (0.20)	212.56	0.28	3.19	-3.32	17.3 (2.2)	858
115	Collinder 121	103.68	-24.30	-3.87 (0.34)	4.08 (0.35)	235.14	-10.14	-5.34	-1.75	31.4 (4.0)	1100
118	NGC 2323	105.67	-8.37	0.34 (0.23)	-1.58 (0.26)	221.66	-1.33	1.56	-0.42	5.4 (1.0)	881
119	vdBergh 92	105.97	-11.49	-5.22 (0.46)	2.52 (0.45)	224.57	-2.49	-4.63	-3.49	17.5 (0.3)	1500
120	NGC 2335	106.71	-10.03	1.45 (0.38)	-3.31 (0.61)	223.60	-1.18	3.61	-0.23	8.7 (0.7)	1417
125	Alessi 21	107.70	-9.34	-3.65 (0.36)	3.04 (0.37)	223.44	0.00	-4.38	-1.83	38.8 (1.8)	500
126	Collinder 132	108.39	-31.03	-5.90 (0.44)	5.09 (1.05)	243.13	-9.30	-7.17	-3.05	26.0 (2.0)	411
127	NGC 2354	108.52	-25.69	-5.41 (0.93)	-1.14 (0.64)	238.36	-6.81	-1.43	-5.34	33.4 (0.3)	3794
128	NGC 2353	108.63	-10.27	-2.81 (0.38)	0.94 (0.39)	224.69	0.38	-2.14	-2.05	32.6 (1.0)	1119
129	Alessi 3	109.08	-46.61	-11.63 (0.39)	12.61 (0.53)	257.84	-15.37	-16.19	-5.66	-2.7 (0.6)	288
132	NGC 2360	109.42	-15.64	-2.62 (0.30)	4.89 (0.32)	229.80	-1.43	-5.55	-0.04	27.2 (0.1)	1887
133	Collinder 135	109.45	-37.16	-10.70 (0.26)	5.31 (0.34)	249.12	-11.19	-9.42	-7.34	24.1 (6.8)	319
134	NGC 2362	109.66	-24.99	-2.25 (0.34)	2.47 (0.34)	238.20	-5.57	-3.23	-0.86	30.0 (14.0)	1389
135	NGC 2367	110.02	-21.89	-2.25 (0.75)	4.91 (0.46)	235.60	-3.84	-5.39	0.29	43.0 (3.7)	2004
136	Collinder 140	110.82	-32.06	-8.50 (0.31)	3.67 (0.40)	245.00	-7.91	-7.14	-5.89	19.9 (3.1)	402
137	NGC 2374	110.98	-13.26	-3.85 (0.21)	-1.14 (0.36)	228.41	1.02	-0.82	-3.93	27.2 (0.1)	1468
139	NGC 2384	111.28	-21.02	-5.89 (0.86)	2.86 (0.51)	235.38	-2.40	-5.30	-3.84	46.0 (3.6)	2116
140	Trumpler 7	111.84	-23.95	-2.26 (0.66)	3.07 (0.92)	238.21	-3.34	-3.77	-0.54	32.9 (2.9)	1474
141	NGC 2396	112.00	-11.72	-2.00 (0.40)	-1.40 (0.33)	227.52	2.63	0.28	-2.43	17.7 (0.9)	588
142	Bochum 5	112.75	-16.93	-2.11 (0.52)	-0.66 (0.65)	232.45	0.77	-0.44	-2.17	27.9 (11.3)	2000
143	Bochum 4	112.90	-17.19	-1.69 (0.58)	0.49 (0.41)	232.75	0.77	-1.24	-1.25	16.0 (3.7)	872
145	NGC 2414	113.31	-15.45	-2.42 (0.61)	1.65 (0.76)	231.41	1.95	-2.61	-1.32	73.9 (0.5)	2888
147	NGC 2422	114.15	-14.48	-6.91 (0.20)	1.87 (0.22)	230.95	3.13	-4.99	-5.13	34.3 (0.8)	491
148	NGC 2423	114.27	-13.87	-0.30 (0.22)	-2.28 (0.19)	230.48	3.53	1.85	-1.37	21.4 (1.8)	766
149	Ruprecht 26	114.30	-15.65	-3.38 (0.46)	-1.34 (0.41)	232.05	2.69	-0.48	-3.60	26.3 (7.2)	1440
150	Melotte 71	114.37	-12.07	-3.59 (0.49)	6.26 (0.43)	228.95	4.49	-7.22	-0.11	50.1 (0.1)	3154

Table B.1: continued

Seq	Name	RA	DEC	PM_{RA} (ePM_{RA})	PM_{DEC} (ePM_{DEC})	GLON	GLAT	PM_{GLON}	PM_{GLAT}	RV (eRV)	d
		deg	deg	mas/yr	mas/yr	deg	deg	mas/yr	mas/yr	km/s	pc
151	Ruprecht 27	114.37	-26.53	-3.65 (0.50)	2.65 (0.94)	241.58	-2.57	-4.09	-1.89	10.9 (1.2)	560
152	NGC 2428	114.85	-16.53	-2.02 (0.47)	1.12 (0.46)	233.08	2.72	-1.97	-1.21	46.7 (2.7)	2100
153	NGC 2430	114.90	-16.35	-4.07 (0.48)	1.28 (0.69)	232.94	2.85	-3.11	-2.92	31.3 (11.8)	650
155	Haffner 13	115.12	-30.08	-6.44 (0.42)	5.40 (0.45)	245.00	-3.73	-7.86	-2.97	68.0 (5.8)	714
156	NGC 2439	115.18	-31.69	-1.94 (0.78)	2.21 (0.55)	246.43	-4.47	-2.88	-0.61	68.0 (0.8)	3855
157	NGC 2432	115.32	-19.15	-3.68 (0.72)	1.62 (0.78)	235.58	1.82	-3.23	-2.40	14.4 (1.8)	2030
158	Ruprecht 151	115.32	-16.29	-4.30 (0.39)	2.10 (0.42)	233.09	3.23	-3.94	-2.71	31.3 (4.8)	2100
159	NGC 2451A	115.32	-38.53	-21.80 (0.25)	15.09 (0.28)	252.50	-7.69	-23.71	-11.87	27.7 (0.5)	188
160	NGC 2437	115.42	-14.81	-4.22 (0.18)	1.20 (0.17)	231.85	4.05	-3.12	-3.09	30.4 (4.0)	1375
162	NGC 2451B	116.11	-37.67	-10.11 (0.59)	4.20 (0.50)	252.05	-6.73	-8.61	-6.77	14.0 (0.3)	430
163	NGC 2447	116.14	-23.86	-3.76 (0.27)	3.91 (0.21)	240.05	0.15	-5.27	-1.30	21.7 (0.2)	1037
164	NGC 2448	116.14	-24.68	-3.80 (0.44)	4.69 (0.38)	240.76	-0.26	-5.96	-0.95	24.4 (4.1)	1040
166	Haffner 16	117.58	-25.46	-5.51 (0.72)	0.62 (1.10)	242.09	0.47	-3.34	-4.43	52.9 (14.2)	3165
167	NGC 2477	118.03	-38.53	-0.23 (0.56)	1.83 (0.29)	253.56	-5.84	-1.70	0.72	7.3 (0.1)	1222
169	NGC 2467	118.06	-26.44	-3.93 (0.83)	1.68 (0.40)	243.15	0.34	-3.46	-2.52	55.8 (9.7)	1355
171	NGC 2482	118.80	-24.26	-5.66 (0.37)	0.75 (0.47)	241.62	2.03	-3.57	-4.46	42.7 (4.2)	1343
174	NGC 2489	119.07	-30.06	-4.05 (2.09)	-0.97 (0.81)	246.71	-0.77	-1.27	-3.97	37.9 (0.2)	3700
175	NGC 2516	119.52	-60.75	-4.13 (0.41)	10.15 (0.22)	273.81	-15.85	-10.91	1.04	24.2 (0.2)	346
178	NGC 2506	120.00	-10.77	-5.87 (0.76)	1.79 (0.68)	230.56	9.93	-4.51	-4.17	87.0 (2.5)	3460
179	Ruprecht 47	120.58	-31.07	-0.74 (1.06)	-0.04 (0.76)	248.25	-0.19	-0.36	-0.65	59.7 (0.0)	3006
180	NGC 2527	121.24	-28.15	-5.36 (0.32)	6.61 (0.29)	246.09	1.85	-8.45	-1.00	42.4 (1.3)	601
182	Vel OB2	122.38	-47.90	-6.10 (0.22)	8.85 (0.22)	263.28	-7.99	-10.74	-0.46	24.0 (9.7)	411
183	NGC 2547	122.53	-49.22	-8.95 (0.27)	4.08 (0.36)	264.46	-8.60	-8.21	-5.42	13.7 (1.6)	457
184	NGC 2539	122.67	-12.84	-3.37 (0.23)	-1.87 (0.26)	233.73	11.11	-0.16	-3.85	29.3 (0.1)	1363
186	NGC 2546	122.98	-37.61	-5.21 (0.19)	4.57 (0.22)	254.83	-2.05	-6.68	-1.85	15.7 (1.2)	919
187	Ruprecht 55	123.12	-32.58	-5.06 (0.72)	1.32 (0.57)	250.69	0.81	-3.89	-3.50	95.3 (2.6)	4892
189	NGC 2548	123.43	-5.75	-0.78 (0.16)	1.55 (0.14)	227.87	15.39	-1.73	0.11	41.5 (0.3)	769
190	vdBergh-Hagen 23	123.52	-36.36	-7.47 (0.28)	7.12 (0.35)	254.02	-1.00	-10.06	-2.28	24.0 (8.0)	437
191	Haffner 26	123.91	-30.83	-4.54 (1.00)	4.31 (0.93)	249.60	2.34	-6.11	-1.38	62.4 (12.1)	1000
192	NGC 2567	124.63	-30.64	-1.52 (0.65)	2.97 (0.48)	249.79	2.96	-3.31	0.41	37.0 (1.0)	1677
193	NGC 2571	124.74	-29.75	-2.92 (0.59)	4.75 (0.56)	249.10	3.53	-5.57	0.25	44.0 (10.3)	1339
196	Pismis 4	128.65	-44.48	-5.55 (0.44)	5.75 (0.29)	262.91	-2.47	-7.93	-1.02	30.0 (5.0)	593
198	Ruprecht 64	129.33	-40.15	-6.14 (0.28)	5.97 (0.28)	259.75	0.53	-8.47	-1.28	26.9 (5.9)	800
199	Pismis 6	129.76	-46.23	-7.05 (0.61)	6.48 (0.45)	264.78	-2.91	-9.43	-1.67	16.8 (4.0)	1668
201	NGC 2632	130.09	19.69	-35.90 (0.13)	-12.88 (0.11)	205.89	32.48	-0.35	-38.14	34.5 (0.1)	187
202	IC 2391	130.14	-53.03	-24.19 (0.49)	23.48 (0.41)	270.36	-6.83	-33.33	-5.08	14.1 (0.2)	176

Table B.1: continued

Seq	Name	RA	DEC	PM_{RA} (ePM_{RA})	PM_{DEC} (ePM_{DEC})	GLON	GLAT	PM_{GLON}	PM_{GLAT}	RV (eRV)	d
		deg	deg	mas/yr	mas/yr	deg	deg	mas/yr	mas/yr	km/s	pc
203	Ruprecht 67	130.41	-43.37	-9.95 (0.88)	2.23 (0.94)	262.79	-0.80	-7.87	-6.48	-15.4 (0.8)	1504
204	Mamajek 1	130.53	-79.03	-30.05 (0.42)	27.57 (0.21)	292.48	-21.65	-39.30	-10.88	15.6 (0.9)	105
205	IC 2395	130.62	-48.11	-4.34 (0.38)	2.42 (0.35)	266.63	-3.59	-4.58	-1.94	9.7 (8.8)	709
207	Bochum 7	131.20	-45.97	-3.74 (0.59)	3.93 (0.78)	265.19	-1.96	-5.40	-0.49	49.0 (2.6)	5754
210	Trumpler 10	131.92	-42.45	-11.90 (0.26)	6.05 (0.25)	262.76	0.64	-12.18	-5.46	20.4 (14.0)	417
212	NGC 2682	132.85	11.80	-8.31 (0.26)	-4.81 (0.22)	215.70	31.92	0.89	-9.56	33.0 (1.6)	908
213	vdBergh-Hagen 56	134.28	-43.25	-4.88 (0.44)	6.08 (0.38)	264.48	1.46	-7.79	0.25	-18.0 (0.0)	680
214	Collinder 205	135.13	-48.99	-3.65 (0.76)	6.63 (0.60)	269.21	-1.85	-7.39	1.61	20.0 (5.6)	1500
216	Platais 8	136.95	-59.14	-15.83 (0.40)	14.80 (0.33)	277.54	-7.79	-21.59	-1.89	7.5 (7.3)	150
218	Platais 9	138.54	-44.14	-24.53 (0.32)	12.01 (0.27)	267.21	3.15	-25.61	-9.48	17.8 (1.5)	200
220	IC 2488	141.91	-57.00	-7.03 (0.41)	5.82 (0.28)	277.83	-4.42	-9.10	-0.68	-2.6 (0.1)	1134
223	Turner 5	143.13	-36.47	0.00 (0.33)	-3.73 (0.30)	264.23	11.05	2.58	-2.69	-1.2 (15.0)	400
224	NGC 2925	143.29	-53.37	-8.94 (0.49)	5.70 (0.40)	275.91	-1.23	-10.44	-1.87	16.0 (7.4)	774
225	Ruprecht 79	145.24	-53.85	-10.35 (1.20)	1.24 (1.31)	277.09	-0.82	-8.61	-5.87	25.2 (2.2)	1979
226	Ruprecht 80	145.51	-44.02	-13.73 (0.79)	6.64 (0.54)	270.75	6.71	-14.70	-4.06	45.7 (1.0)	2500
228	NGC 3033	147.15	-56.42	-3.55 (1.21)	4.13 (1.04)	279.59	-2.07	-5.37	0.92	26.7 (0.1)	922
230	NGC 3036	147.31	-62.67	-7.43 (0.92)	-1.25 (1.05)	283.66	-6.83	-4.91	-5.72	11.8 (1.0)	1200
231	Pismis 16	147.81	-53.17	-6.28 (0.87)	1.40 (0.75)	277.82	0.68	-5.76	-2.87	13.7 (5.3)	1824
234	NGC 3114	150.49	-60.10	-7.43 (0.19)	4.05 (0.22)	283.25	-3.87	-8.37	-1.23	-3.5 (0.2)	911
239	Ruprecht 161	152.19	-61.29	-8.20 (0.69)	3.04 (0.63)	284.63	-4.34	-8.44	-2.30	9.4 (3.7)	940
243	IC 2581	156.87	-57.63	-6.77 (0.64)	3.70 (0.84)	284.59	0.02	-7.71	-0.39	-4.6 (3.5)	2446
245	Loden 143	157.11	-58.78	-11.71 (0.45)	1.86 (0.43)	285.30	-0.89	-10.97	-4.50	-0.4 (9.8)	600
248	Collinder 223	157.59	-59.82	-7.17 (0.88)	1.08 (0.65)	286.05	-1.65	-6.70	-2.76	8.5 (1.1)	1686
249	Ruprecht 90	157.95	-58.24	-6.80 (0.61)	3.47 (0.51)	285.40	-0.20	-7.62	-0.48	-31.5 (14.6)	6000
251	Loden 153	158.67	-58.13	-5.85 (0.68)	4.13 (0.75)	285.67	0.09	-7.13	0.65	-10.3 (2.4)	2670
253	NGC 3293	158.95	-58.23	-7.64 (0.54)	3.08 (0.62)	285.85	0.07	-8.16	-1.12	-12.0 (0.6)	2471
254	NGC 3324	159.33	-58.64	-7.81 (0.63)	3.77 (0.65)	286.22	-0.19	-8.65	-0.56	-7.2 (2.4)	2301
255	vdBergh-Hagen 99	159.46	-59.13	-14.10 (0.76)	0.55 (1.26)	286.52	-0.58	-12.56	-6.43	13.3 (2.1)	531
258	Melotte 101	160.54	-65.10	-6.09 (0.48)	2.45 (0.64)	289.86	-5.56	-6.52	-0.76	20.3 (10.4)	1995
259	IC 2602	160.59	-64.40	-17.16 (0.37)	11.11 (0.29)	289.54	-4.94	-20.38	1.58	5.2 (3.0)	160
260	Bochum 10	160.60	-59.13	-6.61 (0.63)	2.56 (0.60)	287.04	-0.30	-7.03	-0.89	-2.2 (0.3)	2027
261	Alessi 5	160.78	-61.17	-14.56 (0.46)	3.77 (0.55)	288.08	-2.05	-14.61	-3.57	6.6 (2.2)	398
262	Collinder 228	160.95	-60.09	-6.66 (0.39)	1.93 (0.48)	287.64	-1.06	-6.78	-1.43	-13.5 (3.3)	1909
263	Trumpler 14	160.98	-59.55	-3.91 (0.54)	3.65 (0.65)	287.40	-0.58	-5.17	1.38	-15.0 (7.9)	2753
264	Trumpler 15	161.17	-59.37	-2.08 (0.93)	3.53 (0.70)	287.41	-0.37	-3.49	2.15	-11.6 (5.8)	2117
265	Trumpler 16	161.29	-59.72	-11.10 (0.39)	4.02 (0.45)	287.62	-0.65	-11.69	-1.62	-25.0 (1.8)	2842

Table B.1: continued

Seq	Name	RA	DEC	PM_{RA} (ePM_{RA})	PM_{DEC} (ePM_{DEC})	GLON	GLAT	PM_{GLON}	PM_{GLAT}	RV (eRV)	d
		deg	deg	mas/yr	mas/yr	deg	deg	mas/yr	mas/yr	km/s	pc
266	Ruprecht 91	161.91	-57.47	-11.10 (0.48)	3.11 (0.91)	286.87	1.49	-11.29	-2.32	-4.1 (11.3)	900
267	Loden 189	162.58	-56.42	-5.73 (0.74)	2.91 (0.84)	286.72	2.59	-6.43	0.03	10.7 (5.2)	720
268	Ruprecht 92	163.29	-61.71	-2.05 (0.74)	0.50 (0.69)	289.39	-1.98	-2.06	-0.45	-10.6 (3.7)	2362
270	Trumpler 17	164.10	-59.20	-2.20 (0.72)	5.70 (0.56)	288.66	0.45	-4.43	4.21	24.5 (8.2)	2189
271	Collinder 236	164.32	-61.11	-3.57 (0.50)	3.02 (0.51)	289.58	-1.23	-4.52	1.21	17.1 (15.1)	800
272	Bochum 12	164.35	-61.72	-3.08 (0.51)	-2.32 (0.58)	289.85	-1.78	-1.80	-3.41	-3.8 (0.8)	2218
273	NGC 3496	164.89	-60.39	-7.30 (0.60)	2.08 (0.56)	289.53	-0.46	-7.50	-1.16	3.2 (7.5)	990
274	Pismis 17	165.27	-59.87	-6.27 (0.43)	3.12 (0.62)	289.48	0.09	-7.00	0.26	-44.6 (5.2)	3504
275	Ruprecht 93	166.09	-61.37	-3.89 (0.85)	0.39 (0.90)	290.46	-1.11	-3.72	-1.20	5.1 (3.5)	1437
276	NGC 3532	166.50	-58.73	-10.54 (0.23)	4.57 (0.17)	289.60	1.39	-11.49	0.03	1.2 (2.2)	497
277	Loden 306	166.50	-61.13	-6.95 (0.67)	0.34 (0.55)	290.55	-0.82	-6.52	-2.44	-33.0 (4.6)	2000
278	Feinstein 1	166.75	-59.82	-6.57 (0.38)	2.26 (0.41)	290.15	0.44	-6.93	-0.49	-13.4 (8.9)	1159
281	NGC 3572	167.61	-60.25	-10.55 (1.20)	1.25 (0.70)	290.71	0.21	-10.23	-2.85	-8.5 (3.3)	2004
283	Trumpler 18	167.88	-60.67	-9.13 (0.54)	0.52 (0.52)	290.99	-0.13	-8.66	-2.95	-17.3 (4.4)	1358
284	NGC 3590	168.25	-60.78	-6.51 (0.64)	1.48 (0.40)	291.20	-0.17	-6.59	-1.04	-7.3 (6.4)	1651
285	Stock 13	168.27	-58.88	-9.80 (0.58)	2.91 (0.43)	290.50	1.60	-10.18	-0.93	1.0 (7.4)	1577
286	IC 2714	169.36	-62.73	-7.38 (0.87)	0.45 (0.69)	292.40	-1.79	-7.06	-2.20	-14.1 (0.3)	1238
287	NGC 3680	171.40	-43.24	-5.38 (0.44)	1.54 (0.45)	286.75	16.92	-5.58	-0.38	8.0 (3.7)	934
288	Ruprecht 94	172.68	-63.45	-4.87 (0.53)	-0.15 (0.51)	294.05	-1.98	-4.59	-1.64	2.0 (1.8)	3400
291	Loden 402	173.17	-60.72	-6.90 (0.93)	-0.53 (0.69)	293.44	0.70	-6.42	-2.57	-3.0 (7.4)	2450
292	IC 2944	174.03	-62.95	-6.20 (0.87)	-1.17 (0.87)	294.49	-1.32	-5.60	-2.90	-0.9 (6.0)	1794
293	NGC 3766	174.06	-61.61	-6.72 (0.48)	1.35 (0.52)	294.11	-0.03	-6.82	-0.63	-15.6 (0.7)	1745
294	vdBergh-Hagen 121	174.52	-63.33	-5.12 (0.48)	1.05 (0.55)	294.81	-1.62	-5.21	-0.43	-3.8 (2.5)	2735
295	IC 2948	174.84	-63.48	-4.58 (0.77)	-0.35 (0.38)	294.99	-1.72	-4.31	-1.60	1.6 (2.1)	2600
296	Stock 14	175.95	-62.52	-5.49 (0.70)	1.20 (0.67)	295.21	-0.66	-5.61	-0.26	-12.3 (2.2)	2146
298	Loden 481	177.99	-61.28	-3.87 (0.44)	1.67 (0.33)	295.84	0.77	-4.15	0.74	-22.0 (14.9)	1520
300	Ruprecht 98	179.67	-64.58	-5.08 (0.76)	-9.55 (0.65)	297.30	-2.28	-3.03	-10.38	-7.6 (1.7)	610
303	NGC 4103	181.66	-61.25	-5.04 (0.45)	-0.95 (0.35)	297.57	1.16	-4.80	-1.81	-12.0 (7.4)	1664
304	ESO 130-06	181.93	-59.30	-10.80 (0.76)	-0.76 (0.56)	297.37	3.10	-10.52	-2.57	-1.2 (3.4)	2200
305	Loden 565	182.02	-60.72	-3.14 (0.71)	-0.96 (0.83)	297.65	1.71	-2.93	-1.47	10.1 (1.0)	650
306	ESO 130-08	182.58	-59.52	-4.37 (0.62)	-1.18 (0.79)	297.73	2.94	-4.13	-1.86	-38.5 (6.3)	800
308	Melotte 111	185.62	25.85	-11.45 (0.32)	-8.98 (0.24)	222.43	83.40	6.23	-13.15	-0.1 (0.2)	87
309	NGC 4349	186.06	-61.87	-6.41 (0.45)	0.33 (0.64)	299.73	0.84	-6.41	-0.35	-13.5 (2.3)	2176
310	Collinder 258	186.79	-60.77	-7.81 (0.51)	-0.73 (0.52)	299.97	1.97	-7.71	-1.46	-14.3 (9.2)	1198
313	NGC 4463	187.48	-64.79	-3.35 (0.81)	0.22 (0.67)	300.64	-2.01	-3.36	-0.06	-24.5 (6.4)	1050
315	NGC 4609	190.57	-62.99	-8.92 (0.55)	-1.67 (0.85)	301.89	-0.13	-8.85	-1.99	22.0 (7.0)	1223

Table B.1: continued

Seq	Name	RA	DEC	PM_{RA} (ePM_{RA})	PM_{DEC} (ePM_{DEC})	GLON	GLAT	PM_{GLON}	PM_{GLAT}	RV (eRV)	d
		deg	deg	mas/yr	mas/yr	deg	deg	mas/yr	mas/yr	km/s	pc
317	Loden 694	193.26	-60.75	-6.23 (0.56)	0.90 (0.62)	303.12	2.12	-6.22	0.94	-23.0 (7.4)	1700
318	NGC 4755	193.41	-60.36	-4.30 (0.28)	-1.17 (0.31)	303.20	2.51	-4.31	-1.13	-20.0 (0.7)	1976
319	NGC 4852	195.03	-59.59	-6.71 (0.59)	0.68 (0.52)	304.03	3.27	-6.68	0.91	-5.0 (3.7)	1330
320	NGC 5045	198.54	-63.39	-5.90 (0.57)	-2.05 (0.65)	305.47	-0.63	-6.06	-1.52	-16.8 (7.2)	1500
322	Stock 16	199.69	-62.51	-3.31 (0.64)	-0.03 (0.68)	306.08	0.20	-3.29	0.32	-41.8 (8.8)	1640
324	Loden 821	201.00	-59.79	-6.13 (0.68)	0.57 (0.78)	307.02	2.83	-6.01	1.34	-12.4 (12.2)	2800
327	Basel 18	202.02	-62.35	-5.31 (1.04)	-5.38 (0.54)	307.16	0.22	-6.02	-4.57	-22.0 (3.0)	2226
328	Hogg 16	202.32	-61.20	-4.68 (1.20)	-1.54 (0.42)	307.47	1.34	-4.85	-0.84	-29.3 (5.8)	1585
333	Loden 915	203.52	-59.25	-8.36 (0.76)	1.00 (0.54)	308.36	3.17	-8.08	2.36	-21.6 (11.8)	500
334	Platais 10	205.42	-59.21	-29.10 (0.43)	-10.73 (0.37)	309.33	3.04	-30.63	-4.89	-8.0 (7.4)	246
335	Loden 1010	206.20	-60.25	-7.88 (0.53)	0.27 (0.61)	309.51	1.94	-7.66	1.88	-18.9 (4.7)	700
336	NGC 5281	206.64	-62.92	-4.84 (0.71)	-2.72 (0.50)	309.15	-0.71	-5.31	-1.63	-15.9 (13.1)	1108
337	Platais 12	208.12	-63.37	-8.05 (0.21)	-4.62 (0.19)	309.71	-1.30	-8.91	-2.61	-11.4 (2.4)	435
338	NGC 5316	208.48	-61.87	-4.91 (0.38)	-1.10 (0.37)	310.22	0.12	-5.03	0.11	8.9 (6.4)	1215
339	Loden 995	208.57	-64.95	-3.97 (0.59)	-0.91 (0.75)	309.52	-2.88	-4.07	0.07	-6.1 (1.2)	2400
343	Ruprecht 110	211.36	-67.47	-12.35 (0.53)	-4.21 (0.66)	309.95	-5.61	-13.04	-0.53	-36.6 (4.0)	1300
344	Loden 1194	211.42	-59.72	-10.07 (0.93)	-3.29 (1.01)	312.17	1.82	-10.59	-0.30	2.0 (3.7)	500
345	NGC 5460	211.86	-48.34	-5.70 (0.27)	-3.58 (0.37)	315.74	12.64	-6.51	-1.73	-12.7 (3.2)	673
349	ESO 175-06	214.68	-56.92	-8.65 (0.62)	-2.43 (0.90)	314.66	3.95	-8.97	0.57	-27.9 (0.0)	550
352	NGC 5606	216.94	-59.63	-4.78 (0.90)	-3.26 (0.74)	314.84	1.00	-5.64	-1.30	-37.5 (0.7)	1805
355	NGC 5662	218.91	-56.62	-5.97 (0.43)	-6.12 (0.34)	316.93	3.40	-7.89	-3.29	-23.2 (1.0)	678
356	Alessi 6	220.06	-66.12	-6.20 (0.53)	-6.22 (0.53)	313.64	-5.53	-8.20	-3.14	20.0 (1.0)	437
357	vdBergh-Hagen 164	222.06	-66.34	-7.36 (0.50)	-11.14 (0.64)	314.28	-6.07	-11.48	-6.81	16.8 (4.4)	550
360	NGC 5822	226.09	-54.40	-7.46 (0.19)	-5.66 (0.25)	321.57	3.59	-9.27	-1.29	-29.7 (0.2)	917
361	NGC 5823	226.38	-55.60	-6.15 (0.80)	-3.53 (1.62)	321.12	2.47	-7.09	-0.05	-19.8 (0.2)	1192
366	NGC 6025	240.82	-60.43	-4.09 (0.30)	-2.50 (0.38)	324.55	-5.88	-4.72	0.85	-3.4 (7.4)	769
367	Nor OB5	242.64	-49.04	-2.27 (0.25)	-2.26 (0.22)	332.98	1.86	-3.20	-0.11	-23.1 (5.1)	1800
369	NGC 6067	243.30	-54.22	-2.55 (0.33)	-2.39 (0.38)	329.74	-2.20	-3.49	0.01	-39.9 (0.2)	1417
371	NGC 6087	244.71	-57.94	-1.44 (0.40)	-2.34 (0.37)	327.72	-5.42	-2.67	-0.65	-10.0 (10.7)	901
374	NGC 6134	246.94	-49.15	0.32 (0.89)	-5.88 (0.48)	334.92	-0.19	-4.02	-4.31	-26.0 (0.2)	913
377	NGC 6167	248.64	-49.77	0.80 (0.79)	-4.40 (0.50)	335.22	-1.42	-2.70	-3.57	-34.7 (1.0)	1108
378	NGC 6178	248.94	-45.64	1.17 (0.97)	-2.04 (0.39)	338.40	1.22	-0.72	-2.24	3.5 (2.1)	1014
379	NGC 6192	250.09	-43.37	1.80 (0.83)	-0.77 (0.39)	340.64	2.13	0.62	-1.86	-7.7 (0.4)	1547
380	NGC 6193	250.33	-48.76	-0.73 (0.46)	-4.78 (0.37)	336.71	-1.57	-4.07	-2.61	-40.0 (8.8)	1155
382	NGC 6204	251.53	-47.02	0.04 (0.75)	-1.45 (0.54)	338.55	-1.03	-1.08	-0.97	-51.0 (5.8)	1085
383	Hogg 22	251.65	-47.08	-0.84 (0.42)	-4.39 (0.44)	338.56	-1.14	-3.89	-2.21	-58.8 (12.9)	1297

Table B.1: continued

Seq	Name	RA	DEC	PM_{RA} (ePM_{RA})	PM_{DEC} (ePM_{DEC})	GLON	GLAT	PM_{GLON}	PM_{GLAT}	RV (eRV)	d
		deg	deg	mas/yr	mas/yr	deg	deg	mas/yr	mas/yr	km/s	pc
384	NGC 6208	252.36	-53.73	-0.91 (0.83)	-4.72 (1.87)	333.75	-5.76	-4.22	-2.31	-32.2 (0.3)	939
385	NGC 6231	253.56	-41.83	-0.39 (0.52)	-1.99 (0.38)	343.46	1.18	-1.79	-0.95	-27.3 (3.0)	1250
387	NGC 6242	253.89	-39.46	0.63 (0.32)	-0.26 (0.30)	345.47	2.47	0.19	-0.65	39.3 (39.5)	1131
388	vdBergh-Hagen 205	254.04	-40.67	-1.12 (0.35)	-1.22 (0.21)	344.59	1.62	-1.65	0.11	-7.0 (0.0)	2160
390	NGC 6250	254.49	-45.94	1.80 (0.45)	-2.80 (0.39)	340.68	-1.92	-1.08	-3.15	-16.8 (0.0)	865
391	NGC 6268	255.54	-39.73	1.26 (0.42)	-0.71 (0.51)	346.04	1.31	0.21	-1.43	-15.1 (0.1)	1029
392	NGC 6281	256.17	-37.99	-2.96 (0.23)	-3.75 (0.23)	347.72	1.98	-4.78	0.08	-15.4 (0.0)	494
393	Sco OB4	258.15	-33.37	0.46 (0.15)	-2.22 (0.15)	352.39	3.44	-1.53	-1.67	-19.0 (7.0)	1100
394	Bochum 13	259.35	-35.55	-0.28 (0.17)	-1.20 (0.39)	351.20	1.37	-1.14	-0.46	-4.0 (8.5)	1077
395	NGC 6322	259.60	-42.93	1.30 (0.54)	-1.80 (0.54)	345.28	-3.05	-0.73	-2.10	-57.0 (35.9)	995
396	vdBergh-Hagen 221	259.66	-32.34	2.84 (0.65)	-3.10 (0.77)	353.97	3.00	-0.91	-4.10	6.3 (3.8)	750
397	IC 4651	261.21	-49.93	-0.81 (0.37)	-2.17 (0.31)	340.09	-7.90	-2.26	-0.52	-31.0 (0.2)	888
399	Antalova 1	262.23	-31.57	-0.24 (0.52)	-3.75 (0.70)	355.84	1.64	-3.26	-1.87	-4.8 (9.9)	850
402	NGC 6383	263.70	-32.57	1.66 (0.40)	-1.56 (0.34)	355.68	0.05	-0.41	-2.24	-1.2 (4.9)	985
403	Trumpler 27	264.09	-33.52	-1.48 (0.53)	-1.33 (0.70)	355.06	-0.74	-1.92	0.53	-27.0 (8.9)	1211
404	Trumpler 28	264.25	-32.48	0.78 (1.02)	-2.12 (0.62)	356.01	-0.30	-1.37	-1.80	-32.8 (11.9)	1343
405	ESO 139-13	264.42	-58.13	-0.57 (1.14)	1.57 (1.22)	333.98	-13.80	1.08	1.27	-33.9 (1.0)	1500
408	NGC 6405	265.08	-32.20	-1.28 (0.33)	-5.72 (0.35)	356.62	-0.74	-5.53	-1.95	-7.3 (1.9)	487
410	Alessi 9	265.98	-47.18	11.59 (0.31)	-9.72 (0.31)	344.13	-9.13	-2.52	-14.91	-48.1 (28.9)	195
411	NGC 6416	266.08	-32.36	-0.88 (0.39)	0.09 (0.42)	356.93	-1.55	-0.38	0.80	-11.2 (12.7)	741
412	IC 4665	266.58	5.72	-0.57 (0.30)	-7.40 (0.36)	30.62	17.08	-6.87	-2.81	-10.3 (1.8)	352
413	NGC 6425	266.76	-31.53	7.44 (0.58)	1.07 (0.97)	357.94	-1.60	4.77	-5.81	5.4 (12.1)	778
414	Collinder 350	267.03	1.35	-3.55 (0.21)	0.02 (0.22)	26.79	14.69	-1.63	3.15	-14.4 (1.0)	280
418	Sco OB5	268.14	-38.64	2.46 (0.37)	-1.80 (0.32)	352.38	-6.20	-0.33	-3.03	-10.5 (6.4)	3310
420	NGC 6475	268.45	-34.79	2.83 (0.15)	-5.14 (0.15)	355.86	-4.49	-3.02	-5.03	-14.7 (0.2)	300
422	NGC 6494	269.26	-18.99	0.65 (0.18)	-1.14 (0.19)	9.88	2.84	-0.66	-1.13	-8.6 (0.4)	628
423	Collinder 359	270.16	2.93	0.22 (0.28)	-8.90 (0.26)	29.72	12.63	-7.82	-4.26	-4.4 (0.4)	640
425	NGC 6514	270.67	-22.97	2.63 (0.61)	-1.01 (0.92)	7.08	-0.28	0.42	-2.79	-5.0 (3.7)	816
426	NGC 6520	270.85	-27.89	3.54 (0.81)	-1.74 (1.03)	2.88	-2.84	0.22	-3.94	-27.6 (0.9)	1577
427	NGC 6531	271.05	-22.49	0.26 (0.42)	-2.66 (0.55)	7.67	-0.35	-2.19	-1.53	-14.7 (5.1)	1205
428	NGC 6530	271.12	-24.36	2.01 (0.45)	-1.81 (0.56)	6.07	-1.32	-0.59	-2.64	-1.9 (7.2)	1322
429	NGC 6546	271.89	-23.33	-1.30 (0.60)	0.30 (0.70)	7.32	-1.43	-0.37	1.28	-16.7 (15.8)	938
430	vdBergh 113	272.22	-21.42	-0.26 (0.45)	-2.47 (0.54)	9.13	-0.77	-2.29	-0.97	14.1 (5.7)	3470
432	Collinder 367	272.43	-23.66	1.16 (0.42)	-2.03 (0.59)	7.27	-2.02	-1.22	-2.00	-3.2 (4.0)	1200
433	NGC 6561	272.62	-16.73	0.02 (0.60)	0.02 (0.50)	13.42	1.16	0.03	-0.01	-20.0 (1.7)	3400
435	Sgr OB7	273.72	-20.40	1.80 (0.26)	-1.20 (0.27)	10.70	-1.51	-0.20	-2.15	-16.8 (7.2)	1860

Table B.1: continued

Seq	Name	RA deg	DEC deg	PM_{RA} (ePM_{RA}) mas/yr	PM_{DEC} (ePM_{DEC}) mas/yr	GLON deg	GLAT deg	PM_{GLON} mas/yr	PM_{GLAT} mas/yr	RV (eRV) km/s	d pc
436	Markarian 38	273.88	-19.00	-1.76 (0.66)	-2.12 (0.43)	12.01	-0.98	-2.70	0.54	-3.2 (9.2)	1545
438	Dias 5	274.41	-19.67	1.92 (1.21)	-0.37 (0.78)	11.65	-1.73	0.58	-1.87	-5.2 (2.2)	1760
439	NGC 6604	274.51	-12.24	-0.36 (0.29)	-2.68 (0.33)	18.24	1.70	-2.53	-0.95	16.5 (1.7)	1696
441	NGC 6611	274.69	-13.81	1.60 (0.33)	-0.35 (0.48)	16.94	0.80	0.45	-1.58	10.0 (1.4)	1719
442	Alessi 19	274.77	12.18	-0.47 (0.22)	-6.97 (0.37)	40.29	12.63	-6.50	-2.57	-6.2 (1.2)	550
443	NGC 6613	274.99	-17.10	-0.72 (0.59)	-1.53 (0.37)	14.18	-1.01	-1.69	-0.09	-14.0 (4.5)	1296
444	NGC 6618	275.14	-16.19	3.04 (1.12)	0.33 (0.67)	15.05	-0.70	1.72	-2.53	-25.3 (19.1)	1814
445	Trumpler 33	276.18	-19.72	-4.69 (1.02)	-0.92 (0.92)	12.39	-3.23	-2.99	3.72	-8.5 (7.7)	1755
446	NGC 6633	276.81	6.51	0.10 (0.22)	-2.00 (0.24)	36.01	8.34	-1.74	-0.98	-29.1 (0.1)	385
447	NGC 6639	277.74	-13.15	2.31 (0.79)	-1.50 (0.63)	18.91	-1.51	-0.26	-2.74	7.0 (1.8)	700
448	Ruprecht 141	277.83	-12.32	0.57 (0.41)	-2.68 (1.06)	19.69	-1.20	-2.11	-1.74	30.7 (1.8)	5500
449	IC 4725	277.92	-19.12	-2.73 (0.35)	-4.95 (0.35)	13.68	-4.41	-5.65	0.16	10.7 (10.4)	620
450	IC 4756	279.73	5.45	-1.11 (0.16)	-3.86 (0.14)	36.37	5.26	-3.95	-0.75	-25.8 (0.2)	484
451	NGC 6694	281.32	-9.38	-2.02 (0.55)	-3.13 (0.48)	23.88	-2.91	-3.71	0.38	4.0 (7.4)	1582
452	Ruprecht 145	282.64	-18.22	6.43 (0.36)	-4.51 (0.46)	16.51	-8.01	-1.23	-7.76	-8.4 (1.0)	770
453	NGC 6705	282.76	-6.27	-6.51 (0.49)	-0.48 (0.41)	27.30	-2.77	-3.38	5.58	31.7 (2.1)	1877
454	NGC 6709	282.82	10.32	2.55 (0.27)	-3.51 (0.31)	42.12	4.72	-1.99	-3.86	-7.8 (5.0)	1075
455	Collinder 394	283.11	-20.20	-3.03 (0.31)	-6.31 (0.42)	14.90	-9.26	-7.00	0.01	-1.9 (6.5)	703
456	Stephenson 1	283.50	36.82	1.66 (0.60)	-2.84 (0.57)	66.81	15.39	-1.98	-2.62	-27.5 (6.4)	373
457	NGC 6716	283.63	-19.90	-1.54 (0.59)	-4.31 (0.44)	15.39	-9.58	-4.55	-0.47	6.0 (7.4)	789
459	NGC 6738	285.33	11.61	4.42 (1.11)	2.65 (0.86)	44.39	3.11	4.37	-2.73	-34.9 (0.9)	700
460	Ruprecht 147	289.17	-16.30	-0.56 (0.19)	-27.74 (0.20)	20.99	-12.81	-25.40	-11.16	41.0 (3.7)	175
464	NGC 6811	294.31	46.39	-5.21 (0.30)	-7.45 (0.23)	79.21	12.02	-9.00	1.28	7.1 (0.1)	1240
465	NGC 6823	295.78	23.30	-2.83 (0.40)	-5.07 (0.29)	59.40	-0.14	-5.81	-0.07	17.0 (5.4)	1893
466	Turner 9	296.20	29.26	0.63 (0.19)	-3.60 (0.20)	64.75	2.51	-2.81	-2.34	-18.5 (6.2)	852
468	Roslund 2	296.35	23.92	-1.88 (0.53)	-4.24 (0.25)	60.19	-0.28	-4.61	-0.50	-4.7 (6.0)	2000
469	NGC 6828	297.57	7.90	-1.12 (1.06)	-2.90 (0.75)	46.82	-9.27	-3.08	-0.44	-21.0 (0.0)	600
470	NGC 6830	297.75	23.10	-0.04 (0.53)	-2.70 (0.64)	60.13	-1.80	-2.34	-1.34	-30.9 (1.0)	1639
471	Roslund 3	299.67	20.48	-0.70 (0.35)	-3.98 (0.46)	58.80	-4.68	-3.77	-1.47	-2.6 (0.3)	1515
476	NGC 6871	301.50	35.78	-3.65 (0.26)	-7.19 (0.42)	72.64	2.06	-8.03	-0.78	-10.5 (2.2)	1574
477	Biurakan 1	301.87	35.70	-3.51 (0.39)	-6.24 (0.56)	72.74	1.76	-7.15	-0.41	-8.0 (2.5)	1600
478	Biurakan 2	302.29	35.48	-3.63 (0.38)	-6.24 (0.42)	72.74	1.35	-7.21	-0.34	-22.0 (9.5)	1106
479	Roslund 5	302.59	33.80	2.75 (0.30)	-2.12 (0.31)	71.47	0.23	-0.27	-3.46	-20.2 (2.5)	418
480	NGC 6883	302.83	35.83	-3.78 (0.28)	-6.58 (0.30)	73.27	1.17	-7.58	-0.44	-10.5 (4.4)	1380
482	NGC 6882	302.94	26.81	1.26 (0.54)	-10.00 (0.85)	65.77	-3.84	-7.69	-6.52	-17.9 (3.4)	342
483	IC 4996	304.12	37.63	-1.78 (0.40)	-5.42 (0.71)	75.35	1.31	-5.49	-1.55	-12.2 (1.5)	1732

Table B.1: continued

Seq	Name	RA	DEC	PM_{RA} (ePM_{RA})	PM_{DEC} (ePM_{DEC})	GLON	GLAT	PM_{GLON}	PM_{GLAT}	RV (eRV)	d
		deg	deg	mas/yr	mas/yr	deg	deg	mas/yr	mas/yr	km/s	pc
484	Collinder 419	304.50	40.72	-2.56 (0.26)	-6.99 (0.16)	78.07	2.79	-7.22	-1.80	-8.3 (0.1)	740
485	Berkeley 86	305.10	38.70	-6.17 (0.91)	-3.11 (0.93)	76.66	1.27	-6.06	3.32	-19.3 (7.8)	1112
486	NGC 6910	305.80	40.78	-3.89 (0.28)	-4.93 (0.35)	78.68	2.01	-6.27	0.37	-32.7 (2.1)	1139
488	NGC 6913	305.98	38.51	-3.80 (0.51)	-5.71 (0.37)	76.90	0.60	-6.86	-0.17	-16.9 (0.6)	1148
490	Cyg OB2	308.31	41.31	-1.60 (0.26)	-4.72 (0.24)	80.21	0.79	-4.75	-1.52	-28.0 (18.0)	1500
491	NGC 6940	308.61	28.28	-1.50 (0.20)	-8.93 (0.24)	69.85	-7.15	-8.10	-4.05	7.7 (0.1)	770
492	Alessi 12	310.87	23.78	3.75 (0.20)	-4.66 (0.24)	67.41	-11.46	-1.49	-5.79	-26.0 (3.7)	537
493	Roslund 7	313.09	37.90	1.20 (0.33)	0.42 (0.22)	79.80	-4.22	1.09	-0.66	-22.0 (3.0)	700
494	NGC 6991	313.63	47.45	7.00 (0.23)	9.26 (0.30)	87.39	1.60	11.59	0.61	-6.0 (3.7)	700
495	NGC 7039	317.70	45.62	-1.68 (0.50)	-4.69 (0.42)	87.88	-1.70	-4.57	-1.97	-11.6 (0.6)	951
498	NGC 7082	322.24	47.13	-1.56 (0.42)	-3.55 (0.40)	91.16	-2.87	-3.58	-1.50	-11.1 (3.4)	1442
499	NGC 7092	322.95	48.45	-8.00 (0.20)	-20.21 (0.22)	92.41	-2.23	-19.63	-9.34	-5.4 (0.4)	311
500	IC 1396	324.73	57.49	-2.21 (0.54)	-4.06 (0.49)	99.28	3.74	-4.35	-1.57	-14.0 (2.2)	835
501	NGC 7160	328.41	62.60	-3.01 (0.41)	-1.77 (0.48)	104.00	6.46	-3.45	0.51	-20.4 (1.9)	794
502	NGC 7209	331.32	46.48	2.49 (0.29)	1.62 (0.33)	95.51	-7.36	2.97	-0.18	-9.7 (0.0)	1167
503	NGC 7235	333.10	57.27	-2.48 (0.88)	-1.74 (1.15)	102.70	0.78	-3.03	-0.02	-53.7 (0.0)	2823
504	NGC 7243	333.78	49.90	0.37 (0.25)	-2.10 (0.23)	98.85	-5.52	-0.88	-1.94	-12.6 (2.5)	808
505	IC 1442	334.12	54.05	-1.77 (0.45)	-2.13 (0.41)	101.36	-2.20	-2.66	-0.78	-25.3 (—)	2346
506	Pismis-Moreno 1	334.69	63.27	0.31 (0.46)	-0.39 (0.99)	106.72	5.31	0.04	-0.50	-23.2 (0.2)	900
508	NGC 7380	341.77	58.12	-3.08 (0.88)	-1.66 (0.86)	107.10	-0.88	-3.50	-0.06	-34.1 (6.1)	2222
509	NGC 7438	344.34	54.34	1.53 (0.57)	-1.18 (0.38)	106.70	-4.90	0.88	-1.72	-17.0 (3.7)	600
510	Cep OB3	346.05	63.40	-1.46 (0.32)	-1.98 (0.37)	111.26	2.98	-2.13	-1.23	-22.9 (3.9)	700
512	NGC 7654	351.19	61.59	-1.72 (0.77)	-2.16 (1.00)	112.81	0.43	-2.33	-1.47	-40.0 (5.6)	1421
513	Czernik 43	351.45	61.32	-2.77 (1.01)	-2.20 (0.76)	112.84	0.13	-3.33	-1.18	-57.9 (2.9)	2500
516	King 12	358.24	61.97	-3.60 (0.97)	-1.25 (0.40)	116.12	-0.13	-3.79	-0.41	-38.0 (6.8)	2378
517	NGC 7788	359.19	61.40	0.29 (0.67)	-2.36 (0.76)	116.43	-0.78	-0.21	-2.37	-24.0 (5.2)	2374
518	NGC 7789	359.31	56.71	3.03 (0.56)	-0.58 (0.54)	115.51	-5.38	2.84	-1.20	-64.0 (1.2)	2337
519	Frolov 1	359.35	61.63	-5.91 (0.65)	-1.35 (1.22)	116.56	-0.57	-6.06	-0.09	16.4 (3.0)	2560
520	NGC 7790	359.59	61.21	-2.13 (0.99)	-1.40 (0.93)	116.58	-1.01	-2.37	-0.94	-80.2 (1.6)	2944
1001	ASCC 1	2.40	62.68	-2.07 (0.72)	0.46 (0.57)	118.15	0.19	-1.97	0.79	-69.7 (4.7)	4000
1003	ASCC 3	7.78	55.28	-1.92 (0.61)	-1.25 (0.59)	120.02	-7.48	-2.01	-1.09	-37.0 (7.4)	1700
1004	ASCC 4	13.29	61.58	0.11 (0.35)	-1.48 (0.44)	123.13	-1.29	0.12	-1.48	-9.2 (9.3)	750
1005	ASCC 5	14.49	55.84	-3.10 (1.05)	-2.91 (0.82)	123.85	-7.02	-3.02	-2.99	-43.0 (3.7)	1500
1006	ASCC 6	26.80	57.73	-1.02 (0.50)	-1.18 (0.53)	130.34	-4.34	-0.74	-1.37	-20.0 (7.4)	1200
1007	ASCC 7	29.73	58.97	-0.57 (1.02)	-3.08 (0.45)	131.54	-2.77	0.25	-3.12	-49.0 (10.7)	2000
1008	ASCC 8	35.20	59.61	-1.24 (0.53)	0.57 (0.59)	134.02	-1.33	-1.36	0.12	-42.1 (0.0)	2200

Table B.1: continued

Seq	Name	RA deg	DEC deg	PM_{RA} (ePM_{RA}) mas/yr	PM_{DEC} (ePM_{DEC}) mas/yr	GLON deg	GLAT deg	PM_{GLON} mas/yr	PM_{GLAT} mas/yr	RV (eRV) km/s	d pc
1009	ASCC 9	41.73	57.73	0.76 (0.78)	-3.03 (0.63)	137.87	-1.76	1.99	-2.41	-41.0 (1.0)	2900
1011	ASCC 11	53.07	44.84	0.15 (0.38)	-5.01 (0.43)	150.56	-9.24	3.04	-3.99	0.7 (5.6)	650
1013	ASCC 13	78.33	44.58	-0.75 (0.27)	-1.66 (0.29)	163.40	3.26	0.91	-1.58	-12.4 (8.5)	800
1014	ASCC 14	80.13	35.22	-0.91 (0.19)	-5.98 (0.58)	171.83	-1.03	4.39	-4.16	-16.9 (0.0)	1100
1016	ASCC 16	81.15	1.80	0.75 (0.22)	-0.18 (0.29)	200.98	-18.35	0.53	0.56	19.3 (9.6)	460
1017	ASCC 17	81.30	30.17	1.33 (0.39)	-6.39 (0.55)	176.56	-3.08	6.04	-2.47	-16.0 (6.1)	2000
1018	ASCC 18	81.54	0.82	0.89 (0.28)	-0.02 (0.25)	202.08	-18.49	0.45	0.77	24.4 (10.5)	500
1019	ASCC 19	81.94	-1.98	0.61 (0.20)	-0.68 (0.26)	204.88	-19.47	0.89	0.22	19.8 (3.2)	350
1020	ASCC 20	82.18	1.63	-0.09 (0.21)	0.51 (0.19)	201.67	-17.53	-0.49	0.17	23.0 (4.8)	450
1021	ASCC 21	82.24	3.65	0.52 (0.25)	-0.62 (0.28)	199.86	-16.49	0.80	0.14	19.8 (1.1)	500
1024	ASCC 24	97.18	-7.02	-5.55 (0.47)	-4.05 (0.41)	216.64	-8.23	1.15	-6.77	16.4 (3.3)	400
1025	ASCC 25	101.38	24.60	0.96 (0.59)	-3.26 (0.74)	190.18	9.72	3.36	-0.54	21.5 (2.4)	1400
1026	ASCC 26	102.60	7.25	-3.05 (0.60)	-0.50 (0.51)	206.35	3.06	-0.94	-2.95	8.0 (7.4)	800
1028	ASCC 28	103.51	-0.17	-1.68 (0.26)	-1.10 (0.36)	213.38	0.50	0.21	-2.00	22.7 (1.8)	800
1029	ASCC 29	103.57	-1.65	-0.49 (0.43)	-0.35 (0.24)	214.72	-0.12	0.09	-0.60	13.5 (10.0)	750
1033	ASCC 33	105.79	-25.05	-3.78 (0.30)	3.78 (0.23)	236.67	-8.73	-5.05	-1.75	14.7 (9.0)	800
1043	ASCC 43	118.27	-28.17	-4.40 (0.37)	0.47 (0.47)	244.73	-0.39	-2.66	-3.53	90.5 (2.7)	1000
1044	Alessi 34	120.42	-50.57	-5.62 (0.57)	6.25 (0.36)	264.92	-10.47	-8.23	-1.69	17.5 (2.8)	1100
1045	ASCC 45	123.96	-35.65	-5.68 (0.60)	3.19 (0.72)	253.63	-0.31	-5.81	-2.94	43.0 (6.0)	3000
1047	Alessi-Teutsch 7	127.95	-39.08	-8.94 (0.45)	5.20 (0.33)	258.26	0.31	-9.48	-4.13	11.0 (7.4)	900
1048	ASCC 48	128.62	-37.61	-11.63 (0.64)	10.72 (0.43)	257.39	1.61	-15.54	-2.92	22.5 (0.0)	400
1050	Alessi 43	132.57	-41.72	-6.39 (0.37)	3.85 (0.41)	262.50	1.48	-7.03	-2.50	17.1 (8.7)	850
1052	ASCC 52	141.99	-54.26	-5.35 (0.37)	5.12 (0.49)	275.96	-2.41	-7.41	0.00	14.1 (0.3)	1500
1057	ASCC 57	152.70	-66.68	-4.15 (0.46)	3.04 (0.47)	287.97	-8.59	-5.14	0.07	2.5 (7.3)	1500
1058	ASCC 58	153.78	-54.97	-12.89 (0.51)	3.15 (0.42)	281.71	1.33	-12.44	-4.63	8.0 (3.7)	600
1060	ASCC 60	158.28	-58.48	-7.35 (0.67)	2.36 (0.37)	285.67	-0.32	-7.54	-1.68	-14.5 (7.4)	800
1062	ASCC 62	162.72	-60.10	-8.72 (0.37)	1.68 (0.45)	288.43	-0.66	-8.55	-2.39	0.1 (2.7)	3000
1063	ASCC 63	163.96	-60.41	-5.63 (0.43)	1.74 (0.70)	289.12	-0.67	-5.83	-0.85	-142.0 (0.0)	3500
1064	ASCC 64	165.76	-60.92	-5.88 (0.49)	1.44 (0.67)	290.14	-0.77	-5.96	-1.07	-8.3 (9.7)	1500
1065	ASCC 65	167.77	-61.12	-6.83 (0.41)	0.88 (0.34)	291.11	-0.57	-6.66	-1.76	-13.4 (3.5)	3500
1067	ASCC 67	175.38	-61.02	-3.64 (0.66)	-0.77 (0.64)	294.56	0.71	-3.30	-1.72	-20.3 (7.4)	1500
1069	ASCC 69	181.65	-69.77	-7.52 (0.31)	-0.64 (0.49)	299.04	-7.23	-7.29	-1.94	2.0 (11.0)	1000
1070	ASCC 70	183.75	-64.43	-5.55 (1.32)	-0.32 (0.54)	299.01	-1.83	-5.45	-1.10	-10.3 (1.1)	2700
1071	ASCC 71	185.17	-67.52	-7.73 (0.38)	-0.30 (0.36)	299.99	-4.82	-7.64	-1.22	-17.9 (4.2)	1300
1073	ASCC 73	189.15	-67.29	-11.72 (0.59)	-0.88 (0.38)	301.49	-4.46	-11.65	-1.56	-15.8 (2.0)	650
1075	ASCC 75	206.79	-62.42	-3.97 (0.99)	-1.44 (0.62)	309.33	-0.24	-4.19	-0.56	-15.0 (3.7)	3000

Table B.1: continued

Seq	Name	RA deg	DEC deg	PM_{RA} (ePM_{RA}) mas/yr	PM_{DEC} (ePM_{DEC}) mas/yr	GLON deg	GLAT deg	PM_{GLON} mas/yr	PM_{GLAT} mas/yr	RV (eRV) km/s	d pc
1076	ASCC 76	208.06	-66.40	-4.12 (0.50)	-3.34 (0.44)	308.97	-4.24	-4.79	-2.28	-18.8 (7.6)	600
1078	ASCC 78	226.27	-68.39	-7.24 (0.57)	-2.54 (0.76)	314.77	-8.64	-7.55	1.38	-19.0 (7.0)	2400
1079	ASCC 79	229.80	-60.73	-2.67 (0.45)	-4.10 (0.42)	320.04	-2.86	-4.45	-2.03	4.5 (2.6)	800
1080	ASCC 80	231.15	-60.14	-2.60 (0.65)	-4.15 (0.52)	320.92	-2.73	-4.46	-2.03	-25.0 (20.0)	1500
1084	ASCC 84	238.72	-60.74	-1.74 (0.70)	-4.87 (0.67)	323.56	-5.44	-4.46	-2.62	-5.0 (0.0)	900
1085	ASCC 85	251.88	-45.46	-0.43 (0.41)	-4.01 (0.34)	339.89	-0.21	-3.34	-2.26	11.2 (8.5)	1200
1086	Alessi-Teutsch 12	255.49	-59.01	-3.34 (0.54)	-7.79 (0.47)	330.63	-10.38	-8.25	-1.95	-6.0 (3.7)	700
1088	ASCC 88	256.69	-35.60	2.89 (0.33)	-2.00 (0.30)	349.88	3.08	0.13	-3.51	1.8 (1.8)	1900
1089	Alessi 24	260.82	-62.64	1.35 (0.45)	-8.31 (0.44)	329.04	-14.56	-6.38	-5.50	-38.6 (19.3)	500
1091	ASCC 91	267.22	-37.36	2.29 (0.32)	-4.92 (0.84)	353.13	-4.93	-3.06	-4.48	-14.5 (1.0)	800
1093	ASCC 93	272.05	-22.26	-2.18 (0.37)	-1.80 (0.69)	8.33	-1.04	-2.63	1.03	-25.1 (3.4)	2500
1094	ASCC 94	273.90	-14.99	0.38 (0.25)	-0.08 (0.37)	15.54	0.92	0.11	-0.37	-26.0 (3.7)	850
1096	Ferrero 1	275.02	-32.37	-1.29 (0.54)	-4.71 (0.49)	0.63	-8.14	-4.78	-0.99	-35.0 (7.4)	750
1097	Alessi 40	279.24	-19.22	-2.09 (0.48)	-6.21 (0.52)	14.16	-5.56	-6.48	-0.94	-16.3 (5.2)	800
1098	ASCC 98	280.65	-33.63	0.69 (0.38)	-5.26 (0.43)	1.54	-12.94	-4.52	-2.78	-54.0 (7.4)	800
1099	ASCC 99	282.27	-18.73	6.90 (0.64)	-2.50 (0.49)	15.89	-7.91	0.78	-7.30	-31.3 (0.4)	280
1100	ASCC 100	285.40	33.57	2.29 (0.43)	-1.51 (0.40)	64.37	12.67	-0.43	-2.71	-22.9 (1.8)	350
1101	ASCC 101	288.40	36.33	0.81 (0.69)	1.87 (0.54)	67.99	11.59	2.04	0.07	-32.0 (2.1)	350
1104	ASCC 104	294.72	18.69	-0.09 (0.31)	-4.65 (0.33)	54.90	-1.55	-4.10	-2.20	-6.6 (1.4)	800
1105	ASCC 105	295.44	27.38	0.91 (0.32)	-3.76 (0.27)	62.78	2.16	-2.82	-2.65	-13.9 (1.9)	500
1106	Alessi 44	295.78	1.60	-1.16 (0.21)	-2.74 (0.36)	40.34	-10.73	-2.96	-0.26	-62.2 (0.2)	500
1107	ASCC 107	297.13	21.96	0.89 (0.42)	-4.48 (0.23)	58.86	-1.89	-3.42	-3.03	-7.0 (3.7)	700
1110	ASCC 110	300.75	33.57	0.60 (0.24)	-4.41 (0.41)	70.45	1.40	-3.42	-2.85	-20.5 (10.9)	800
1111	ASCC 111	302.80	37.45	-0.45 (0.37)	-3.90 (0.27)	74.62	2.08	-3.51	-1.76	-14.2 (7.0)	1600
1114	ASCC 114	325.00	53.97	-3.62 (0.25)	-3.38 (0.32)	97.07	1.00	-4.95	-0.15	-22.0 (4.9)	550
1115	ASCC 115	329.22	51.48	0.15 (0.74)	-1.28 (0.43)	97.45	-2.54	-0.67	-1.10	-9.0 (5.8)	600
1116	ASCC 116	329.64	54.49	-3.51 (0.89)	-4.74 (0.62)	99.49	-0.32	-5.67	-1.62	-30.6 (3.7)	5000
1117	ASCC 117	331.24	62.27	-2.31 (0.34)	0.03 (0.66)	104.85	5.39	-1.84	1.40	-11.4 (1.0)	1200
1118	Alessi-Teutsch 5	332.10	61.10	-2.19 (0.57)	-4.03 (0.49)	104.48	4.21	-4.13	-2.00	-42.0 (10.7)	900
1120	ASCC 120	337.65	57.21	-2.99 (0.55)	-1.54 (0.75)	104.73	-0.60	-3.36	0.21	-60.8 (1.8)	2500
1121	ASCC 121	337.68	54.90	-2.49 (0.51)	-0.70 (0.37)	103.56	-2.59	-2.50	0.68	-64.3 (7.4)	2500
1122	ASCC 122	338.31	39.61	-0.29 (0.42)	-4.19 (0.39)	95.91	-15.90	-2.45	-3.41	-6.1 (3.6)	700
1123	ASCC 123	340.65	54.26	12.50 (0.44)	-1.06 (0.31)	104.74	-4.00	10.49	-6.88	-6.5 (6.5)	250
1125	ASCC 125	344.07	62.75	-2.23 (0.52)	-3.44 (0.52)	110.17	2.76	-3.49	-2.15	-17.9 (3.3)	1500
1126	ASCC 126	346.57	51.05	-0.66 (0.70)	-3.01 (0.42)	106.58	-8.46	-1.80	-2.50	-12.7 (1.8)	800
1127	ASCC 127	347.10	64.85	6.89 (0.52)	-2.23 (0.50)	112.26	4.13	5.49	-4.73	-9.9 (2.1)	350

Table B.2: Cartesian parameters for the final working sample: XYZ-coordinates, UVW-velocities, along with ages, and metallicities.

Seq	Name	X (eX) kpc	Y (eY) kpc	Z (eZ) kpc	U (eU) km/s	V (eV) km/s	W (eW) km/s	Age logt	Met dex	REF
2	Berkeley 59	0.471 (0.047)	0.878 (0.088)	0.087 (0.009)	-10.0 (8.6)	8.3 (10.2)	14.3 (4.9)	6.80	—	—
3	Blanco 1	-0.050 (0.005)	0.013 (0.001)	-0.264 (0.026)	13.4 (2.7)	3.4 (1.7)	-0.8 (0.6)	8.32	-0.19	CC14
4	Alessi 20	0.208 (0.021)	0.398 (0.040)	-0.029 (0.003)	9.1 (3.8)	-5.3 (2.1)	-0.4 (2.3)	8.22	—	—
5	Mayer 1	0.702 (0.070)	1.244 (0.124)	-0.023 (0.003)	-20.6 (10.2)	13.9 (6.1)	-28.2 (7.6)	7.74	—	—
8	NGC 129	0.818 (0.082)	1.402 (0.140)	-0.072 (0.008)	4.6 (11.7)	-14.3 (7.0)	4.8 (7.7)	7.87	—	—
10	NGC 225	0.348 (0.035)	0.557 (0.056)	-0.012 (0.002)	-17.1 (4.7)	-6.1 (3.0)	14.1 (3.2)	8.19	—	—
12	IC 1590	1.295 (0.130)	1.985 (0.198)	-0.259 (0.026)	14.1 (17.5)	-6.4 (12.6)	-7.9 (11.4)	6.84	—	—
13	Alessi 1	0.427 (0.043)	0.651 (0.065)	-0.184 (0.018)	29.2 (6.7)	-2.0 (4.7)	-24.9 (4.7)	8.85	—	—
14	NGC 381	0.606 (0.061)	0.867 (0.087)	-0.022 (0.003)	5.2 (8.5)	-8.3 (7.4)	0.1 (5.1)	8.77	0.07	A02
15	Platais 2	0.107 (0.011)	0.136 (0.014)	-0.102 (0.010)	3.8 (3.9)	1.6 (4.6)	-2.4 (3.4)	8.54	—	—
17	NGC 457	1.445 (0.145)	1.944 (0.194)	-0.185 (0.019)	16.2 (17.3)	-0.7 (13.1)	-12.0 (11.6)	7.38	—	—
18	NGC 581	1.352 (0.135)	1.727 (0.173)	-0.069 (0.008)	4.1 (15.5)	-17.5 (12.4)	8.6 (10.4)	7.44	—	—
19	NGC 637	1.345 (0.135)	1.689 (0.169)	0.065 (0.007)	15.0 (15.6)	-26.3 (12.8)	-14.6 (10.5)	7.21	—	—
20	NGC 654	1.287 (0.129)	1.584 (0.158)	-0.013 (0.003)	16.3 (21.4)	13.5 (23.0)	9.1 (9.7)	7.30	—	—
22	NGC 663	1.240 (0.124)	1.507 (0.151)	-0.032 (0.004)	-6.0 (13.5)	2.7 (11.2)	-17.3 (9.6)	7.14	—	—
25	NGC 752	0.308 (0.031)	0.286 (0.029)	-0.181 (0.018)	11.7 (3.5)	-7.7 (3.8)	-16.3 (2.8)	9.14	—	—
27	Stock 5	0.717 (0.072)	0.833 (0.083)	0.050 (0.005)	-0.7 (7.6)	-0.4 (6.6)	-1.8 (5.3)	7.73	—	—
28	Stock 2	0.261 (0.026)	0.276 (0.028)	-0.013 (0.001)	30.1 (4.0)	-5.3 (3.8)	-7.0 (2.3)	8.17	-0.14	Cl96
29	NGC 869	1.457 (0.146)	1.476 (0.148)	-0.135 (0.014)	2.4 (13.6)	-12.9 (13.5)	-2.2 (9.9)	7.28	-0.30	Go00
30	NGC 884	1.655 (0.166)	1.655 (0.165)	-0.147 (0.015)	2.8 (15.2)	-7.8 (15.2)	2.0 (11.1)	7.10	-0.30	Go00
32	Stock 7	0.491 (0.049)	0.496 (0.050)	0.001 (0.001)	-8.5 (6.3)	20.1 (6.3)	-0.7 (3.4)	7.13	—	—
33	IC 1805	1.327 (0.133)	1.340 (0.134)	0.030 (0.004)	-11.2 (16.1)	-14.9 (16.0)	-7.2 (9.1)	6.73	—	—
34	NGC 957	1.310 (0.131)	1.253 (0.125)	-0.084 (0.009)	3.5 (11.7)	-26.2 (12.2)	-0.3 (8.6)	6.84	—	—
35	Trumpler 2	0.476 (0.048)	0.438 (0.044)	-0.045 (0.005)	-11.0 (9.4)	-14.5 (9.0)	-5.5 (3.5)	7.93	—	—
36	NGC 1039	0.387 (0.039)	0.285 (0.028)	-0.134 (0.013)	-8.4 (2.8)	-0.9 (3.7)	-6.5 (2.7)	8.42	—	—
37	NGC 1027	0.553 (0.055)	0.539 (0.054)	0.021 (0.002)	9.0 (5.6)	30.5 (5.7)	8.9 (3.7)	8.55	—	—
38	IC 1848	1.469 (0.147)	1.360 (0.136)	0.032 (0.004)	-6.7 (12.8)	7.0 (13.7)	-9.3 (9.6)	6.65	—	—
39	Collinder 33	0.744 (0.074)	0.668 (0.067)	0.023 (0.003)	6.4 (11.5)	5.1 (11.1)	26.7 (5.1)	8.36	—	—
41	Stock 23	0.291 (0.029)	0.244 (0.024)	0.014 (0.001)	-16.1 (3.9)	2.4 (3.8)	3.8 (1.8)	7.51	—	—
42	Melotte 20	0.159 (0.016)	0.102 (0.010)	-0.021 (0.002)	6.5 (2.1)	-14.2 (2.9)	-0.6 (1.2)	7.55	0.04	N80
44	Alessi 13	0.033 (0.003)	-0.052 (0.005)	-0.091 (0.009)	2.4 (1.5)	-11.6 (2.1)	3.2 (2.7)	8.72	0.06	CC14
45	NGC 1342	0.581 (0.058)	0.271 (0.027)	-0.176 (0.018)	-10.7 (2.4)	2.6 (4.6)	1.7 (3.1)	8.21	-0.16	G00
46	IC 348	0.354 (0.035)	0.125 (0.013)	-0.121 (0.012)	14.6 (3.4)	2.1 (3.2)	-3.5 (2.1)	7.79	—	—
47	Melotte 22	0.116 (0.012)	0.028 (0.003)	-0.052 (0.005)	-2.1 (1.0)	-14.6 (2.8)	-6.8 (1.3)	8.08	-0.04	CC14
48	Tombaugh 5	0.807 (0.081)	0.587 (0.059)	0.062 (0.006)	6.3 (5.3)	5.0 (7.2)	-3.2 (4.9)	8.73	—	—
49	NGC 1502	0.656 (0.066)	0.482 (0.048)	0.109 (0.011)	-8.2 (5.6)	3.1 (6.4)	1.8 (3.9)	6.80	—	—

Table B.2: continued

Seq	Name	X (eX) kpc	Y (eY) kpc	Z (eZ) kpc	U (eU) km/s	V (eV) km/s	W (eW) km/s	Age logt	Met dex	REF
50	NGC 1528	0.685 (0.069)	0.364 (0.036)	0.003 (0.001)	-3.4 (3.1)	-1.3 (5.6)	4.9 (3.7)	8.43	—	—
51	NGC 1545	0.636 (0.064)	0.319 (0.032)	0.002 (0.001)	-13.0 (2.7)	8.3 (4.9)	0.9 (3.4)	8.15	—	—
52	NGC 1582	0.560 (0.056)	0.212 (0.021)	-0.032 (0.003)	2.9 (1.8)	11.5 (3.9)	9.0 (2.9)	8.60	—	—
53	Platais 3	0.145 (0.014)	0.127 (0.013)	0.055 (0.006)	12.4 (3.2)	5.6 (3.1)	0.2 (1.7)	8.70	—	—
54	NGC 1647	0.516 (0.052)	-0.003 (0.001)	-0.156 (0.016)	-13.4 (0.8)	11.2 (2.6)	2.4 (2.5)	7.96	—	—
56	NGC 1662	0.404 (0.040)	-0.054 (0.005)	-0.157 (0.016)	-26.3 (0.9)	15.5 (2.2)	5.6 (2.1)	8.68	-0.10	T97
57	NGC 1664	1.138 (0.114)	0.377 (0.038)	-0.009 (0.002)	13.7 (2.9)	-1.1 (7.7)	-26.6 (6.6)	8.72	—	—
58	Berkeley 14A	1.051 (0.105)	0.324 (0.032)	0.014 (0.002)	7.1 (4.2)	5.6 (6.9)	-5.1 (5.4)	6.97	—	—
60	NGC 1746	0.747 (0.075)	0.012 (0.002)	-0.140 (0.014)	-9.3 (3.7)	8.1 (3.6)	-5.0 (3.8)	8.19	—	—
61	Platais 4	0.271 (0.027)	-0.003 (0.000)	-0.052 (0.005)	3.5 (5.0)	3.6 (1.5)	2.3 (1.6)	8.24	—	—
62	NGC 1778	1.426 (0.143)	0.280 (0.028)	-0.052 (0.006)	7.7 (2.2)	1.6 (8.0)	-10.4 (7.1)	8.18	—	—
64	NGC 1817	1.910 (0.191)	-0.206 (0.021)	-0.447 (0.045)	41.8 (2.5)	-15.4 (10.1)	-22.6 (9.3)	8.25	—	—
65	NGC 1901	-0.053 (0.005)	-0.336 (0.034)	-0.226 (0.023)	-1.4 (2.3)	11.0 (1.2)	5.7 (1.6)	8.93	-0.02	CC14
66	NGC 1893	3.258 (0.326)	0.367 (0.037)	-0.097 (0.011)	4.0 (5.7)	-42.3 (17.3)	-26.9 (15.9)	6.82	—	—
68	Collinder 65	0.301 (0.030)	-0.047 (0.005)	-0.058 (0.006)	6.1 (4.5)	0.7 (2.0)	0.2 (1.7)	7.41	—	—
69	NGC 1907	1.319 (0.132)	0.171 (0.017)	0.007 (0.002)	-2.2 (1.4)	-4.3 (7.0)	-3.9 (6.4)	7.94	—	—
70	Stock 8	1.809 (0.181)	0.210 (0.021)	-0.006 (0.003)	-7.7 (2.8)	-7.1 (9.3)	-21.8 (9.1)	7.61	—	—
71	NGC 1912	1.056 (0.106)	0.143 (0.014)	0.013 (0.002)	-1.2 (1.1)	-9.7 (5.9)	-7.0 (5.2)	8.56	—	—
72	Collinder 69	0.413 (0.041)	-0.113 (0.011)	-0.092 (0.009)	15.8 (1.6)	0.8 (2.6)	-0.0 (2.1)	6.76	—	—
73	NGC 1981	0.334 (0.033)	-0.178 (0.018)	-0.130 (0.013)	10.2 (2.6)	0.4 (3.0)	2.2 (2.0)	7.50	—	—
74	NGC 1976	0.329 (0.033)	-0.183 (0.018)	-0.132 (0.013)	7.7 (4.5)	-3.4 (3.7)	2.1 (2.5)	7.71	—	—
75	NGC 1977	0.415 (0.042)	-0.225 (0.023)	-0.164 (0.016)	2.1 (2.7)	-4.8 (3.7)	4.2 (2.4)	7.08	—	—
76	NGC 1980	0.451 (0.045)	-0.255 (0.026)	-0.184 (0.018)	1.9 (2.4)	-0.1 (3.9)	3.2 (2.5)	6.67	—	—
77	Collinder 70	0.338 (0.034)	-0.158 (0.016)	-0.117 (0.012)	13.0 (4.3)	-1.8 (3.3)	-1.0 (2.3)	6.71	0.14	CC14
78	NGC 1960	1.312 (0.131)	0.126 (0.013)	0.025 (0.003)	-4.3 (4.6)	-13.8 (7.0)	-6.7 (6.4)	7.62	—	—
80	Sigma Ori	0.340 (0.034)	-0.172 (0.017)	-0.119 (0.012)	10.9 (1.6)	-4.1 (2.8)	5.1 (1.9)	6.82	—	—
81	Stock 10	0.375 (0.038)	0.055 (0.006)	0.024 (0.002)	-20.6 (3.6)	11.4 (2.0)	-0.1 (1.9)	8.42	—	—
82	NGC 2099	1.380 (0.138)	0.057 (0.006)	0.075 (0.008)	2.3 (0.5)	-37.4 (8.3)	0.7 (6.6)	8.54	0.09	T97
84	NGC 2129	1.505 (0.150)	-0.174 (0.018)	0.003 (0.002)	-3.1 (1.7)	7.8 (7.6)	6.2 (7.2)	7.08	—	—
86	NGC 2169	0.993 (0.099)	-0.277 (0.028)	-0.053 (0.005)	2.8 (2.4)	2.0 (6.2)	-8.8 (5.1)	6.89	—	—
87	NGC 2168	0.824 (0.082)	-0.095 (0.010)	0.032 (0.003)	-21.8 (0.7)	-0.5 (4.4)	9.4 (3.9)	8.18	-0.16	T97
91	Platais 6	0.313 (0.031)	-0.148 (0.015)	-0.038 (0.004)	-3.9 (13.5)	4.7 (6.8)	-3.5 (2.5)	7.79	—	—
93	Collinder 89	0.789 (0.079)	-0.120 (0.012)	0.053 (0.005)	12.1 (7.6)	1.3 (4.4)	6.3 (3.8)	7.50	—	—
95	NGC 2232	0.265 (0.027)	-0.183 (0.018)	-0.042 (0.004)	1.7 (1.7)	0.8 (2.3)	-2.5 (1.7)	7.49	—	—
96	Collinder 95	0.516 (0.052)	-0.207 (0.021)	0.000 (0.001)	-28.5 (7.1)	8.8 (4.7)	-2.7 (2.8)	8.36	—	—
97	Collinder 97	0.452 (0.045)	-0.214 (0.021)	-0.015 (0.002)	5.1 (1.7)	2.7 (3.4)	-3.5 (2.6)	8.32	—	—

Table B.2: continued

Seq	Name	X (eX) kpc	Y (eY) kpc	Z (eZ) kpc	U (eU) km/s	V (eV) km/s	W (eW) km/s	Age logt	Met dex	REF
98	NGC 2244	1.295 (0.129)	-0.640 (0.064)	-0.052 (0.006)	-2.5 (6.9)	4.5 (10.2)	-2.8 (6.9)	6.70	—	—
99	NGC 2240	0.440 (0.044)	0.006 (0.001)	0.092 (0.009)	8.2 (1.1)	-13.8 (3.4)	2.8 (2.2)	9.50	—	—
100	Basel 8	1.215 (0.121)	-0.537 (0.054)	-0.004 (0.002)	-19.9 (8.0)	-3.7 (9.6)	3.4 (6.3)	7.68	—	—
102	NGC 2251	1.218 (0.122)	-0.531 (0.053)	0.002 (0.002)	-8.4 (4.2)	-12.3 (9.2)	2.9 (6.3)	8.43	0.25	Pr05
104	Collinder 106	1.438 (0.144)	-0.702 (0.070)	-0.011 (0.002)	4.4 (7.2)	16.6 (11.3)	-1.1 (7.6)	6.74	—	—
105	Collinder 107	1.288 (0.129)	-0.666 (0.067)	-0.019 (0.003)	-14.0 (7.7)	10.7 (10.5)	-10.9 (7.1)	7.03	—	—
107	NGC 2264	0.607 (0.061)	-0.257 (0.026)	0.025 (0.003)	1.7 (2.3)	-1.3 (4.5)	-4.7 (3.4)	6.81	—	—
109	NGC 2270	1.225 (0.122)	-0.678 (0.068)	-0.002 (0.002)	-1.8 (6.6)	-21.3 (10.2)	-3.3 (6.7)	8.64	—	—
110	NGC 2287	0.429 (0.043)	-0.530 (0.053)	-0.126 (0.013)	-6.2 (4.9)	-2.8 (4.0)	-10.0 (3.5)	8.45	—	—
111	NGC 2281	0.532 (0.053)	0.047 (0.005)	0.162 (0.016)	13.8 (3.6)	-0.4 (3.1)	-4.6 (3.2)	8.70	0.13	G00
112	NGC 2301	0.723 (0.072)	-0.462 (0.046)	0.004 (0.001)	-14.5 (4.5)	-7.3 (6.4)	-6.3 (4.3)	8.31	0.06	T97
115	Collinder 121	0.619 (0.062)	-0.889 (0.089)	-0.194 (0.019)	5.4 (8.1)	4.6 (6.4)	-4.7 (5.3)	7.08	—	—
118	NGC 2323	0.658 (0.066)	-0.585 (0.059)	-0.020 (0.002)	-25.9 (5.5)	4.5 (6.1)	5.6 (4.2)	8.13	—	—
119	vdBergh 92	1.068 (0.107)	-1.052 (0.105)	-0.065 (0.007)	-3.6 (9.6)	25.4 (9.8)	-17.4 (7.5)	7.59	—	—
120	NGC 2335	1.026 (0.103)	-0.977 (0.098)	-0.029 (0.004)	-46.8 (9.4)	-10.1 (9.8)	5.9 (6.7)	8.08	-0.03	T97
125	Alessi 21	0.363 (0.036)	-0.344 (0.034)	0.000 (0.001)	16.4 (3.4)	-6.7 (3.5)	2.9 (2.4)	7.47	—	—
126	Collinder 132	0.183 (0.018)	-0.362 (0.036)	-0.066 (0.007)	4.1 (3.0)	-3.6 (2.3)	-2.1 (2.0)	7.51	—	—
127	NGC 2354	1.976 (0.198)	-3.207 (0.321)	-0.450 (0.045)	-64.8 (27.2)	9.5 (17.3)	-86.3 (20.3)	8.10	-0.11	CC14
128	NGC 2353	0.796 (0.080)	-0.787 (0.079)	0.007 (0.002)	0.1 (7.2)	-1.8 (7.3)	-3.6 (5.4)	7.05	—	—
129	Alessi 3	0.058 (0.006)	-0.271 (0.027)	-0.076 (0.008)	3.4 (2.1)	21.2 (0.9)	0.9 (1.5)	8.87	-0.28	CC14
132	NGC 2360	1.218 (0.122)	-1.441 (0.144)	-0.047 (0.005)	6.4 (13.0)	25.0 (11.1)	6.8 (8.9)	8.59	—	—
133	Collinder 135	0.112 (0.011)	-0.292 (0.029)	-0.062 (0.006)	3.3 (3.2)	-3.0 (6.3)	-7.8 (2.3)	7.54	-0.22	CC14
134	NGC 2362	0.728 (0.073)	-1.175 (0.117)	-0.135 (0.014)	-8.3 (12.3)	-0.8 (13.4)	0.4 (6.7)	6.64	—	—
135	NGC 2367	1.130 (0.113)	-1.650 (0.165)	-0.134 (0.014)	11.7 (14.4)	6.9 (10.4)	8.9 (9.5)	7.01	—	—
136	Collinder 140	0.168 (0.017)	-0.361 (0.036)	-0.055 (0.006)	0.6 (3.1)	1.4 (3.1)	-6.0 (2.2)	7.57	-0.10	G00
137	NGC 2374	0.974 (0.097)	-1.098 (0.110)	0.026 (0.003)	-17.0 (10.0)	-3.6 (8.9)	-20.0 (7.5)	8.68	—	—
139	NGC 2384	1.201 (0.120)	-1.740 (0.174)	-0.089 (0.009)	11.6 (15.2)	7.4 (11.0)	-32.0 (10.7)	7.13	—	—
140	Trumpler 7	0.775 (0.078)	-1.251 (0.125)	-0.086 (0.009)	-4.3 (10.6)	-0.8 (7.1)	2.6 (7.0)	7.72	—	—
141	NGC 2396	0.397 (0.040)	-0.433 (0.043)	0.027 (0.003)	-9.8 (4.0)	-1.3 (3.7)	0.9 (2.9)	8.52	—	—
142	Bochum 5	1.219 (0.122)	-1.586 (0.159)	0.027 (0.004)	-32.6 (15.8)	-6.1 (14.2)	-13.4 (9.7)	8.45	-0.17	CC14
143	Bochum 4	0.528 (0.053)	-0.694 (0.069)	0.012 (0.002)	-14.7 (6.6)	3.0 (5.6)	2.1 (4.2)	7.25	—	—
145	NGC 2414	1.800 (0.180)	-2.256 (0.226)	0.098 (0.011)	2.9 (20.1)	-21.3 (16.2)	-9.7 (13.8)	6.94	—	—
147	NGC 2422	0.309 (0.031)	-0.381 (0.038)	0.027 (0.003)	11.1 (3.4)	-7.4 (2.9)	-3.2 (2.6)	8.12	-0.03	CC14
148	NGC 2423	0.487 (0.049)	-0.590 (0.059)	0.047 (0.005)	-17.1 (5.6)	-8.4 (4.8)	2.9 (3.7)	8.98	0.07	CC14
149	Ruprecht 26	0.885 (0.088)	-1.134 (0.113)	0.068 (0.007)	-21.2 (11.1)	-6.4 (9.8)	-17.1 (7.3)	7.49	0.31	CC14
150	Melotte 71	2.065 (0.207)	-2.371 (0.237)	0.247 (0.025)	39.6 (21.9)	48.0 (19.2)	5.9 (14.9)	8.37	-0.22	CC14

Table B.2: continued

Seq	Name	X (eX) kpc	Y (eY) kpc	Z (eZ) kpc	U (eU) km/s	V (eV) km/s	W (eW) km/s	Age logt	Met dex	REF
151	Ruprecht 27	0.266 (0.027)	-0.492 (0.049)	-0.025 (0.003)	-8.4 (4.0)	8.1 (2.4)	2.0 (2.7)	8.41	—	—
152	NGC 2428	1.260 (0.126)	-1.677 (0.168)	0.100 (0.010)	-11.6 (14.9)	-12.2 (11.5)	-4.0 (10.0)	8.68	-0.14	CC14
153	NGC 2430	0.391 (0.039)	-0.518 (0.052)	0.032 (0.003)	3.1 (8.5)	-7.1 (10.1)	-0.7 (3.3)	8.68	0.13	CC14
155	Haffner 13	0.301 (0.030)	-0.646 (0.065)	-0.046 (0.005)	25.3 (5.5)	-37.3 (5.8)	-6.7 (3.5)	7.51	—	—
156	NGC 2439	1.537 (0.154)	-3.523 (0.352)	-0.300 (0.031)	-31.6 (26.1)	-26.2 (12.1)	-6.0 (18.3)	6.82	—	—
157	NGC 2432	1.147 (0.115)	-1.674 (0.167)	0.064 (0.007)	-21.3 (14.4)	18.7 (10.2)	-16.3 (9.9)	8.18	—	—
158	Ruprecht 151	1.259 (0.126)	-1.676 (0.168)	0.118 (0.012)	-4.6 (15.0)	11.1 (11.9)	-19.6 (10.3)	8.49	-0.10	CC14
159	NGC 2451A	0.056 (0.006)	-0.178 (0.018)	-0.025 (0.003)	13.6 (2.0)	-6.5 (0.8)	-6.8 (1.4)	7.76	-0.53	CC14
160	NGC 2437	0.847 (0.085)	-1.079 (0.108)	0.097 (0.010)	-3.5 (9.9)	0.7 (8.3)	-12.1 (6.8)	8.16	-0.75	CC14
162	NGC 2451B	0.132 (0.013)	-0.406 (0.041)	-0.050 (0.005)	-0.2 (2.7)	5.8 (1.0)	-7.7 (2.4)	7.88	-0.45	Ly81
163	NGC 2447	0.518 (0.052)	-0.899 (0.090)	0.003 (0.001)	-0.9 (7.3)	6.8 (4.4)	0.8 (5.0)	8.76	-0.10	CC14
164	NGC 2448	0.508 (0.051)	-0.907 (0.091)	-0.005 (0.002)	3.2 (7.6)	5.7 (5.6)	2.5 (5.0)	7.19	—	—
166	Haffner 16	1.481 (0.148)	-2.797 (0.280)	0.026 (0.005)	-17.0 (23.1)	-9.7 (17.5)	-59.1 (16.4)	7.51	-0.11	CC14
167	NGC 2477	0.344 (0.034)	-1.166 (0.117)	-0.124 (0.013)	-30.0 (7.6)	7.8 (2.5)	11.6 (5.8)	8.61	-0.19	CC14
169	NGC 2467	0.612 (0.061)	-1.209 (0.121)	0.008 (0.002)	2.4 (10.4)	-27.0 (10.0)	-8.7 (6.6)	8.05	—	—
171	NGC 2482	0.638 (0.064)	-1.181 (0.118)	0.048 (0.005)	-1.2 (9.6)	-14.8 (6.5)	-20.2 (7.0)	8.48	-0.08	CC14
174	NGC 2489	1.463 (0.146)	-3.398 (0.340)	-0.050 (0.007)	-67.8 (25.5)	-11.0 (11.5)	-62.4 (18.9)	7.25	0.08	T97
175	NGC 2516	-0.022 (0.002)	-0.332 (0.033)	-0.094 (0.009)	-2.7 (1.9)	-13.0 (0.5)	2.0 (1.6)	8.08	-0.37	CC14
178	NGC 2506	2.165 (0.217)	-2.632 (0.263)	0.597 (0.060)	36.6 (24.0)	-13.7 (20.1)	-53.7 (17.5)	9.05	—	—
179	Ruprecht 47	1.114 (0.111)	-2.792 (0.279)	-0.010 (0.004)	-59.3 (20.7)	-40.0 (8.7)	-2.2 (14.3)	8.07	—	—
180	NGC 2527	0.243 (0.024)	-0.549 (0.055)	0.019 (0.002)	14.7 (4.2)	-16.8 (2.3)	5.5 (2.9)	8.85	0.06	CC14
182	Vel OB2	0.048 (0.005)	-0.404 (0.040)	-0.057 (0.006)	2.9 (2.5)	-9.1 (9.5)	3.2 (2.4)	7.26	-0.29	CC14
183	NGC 2547	0.044 (0.004)	-0.450 (0.045)	-0.068 (0.007)	-3.1 (2.3)	2.0 (1.6)	-6.3 (2.4)	7.70	-0.16	T97
184	NGC 2539	0.791 (0.079)	-1.078 (0.108)	0.263 (0.026)	-18.8 (9.8)	-13.6 (7.4)	-15.2 (6.8)	8.75	—	—
186	NGC 2546	0.240 (0.024)	-0.886 (0.089)	-0.033 (0.004)	-1.7 (5.5)	5.0 (2.0)	-1.2 (4.4)	7.92	0.12	T97
187	Ruprecht 55	1.618 (0.162)	-4.616 (0.462)	0.069 (0.010)	-19.4 (31.2)	-46.9 (11.9)	-73.2 (24.6)	6.97	—	—
189	NGC 2548	0.497 (0.050)	-0.550 (0.055)	0.204 (0.020)	6.6 (5.2)	-13.0 (4.7)	15.7 (3.5)	8.75	0.08	T97
190	vdBergh-Hagen 23	0.120 (0.012)	-0.420 (0.042)	-0.008 (0.001)	5.6 (3.5)	-5.2 (7.7)	2.1 (2.1)	7.14	—	—
191	Haffner 26	0.348 (0.035)	-0.937 (0.094)	0.041 (0.004)	13.8 (7.7)	-36.2 (11.6)	2.8 (4.8)	7.47	—	—
192	NGC 2567	0.579 (0.058)	-1.572 (0.157)	0.087 (0.009)	-15.3 (10.9)	-12.7 (4.4)	11.6 (7.9)	8.64	-0.07	CC14
193	NGC 2571	0.477 (0.048)	-1.249 (0.125)	0.082 (0.008)	4.8 (9.4)	-15.8 (10.2)	10.7 (6.4)	7.22	0.05	Cm85
196	Pismis 4	0.073 (0.007)	-0.588 (0.059)	-0.026 (0.003)	0.2 (3.1)	-14.9 (5.0)	3.1 (2.8)	8.11	-0.20	Pi95
198	Ruprecht 64	0.142 (0.014)	-0.787 (0.079)	0.007 (0.001)	5.3 (4.5)	-8.7 (5.9)	2.6 (3.8)	8.45	—	—
199	Pismis 6	0.152 (0.015)	-1.659 (0.166)	-0.085 (0.009)	20.6 (8.7)	2.9 (4.1)	-6.6 (8.0)	7.58	—	—
201	NGC 2632	0.142 (0.014)	-0.069 (0.007)	0.100 (0.010)	31.3 (1.8)	-8.4 (1.5)	-3.9 (3.0)	8.90	0.10	CC14
202	IC 2391	-0.001 (0.000)	-0.175 (0.017)	-0.021 (0.002)	13.4 (2.4)	-1.8 (0.2)	1.3 (0.9)	7.88	-0.15	CC14

Table B.2: continued

Seq	Name	X (eX) kpc	Y (eY) kpc	Z (eZ) kpc	U (eU) km/s	V (eV) km/s	W (eW) km/s	Age logt	Met dex	REF
203	Ruprecht 67	0.189 (0.019)	-1.492 (0.149)	-0.021 (0.003)	3.2 (7.8)	35.1 (1.4)	-38.7 (8.5)	8.38	—	—
204	Mamajek 1	-0.037 (0.004)	-0.090 (0.009)	-0.039 (0.004)	1.2 (1.8)	-7.1 (1.1)	-4.0 (0.8)	6.90	—	—
205	IC 2395	0.042 (0.004)	-0.706 (0.071)	-0.044 (0.005)	-13.0 (3.5)	3.7 (8.8)	0.2 (3.5)	7.08	0.00	Cl03B
207	Bochum 7	0.482 (0.049)	-5.730 (0.573)	-0.197 (0.021)	-16.3 (28.2)	-23.4 (3.9)	-7.4 (27.3)	7.08	—	—
210	Trumpler 10	0.053 (0.005)	-0.414 (0.041)	0.005 (0.001)	5.7 (3.0)	-5.4 (13.9)	-3.4 (2.3)	7.38	-0.13	Ly84
212	NGC 2682	0.626 (0.063)	-0.450 (0.045)	0.480 (0.048)	15.7 (5.5)	-20.2 (6.8)	-16.9 (5.2)	9.41	-0.10	CC14
213	vdBergh-Hagen 56	0.065 (0.007)	-0.677 (0.068)	0.017 (0.002)	-4.8 (3.4)	32.3 (0.4)	7.5 (3.2)	7.24	—	—
214	Collinder 205	0.021 (0.003)	-1.499 (0.150)	-0.048 (0.005)	2.1 (7.2)	-7.7 (5.6)	18.0 (7.2)	7.03	—	—
216	Platais 8	-0.020 (0.002)	-0.147 (0.015)	-0.020 (0.002)	0.7 (1.7)	2.7 (7.2)	4.8 (1.2)	7.75	-0.30	CC14
218	Platais 9	0.010 (0.001)	-0.199 (0.020)	0.011 (0.001)	10.2 (2.1)	-5.2 (1.5)	-0.8 (1.3)	8.09	—	—
220	IC 2488	-0.154 (0.015)	-1.120 (0.112)	-0.087 (0.009)	8.5 (6.1)	7.9 (1.0)	3.4 (5.4)	8.53	0.10	Cl03A
223	Turner 5	0.039 (0.004)	-0.391 (0.039)	0.077 (0.008)	-25.3 (2.9)	11.6 (14.6)	1.7 (3.5)	8.49	-0.21	CC14
224	NGC 2925	-0.080 (0.008)	-0.770 (0.077)	-0.017 (0.002)	5.9 (4.3)	-7.9 (7.4)	-0.1 (3.7)	8.05	—	—
225	Ruprecht 79	-0.244 (0.025)	-1.964 (0.196)	-0.028 (0.004)	13.7 (10.4)	-22.7 (2.7)	-48.3 (10.9)	7.84	—	—
226	Ruprecht 80	-0.033 (0.005)	-2.483 (0.248)	0.292 (0.029)	95.3 (15.9)	-41.5 (1.8)	-35.1 (12.7)	8.33	-0.37	CC14
228	NGC 3033	-0.154 (0.015)	-0.909 (0.091)	-0.033 (0.004)	-15.8 (4.9)	-18.7 (0.9)	10.1 (4.4)	8.62	—	—
230	NGC 3036	-0.281 (0.028)	-1.158 (0.116)	-0.143 (0.014)	-16.2 (6.9)	-2.7 (2.2)	-27.5 (6.5)	8.61	-0.71	CC14
231	Pismis 16	-0.248 (0.025)	-1.807 (0.181)	0.022 (0.003)	-11.7 (9.4)	-9.1 (5.4)	-17.4 (9.0)	7.72	—	—
234	NGC 3114	-0.208 (0.021)	-0.885 (0.088)	-0.061 (0.006)	2.2 (5.3)	7.1 (1.4)	1.7 (4.3)	8.24	—	—
239	Ruprecht 161	-0.237 (0.024)	-0.907 (0.091)	-0.071 (0.007)	-0.2 (5.7)	-6.3 (3.9)	-4.2 (4.6)	8.39	—	—
243	IC 2581	-0.616 (0.062)	-2.367 (0.237)	0.001 (0.003)	13.1 (14.5)	-7.1 (5.3)	2.7 (11.6)	7.22	-0.34	G00
245	Loden 143	-0.158 (0.016)	-0.579 (0.058)	-0.009 (0.001)	4.9 (4.6)	4.0 (9.5)	-5.7 (3.1)	8.45	—	—
248	Collinder 223	-0.466 (0.047)	-1.620 (0.162)	-0.049 (0.005)	-4.7 (10.2)	-11.1 (3.3)	-15.5 (8.3)	8.41	-0.22	CC14
249	Ruprecht 90	-1.593 (0.160)	-5.785 (0.578)	-0.021 (0.009)	48.8 (36.3)	-17.6 (17.8)	-6.5 (28.5)	7.10	—	—
251	Loden 153	-0.721 (0.072)	-2.571 (0.257)	0.004 (0.004)	9.5 (16.0)	-3.6 (5.4)	15.4 (12.7)	6.74	0.19	CC14
253	NGC 3293	-0.675 (0.068)	-2.377 (0.238)	0.003 (0.003)	20.4 (15.1)	-3.7 (4.7)	-5.9 (11.8)	6.94	—	—
254	NGC 3324	-0.643 (0.064)	-2.209 (0.221)	-0.008 (0.003)	22.4 (14.3)	-8.4 (5.0)	1.1 (10.9)	6.72	-0.47	CC14
255	vdBergh-Hagen 99	-0.151 (0.015)	-0.509 (0.051)	-0.005 (0.001)	3.1 (3.7)	-9.9 (2.3)	-9.2 (3.0)	7.86	0.09	CC14
258	Melotte 101	-0.675 (0.068)	-1.868 (0.187)	-0.193 (0.020)	-9.6 (13.3)	-28.3 (10.9)	-3.7 (9.5)	8.35	—	—
259	IC 2602	-0.053 (0.005)	-0.150 (0.015)	-0.014 (0.001)	-0.8 (1.8)	1.7 (2.8)	7.8 (0.8)	7.83	-0.09	CC14
260	Bochum 10	-0.594 (0.059)	-1.938 (0.194)	-0.011 (0.003)	2.5 (12.5)	-6.6 (4.1)	-1.4 (9.6)	6.93	—	—
261	Alessi 5	-0.123 (0.012)	-0.378 (0.038)	-0.014 (0.002)	4.4 (3.1)	-2.9 (2.4)	0.1 (2.0)	7.71	-0.38	CC14
262	Collinder 228	-0.578 (0.058)	-1.819 (0.182)	-0.035 (0.004)	3.1 (11.9)	5.5 (5.1)	-5.8 (9.1)	6.68	—	—
263	Trumpler 14	-0.823 (0.082)	-2.627 (0.263)	-0.028 (0.005)	-12.9 (17.1)	4.6 (9.5)	25.1 (13.2)	6.67	—	—
264	Trumpler 15	-0.633 (0.063)	-2.020 (0.202)	-0.014 (0.003)	-28.1 (13.2)	11.4 (7.1)	28.7 (10.3)	7.08	—	—
265	Trumpler 16	-0.860 (0.086)	-2.708 (0.271)	-0.032 (0.005)	73.8 (19.4)	-13.0 (6.8)	-14.6 (13.6)	6.90	—	—

Table B.2: continued

Seq	Name	X (eX) kpc	Y (eY) kpc	Z (eZ) kpc	U (eU) km/s	V (eV) km/s	W (eW) km/s	Age logt	Met dex	REF
266	Ruprecht 91	-0.261 (0.026)	-0.861 (0.086)	0.023 (0.003)	14.1 (6.8)	1.2 (11.0)	-2.6 (4.4)	8.63	—	—
267	Loden 189	-0.207 (0.021)	-0.689 (0.069)	0.033 (0.003)	-10.5 (4.6)	-4.9 (5.2)	8.0 (3.4)	8.64	0.20	CC14
268	Ruprecht 92	-0.784 (0.078)	-2.227 (0.223)	-0.082 (0.009)	-45.4 (15.4)	13.2 (6.7)	1.8 (11.2)	7.53	0.20	CC14
270	Trumpler 17	-0.700 (0.070)	-2.074 (0.207)	0.017 (0.003)	-30.6 (14.0)	-26.7 (9.2)	51.2 (11.3)	7.51	—	—
271	Collinder 236	-0.268 (0.027)	-0.754 (0.075)	-0.017 (0.002)	-19.8 (7.2)	-10.5 (14.4)	11.3 (3.8)	8.37	0.04	CC14
272	Bochum 12	-0.753 (0.075)	-2.085 (0.209)	-0.069 (0.008)	-47.3 (14.6)	9.0 (5.7)	-29.2 (11.1)	7.68	—	—
273	NGC 3496	-0.331 (0.033)	-0.933 (0.093)	-0.008 (0.002)	-3.0 (6.9)	-3.3 (7.4)	1.7 (4.7)	8.62	—	—
274	Pismis 17	-1.169 (0.117)	-3.303 (0.330)	0.006 (0.005)	24.2 (22.5)	13.4 (9.8)	11.5 (16.6)	7.32	-0.14	CC14
275	Ruprecht 93	-0.502 (0.050)	-1.346 (0.135)	-0.028 (0.003)	-24.4 (9.4)	-2.3 (4.9)	-1.3 (6.9)	8.64	0.15	CC14
276	NGC 3532	-0.167 (0.017)	-0.468 (0.047)	0.012 (0.001)	2.8 (3.5)	1.4 (2.5)	7.4 (2.4)	8.45	-0.02	CC14
277	Loden 306	-0.702 (0.070)	-1.873 (0.187)	-0.029 (0.004)	8.6 (13.1)	20.4 (6.7)	-15.7 (9.8)	6.76	—	—
278	Feinstein 1	-0.399 (0.040)	-1.088 (0.109)	0.009 (0.002)	1.0 (8.1)	10.8 (8.9)	4.5 (5.5)	6.97	—	—
281	NGC 3572	-0.709 (0.071)	-1.874 (0.187)	0.007 (0.003)	32.9 (13.8)	-15.7 (6.3)	-19.8 (9.9)	6.88	—	—
283	Trumpler 18	-0.486 (0.049)	-1.268 (0.127)	-0.003 (0.002)	14.0 (9.2)	7.4 (5.5)	-11.8 (6.7)	7.77	—	—
284	NGC 3590	-0.597 (0.060)	-1.539 (0.154)	-0.005 (0.002)	-1.0 (11.1)	-0.8 (7.5)	-1.0 (7.9)	7.55	—	—
285	Stock 13	-0.552 (0.055)	-1.477 (0.148)	0.044 (0.005)	20.8 (11.1)	-16.7 (8.1)	0.7 (7.5)	7.37	—	—
286	IC 2714	-0.472 (0.047)	-1.144 (0.114)	-0.039 (0.004)	2.9 (8.3)	8.8 (3.6)	-5.7 (6.0)	8.41	—	—
287	NGC 3680	-0.258 (0.026)	-0.856 (0.086)	0.272 (0.027)	-12.6 (5.8)	-3.1 (4.0)	10.1 (4.4)	9.09	-0.17	CC14
288	Ruprecht 94	-1.385 (0.139)	-3.103 (0.310)	-0.117 (0.013)	-27.7 (23.0)	-21.3 (10.9)	-20.6 (16.3)	7.19	—	—
291	Loden 402	-0.975 (0.098)	-2.248 (0.225)	0.030 (0.005)	-1.8 (16.8)	-16.8 (10.1)	-22.4 (12.0)	8.20	—	—
292	IC 2944	-0.743 (0.074)	-1.632 (0.163)	-0.041 (0.005)	-10.4 (12.5)	-7.6 (8.0)	-17.9 (8.9)	6.90	—	—
293	NGC 3766	-0.713 (0.071)	-1.593 (0.159)	-0.001 (0.002)	4.6 (11.9)	2.0 (5.6)	2.0 (8.3)	7.52	—	—
294	vdBergh-Hagen 121	-1.147 (0.115)	-2.482 (0.248)	-0.077 (0.009)	-14.8 (18.7)	-14.6 (9.3)	0.9 (13.0)	6.64	—	—
295	IC 2948	-1.098 (0.110)	-2.356 (0.236)	-0.078 (0.009)	-26.5 (17.8)	-13.0 (8.9)	-13.4 (12.5)	6.75	—	—
296	Stock 14	-0.914 (0.091)	-1.941 (0.194)	-0.025 (0.004)	-6.0 (14.7)	-2.6 (7.5)	4.4 (10.2)	7.00	—	—
298	Loden 481	-0.662 (0.066)	-1.368 (0.137)	0.020 (0.003)	-10.5 (12.3)	17.8 (14.5)	12.5 (7.2)	8.19	—	—
300	Ruprecht 98	-0.280 (0.028)	-0.542 (0.054)	-0.024 (0.003)	-12.5 (4.3)	15.3 (2.7)	-22.8 (4.2)	8.78	—	—
303	NGC 4103	-0.770 (0.077)	-1.475 (0.147)	0.034 (0.004)	-11.0 (12.1)	3.6 (9.1)	-6.9 (8.0)	7.59	—	—
304	ESO 130-06	-1.010 (0.101)	-1.951 (0.195)	0.119 (0.012)	34.2 (16.4)	-40.2 (9.3)	-18.2 (10.8)	8.33	-1.52	CC14
305	Loden 565	-0.302 (0.030)	-0.576 (0.058)	0.019 (0.002)	-22.0 (4.6)	-1.8 (2.6)	3.2 (3.1)	8.05	—	—
306	ESO 130-08	-0.372 (0.037)	-0.707 (0.071)	0.041 (0.004)	2.7 (6.3)	37.8 (6.4)	-1.3 (3.9)	9.02	-0.25	CC14
308	Melotte 111	0.007 (0.001)	-0.007 (0.001)	0.086 (0.009)	-8.0 (0.8)	5.7 (0.8)	5.2 (0.2)	8.78	—	—
309	NGC 4349	-1.079 (0.108)	-1.889 (0.189)	0.032 (0.004)	2.7 (15.5)	-10.8 (9.3)	3.8 (10.3)	8.32	-0.02	CC14
310	Collinder 258	-0.598 (0.060)	-1.037 (0.104)	0.041 (0.004)	7.0 (9.8)	1.3 (9.5)	-1.1 (5.7)	8.05	—	—
313	NGC 4463	-0.535 (0.053)	-0.903 (0.090)	-0.037 (0.004)	-7.4 (8.1)	23.7 (7.1)	7.3 (5.0)	7.97	—	—
315	NGC 4609	-0.646 (0.065)	-1.038 (0.104)	-0.003 (0.002)	-6.0 (9.7)	-34.8 (8.3)	-4.4 (5.9)	7.78	0.05	Cl89

Table B.2: continued

Seq	Name	X (eX) kpc	Y (eY) kpc	Z (eZ) kpc	U (eU) km/s	V (eV) km/s	W (eW) km/s	Age logt	Met dex	REF
317	Loden 694	-0.928 (0.093)	-1.423 (0.142)	0.063 (0.007)	6.1 (12.8)	2.6 (10.2)	14.8 (8.1)	7.38	—	—
318	NGC 4755	-1.081 (0.108)	-1.652 (0.165)	0.087 (0.009)	-10.4 (14.0)	4.5 (9.4)	-3.1 (9.4)	6.98	—	—
319	NGC 4852	-0.743 (0.074)	-1.100 (0.110)	0.076 (0.008)	-1.9 (9.8)	-8.4 (7.3)	13.7 (6.3)	8.63	—	—
320	NGC 5045	-0.870 (0.087)	-1.222 (0.122)	-0.016 (0.003)	1.9 (11.5)	-0.7 (9.7)	-3.6 (7.2)	7.11	—	—
322	Stock 16	-0.966 (0.097)	-1.325 (0.133)	0.006 (0.002)	-0.6 (12.7)	29.2 (11.1)	9.6 (7.8)	6.78	—	—
324	Loden 821	-1.684 (0.168)	-2.233 (0.223)	0.138 (0.014)	0.8 (21.1)	-28.1 (18.0)	26.3 (13.4)	7.29	-0.10	CC14
327	Basel 18	-1.345 (0.134)	-1.774 (0.177)	0.009 (0.003)	5.6 (15.8)	-11.1 (12.3)	-41.0 (11.6)	7.92	0.04	CC14
328	Hogg 16	-0.964 (0.096)	-1.258 (0.126)	0.037 (0.004)	2.6 (11.7)	11.5 (9.8)	0.7 (7.5)	7.26	—	—
333	Loden 915	-0.310 (0.031)	-0.391 (0.039)	0.028 (0.003)	8.4 (8.1)	16.7 (9.6)	12.0 (2.5)	8.44	—	—
334	Platais 10	-0.156 (0.016)	-0.190 (0.019)	0.013 (0.001)	17.8 (5.6)	-5.0 (6.2)	1.3 (1.4)	8.20	—	—
335	Loden 1010	-0.445 (0.045)	-0.540 (0.054)	0.024 (0.003)	7.4 (5.8)	9.8 (5.5)	13.1 (3.4)	8.69	—	—
336	NGC 5281	-0.699 (0.070)	-0.859 (0.086)	-0.014 (0.002)	-1.3 (11.3)	5.7 (12.0)	-1.4 (5.3)	7.76	—	—
337	Platais 12	-0.278 (0.028)	-0.335 (0.033)	-0.010 (0.001)	2.8 (3.5)	8.6 (3.2)	1.9 (2.1)	8.23	-0.01	CC14
338	NGC 5316	-0.785 (0.078)	-0.928 (0.093)	0.003 (0.002)	-18.6 (9.3)	-14.8 (8.6)	7.9 (5.8)	8.19	0.04	CC14
339	Loden 995	-1.525 (0.153)	-1.849 (0.185)	-0.121 (0.013)	-20.8 (16.6)	-15.2 (13.8)	6.6 (11.4)	8.34	-0.13	CC14
343	Ruprecht 110	-0.831 (0.083)	-0.992 (0.099)	-0.127 (0.013)	48.4 (10.4)	-12.7 (9.0)	5.7 (6.2)	8.74	-0.36	CC14
344	Loden 1194	-0.335 (0.034)	-0.370 (0.037)	0.016 (0.002)	-2.4 (4.4)	-6.9 (4.3)	6.8 (2.4)	8.53	—	—
345	NGC 5460	-0.470 (0.047)	-0.458 (0.046)	0.147 (0.015)	0.3 (4.9)	4.3 (5.0)	1.2 (3.2)	8.31	—	—
349	ESO 175-06	-0.386 (0.039)	-0.390 (0.039)	0.038 (0.004)	16.1 (3.7)	14.8 (3.7)	7.3 (2.6)	8.60	—	—
352	NGC 5606	-1.273 (0.127)	-1.280 (0.128)	0.032 (0.004)	15.9 (11.8)	2.4 (11.7)	-4.1 (8.6)	6.84	—	—
355	NGC 5662	-0.494 (0.049)	-0.462 (0.046)	0.040 (0.004)	11.6 (4.4)	8.0 (4.7)	-4.1 (3.4)	7.64	-0.03	Cl91
356	Alessi 6	-0.300 (0.030)	-0.315 (0.031)	-0.042 (0.004)	-19.1 (3.1)	-14.2 (2.9)	-1.8 (2.2)	8.30	-0.15	CC14
357	vdBergh-Hagen 164	-0.382 (0.038)	-0.392 (0.039)	-0.058 (0.006)	-9.2 (5.0)	-20.2 (4.9)	-13.1 (3.2)	7.14	—	—
360	NGC 5822	-0.717 (0.072)	-0.569 (0.057)	0.057 (0.006)	22.9 (5.5)	-2.5 (6.8)	0.6 (4.4)	8.83	—	—
361	NGC 5823	-0.927 (0.093)	-0.748 (0.075)	0.051 (0.005)	10.5 (7.0)	-8.3 (8.5)	6.8 (5.6)	8.90	—	—
366	NGC 6025	-0.623 (0.062)	-0.444 (0.044)	-0.079 (0.008)	-9.2 (7.2)	-1.2 (7.0)	9.6 (3.7)	7.96	0.19	G00
367	Nor OB5	-1.603 (0.160)	-0.817 (0.082)	0.058 (0.006)	1.1 (8.1)	-4.3 (12.8)	6.2 (8.5)	7.11	-2.06	CC14
369	NGC 6067	-1.223 (0.122)	-0.714 (0.071)	-0.054 (0.006)	17.2 (6.1)	9.9 (10.1)	8.1 (6.7)	8.01	0.14	T97
371	NGC 6087	-0.758 (0.076)	-0.479 (0.048)	-0.085 (0.009)	-7.9 (9.9)	6.6 (8.6)	4.3 (4.4)	7.93	-0.01	G00
374	NGC 6134	-0.827 (0.083)	-0.387 (0.039)	-0.003 (0.001)	10.9 (3.1)	5.9 (6.4)	-11.4 (4.7)	8.53	0.15	T97
377	NGC 6167	-1.006 (0.101)	-0.464 (0.046)	-0.027 (0.003)	15.7 (3.8)	12.3 (7.6)	-11.0 (5.6)	8.16	—	—
378	NGC 6178	-0.943 (0.094)	-0.373 (0.037)	0.022 (0.003)	-21.9 (3.4)	5.9 (6.7)	-3.3 (4.9)	7.51	—	—
379	NGC 6192	-1.459 (0.146)	-0.512 (0.051)	0.057 (0.006)	-18.2 (3.7)	16.4 (9.8)	-6.2 (7.5)	8.13	0.12	Pn03
380	NGC 6193	-1.060 (0.106)	-0.456 (0.046)	-0.032 (0.004)	23.9 (8.8)	5.8 (8.7)	-6.3 (5.7)	6.90	—	—
382	NGC 6204	-1.010 (0.101)	-0.397 (0.040)	-0.020 (0.002)	29.2 (6.2)	23.9 (7.4)	2.9 (5.2)	8.28	-1.05	CC14
383	Hogg 22	-1.207 (0.121)	-0.474 (0.047)	-0.026 (0.003)	41.2 (12.6)	9.4 (9.9)	-5.5 (6.3)	6.70	—	—

Table B.2: continued

Seq	Name	X (eX) kpc	Y (eY) kpc	Z (eZ) kpc	U (eU) km/s	V (eV) km/s	W (eW) km/s	Age logt	Met dex	REF
384	NGC 6208	-0.838 (0.084)	-0.413 (0.041)	-0.094 (0.010)	17.2 (3.4)	8.4 (6.6)	-0.9 (4.5)	9.07	-0.03	Pi95
385	NGC 6231	-1.198 (0.120)	-0.356 (0.036)	0.026 (0.003)	9.8 (3.8)	7.7 (7.7)	1.2 (6.0)	6.81	—	—
387	NGC 6242	-1.094 (0.109)	-0.283 (0.028)	0.049 (0.005)	-55.7 (38.3)	1.4 (11.9)	5.8 (5.6)	7.63	—	—
388	vdBergh-Hagen 205	-2.082 (0.208)	-0.574 (0.057)	0.061 (0.007)	-14.0 (3.9)	-5.6 (12.9)	8.6 (10.2)	7.12	—	—
390	NGC 6250	-0.816 (0.082)	-0.286 (0.029)	-0.029 (0.003)	0.4 (2.1)	12.2 (5.5)	-5.4 (4.3)	7.42	—	—
391	NGC 6268	-0.998 (0.100)	-0.248 (0.025)	0.024 (0.003)	-2.0 (1.6)	15.0 (5.9)	0.0 (4.9)	8.24	—	—
392	NGC 6281	-0.482 (0.048)	-0.105 (0.011)	0.017 (0.002)	5.1 (0.7)	3.5 (3.0)	7.0 (2.3)	8.51	0.00	Pi95
393	Sco OB4	-1.088 (0.109)	-0.145 (0.015)	0.066 (0.007)	5.9 (7.0)	4.8 (5.8)	-2.4 (5.3)	6.82	-0.09	CC14
394	Bochum 13	-1.064 (0.106)	-0.165 (0.017)	0.026 (0.003)	-9.2 (8.5)	5.2 (5.8)	4.9 (5.1)	7.08	—	—
395	NGC 6322	-0.961 (0.096)	-0.252 (0.025)	-0.053 (0.005)	40.1 (34.7)	21.7 (10.8)	-0.0 (5.2)	7.16	—	—
396	vdBergh-Hagen 221	-0.745 (0.074)	-0.079 (0.008)	0.039 (0.004)	-18.3 (3.8)	6.8 (3.8)	-6.9 (3.8)	8.01	—	—
397	IC 4651	-0.827 (0.083)	-0.300 (0.030)	-0.122 (0.012)	14.7 (2.3)	12.3 (5.7)	8.2 (4.2)	8.92	-0.13	CC14
399	Antalova 1	-0.847 (0.085)	-0.062 (0.006)	0.024 (0.003)	-5.6 (9.9)	-2.1 (4.4)	-0.4 (4.1)	8.50	-0.66	CC14
402	NGC 6383	-0.982 (0.098)	-0.074 (0.008)	0.001 (0.001)	-10.2 (4.9)	8.6 (4.8)	-3.3 (4.8)	6.71	—	—
403	Trumpler 27	-1.206 (0.121)	-0.104 (0.011)	-0.016 (0.002)	15.5 (8.9)	1.4 (6.1)	10.6 (5.7)	7.47	-0.19	CC14
404	Trumpler 28	-1.340 (0.134)	-0.093 (0.010)	-0.007 (0.002)	21.3 (11.9)	3.5 (6.6)	-4.1 (6.5)	6.89	0.33	CC14
405	ESO 139-13	-1.309 (0.131)	-0.639 (0.064)	-0.358 (0.036)	-2.8 (5.6)	30.5 (10.4)	20.0 (7.0)	8.78	-0.32	CC14
408	NGC 6405	-0.486 (0.049)	-0.029 (0.003)	-0.006 (0.001)	-2.1 (1.9)	-1.1 (2.7)	2.8 (2.4)	7.91	0.20	CC14
410	Alessi 9	-0.185 (0.019)	-0.053 (0.005)	-0.031 (0.003)	37.5 (27.5)	23.0 (7.9)	1.0 (4.9)	8.42	-0.58	CC14
411	NGC 6416	-0.740 (0.074)	-0.040 (0.004)	-0.020 (0.002)	0.6 (12.7)	10.1 (3.6)	10.3 (3.5)	8.78	-0.61	CC14
412	IC 4665	-0.290 (0.029)	0.171 (0.017)	0.103 (0.010)	-3.3 (2.2)	-2.6 (2.8)	-1.6 (1.7)	7.63	—	—
413	NGC 6425	-0.777 (0.078)	-0.028 (0.003)	-0.022 (0.002)	-15.7 (12.1)	28.1 (4.1)	-14.4 (4.3)	8.34	0.09	Pi95
414	Collinder 350	-0.242 (0.024)	0.122 (0.012)	0.071 (0.007)	6.3 (1.4)	2.9 (2.0)	6.8 (1.4)	8.61	—	—
418	Sco OB5	-3.262 (0.326)	-0.436 (0.044)	-0.357 (0.036)	-5.4 (7.1)	3.9 (16.9)	-40.3 (16.3)	6.86	—	—
420	NGC 6475	-0.298 (0.030)	-0.022 (0.002)	-0.023 (0.002)	5.5 (0.3)	8.3 (1.5)	1.2 (1.6)	8.22	—	—
422	NGC 6494	-0.618 (0.062)	0.108 (0.011)	0.031 (0.003)	1.5 (0.8)	7.6 (3.3)	3.3 (3.0)	8.52	—	—
423	Collinder 359	-0.542 (0.054)	0.310 (0.031)	0.140 (0.014)	-11.4 (2.9)	-10.2 (4.9)	-8.1 (3.2)	7.45	—	—
425	NGC 6514	-0.810 (0.081)	0.101 (0.010)	-0.004 (0.001)	-1.5 (3.7)	11.7 (4.2)	-3.6 (4.0)	7.28	—	—
426	NGC 6520	-1.573 (0.157)	0.079 (0.008)	-0.078 (0.008)	21.8 (1.1)	9.7 (7.6)	-20.7 (8.0)	7.75	—	—
427	NGC 6531	-1.194 (0.119)	0.161 (0.016)	-0.007 (0.002)	7.9 (5.2)	-4.3 (6.3)	-1.4 (5.8)	6.82	—	—
428	NGC 6530	-1.314 (0.131)	0.140 (0.014)	-0.030 (0.004)	-3.7 (7.2)	6.0 (6.6)	-9.2 (6.5)	6.67	—	—
429	NGC 6546	-0.930 (0.093)	0.119 (0.012)	-0.023 (0.003)	10.0 (15.7)	6.8 (5.2)	13.4 (4.5)	8.72	-0.33	CC14
430	vdBergh 113	-3.426 (0.343)	0.551 (0.055)	-0.047 (0.007)	-13.9 (6.6)	-28.2 (18.6)	-8.7 (16.5)	7.50	-0.36	CC14
432	Collinder 367	-1.190 (0.119)	0.152 (0.015)	-0.042 (0.005)	-2.6 (4.1)	2.8 (6.2)	-3.9 (5.8)	6.84	—	—
433	NGC 6561	-3.306 (0.331)	0.789 (0.079)	0.069 (0.008)	31.8 (5.4)	2.8 (19.4)	6.2 (16.1)	6.92	—	—
435	Sgr OB7	-1.827 (0.183)	0.345 (0.035)	-0.049 (0.006)	16.7 (7.4)	4.2 (10.1)	-11.0 (9.0)	6.64	-0.06	CC14

Table B.2: continued

Seq	Name	X (eX) kpc	Y (eY) kpc	Z (eZ) kpc	U (eU) km/s	V (eV) km/s	W (eW) km/s	Age logt	Met dex	REF
436	Markarian 38	-1.511 (0.151)	0.321 (0.032)	-0.026 (0.003)	-1.7 (9.2)	-10.4 (9.0)	11.4 (7.3)	6.95	0.18	CC14
438	Dias 5	-1.723 (0.172)	0.355 (0.036)	-0.053 (0.006)	6.9 (3.1)	12.9 (9.7)	-7.9 (8.5)	7.14	—	—
439	NGC 6604	-1.610 (0.161)	0.531 (0.053)	0.050 (0.006)	-17.1 (4.1)	-4.6 (10.7)	-0.4 (8.1)	6.64	—	—
441	NGC 6611	-1.644 (0.164)	0.501 (0.050)	0.024 (0.003)	-4.3 (3.7)	15.9 (10.5)	-5.7 (8.2)	6.72	—	—
442	Alessi 19	-0.409 (0.041)	0.347 (0.035)	0.120 (0.012)	-7.3 (3.4)	-4.5 (3.9)	-2.4 (2.6)	8.05	—	—
443	NGC 6613	-1.256 (0.126)	0.317 (0.032)	-0.023 (0.003)	10.3 (4.8)	-3.5 (7.6)	7.1 (6.1)	7.52	—	—
444	NGC 6618	-1.752 (0.175)	0.471 (0.047)	-0.022 (0.003)	32.0 (18.7)	16.9 (11.9)	-14.1 (8.9)	6.78	0.13	CC14
445	Trumpler 33	-1.711 (0.171)	0.376 (0.038)	-0.099 (0.010)	2.2 (8.0)	-16.4 (10.2)	39.2 (8.9)	7.84	-1.54	CC14
446	NGC 6633	-0.308 (0.031)	0.224 (0.022)	0.056 (0.006)	18.0 (2.0)	-7.9 (2.7)	0.4 (1.8)	8.76	—	—
447	NGC 6639	-0.662 (0.066)	0.227 (0.023)	-0.018 (0.002)	-9.9 (2.4)	12.3 (4.5)	-1.9 (3.4)	8.86	—	—
448	Ruprecht 141	-5.177 (0.518)	1.853 (0.185)	-0.115 (0.014)	-5.0 (13.6)	-37.6 (35.4)	-37.7 (26.5)	6.92	—	—
449	IC 4725	-0.601 (0.060)	0.146 (0.015)	-0.048 (0.005)	-19.8 (10.1)	-2.6 (4.6)	7.2 (3.0)	7.83	-0.26	CC14
450	IC 4756	-0.388 (0.039)	0.286 (0.029)	0.044 (0.004)	13.6 (2.6)	-11.1 (3.4)	2.5 (2.3)	8.79	—	—
451	NGC 6694	-1.445 (0.144)	0.640 (0.064)	-0.080 (0.008)	-6.9 (8.4)	-14.0 (11.3)	10.7 (7.5)	8.30	—	—
452	Ruprecht 145	-0.731 (0.073)	0.217 (0.022)	-0.107 (0.011)	7.0 (1.9)	3.0 (4.7)	-18.8 (4.6)	8.64	-0.13	CC14
453	NGC 6705	-1.666 (0.167)	0.860 (0.086)	-0.091 (0.009)	-29.9 (7.3)	-1.7 (13.2)	56.3 (10.2)	8.07	—	—
454	NGC 6709	-0.795 (0.079)	0.719 (0.072)	0.088 (0.009)	8.1 (7.5)	-0.9 (8.0)	-14.3 (5.5)	8.14	—	—
455	Collinder 394	-0.671 (0.067)	0.178 (0.018)	-0.113 (0.011)	-8.8 (6.3)	-12.1 (5.0)	8.3 (3.5)	7.86	—	—
456	Stephenson 1	-0.142 (0.014)	0.331 (0.033)	0.099 (0.010)	6.7 (3.5)	-12.8 (5.8)	-5.6 (2.4)	7.69	—	—
457	NGC 6716	-0.750 (0.075)	0.206 (0.021)	-0.131 (0.013)	-13.7 (7.2)	-4.1 (5.3)	5.4 (3.9)	7.47	-0.31	Cm85
459	NGC 6738	-0.499 (0.050)	0.489 (0.049)	0.038 (0.004)	38.7 (4.8)	-2.5 (4.9)	-4.3 (3.4)	9.16	—	—
460	Ruprecht 147	-0.159 (0.016)	0.061 (0.006)	-0.039 (0.004)	-50.7 (3.5)	5.6 (2.6)	-10.5 (1.5)	9.39	—	—
464	NGC 6811	-0.227 (0.023)	1.191 (0.119)	0.258 (0.026)	-28.9 (7.0)	7.1 (1.9)	14.7 (5.8)	8.76	—	—
465	NGC 6823	-0.964 (0.096)	1.629 (0.163)	-0.005 (0.003)	-18.2 (13.7)	-1.5 (9.4)	6.6 (9.0)	7.01	—	—
466	Turner 9	-0.363 (0.036)	0.770 (0.077)	0.037 (0.004)	9.2 (6.4)	-9.8 (6.3)	-3.5 (4.2)	8.06	—	—
468	Roslund 2	-0.994 (0.099)	1.735 (0.174)	-0.010 (0.003)	2.7 (14.4)	-15.4 (9.8)	2.6 (9.5)	6.89	—	—
469	NGC 6828	-0.405 (0.041)	0.432 (0.043)	-0.097 (0.010)	10.4 (4.0)	-9.9 (3.7)	10.7 (2.8)	8.56	—	—
470	NGC 6830	-0.816 (0.082)	1.421 (0.142)	-0.051 (0.006)	29.4 (11.7)	-25.4 (7.0)	-1.6 (7.8)	7.52	—	—
471	Roslund 3	-0.782 (0.078)	1.292 (0.129)	-0.124 (0.013)	4.8 (10.7)	-6.2 (6.7)	-1.5 (7.2)	7.61	—	—
476	NGC 6871	-0.469 (0.047)	1.501 (0.150)	0.057 (0.006)	-22.2 (9.9)	-16.5 (4.0)	0.5 (7.5)	6.99	—	—
477	Biurakan 1	-0.475 (0.047)	1.527 (0.153)	0.049 (0.005)	-16.9 (9.9)	-12.4 (4.1)	3.4 (7.6)	7.25	—	—
478	Biurakan 2	-0.328 (0.033)	1.056 (0.106)	0.026 (0.003)	-10.0 (7.4)	-20.8 (9.3)	4.7 (5.2)	7.14	—	—
479	Roslund 5	-0.133 (0.013)	0.396 (0.040)	0.002 (0.001)	7.4 (2.9)	-7.6 (2.6)	0.2 (2.1)	7.77	—	—
480	NGC 6883	-0.397 (0.040)	1.321 (0.132)	0.028 (0.003)	-17.6 (8.6)	-12.9 (5.0)	3.9 (6.5)	7.53	—	—
482	NGC 6882	-0.140 (0.014)	0.311 (0.031)	-0.023 (0.002)	-4.6 (2.7)	-10.3 (3.3)	-1.9 (1.9)	8.16	-0.02	L94
483	IC 4996	-0.438 (0.044)	1.675 (0.168)	0.040 (0.005)	-4.0 (10.1)	-11.7 (3.3)	-6.1 (8.3)	6.80	—	—

Table B.2: continued

Seq	Name	X (eX) kpc	Y (eY) kpc	Z (eZ) kpc	U (eU) km/s	V (eV) km/s	W (eW) km/s	Age logt	Met dex	REF
484	Collinder 419	-0.153 (0.015)	0.723 (0.072)	0.036 (0.004)	-12.7 (4.1)	-1.4 (1.0)	0.3 (3.6)	6.85	—	—
485	Berkeley 86	-0.257 (0.026)	1.082 (0.108)	0.025 (0.003)	-6.2 (6.6)	-15.0 (7.8)	24.1 (5.6)	6.96	—	—
486	NGC 6910	-0.223 (0.022)	1.116 (0.112)	0.040 (0.004)	-5.5 (6.3)	-27.2 (2.5)	7.8 (5.4)	7.33	—	—
488	NGC 6913	-0.260 (0.026)	1.118 (0.112)	0.012 (0.002)	-11.2 (6.5)	-13.4 (1.8)	6.0 (5.4)	7.12	—	—
490	Cyg OB2	-0.255 (0.026)	1.478 (0.148)	0.021 (0.003)	2.7 (8.5)	-21.7 (17.8)	-4.1 (7.2)	6.72	—	—
491	NGC 6940	-0.263 (0.026)	0.717 (0.072)	-0.096 (0.010)	-19.3 (5.1)	6.8 (2.0)	-7.5 (3.9)	8.94	0.01	T97
492	Alessi 12	-0.202 (0.020)	0.486 (0.049)	-0.107 (0.011)	11.6 (3.9)	-16.0 (3.8)	-1.0 (3.0)	7.90	—	—
493	Roslund 7	-0.124 (0.012)	0.687 (0.069)	-0.052 (0.005)	17.0 (4.4)	-9.4 (3.1)	6.9 (3.3)	8.67	—	—
494	NGC 6991	-0.032 (0.003)	0.699 (0.070)	0.020 (0.002)	48.5 (6.7)	7.6 (3.7)	9.0 (3.3)	9.11	—	—
495	NGC 7039	-0.035 (0.004)	0.950 (0.095)	-0.028 (0.003)	-3.5 (4.6)	-0.8 (0.6)	-1.3 (4.6)	8.83	—	—
498	NGC 7082	0.029 (0.004)	1.440 (0.144)	-0.072 (0.007)	5.5 (7.0)	0.8 (3.4)	-2.5 (6.9)	7.91	-0.01	G00
499	NGC 7092	0.013 (0.001)	0.310 (0.031)	-0.012 (0.001)	-30.1 (2.5)	7.2 (0.4)	-6.4 (2.0)	8.57	0.01	Pa86
500	IC 1396	0.134 (0.013)	0.822 (0.082)	0.054 (0.006)	-6.0 (4.4)	1.5 (2.3)	0.3 (4.0)	6.69	—	—
501	NGC 7160	0.191 (0.019)	0.766 (0.077)	0.089 (0.009)	-5.8 (4.7)	-4.5 (2.3)	7.4 (3.8)	7.66	—	—
502	NGC 7209	0.111 (0.011)	1.152 (0.115)	-0.149 (0.015)	37.9 (7.5)	0.8 (1.1)	7.0 (5.5)	8.65	-0.12	Pi95
503	NGC 7235	0.621 (0.062)	2.754 (0.275)	0.038 (0.005)	14.9 (16.2)	-30.6 (4.0)	6.4 (13.4)	6.76	—	—
504	NGC 7243	0.124 (0.012)	0.795 (0.079)	-0.078 (0.008)	7.1 (4.6)	-0.5 (2.6)	0.7 (3.9)	8.09	—	—
505	IC 1442	0.462 (0.046)	2.298 (0.230)	-0.090 (0.010)	19.8 (—)	-6.7 (—)	-1.0 (—)	7.71	—	—
506	Pismis-Moreno 1	0.258 (0.026)	0.858 (0.086)	0.083 (0.008)	7.8 (5.9)	-9.8 (1.9)	3.6 (4.3)	7.55	—	—
508	NGC 7380	0.653 (0.065)	2.124 (0.212)	-0.034 (0.005)	3.7 (13.8)	-8.9 (7.4)	6.8 (10.5)	6.72	—	—
509	NGC 7438	0.172 (0.017)	0.573 (0.057)	-0.051 (0.005)	3.8 (4.1)	-5.2 (3.8)	3.4 (2.9)	8.93	—	—
510	Cep OB3	0.253 (0.025)	0.651 (0.065)	0.036 (0.004)	-6.3 (4.9)	-6.3 (4.1)	2.3 (3.3)	7.44	—	—
512	NGC 7654	0.551 (0.055)	1.310 (0.131)	0.011 (0.002)	-3.4 (9.8)	-18.0 (6.7)	-2.9 (6.8)	7.84	—	—
513	Czernik 43	0.970 (0.097)	2.304 (0.230)	0.006 (0.004)	-4.9 (16.8)	-24.7 (7.9)	-6.9 (11.9)	7.70	—	—
516	King 12	1.047 (0.105)	2.135 (0.214)	-0.005 (0.003)	-5.8 (16.7)	-1.9 (10.4)	2.6 (11.3)	7.12	—	—
517	NGC 7788	1.057 (0.106)	2.126 (0.213)	-0.032 (0.005)	36.1 (17.2)	-7.3 (9.9)	-19.5 (11.6)	7.48	—	—
518	NGC 7789	1.002 (0.100)	2.100 (0.210)	-0.219 (0.022)	48.9 (17.7)	-58.9 (8.9)	-2.5 (11.1)	9.23	—	—
519	Frolov 1	1.145 (0.115)	2.290 (0.229)	-0.025 (0.004)	-4.9 (17.8)	61.2 (9.6)	5.6 (12.1)	7.66	—	—
520	NGC 7790	1.317 (0.132)	2.632 (0.263)	-0.052 (0.007)	-2.6 (20.6)	-43.3 (10.8)	-5.1 (14.0)	7.91	—	—
1001	ASCC 1	1.887 (0.189)	3.527 (0.353)	0.013 (0.006)	21.7 (28.4)	-29.1 (16.2)	22.1 (19.0)	8.25	—	—
1003	ASCC 3	0.843 (0.084)	1.459 (0.146)	-0.221 (0.022)	-2.0 (12.7)	-11.6 (9.7)	0.5 (8.1)	7.90	—	—
1004	ASCC 4	0.410 (0.041)	0.628 (0.063)	-0.017 (0.002)	3.1 (7.5)	4.4 (8.6)	1.9 (3.6)	8.34	—	—
1005	ASCC 5	0.829 (0.083)	1.236 (0.124)	-0.183 (0.018)	-18.3 (10.9)	-12.6 (7.9)	-11.1 (7.4)	7.03	—	—
1006	ASCC 6	0.775 (0.077)	0.912 (0.091)	-0.091 (0.009)	-0.8 (9.6)	0.1 (9.1)	-0.4 (5.8)	8.17	—	—
1007	ASCC 7	1.325 (0.132)	1.495 (0.150)	-0.097 (0.010)	0.1 (15.4)	-25.4 (14.6)	-21.4 (9.9)	7.36	—	—
1008	ASCC 8	1.528 (0.153)	1.582 (0.158)	-0.051 (0.006)	-5.4 (14.4)	-6.2 (13.9)	8.7 (10.4)	6.76	—	—

Table B.2: continued

Seq	Name	X (eX) kpc	Y (eY) kpc	Z (eZ) kpc	U (eU) km/s	V (eV) km/s	W (eW) km/s	Age logt	Met dex	REF
1009	ASCC 9	2.150 (0.215)	1.944 (0.194)	-0.089 (0.010)	31.3 (18.1)	-33.3 (20.0)	-25.9 (14.1)	6.79	—	—
1011	ASCC 11	0.559 (0.056)	0.315 (0.032)	-0.104 (0.010)	2.8 (5.6)	3.9 (5.5)	-6.3 (3.4)	8.61	—	—
1013	ASCC 13	0.765 (0.077)	0.228 (0.023)	0.045 (0.005)	-13.7 (8.3)	6.3 (5.4)	0.9 (3.9)	7.71	—	—
1014	ASCC 14	1.089 (0.109)	0.156 (0.016)	-0.020 (0.002)	-19.0 (1.0)	-11.6 (6.1)	-14.3 (5.6)	8.61	—	—
1016	ASCC 16	0.408 (0.041)	-0.156 (0.016)	-0.145 (0.014)	3.3 (8.6)	4.7 (4.4)	3.7 (3.7)	6.93	—	—
1017	ASCC 17	1.994 (0.199)	0.120 (0.012)	-0.107 (0.011)	-19.9 (6.2)	-43.3 (11.1)	-15.5 (9.8)	7.12	—	—
1018	ASCC 18	0.439 (0.044)	-0.178 (0.018)	-0.159 (0.016)	7.2 (9.4)	2.6 (5.0)	2.8 (4.0)	7.12	—	—
1019	ASCC 19	0.299 (0.030)	-0.139 (0.014)	-0.117 (0.012)	3.1 (3.0)	3.0 (2.7)	2.2 (1.9)	7.64	—	—
1020	ASCC 20	0.399 (0.040)	-0.158 (0.016)	-0.136 (0.014)	7.0 (4.5)	5.3 (3.4)	2.0 (2.5)	7.35	—	—
1021	ASCC 21	0.451 (0.045)	-0.163 (0.016)	-0.142 (0.014)	3.3 (1.7)	4.3 (3.2)	3.2 (2.3)	7.11	—	—
1024	ASCC 24	0.318 (0.032)	-0.236 (0.024)	-0.057 (0.006)	-5.8 (3.4)	2.0 (3.5)	-7.0 (2.3)	6.96	—	—
1025	ASCC 25	1.358 (0.136)	-0.244 (0.024)	0.236 (0.024)	1.4 (3.0)	-11.8 (7.8)	6.1 (6.6)	8.86	—	—
1026	ASCC 26	0.716 (0.072)	-0.355 (0.035)	0.043 (0.004)	-9.9 (7.2)	12.4 (6.4)	-4.0 (4.0)	8.09	—	—
1028	ASCC 28	0.668 (0.067)	-0.440 (0.044)	0.007 (0.001)	-3.0 (4.1)	-0.3 (5.8)	-0.3 (3.9)	8.34	—	—
1029	ASCC 29	0.616 (0.062)	-0.427 (0.043)	-0.002 (0.001)	-10.3 (9.0)	4.9 (7.8)	5.1 (3.6)	8.06	—	—
1033	ASCC 33	0.434 (0.043)	-0.661 (0.066)	-0.121 (0.012)	-4.3 (7.5)	11.7 (8.4)	0.0 (4.0)	7.26	-0.17	CC14
1043	ASCC 43	0.427 (0.043)	-0.904 (0.090)	-0.007 (0.002)	15.7 (7.0)	-63.8 (4.2)	-10.1 (5.0)	8.28	—	—
1044	Alessi 34	0.096 (0.010)	-1.077 (0.108)	-0.200 (0.020)	4.6 (5.6)	0.3 (2.9)	-4.1 (5.2)	7.89	—	—
1045	ASCC 45	0.846 (0.085)	-2.878 (0.288)	-0.016 (0.004)	2.7 (18.2)	-4.6 (8.2)	-34.7 (14.8)	7.12	—	—
1047	Alessi-Teutsch 7	0.183 (0.018)	-0.881 (0.088)	0.005 (0.001)	8.2 (5.4)	9.5 (7.3)	-10.4 (4.6)	7.88	—	—
1048	ASCC 48	0.087 (0.009)	-0.390 (0.039)	0.011 (0.001)	13.5 (2.9)	-3.6 (0.7)	2.2 (2.0)	9.09	—	—
1050	Alessi 43	0.111 (0.011)	-0.842 (0.084)	0.022 (0.002)	-2.3 (4.5)	-1.5 (8.6)	-2.5 (4.2)	7.48	—	—
1052	ASCC 52	-0.156 (0.016)	-1.491 (0.149)	-0.063 (0.007)	0.5 (7.5)	-7.8 (1.0)	6.4 (7.1)	8.75	—	—
1057	ASCC 57	-0.458 (0.046)	-1.411 (0.141)	-0.224 (0.022)	-14.6 (9.6)	-2.3 (7.7)	5.4 (7.1)	8.70	-0.30	CC14
1058	ASCC 58	-0.122 (0.012)	-0.587 (0.059)	0.014 (0.002)	7.4 (3.9)	-3.6 (3.7)	-5.7 (3.1)	7.04	—	—
1060	ASCC 60	-0.216 (0.022)	-0.770 (0.077)	-0.004 (0.001)	0.8 (5.2)	17.8 (7.3)	0.9 (3.8)	8.36	—	—
1062	ASCC 62	-0.948 (0.095)	-2.846 (0.285)	-0.035 (0.005)	27.7 (19.3)	-27.7 (7.3)	-27.1 (14.6)	7.50	—	—
1063	ASCC 63	-1.146 (0.115)	-3.307 (0.331)	-0.041 (0.006)	37.6 (22.2)	112.8 (8.2)	-5.6 (16.6)	7.24	—	—
1064	ASCC 64	-0.516 (0.052)	-1.408 (0.141)	-0.020 (0.003)	-5.5 (10.2)	4.5 (9.9)	-0.5 (7.2)	7.92	—	—
1065	ASCC 65	-1.260 (0.126)	-3.265 (0.327)	-0.035 (0.006)	8.8 (23.0)	-17.0 (10.0)	-22.2 (16.8)	7.09	—	—
1067	ASCC 67	-0.623 (0.062)	-1.364 (0.136)	0.019 (0.003)	-17.3 (10.7)	19.5 (8.3)	-5.1 (7.2)	7.67	—	—
1069	ASCC 69	-0.482 (0.048)	-0.867 (0.087)	-0.126 (0.013)	-3.6 (8.9)	-6.2 (10.4)	-3.7 (5.0)	7.91	—	—
1070	ASCC 70	-1.309 (0.131)	-2.360 (0.236)	-0.086 (0.009)	-8.2 (19.0)	-14.5 (11.0)	-7.6 (12.9)	6.92	—	—
1071	ASCC 71	-0.648 (0.065)	-1.122 (0.112)	-0.109 (0.011)	9.6 (9.6)	3.4 (6.7)	-0.2 (6.2)	7.88	—	—
1073	ASCC 73	-0.338 (0.034)	-0.553 (0.055)	-0.051 (0.005)	14.4 (5.1)	6.4 (3.6)	3.0 (3.1)	8.19	—	—
1075	ASCC 75	-1.901 (0.190)	-2.321 (0.232)	-0.013 (0.004)	-17.6 (20.9)	-17.1 (17.4)	-0.9 (14.2)	6.65	—	—

Table B.2: continued

Seq	Name	X (eX) kpc	Y (eY) kpc	Z (eZ) kpc	U (eU) km/s	V (eV) km/s	W (eW) km/s	Age logt	Met dex	REF
1076	ASCC 76	-0.376 (0.038)	-0.465 (0.047)	-0.044 (0.005)	0.4 (6.3)	17.7 (6.8)	1.5 (3.0)	7.45	—	—
1078	ASCC 78	-1.671 (0.167)	-1.685 (0.168)	-0.361 (0.036)	16.6 (16.7)	-39.2 (16.6)	20.4 (11.4)	8.48	-0.06	CC14
1079	ASCC 79	-0.612 (0.061)	-0.513 (0.051)	-0.040 (0.004)	-15.9 (5.1)	-4.6 (5.8)	-1.3 (3.9)	6.86	—	—
1080	ASCC 80	-1.163 (0.116)	-0.945 (0.094)	-0.071 (0.007)	4.5 (17.7)	1.7 (16.4)	-7.0 (7.3)	7.93	—	—
1084	ASCC 84	-0.721 (0.072)	-0.532 (0.053)	-0.085 (0.009)	-7.9 (4.8)	-0.9 (6.4)	-4.6 (4.4)	7.68	—	—
1085	ASCC 85	-1.127 (0.113)	-0.413 (0.041)	-0.004 (0.002)	-24.7 (8.6)	-11.5 (8.4)	-5.7 (5.8)	7.42	—	—
1086	Alessi-Teutsch 12	-0.600 (0.060)	-0.338 (0.034)	-0.126 (0.013)	0.8 (4.5)	-9.3 (5.6)	0.4 (3.4)	7.07	—	—
1088	ASCC 88	-1.868 (0.187)	-0.333 (0.033)	0.102 (0.011)	-22.2 (2.7)	9.6 (10.2)	-23.8 (9.5)	7.17	—	—
1089	Alessi 24	-0.415 (0.042)	-0.249 (0.025)	-0.126 (0.013)	26.3 (16.2)	19.3 (10.3)	2.7 (5.5)	7.03	-0.13	CC14
1091	ASCC 91	-0.791 (0.079)	-0.095 (0.010)	-0.069 (0.007)	5.1 (1.2)	1.1 (4.2)	-8.7 (4.1)	8.65	-0.04	CC14
1093	ASCC 93	-2.473 (0.247)	0.362 (0.036)	-0.045 (0.006)	20.6 (4.1)	-26.3 (13.3)	20.0 (11.9)	7.22	—	—
1094	ASCC 94	-0.819 (0.082)	0.228 (0.023)	0.014 (0.002)	22.0 (3.9)	4.1 (5.1)	5.2 (4.0)	8.78	—	—
1096	Ferrero 1	-0.742 (0.074)	0.008 (0.001)	-0.106 (0.011)	25.7 (7.3)	-6.6 (4.0)	8.7 (3.7)	8.27	—	—
1097	Alessi 40	-0.772 (0.077)	0.195 (0.020)	-0.078 (0.008)	6.0 (5.2)	-17.1 (5.3)	5.8 (3.8)	7.88	0.13	CC14
1098	ASCC 98	-0.779 (0.078)	0.021 (0.002)	-0.179 (0.018)	45.6 (7.3)	-7.9 (4.2)	9.2 (4.2)	8.33	—	—
1099	ASCC 99	-0.267 (0.027)	0.076 (0.008)	-0.039 (0.004)	24.0 (0.7)	3.6 (1.7)	2.2 (1.6)	8.71	—	—
1100	ASCC 100	-0.148 (0.015)	0.308 (0.031)	0.077 (0.008)	7.8 (2.6)	-7.8 (2.0)	-3.1 (1.7)	8.01	—	—
1101	ASCC 101	-0.128 (0.013)	0.318 (0.032)	0.070 (0.007)	14.4 (2.7)	-16.0 (2.2)	0.2 (1.7)	8.52	—	—
1104	ASCC 104	-0.460 (0.046)	0.654 (0.065)	-0.022 (0.002)	-0.2 (5.7)	-3.3 (4.2)	-0.7 (3.9)	7.71	—	—
1105	ASCC 105	-0.229 (0.023)	0.444 (0.044)	0.019 (0.002)	3.1 (3.6)	-3.6 (2.5)	0.2 (2.5)	8.00	—	—
1106	Alessi 44	-0.374 (0.037)	0.318 (0.032)	-0.093 (0.009)	41.5 (3.0)	-33.6 (3.4)	19.5 (2.3)	8.42	—	—
1107	ASCC 107	-0.362 (0.036)	0.599 (0.060)	-0.023 (0.003)	1.1 (5.3)	-0.8 (4.4)	-2.3 (3.5)	8.41	—	—
1110	ASCC 110	-0.268 (0.027)	0.754 (0.075)	0.020 (0.002)	5.8 (6.3)	-11.9 (10.5)	-4.3 (4.0)	8.75	—	—
1111	ASCC 111	-0.424 (0.042)	1.542 (0.154)	0.058 (0.006)	11.0 (9.7)	-9.0 (7.4)	-7.1 (7.7)	7.05	—	—
1114	ASCC 114	0.068 (0.007)	0.546 (0.055)	0.010 (0.001)	-9.9 (2.9)	-8.2 (4.9)	6.5 (2.6)	7.75	—	—
1115	ASCC 115	0.078 (0.008)	0.594 (0.059)	-0.027 (0.003)	3.8 (3.4)	3.2 (5.8)	4.4 (2.9)	8.59	—	—
1116	ASCC 116	0.824 (0.083)	4.931 (0.493)	-0.028 (0.007)	-11.4 (26.4)	4.9 (6.2)	-31.2 (24.0)	7.03	—	—
1117	ASCC 117	0.306 (0.031)	1.155 (0.115)	0.113 (0.011)	9.2 (7.3)	3.3 (2.4)	14.9 (5.7)	6.67	—	—
1118	Alessi-Teutsch 5	0.224 (0.022)	0.869 (0.087)	0.066 (0.007)	-12.9 (5.9)	-23.3 (10.4)	-3.9 (4.4)	7.02	—	—
1120	ASCC 120	0.636 (0.064)	2.418 (0.242)	-0.026 (0.004)	3.1 (14.8)	-35.8 (4.6)	10.1 (11.9)	7.08	—	—
1121	ASCC 121	0.586 (0.059)	2.428 (0.243)	-0.113 (0.012)	13.6 (14.8)	-42.4 (8.2)	17.4 (11.9)	7.73	—	—
1122	ASCC 122	0.069 (0.007)	0.670 (0.067)	-0.192 (0.019)	0.7 (3.7)	3.8 (3.6)	-2.6 (3.5)	6.98	—	—
1123	ASCC 123	0.063 (0.006)	0.241 (0.024)	-0.017 (0.002)	7.4 (2.9)	2.0 (6.3)	-0.6 (1.5)	8.41	—	—
1125	ASCC 125	0.517 (0.052)	1.406 (0.141)	0.072 (0.008)	0.1 (9.8)	5.1 (4.9)	-8.3 (7.3)	7.01	—	—
1126	ASCC 126	0.226 (0.023)	0.758 (0.076)	-0.118 (0.012)	1.1 (5.0)	0.7 (2.4)	-1.2 (3.9)	7.26	—	—
1127	ASCC 127	0.132 (0.013)	0.323 (0.032)	0.025 (0.003)	4.4 (2.9)	0.1 (2.3)	-1.1 (1.8)	7.82	—	—

Abbreviated literature references in Tab. B.2:

- A02: Ann et al. (2002)
- Cm85: Cameron (1985)
- Cl89: Clariá et al. (1989)
- Cl91: Clariá et al. (1991)
- Cl96: Clariá et al. (1996)
- Cl03A: Clariá et al. (2003a)
- Cl03B: Clariá et al. (2003b)
- CC14: Conrad et al. (2014)
- G00: Gratton (2000)
- Go00: Gonzalez & Wallerstein (2000)
- L94: Luck (1994)
- Ly81: Lynga (1981)
- Ly84: Lynga & Wramdemark (1984)
- N80: Nissen (1980)
- Pa86: Palous & Hauck (1986)
- Pr05: Parisi et al. (2005)
- Pn03: Paunzen et al. (2003)
- Pi95: Piatti et al. (1995)
- T97: Twarog et al. (1997)

Appendix C

Additional information on the found OC groupings

Section C.1

For linking lengths 100 pc and 10 km/s

In Sect. 4.4 I summarised the characteristics of the identified OC gropings in the COCD working sample using the first set of linking lengths (100 pc and 10 km/s) and listed those in Tab. 4.1 and 4.2. Although not all groupings were genuine, especially the pairs, the larger groups and complexes were most likely real. Each OC grouping covered a rather narrow volume in coordinate and velocity space and, in particular the complex was indicated to originate from the same star forming region. For a general overview I again display the distribution of all detected OC groupings using the first set of linking lengths in Fig. C.1, as already shown in Sect. 4.2.

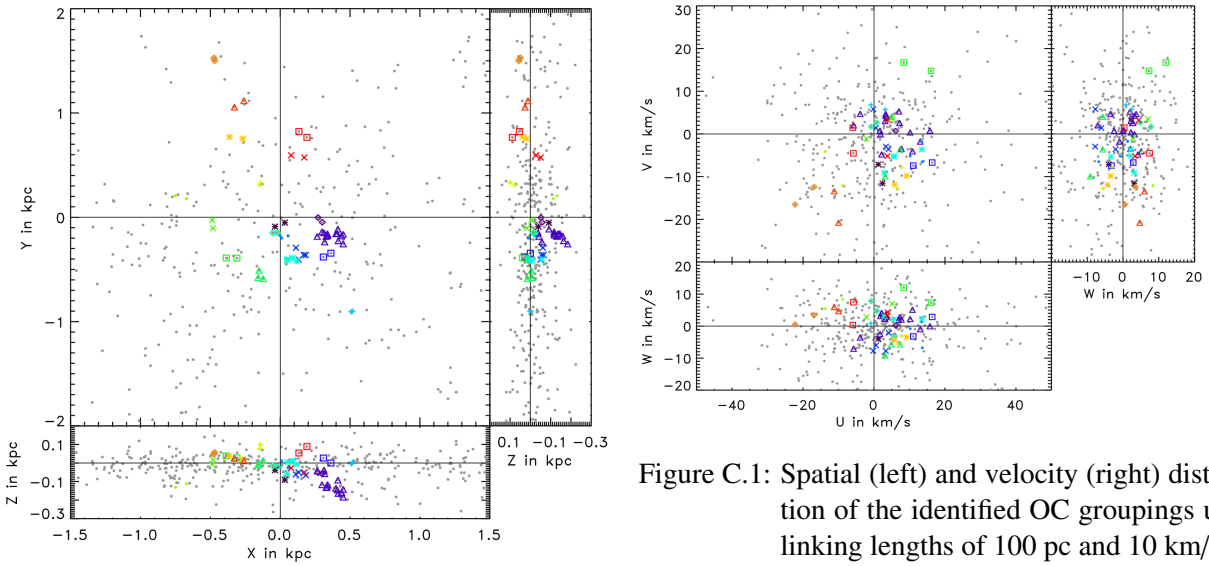

Figure C.1: Spatial (left) and velocity (right) distribution of the identified OC groupings using linking lengths of 100 pc and 10 km/s.

In the following figures (Fig. C.2-C.20) I illustrate the various parameter distributions for each detected grouping to visualise the numbers listed in Tab. 4.2. For each grouping the panels a)-c) show the spatial distribution of the members in the XY-, XZ- and YZ-planes, while panels d)-f) illustrate the distribution for each grouping in velocity space projected onto the UV-, UW- and VW-planes. The spread in age and metallicity are presented in the panels g) and h), respectively. Since $[M/H]$ information were only available for about a quarter of the clusters in the working sample, for the majority of grouping members $[M/H]$ data were missing and, because of this, the corresponding panel in the Fig. C.2-C.20 either harbour fewer data points or are empty.

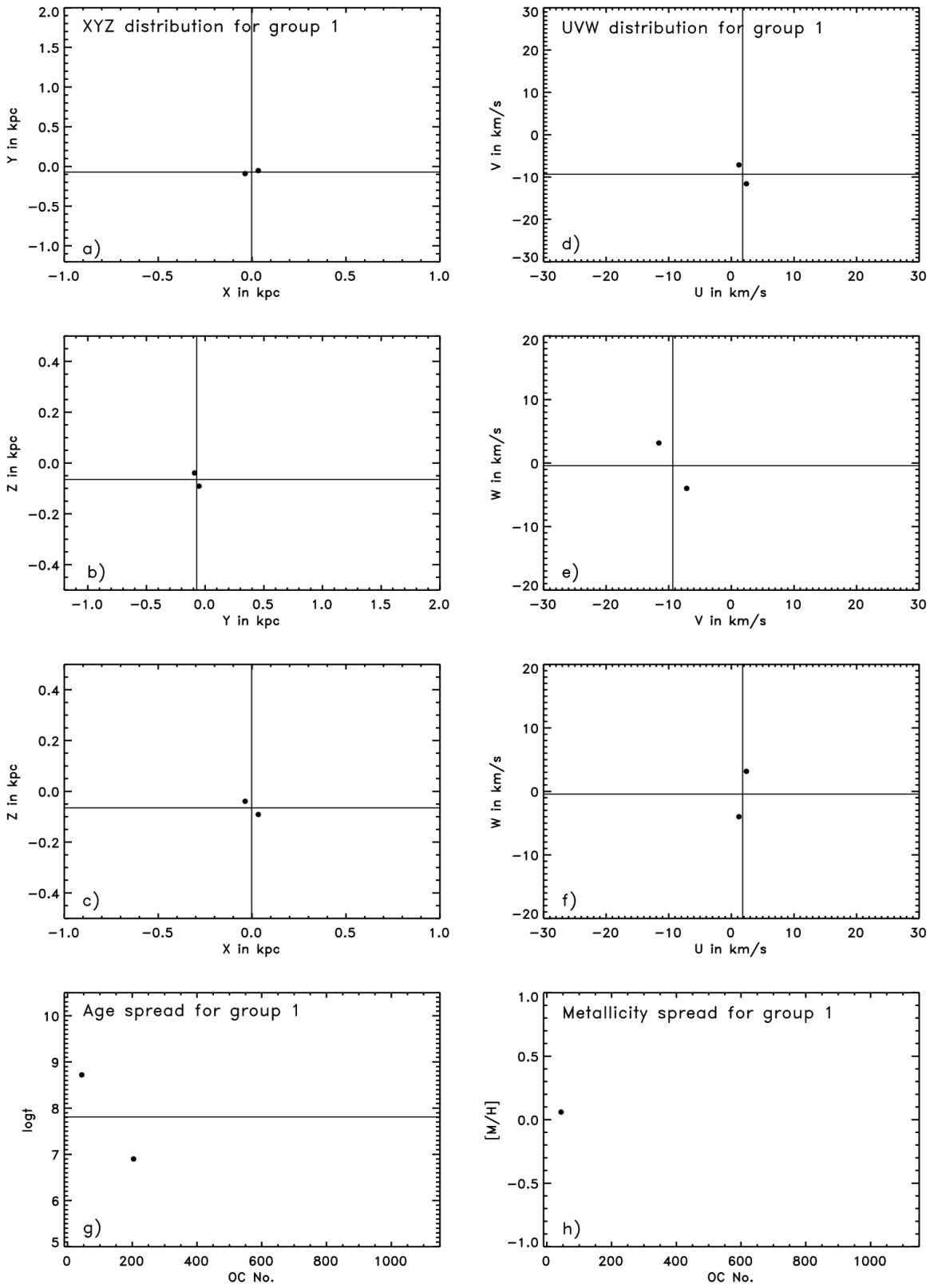

Figure C.2: Parameter distributions for the members of the open cluster grouping No. 1. a-c) spatial distribution; d-f) velocity distribution; g) age spread; h) metallicity spread. The solid lines show the corresponding averaged values for the open cluster grouping No. 1.

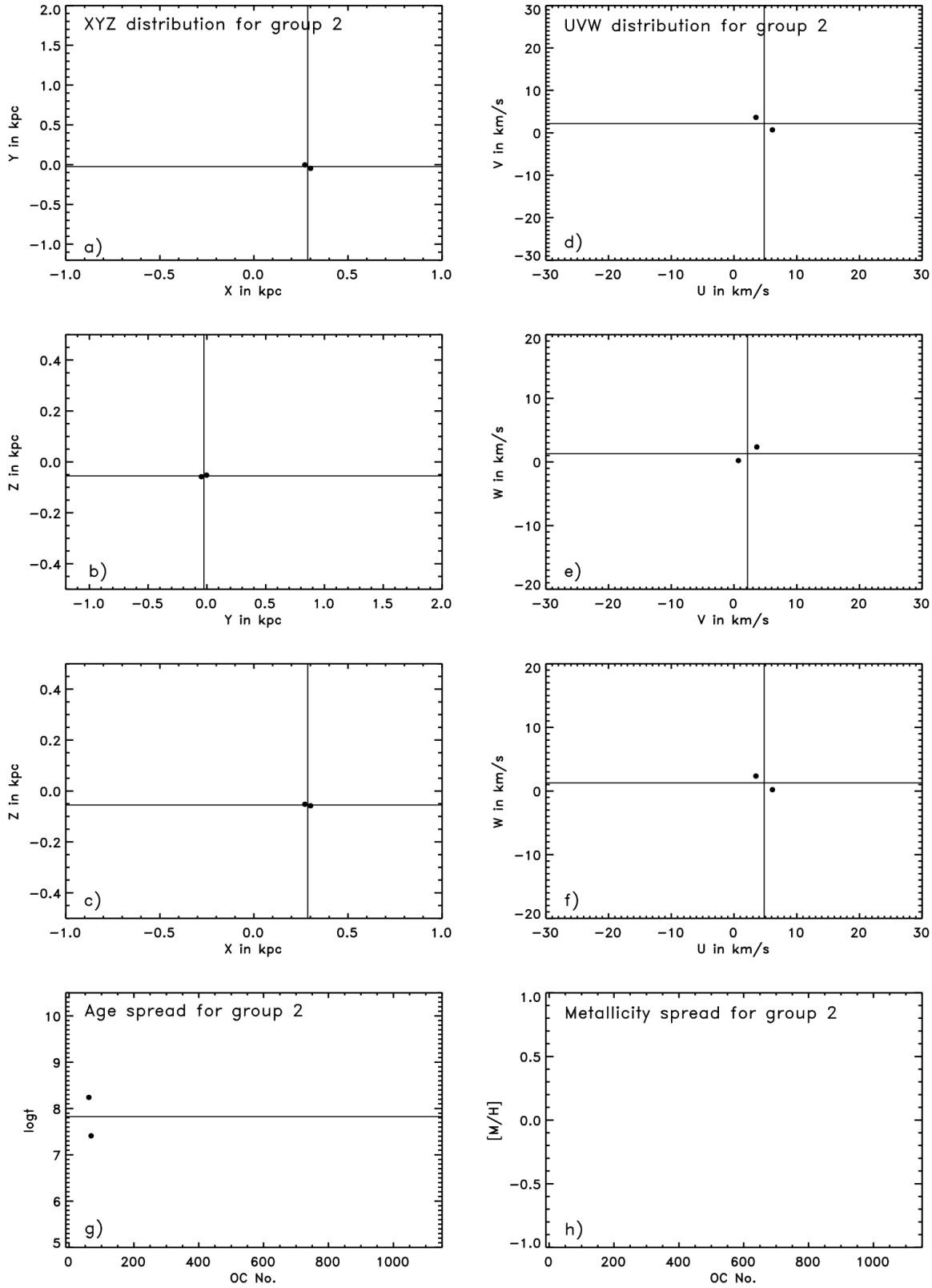

Figure C.3: Parameter distributions for the members of the open cluster grouping No. 2. a-c) spatial distribution; d-f) velocity distribution; g) age spread; h) metallicity spread. The solid lines show the corresponding averaged values for the open cluster grouping No. 2.

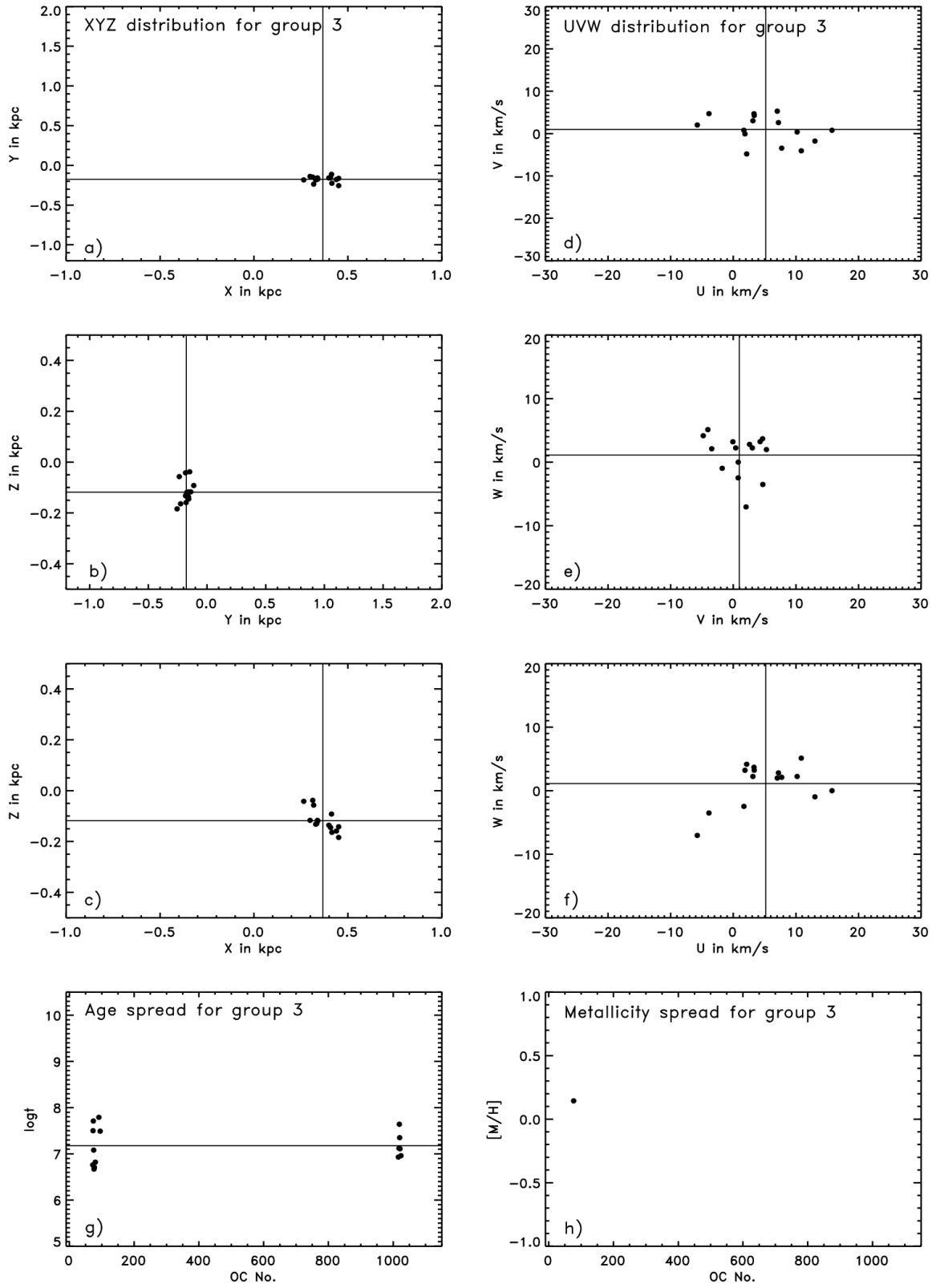

Figure C.4: Parameter distributions for the members of the open cluster grouping No. 3, as already shown in Sect. 4.4. a-c) spatial distribution; d-f) velocity distribution; g) age spread; h) metallicity spread. The solid lines show the corresponding averaged values for the open cluster grouping No. 3.

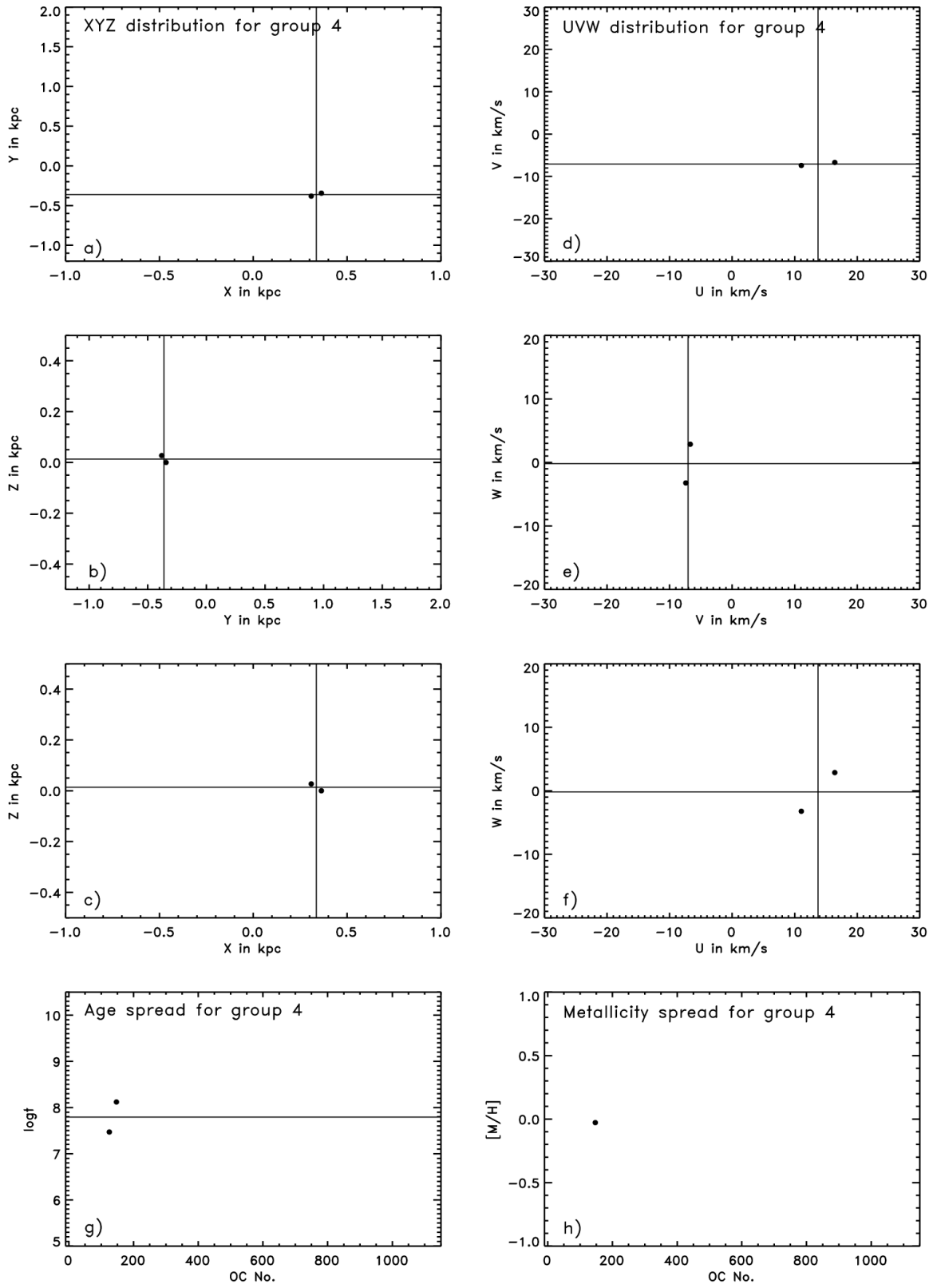

Figure C.5: Parameter distributions for the members of the open cluster grouping No. 4. a-c) spatial distribution; d-f) velocity distribution; g) age spread; h) metallicity spread. The solid lines show the corresponding averaged values for the open cluster grouping No. 4.

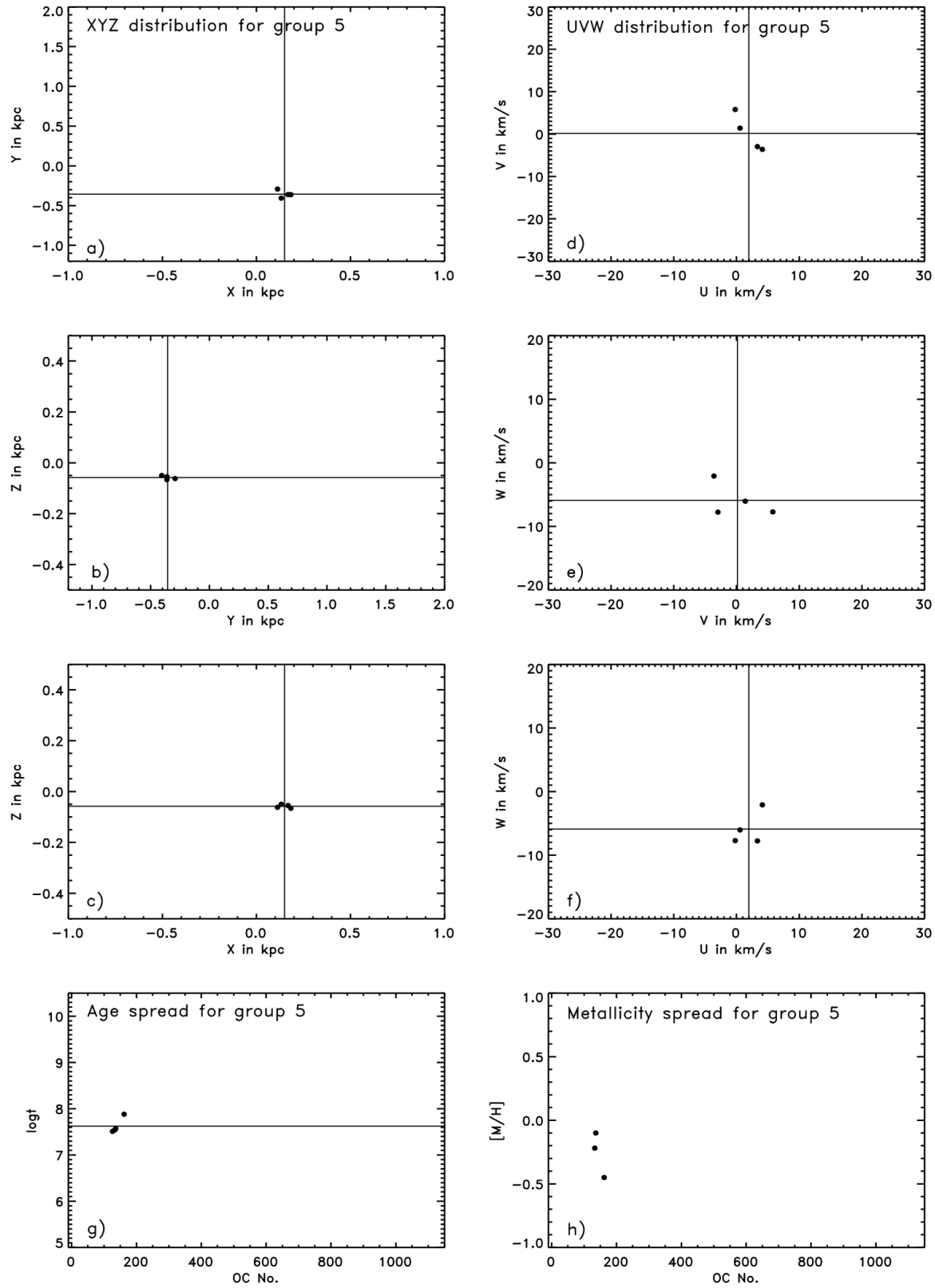

Figure C.6: Parameter distributions for the members of the open cluster grouping No. 5. a-c) spatial distribution; d-f) velocity distribution; g) age spread; h) metallicity spread. The solid lines show the corresponding averaged values for the open cluster grouping No. 5.

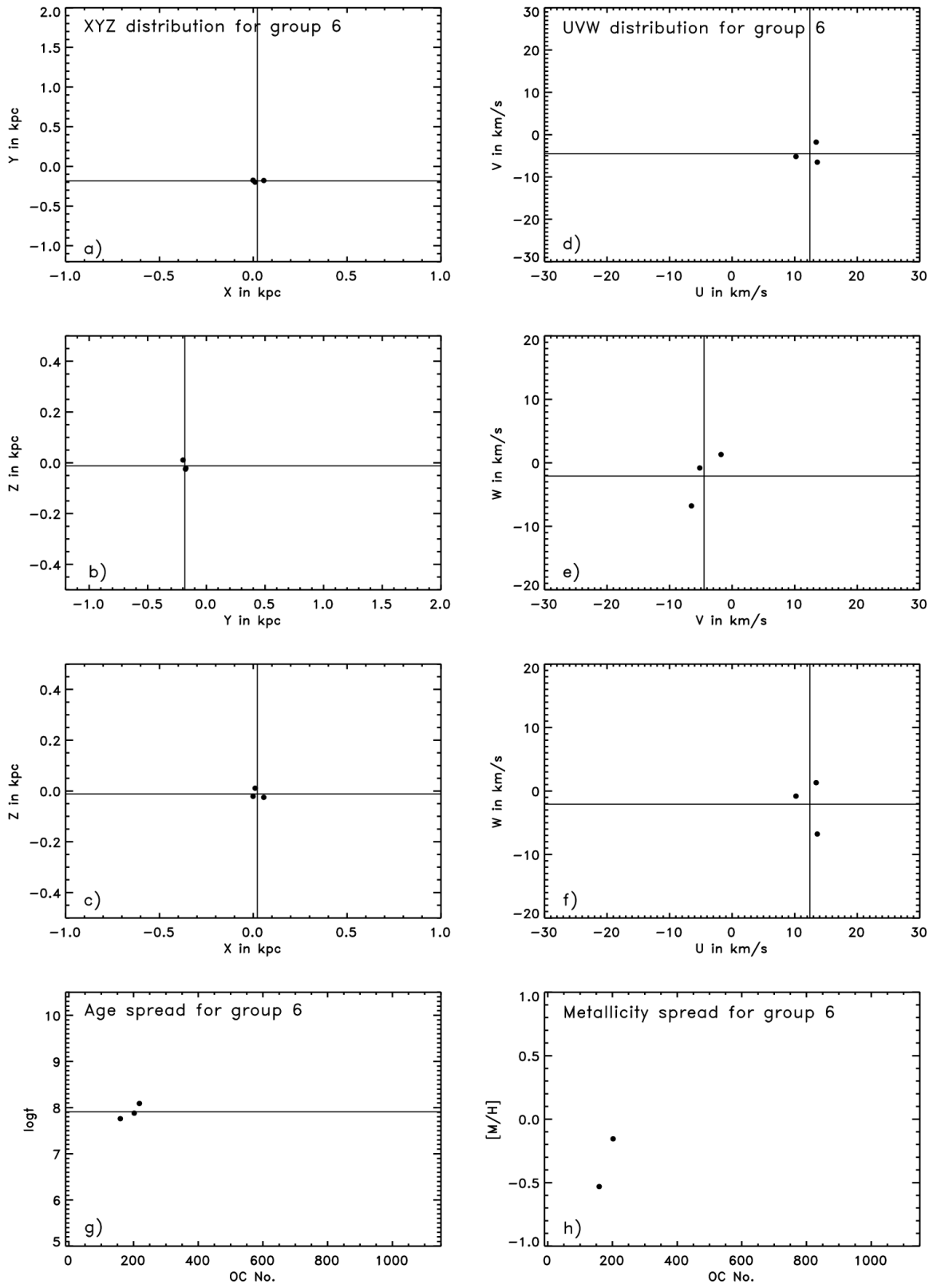

Figure C.7: Parameter distributions for the members of the open cluster grouping No. 6. a-c) spatial distribution; d-f) velocity distribution; g) age spread; h) metallicity spread. The solid lines show the corresponding averaged values for the open cluster grouping No. 6.

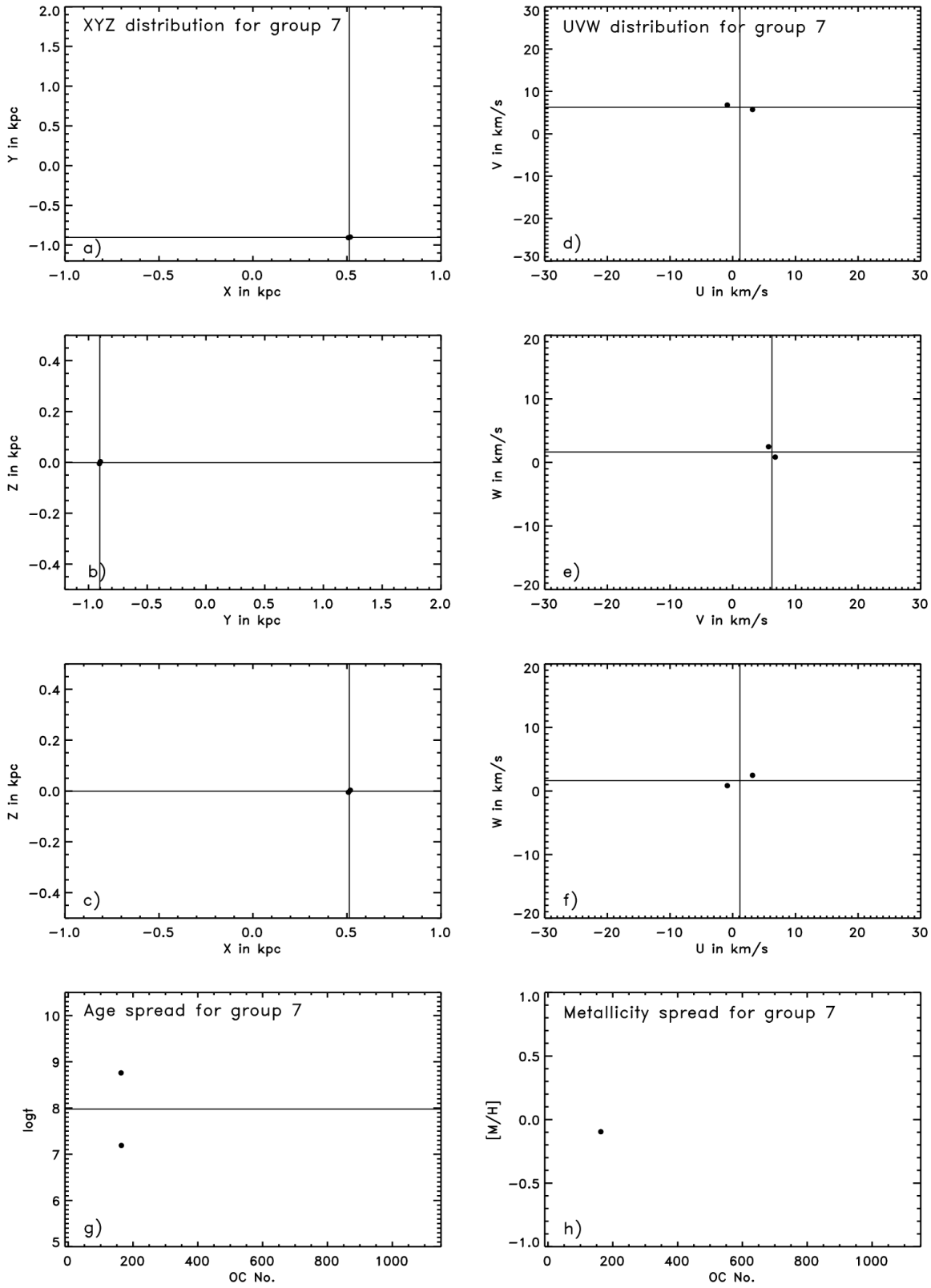

Figure C.8: Parameter distributions for the members of the open cluster grouping No. 7. a-c) spatial distribution; d-f) velocity distribution; g) age spread; h) metallicity spread. The solid lines show the corresponding averaged values for the open cluster grouping No. 7.

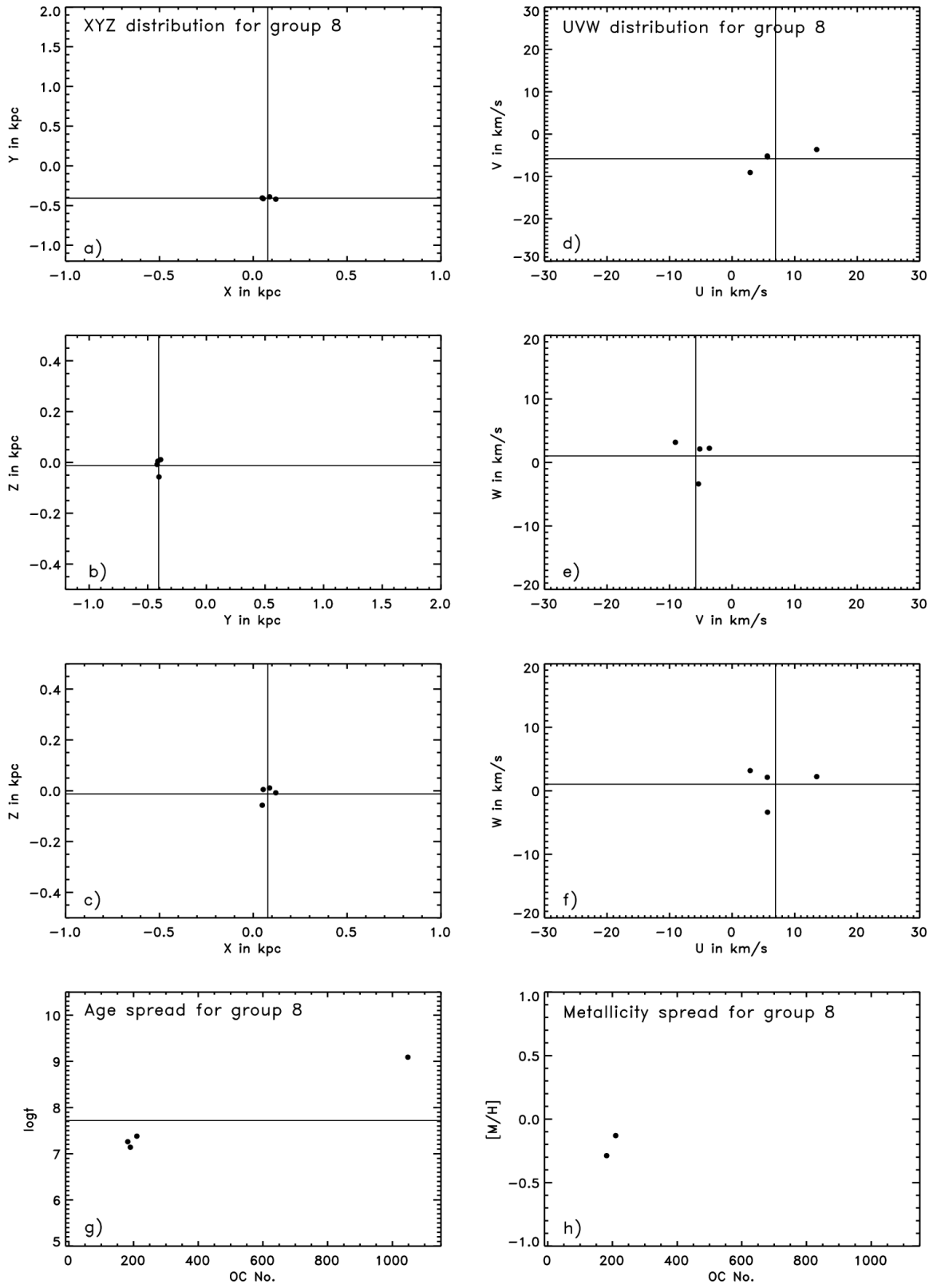

Figure C.9: Parameter distributions for the members of the open cluster grouping No. 8. a-c) spatial distribution; d-f) velocity distribution; g) age spread; h) metallicity spread. The solid lines show the corresponding averaged values for the open cluster grouping No. 8.

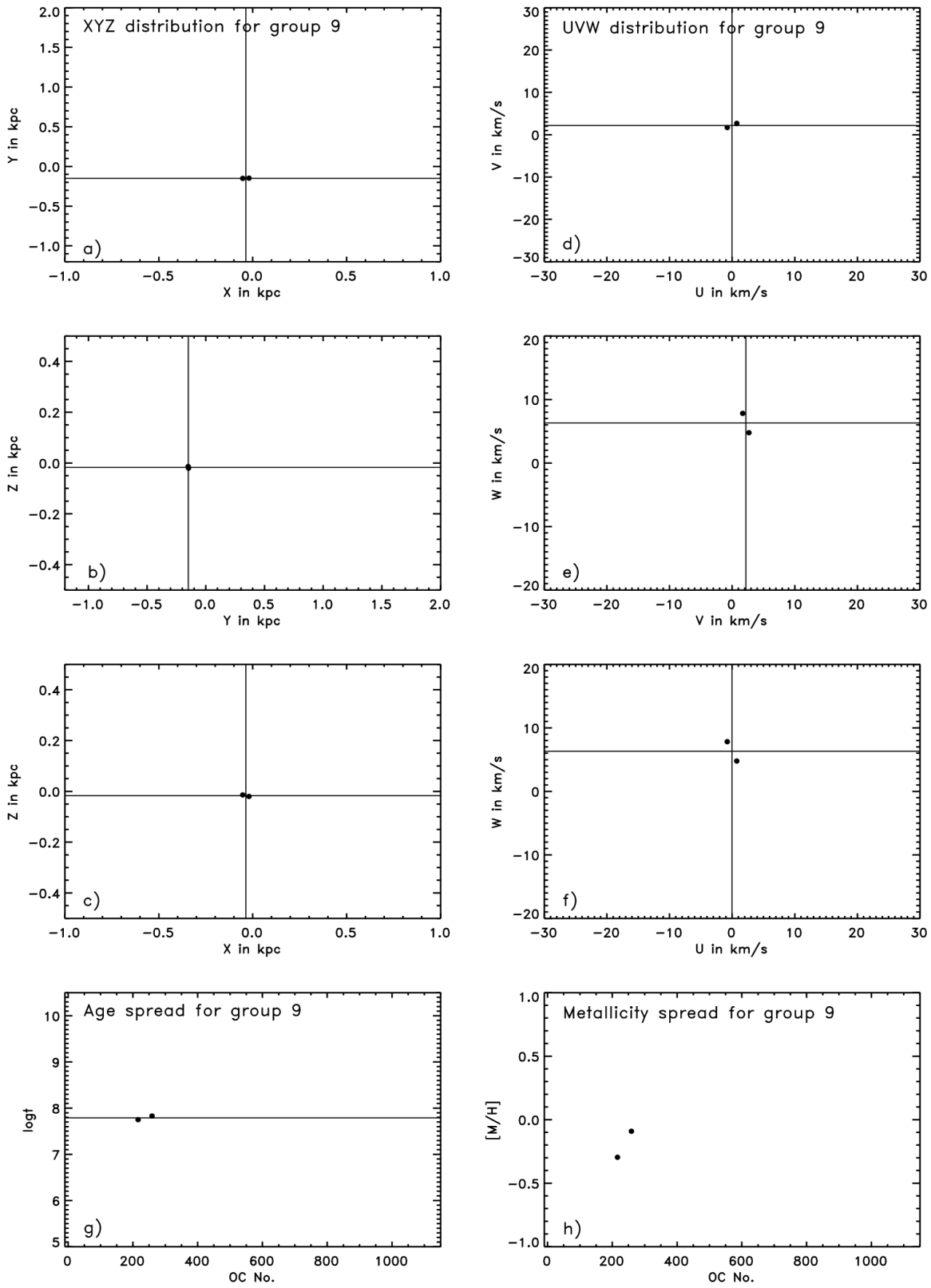

Figure C.10: Parameter distributions for the members of the open cluster grouping No. 9. a-c) spatial distribution; d-f) velocity distribution; g) age spread; h) metallicity spread. The solid lines show the corresponding averaged values for the open cluster grouping No. 9.

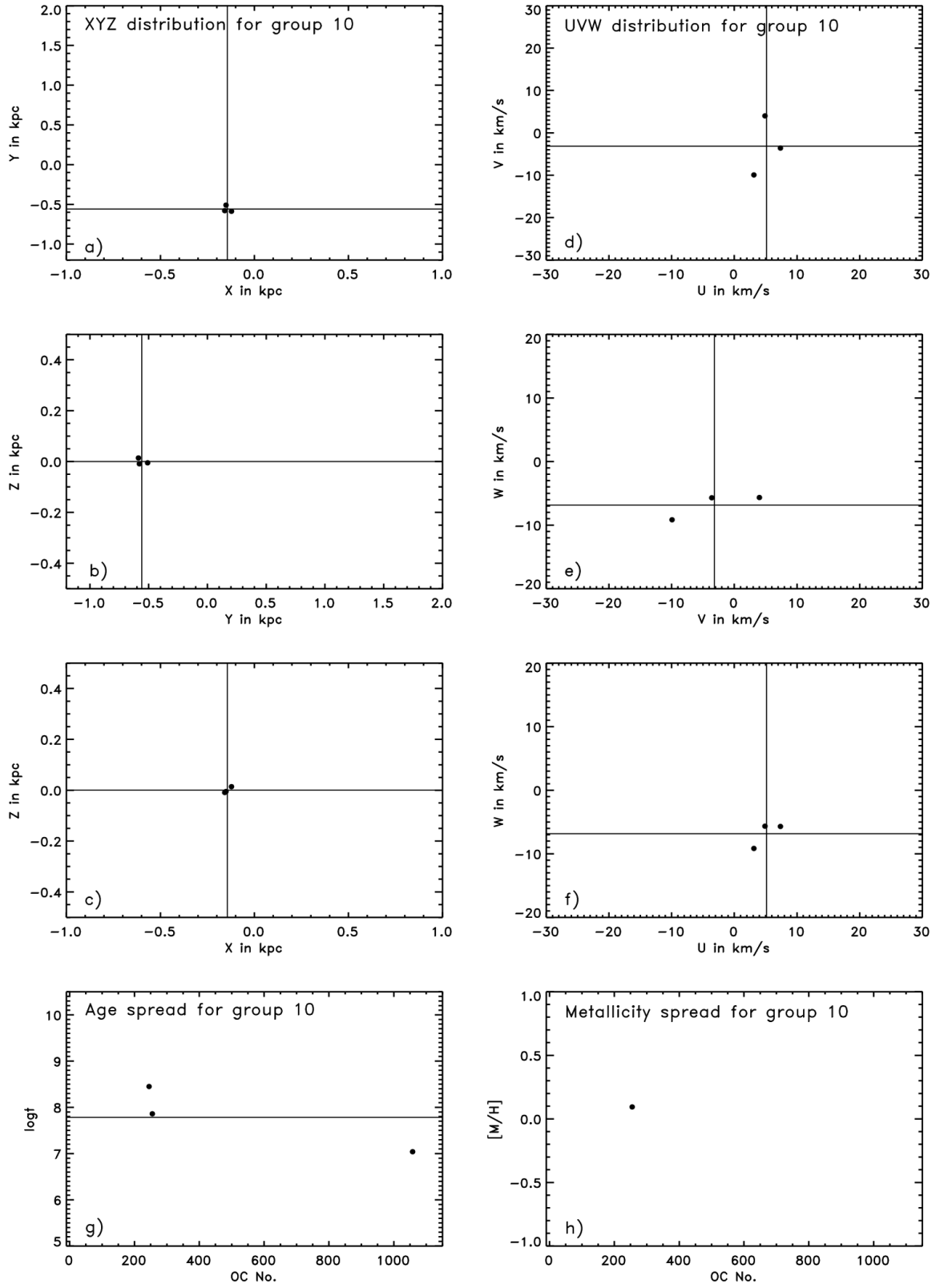

Figure C.11: Parameter distributions for the members of the open cluster grouping No. 10. a-c) spatial distribution; d-f) velocity distribution; g) age spread; h) metallicity spread. The solid lines show the corresponding averaged values for the open cluster grouping No. 10.

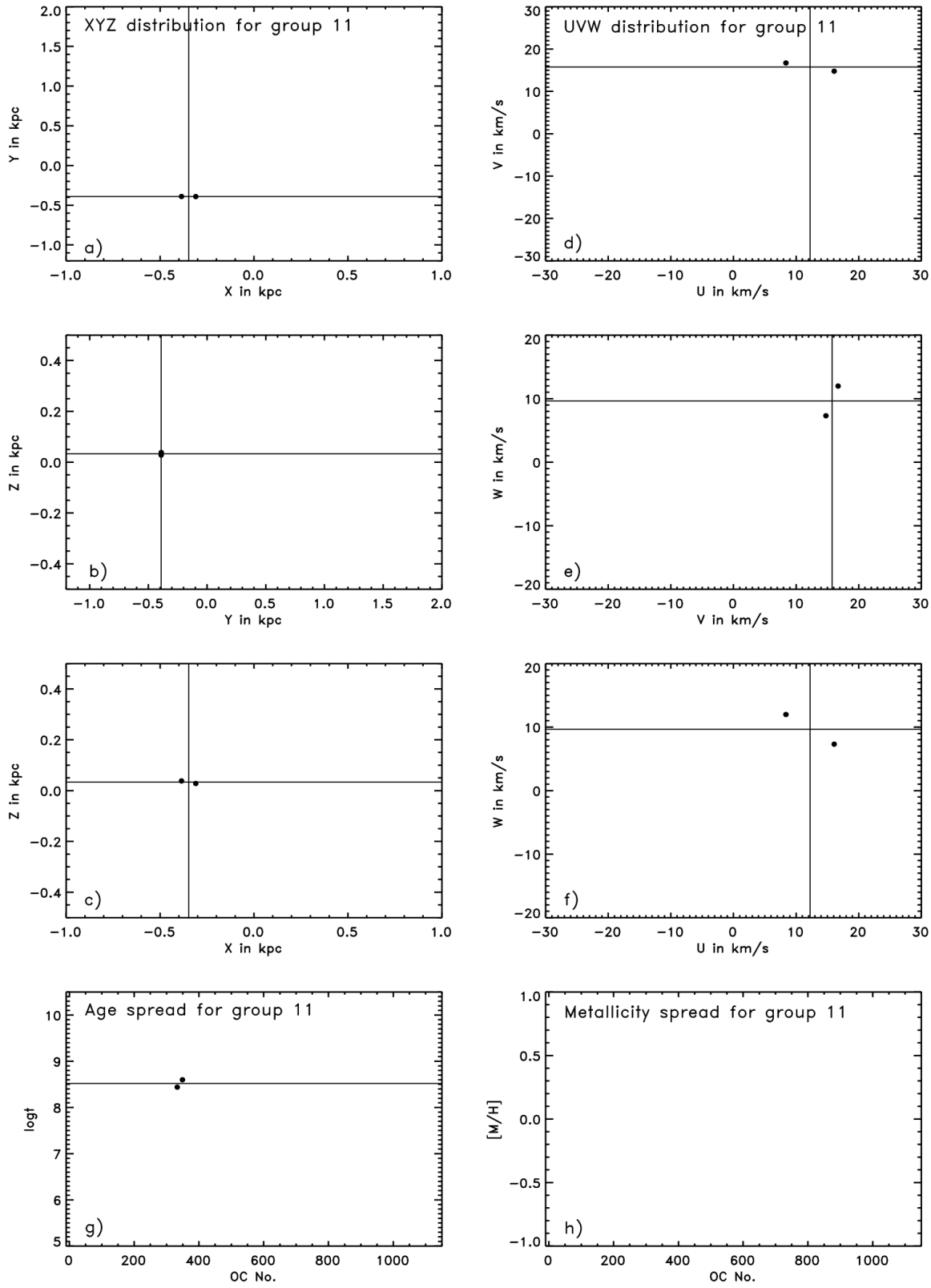

Figure C.12: Parameter distributions for the members of the open cluster grouping No. 11. a-c) spatial distribution; d-f) velocity distribution; g) age spread; h) metallicity spread. The solid lines show the corresponding averaged values for the open cluster grouping No. 11.

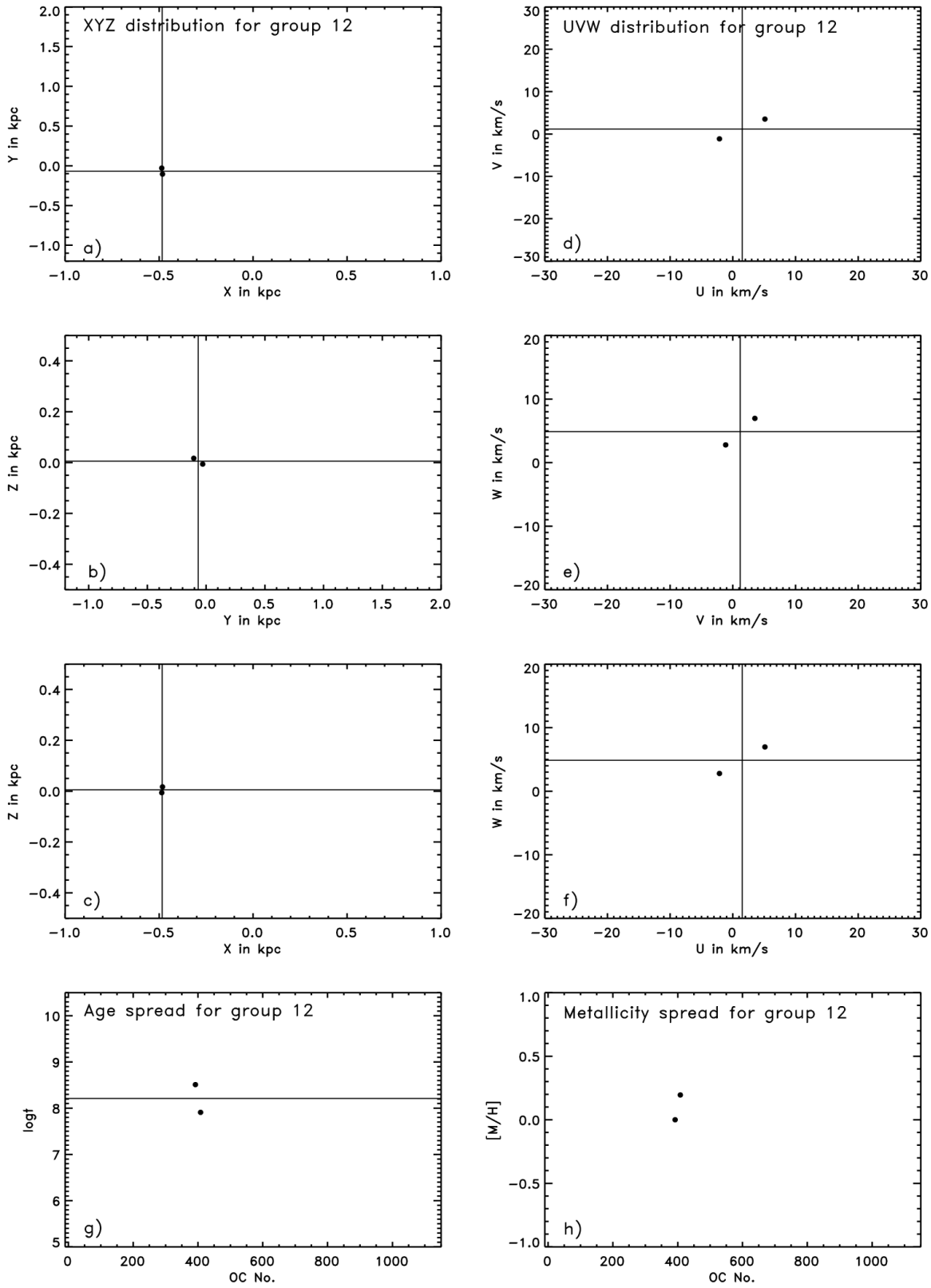

Figure C.13: Parameter distributions for the members of the open cluster grouping No. 12. a-c) spatial distribution; d-f) velocity distribution; g) age spread; h) metallicity spread. The solid lines show the corresponding averaged values for the open cluster grouping No. 12.

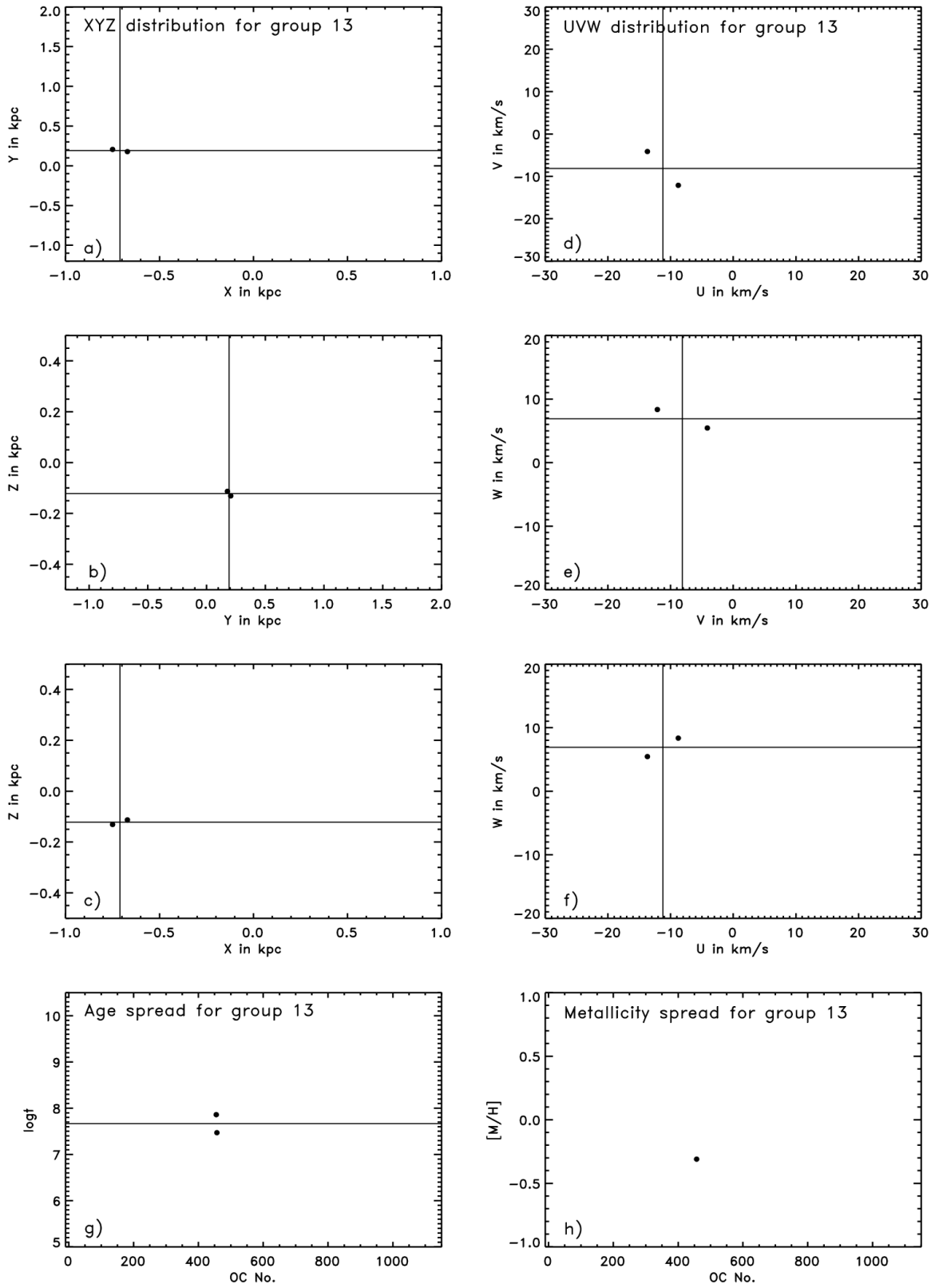

Figure C.14: Parameter distributions for the members of the open cluster grouping No. 13. a-c) spatial distribution; d-f) velocity distribution; g) age spread; h) metallicity spread. The solid lines show the corresponding averaged values for the open cluster grouping No. 13.

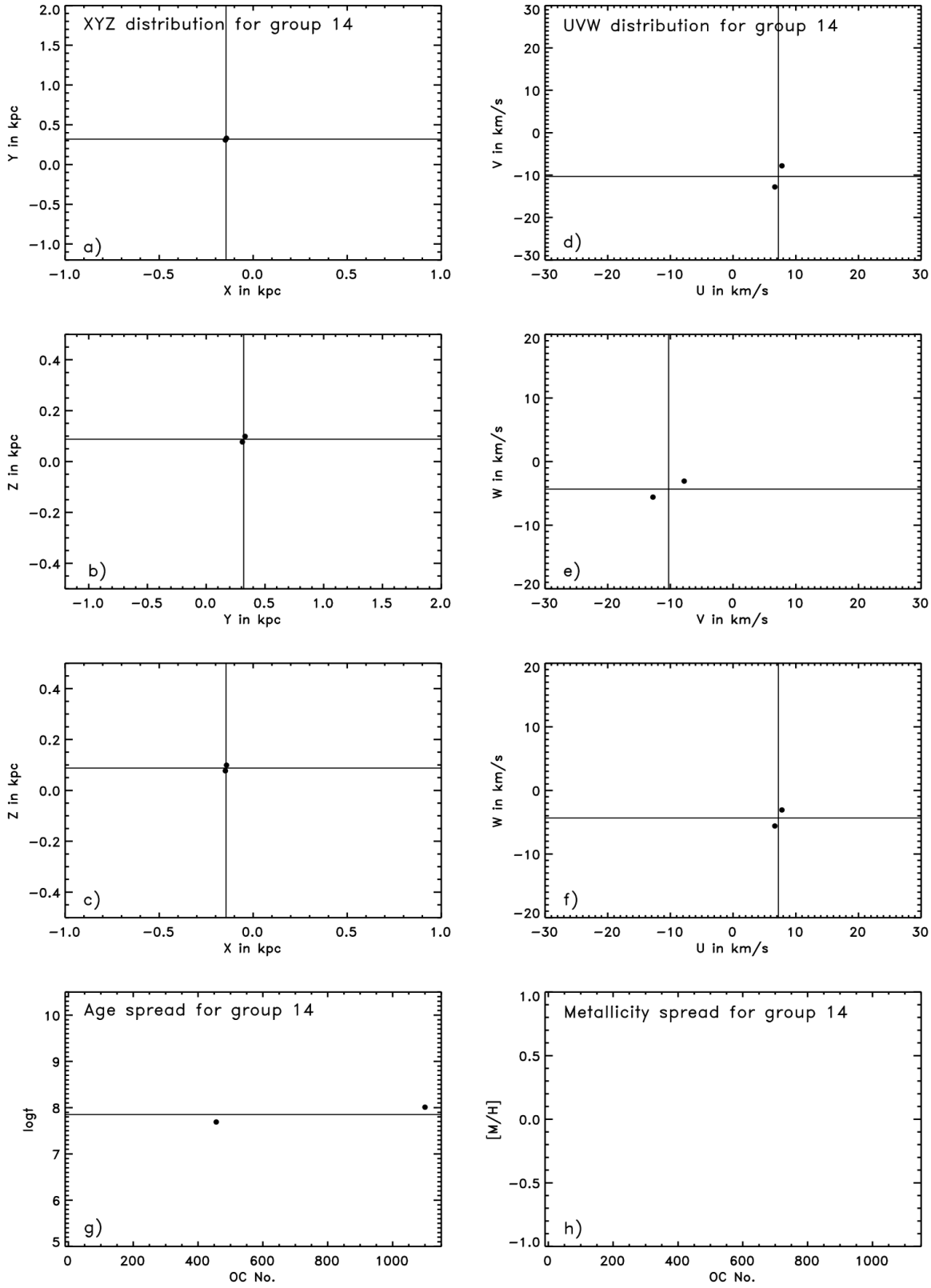

Figure C.15: Parameter distributions for the members of the open cluster grouping No. 14. a-c) spatial distribution; d-f) velocity distribution; g) age spread; h) metallicity spread. The solid lines show the corresponding averaged values for the open cluster grouping No. 14.

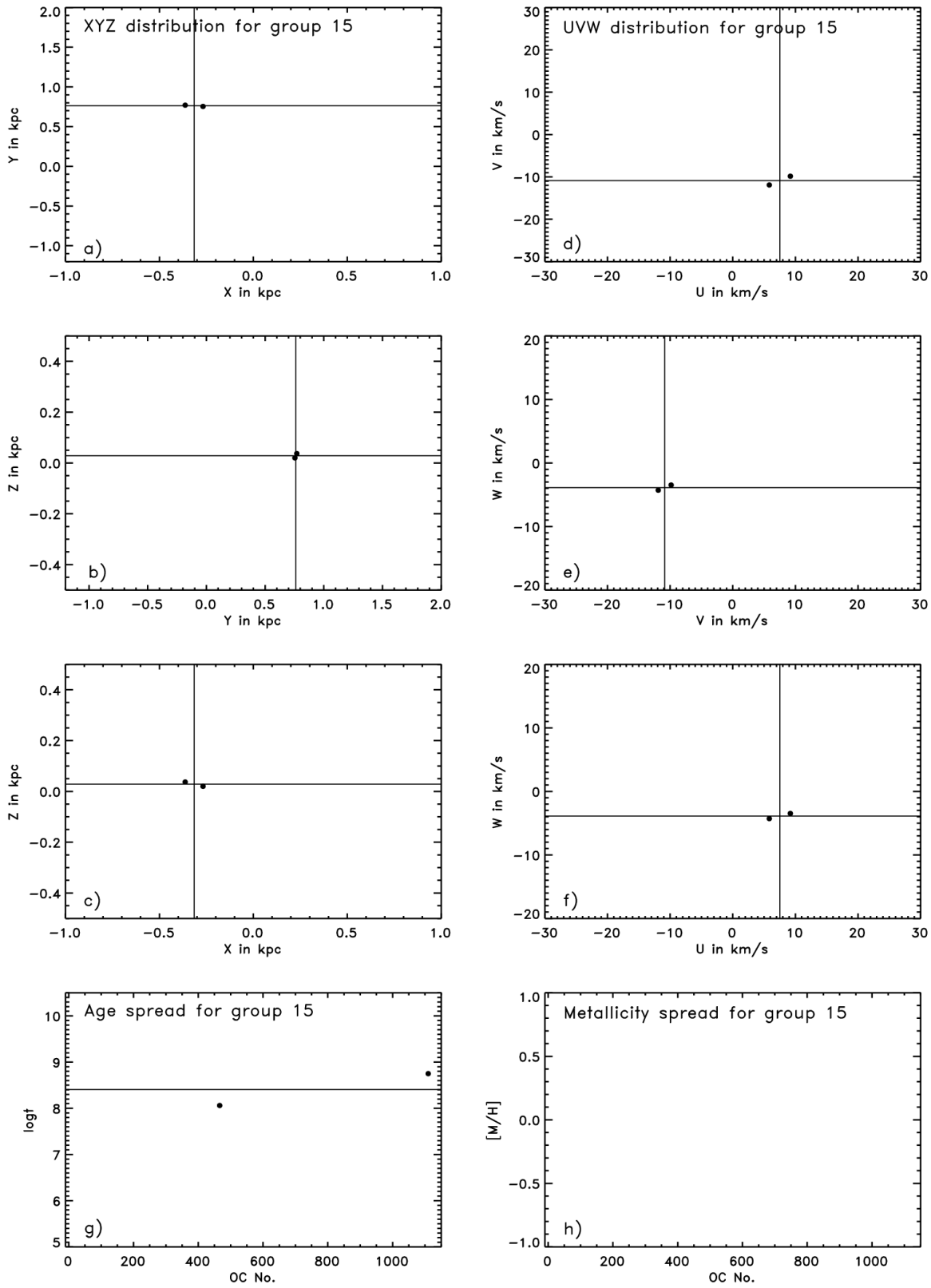

Figure C.16: Parameter distributions for the members of the open cluster grouping No. 15. a-c) spatial distribution; d-f) velocity distribution; g) age spread; h) metallicity spread. The solid lines show the corresponding averaged values for the open cluster grouping No. 15.

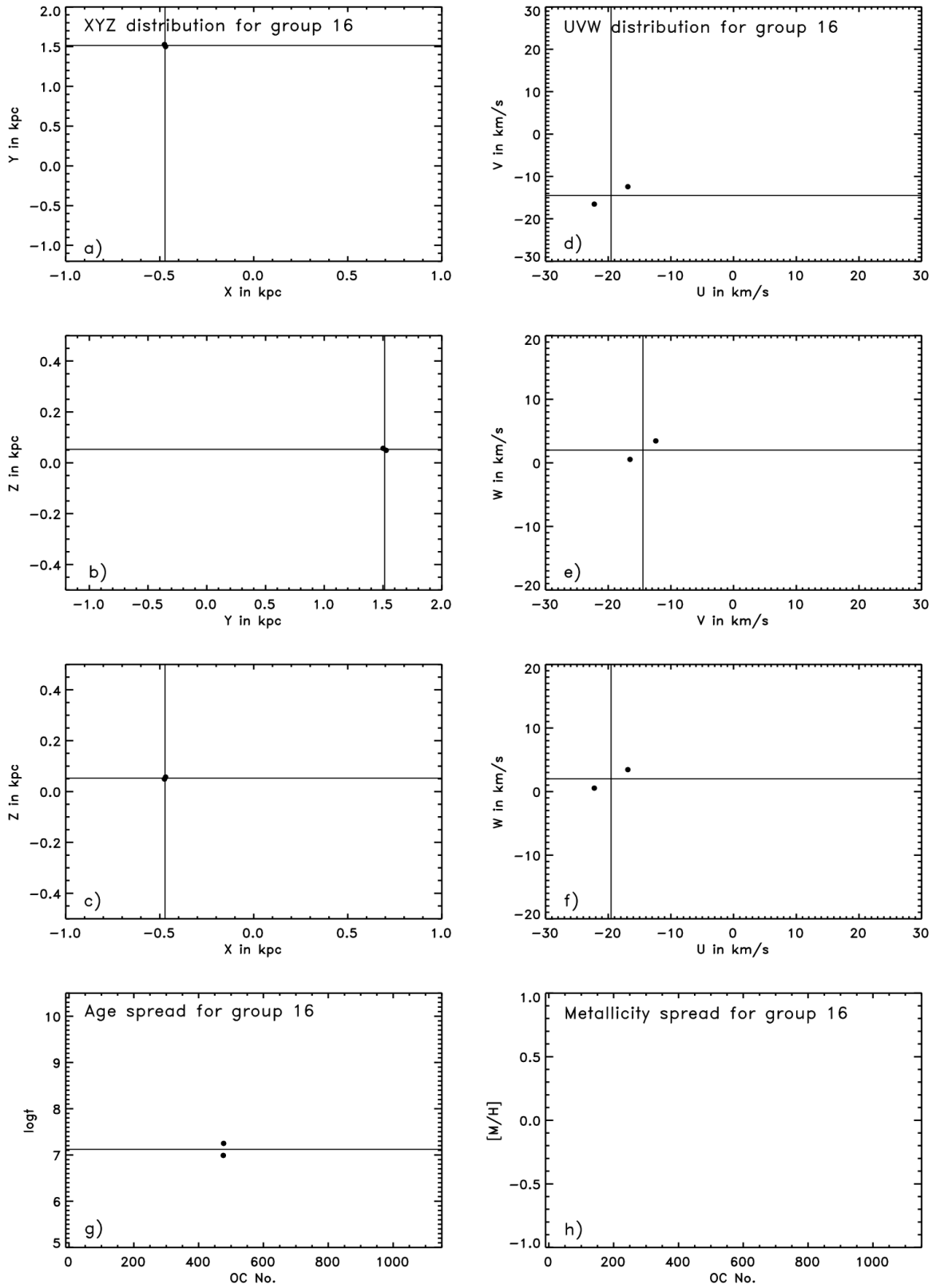

Figure C.17: Parameter distributions for the members of the open cluster grouping No. 16. a-c) spatial distribution; d-f) velocity distribution; g) age spread; h) metallicity spread. The solid lines show the corresponding averaged values for the open cluster grouping No. 16.

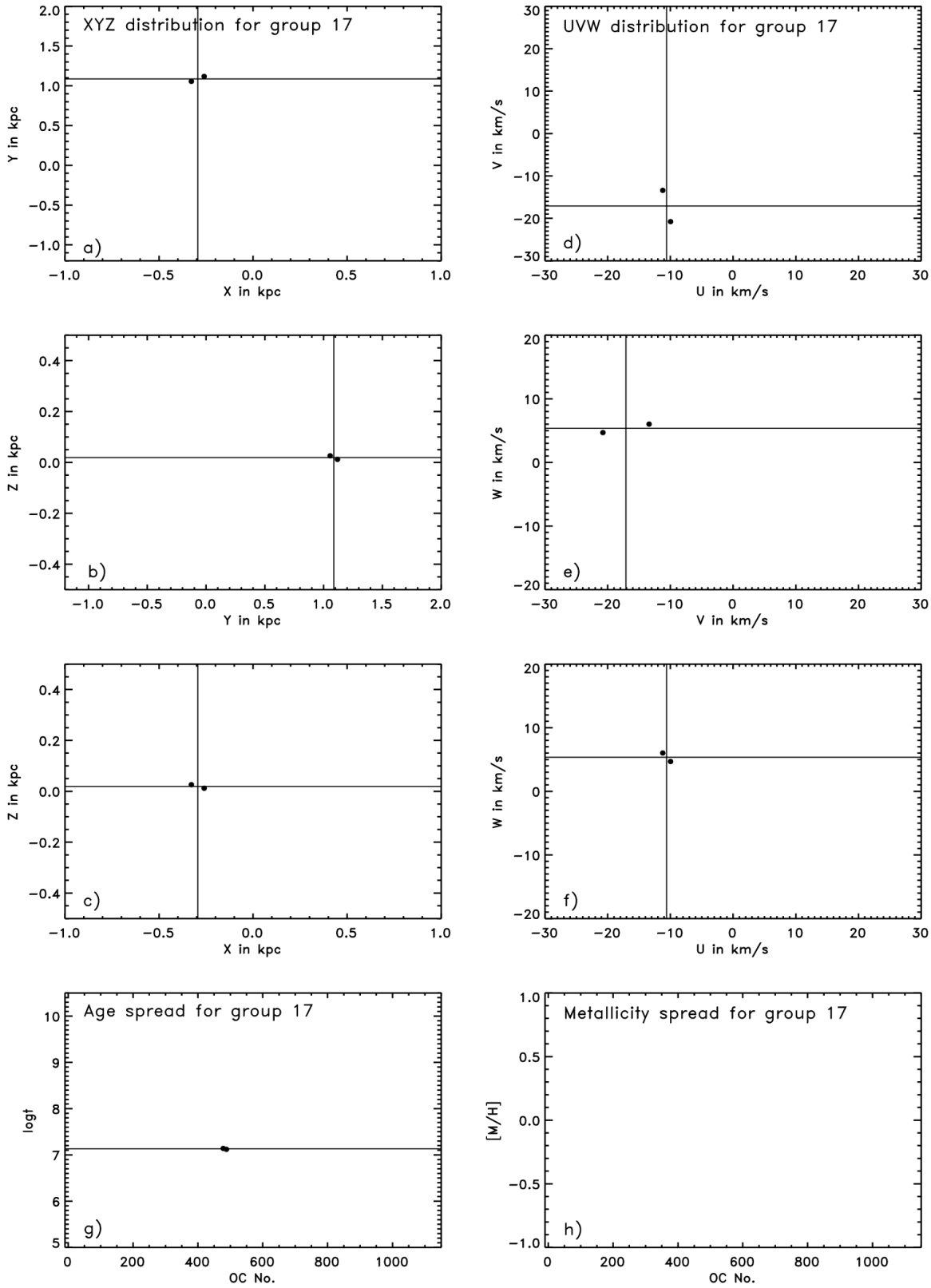

Figure C.18: Parameter distributions for the members of the open cluster grouping No. 17. a-c) spatial distribution; d-f) velocity distribution; g) age spread; h) metallicity spread. The solid lines show the corresponding averaged values for the open cluster grouping No. 17.

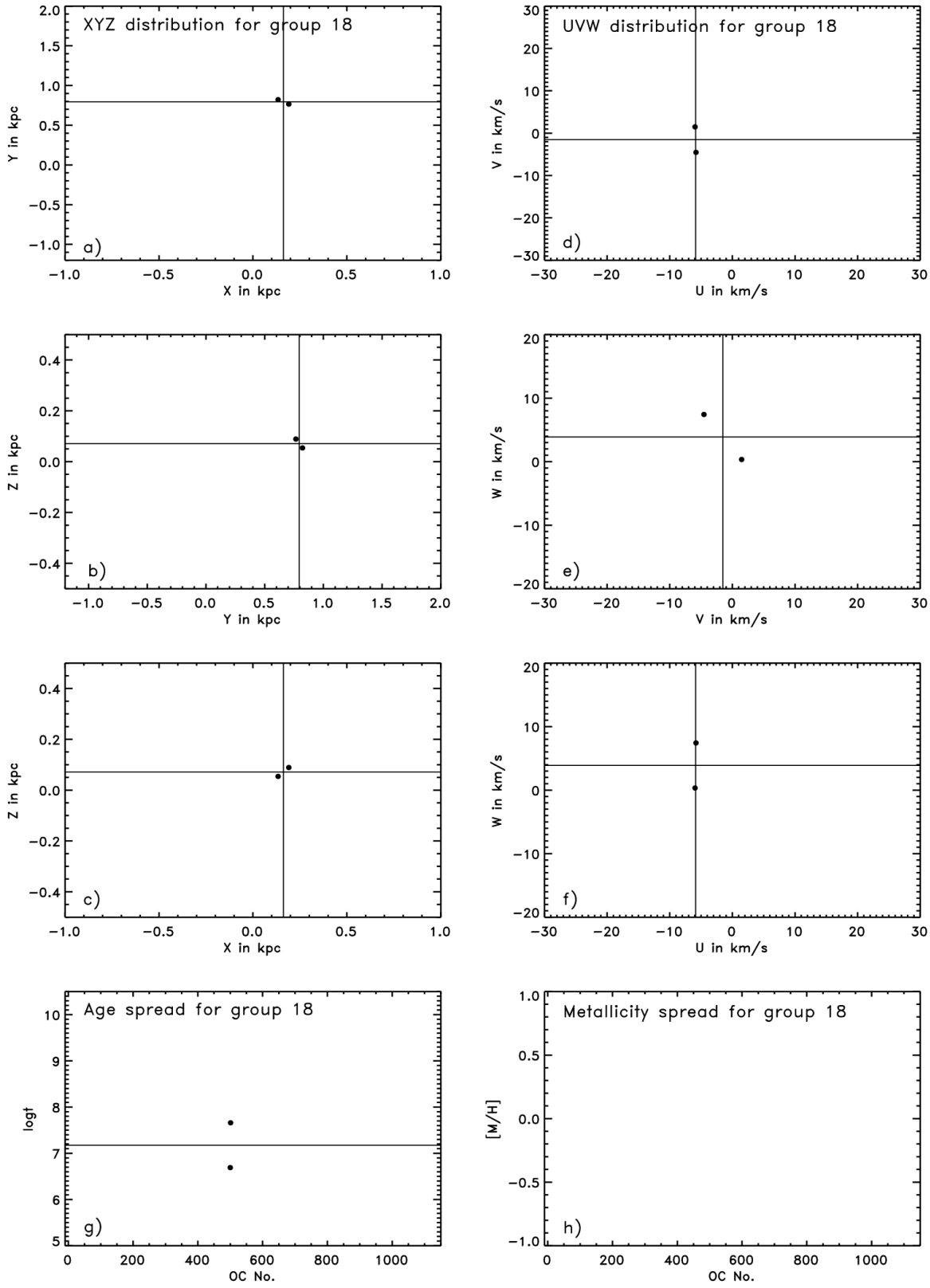

Figure C.19: Parameter distributions for the members of the open cluster grouping No. 18. a-c) spatial distribution; d-f) velocity distribution; g) age spread; h) metallicity spread. The solid lines show the corresponding averaged values for the open cluster grouping No. 18.

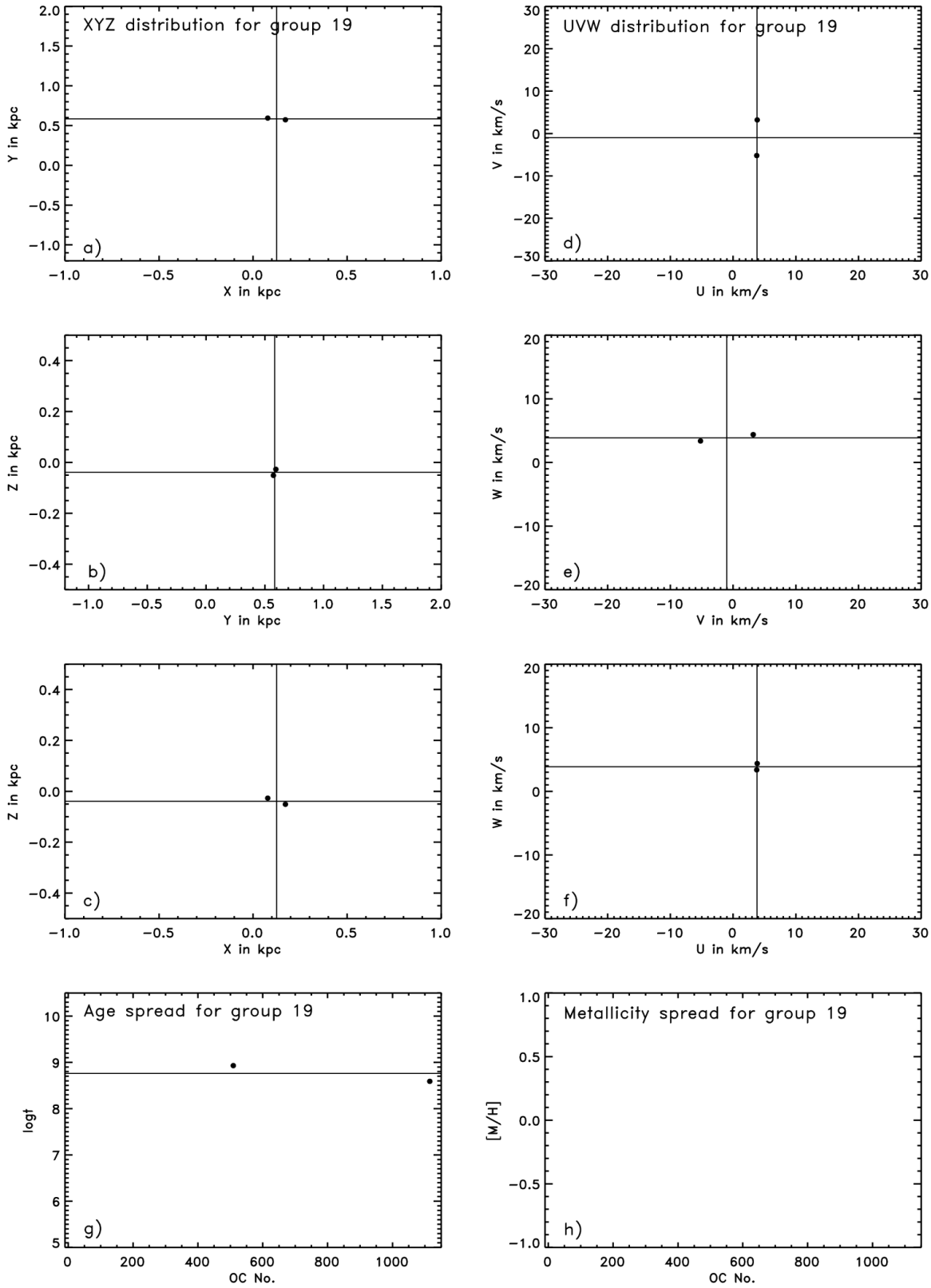

Figure C.20: Parameter distributions for the members of the open cluster grouping No. 19. a-c) spatial distribution; d-f) velocity distribution; g) age spread; h) metallicity spread. The solid lines show the corresponding averaged values for the open cluster grouping No. 19.

Section C.2

For linking lengths 100 pc and 20 km/s

In Sect. 4.4 I summarised the mean characteristics and individual parameters for the members of the OC groupings identified with the first set of linking lengths (100 pc and 10 km/s) in Tab. 4.1 and 4.2, respectively. For the second set of linking lengths (100 pc and 20 km/s) 42 OC groupings were detected. The XYZ-coordinates, UVW-velocities, distances, ages, and metallicities for the members of the groupings are given in Tab. C.1, while the corresponding mean values, except for the metallicities, are listed in Tab. C.2. The mean $[M/H]$ could not be included in Tab. C.2, because of missing respective information for the majority of the members (see Tab. C.1). The tables for the second set of linking lengths (100 pc and 20 km/s) are provided here for comparison with the results for the first set of linking lengths (100 pc and 10 km/s) in Sect. 4.4.

Table C.1: Parameters for the members of the identified OC groupings using linking lengths 100 pc and 20 km/s, namely identifiers, XYZ-coordinates, UVW-velocities, distances, ages, and metallicities.

OCC No.	Seq	Name	X kpc	Y kpc	Z kpc	U km/s	V km/s	W km/s	d kpc	log t dex	$[M/H]$ dex
1	42	Melotte 20	0.159	0.102	-0.021	6.5	-14.2	-0.6	0.190	7.55	0.04
	47	Melotte 22	0.116	0.028	-0.052	-2.1	-14.6	-6.8	0.130	8.08	-0.04
2	44	Alessi 13	0.033	-0.052	-0.091	2.4	-11.6	3.2	0.110	8.72	0.06
	159	NGC 2451A	0.056	-0.178	-0.025	13.6	-6.5	-6.8	0.188	7.76	-0.53
	202	IC 2391	-0.001	-0.175	-0.021	13.4	-1.8	1.3	0.176	7.88	-0.15
	204	Mamajek 1	-0.037	-0.090	-0.039	1.2	-7.1	-4.0	0.105	6.90	—
	216	Platais 8	-0.020	-0.147	-0.020	0.7	2.7	4.8	0.150	7.75	-0.30
	218	Platais 9	0.010	-0.199	0.011	10.2	-5.2	-0.8	0.200	8.09	—
	259	IC 2602	-0.053	-0.150	-0.014	-0.8	1.7	7.8	0.160	7.83	-0.09
3	45	NGC 1342	0.581	0.271	-0.176	-10.7	2.6	1.7	0.665	8.21	-0.16
	1011	ASCC 11	0.559	0.315	-0.104	2.8	3.9	-6.3	0.650	8.61	—
4	50	NGC 1528	0.685	0.364	0.003	-3.4	-1.3	4.9	0.776	8.43	—
	51	NGC 1545	0.636	0.319	0.002	-13.0	8.3	0.9	0.711	8.15	—
5	61	Platais 4	0.271	-0.003	-0.052	3.5	3.6	2.3	0.276	8.24	—
	68	Collinder 65	0.301	-0.047	-0.058	6.1	0.7	0.2	0.310	7.41	—
6	69	NGC 1907	1.319	0.171	0.007	-2.2	-4.3	-3.9	1.330	7.94	—
	78	NGC 1960	1.312	0.126	0.025	-4.3	-13.8	-6.7	1.318	7.62	—
7	71	NGC 1912	1.056	0.143	0.013	-1.2	-9.7	-7.0	1.066	8.56	—
	1014	ASCC 14	1.089	0.156	-0.020	-19.0	-11.6	-14.3	1.100	8.61	—
8	72	Collinder 69	0.413	-0.113	-0.092	15.8	0.8	-0.0	0.438	6.76	—
	73	NGC 1981	0.334	-0.178	-0.130	10.2	0.4	2.2	0.400	7.50	—
	74	NGC 1976	0.329	-0.183	-0.132	7.7	-3.4	2.1	0.399	7.71	—
	75	NGC 1977	0.415	-0.225	-0.164	2.1	-4.8	4.2	0.500	7.08	—
	76	NGC 1980	0.451	-0.255	-0.184	1.9	-0.1	3.2	0.550	6.67	—
	77	Collinder 70	0.338	-0.158	-0.117	13.0	-1.8	-1.0	0.391	6.71	0.14
	80	Sigma Ori	0.340	-0.172	-0.119	10.9	-4.1	5.1	0.399	6.82	—
	91	Platais 6	0.313	-0.148	-0.038	-3.9	4.7	-3.5	0.348	7.79	—
	95	NGC 2232	0.265	-0.183	-0.042	1.7	0.8	-2.5	0.325	7.49	—
	1016	ASCC 16	0.408	-0.156	-0.145	3.3	4.7	3.7	0.460	6.93	—
	1018	ASCC 18	0.439	-0.178	-0.159	7.2	2.6	2.8	0.500	7.12	—
	1019	ASCC 19	0.299	-0.139	-0.117	3.1	3.0	2.2	0.350	7.64	—
	1020	ASCC 20	0.399	-0.158	-0.136	7.0	5.3	2.0	0.450	7.35	—
	1021	ASCC 21	0.451	-0.163	-0.142	3.3	4.3	3.2	0.500	7.11	—
	1024	ASCC 24	0.318	-0.236	-0.057	-5.8	2.0	-7.0	0.400	6.96	—

Table C.1: continued

OCC No.	Seq	Name	X kpc	Y kpc	Z kpc	U km/s	V km/s	W km/s	d kpc	log t dex	$[M/H]$ dex
9	98	NGC 2244	1.295	-0.640	-0.052	-2.5	4.5	-2.8	1.445	6.70	—
	105	Collinder 107	1.288	-0.666	-0.019	-14.0	10.7	-10.9	1.450	7.03	—
10	100	Basel 8	1.215	-0.537	-0.004	-19.9	-3.7	3.4	1.328	7.68	—
	102	NGC 2251	1.218	-0.531	0.002	-8.4	-12.3	2.9	1.329	8.43	0.25
11	112	NGC 2301	0.723	-0.462	0.004	-14.5	-7.3	-6.3	0.858	8.31	0.06
	1028	ASCC 28	0.668	-0.440	0.007	-3.0	-0.3	-0.3	0.800	8.34	—
	1029	ASCC 29	0.616	-0.427	-0.002	-10.3	4.9	5.1	0.750	8.06	—
12	125	Alessi 21	0.363	-0.344	0.000	16.4	-6.7	2.9	0.500	7.47	—
	147	NGC 2422	0.309	-0.381	0.027	11.1	-7.4	-3.2	0.491	8.12	-0.03
13	126	Collinder 132	0.183	-0.362	-0.066	4.1	-3.6	-2.1	0.411	7.51	—
	133	Collinder 135	0.112	-0.292	-0.062	3.3	-3.0	-7.8	0.319	7.54	-0.22
	136	Collinder 140	0.168	-0.361	-0.055	0.6	1.4	-6.0	0.402	7.57	-0.10
	162	NGC 2451B	0.132	-0.406	-0.050	-0.2	5.8	-7.7	0.430	7.88	-0.45
	182	Vel OB2	0.048	-0.404	-0.057	2.9	-9.1	3.2	0.411	7.26	-0.29
	183	NGC 2547	0.044	-0.450	-0.068	-3.1	2.0	-6.3	0.457	7.70	-0.16
	190	vdBergh-Hagen 23	0.120	-0.420	-0.008	5.6	-5.2	2.1	0.437	7.14	—
	210	Trumpler 10	0.053	-0.414	0.005	5.7	-5.4	-3.4	0.417	7.38	-0.13
	1048	ASCC 48	0.087	-0.390	0.011	13.5	-3.6	2.2	0.400	9.09	—
14	141	NGC 2396	0.397	-0.433	0.027	-9.8	-1.3	0.9	0.588	8.52	—
	153	NGC 2430	0.391	-0.518	0.032	3.1	-7.1	-0.7	0.650	8.68	0.13
15	149	Ruprecht 26	0.885	-1.134	0.068	-21.2	-6.4	-17.1	1.440	7.49	0.31
	160	NGC 2437	0.847	-1.079	0.097	-3.5	0.7	-12.1	1.375	8.16	-0.75
16	163	NGC 2447	0.518	-0.899	0.003	-0.9	6.8	0.8	1.037	8.76	-0.10
	164	NGC 2448	0.508	-0.907	-0.005	3.2	5.7	2.5	1.040	7.19	—
17	169	NGC 2467	0.612	-1.209	0.008	2.4	-27.0	-8.7	1.355	8.05	—
	171	NGC 2482	0.638	-1.181	0.048	-1.2	-14.8	-20.2	1.343	8.48	-0.08
18	186	NGC 2546	0.240	-0.886	-0.033	-1.7	5.0	-1.2	0.919	7.92	0.12
	198	Ruprecht 64	0.142	-0.787	0.007	5.3	-8.7	2.6	0.800	8.45	—
	1047	Alessi-Teutsch 7	0.183	-0.881	0.005	8.2	9.5	-10.4	0.900	7.88	—
	1050	Alessi 43	0.111	-0.842	0.022	-2.3	-1.5	-2.5	0.850	7.48	—
19	234	NGC 3114	-0.208	-0.885	-0.061	2.2	7.1	1.7	0.911	8.24	—
	239	Ruprecht 161	-0.237	-0.907	-0.071	-0.2	-6.3	-4.2	0.940	8.39	—
20	243	IC 2581	-0.616	-2.367	0.001	13.1	-7.1	2.7	2.446	7.22	-0.34
	253	NGC 3293	-0.675	-2.377	0.003	20.4	-3.7	-5.9	2.471	6.94	—
21	245	Loden 143	-0.158	-0.579	-0.009	4.9	4.0	-5.7	0.600	8.45	—
	255	vdBergh-Hagen 99	-0.151	-0.509	-0.005	3.1	-9.9	-9.2	0.531	7.86	0.09
	1058	ASCC 58	-0.122	-0.587	0.014	7.4	-3.6	-5.7	0.600	7.04	—
22	298	Loden 481	-0.662	-1.368	0.020	-10.5	17.8	12.5	1.520	8.19	—
	1067	ASCC 67	-0.623	-1.364	0.019	-17.3	19.5	-5.1	1.500	7.67	—
23	333	Loden 915	-0.310	-0.391	0.028	8.4	16.7	12.0	0.500	8.44	—
	337	Platais 12	-0.278	-0.335	-0.010	2.8	8.6	1.9	0.435	8.23	-0.01
	344	Loden 1194	-0.335	-0.370	0.016	-2.4	-6.9	6.8	0.500	8.53	—
	349	ESO 175-06	-0.386	-0.390	0.038	16.1	14.8	7.3	0.550	8.60	—
24	335	Loden 1010	-0.445	-0.540	0.024	7.4	9.8	13.1	0.700	8.69	—
	355	NGC 5662	-0.494	-0.462	0.040	11.6	8.0	-4.1	0.678	7.64	-0.03
25	366	NGC 6025	-0.623	-0.444	-0.079	-9.2	-1.2	9.6	0.769	7.96	0.19
	1079	ASCC 79	-0.612	-0.513	-0.040	-15.9	-4.6	-1.3	0.800	6.86	—
26	371	NGC 6087	-0.758	-0.479	-0.085	-7.9	6.6	4.3	0.901	7.93	-0.01
	1084	ASCC 84	-0.721	-0.532	-0.085	-7.9	-0.9	-4.6	0.900	7.68	—
27	374	NGC 6134	-0.827	-0.387	-0.003	10.9	5.9	-11.4	0.913	8.53	0.15
	384	NGC 6208	-0.838	-0.413	-0.094	17.2	8.4	-0.9	0.939	9.07	-0.03

Table C.1: continued

OCC No.	Seq	Name	X kpc	Y kpc	Z kpc	U km/s	V km/s	W km/s	d kpc	log t dex	$[M/H]$ dex
28	377	NGC 6167	-1.006	-0.464	-0.027	15.7	12.3	-11.0	1.108	8.16	—
	380	NGC 6193	-1.060	-0.456	-0.032	23.9	5.8	-6.3	1.155	6.90	—
29	390	NGC 6250	-0.816	-0.286	-0.029	0.4	12.2	-5.4	0.865	7.42	—
	397	IC 4651	-0.827	-0.300	-0.122	14.7	12.3	8.2	0.888	8.92	-0.13
30	392	NGC 6281	-0.482	-0.105	0.017	5.1	3.5	7.0	0.494	8.51	0.00
	408	NGC 6405	-0.486	-0.029	-0.006	-2.1	-1.1	2.8	0.487	7.91	0.20
31	393	Sco OB4	-1.088	-0.145	0.066	5.9	4.8	-2.4	1.100	6.82	-0.09
	394	Bochum 13	-1.064	-0.165	0.026	-9.2	5.2	4.9	1.077	7.08	—
32	412	IC 4665	-0.290	0.171	0.103	-3.3	-2.6	-1.6	0.352	7.63	—
	414	Collinder 350	-0.242	0.122	0.071	6.3	2.9	6.8	0.280	8.61	—
33	427	NGC 6531	-1.194	0.161	-0.007	7.9	-4.3	-1.4	1.205	6.82	—
	432	Collinder 367	-1.190	0.152	-0.042	-2.6	2.8	-3.9	1.200	6.84	—
34	455	Collinder 394	-0.671	0.178	-0.113	-8.8	-12.1	8.3	0.703	7.86	—
	457	NGC 6716	-0.750	0.206	-0.131	-13.7	-4.1	5.4	0.789	7.47	-0.31
35	456	Stephenson 1	-0.142	0.331	0.099	6.7	-12.8	-5.6	0.373	7.69	—
	479	Roslund 5	-0.133	0.396	0.002	7.4	-7.6	0.2	0.418	7.77	—
	482	NGC 6882	-0.140	0.311	-0.023	-4.6	-10.3	-1.9	0.342	8.16	-0.02
	1100	ASCC 100	-0.148	0.308	0.077	7.8	-7.8	-3.1	0.350	8.01	—
	1101	ASCC 101	-0.128	0.318	0.070	14.4	-16.0	0.2	0.350	8.52	—
36	466	Turner 9	-0.363	0.770	0.037	9.2	-9.8	-3.5	0.852	8.06	—
	1110	ASCC 110	-0.268	0.754	0.020	5.8	-11.9	-4.3	0.800	8.75	—
37	476	NGC 6871	-0.469	1.501	0.057	-22.2	-16.5	0.5	1.574	6.99	—
	477	Biurakan 1	-0.475	1.527	0.049	-16.9	-12.4	3.4	1.600	7.25	—
38	478	Biurakan 2	-0.328	1.056	0.026	-10.0	-20.8	4.7	1.106	7.14	—
	485	Berkeley 86	-0.257	1.082	0.025	-6.2	-15.0	24.1	1.112	6.96	—
	486	NGC 6910	-0.223	1.116	0.040	-5.5	-27.2	7.8	1.139	7.33	—
	488	NGC 6913	-0.260	1.118	0.012	-11.2	-13.4	6.0	1.148	7.12	—
39	500	IC 1396	0.134	0.822	0.054	-6.0	1.5	0.3	0.835	6.69	—
	501	NGC 7160	0.191	0.766	0.089	-5.8	-4.5	7.4	0.794	7.66	—
40	509	NGC 7438	0.172	0.573	-0.051	3.8	-5.2	3.4	0.600	8.93	—
	1114	ASCC 114	0.068	0.546	0.010	-9.9	-8.2	6.5	0.550	7.75	—
	1115	ASCC 115	0.078	0.594	-0.027	3.8	3.2	4.4	0.600	8.59	—
41	1073	ASCC 73	-0.338	-0.553	-0.051	14.4	6.4	3.0	0.650	8.19	—
	1076	ASCC 76	-0.376	-0.465	-0.044	0.4	17.7	1.5	0.600	7.45	—
42	1096	Ferrero 1	-0.742	0.008	-0.106	25.7	-6.6	8.7	0.750	8.27	—
	1098	ASCC 98	-0.779	0.021	-0.179	45.6	-7.9	9.2	0.800	8.33	—

Table C.2: Parameters for the identified OC groupings with linking lengths 100 pc and 20 km/s: Number of OC grouping and members, XYZ-coordinates, UVW-velocities, distances, and ages.*

Group number	No. of members	X_{mean} kpc	Y_{mean} kpc	Z_{mean} kpc	U_{mean} km/s	V_{mean} km/s	W_{mean} km/s	d_{mean} kpc	$\log t_{mean}$ dex
1	2	0.137 (0.030)	0.065 (0.052)	-0.036 (0.022)	2.2 (6.0)	-14.4 (0.3)	-3.7 (4.4)	0.160 (0.042)	7.82 (0.37)
2	7	-0.002 (0.038)	-0.142 (0.052)	-0.028 (0.031)	5.8 (6.3)	-4.0 (5.1)	0.8 (5.1)	0.156 (0.037)	7.85 (0.54)
3	2	0.570 (0.016)	0.293 (0.031)	-0.140 (0.051)	-4.0 (9.6)	3.3 (0.9)	-2.3 (5.7)	0.657 (0.011)	8.41 (0.28)
4	2	0.660 (0.035)	0.341 (0.032)	0.002 (0.001)	-8.2 (6.9)	3.5 (6.8)	2.9 (2.8)	0.744 (0.046)	8.29 (0.20)
5	2	0.286 (0.021)	-0.025 (0.031)	-0.055 (0.004)	4.8 (1.9)	2.2 (2.1)	1.3 (1.5)	0.293 (0.024)	7.82 (0.59)
6	2	1.316 (0.005)	0.148 (0.032)	0.016 (0.013)	-3.2 (1.4)	-9.0 (6.7)	-5.3 (2.0)	1.324 (0.008)	7.78 (0.23)
7	2	1.072 (0.023)	0.150 (0.009)	-0.003 (0.023)	-10.1 (12.6)	-10.6 (1.3)	-10.6 (5.1)	1.083 (0.024)	8.59 (0.04)
8	15	0.367 (0.060)	-0.176 (0.038)	-0.118 (0.044)	5.2 (5.9)	1.0 (3.3)	1.1 (3.3)	0.427 (0.065)	7.18 (0.38)
9	2	1.291 (0.005)	-0.653 (0.018)	-0.036 (0.023)	-8.2 (8.1)	7.6 (4.4)	-6.9 (5.7)	1.448 (0.004)	6.86 (0.23)
10	2	1.217 (0.002)	-0.534 (0.004)	-0.001 (0.004)	-14.2 (8.1)	-8.0 (6.0)	3.1 (0.4)	1.329 (0.001)	8.06 (0.53)
11	3	0.669 (0.054)	-0.443 (0.018)	0.003 (0.005)	-9.2 (5.8)	-0.9 (6.1)	-0.5 (5.7)	0.803 (0.054)	8.24 (0.15)
12	2	0.336 (0.038)	-0.363 (0.026)	0.014 (0.019)	13.7 (3.8)	-7.1 (0.5)	-0.2 (4.3)	0.495 (0.006)	7.80 (0.46)
13	9	0.105 (0.051)	-0.389 (0.046)	-0.039 (0.032)	3.6 (4.7)	-2.3 (4.5)	-2.9 (4.4)	0.409 (0.038)	7.67 (0.58)
14	2	0.394 (0.004)	-0.475 (0.060)	0.030 (0.004)	-3.4 (9.1)	-4.2 (4.1)	0.1 (1.1)	0.619 (0.044)	8.60 (0.11)
15	2	0.866 (0.027)	-1.106 (0.039)	0.083 (0.021)	-12.4 (12.5)	-2.9 (5.0)	-14.6 (3.5)	1.407 (0.046)	7.82 (0.47)
16	2	0.513 (0.007)	-0.903 (0.006)	-0.001 (0.006)	1.1 (2.8)	6.3 (0.8)	1.6 (1.2)	1.038 (0.002)	7.98 (1.11)
17	2	0.625 (0.018)	-1.195 (0.020)	0.028 (0.028)	0.6 (2.5)	-20.9 (8.6)	-14.5 (8.1)	1.349 (0.008)	8.26 (0.30)
18	4	0.169 (0.056)	-0.849 (0.046)	0.000 (0.023)	2.4 (5.2)	1.1 (7.9)	-2.9 (5.4)	0.867 (0.053)	7.93 (0.40)
19	2	-0.222 (0.021)	-0.896 (0.016)	-0.066 (0.007)	1.0 (1.8)	0.4 (9.4)	-1.2 (4.2)	0.925 (0.021)	8.32 (0.11)
20	2	-0.646 (0.042)	-2.372 (0.007)	0.002 (0.001)	16.8 (5.1)	-5.4 (2.4)	-1.6 (6.1)	2.458 (0.018)	7.08 (0.20)
21	3	-0.144 (0.019)	-0.558 (0.043)	0.000 (0.012)	5.1 (2.1)	-3.2 (7.0)	-6.8 (2.0)	0.577 (0.040)	7.78 (0.71)
22	2	-0.643 (0.028)	-1.366 (0.003)	0.019 (0.001)	-13.9 (4.8)	18.6 (1.2)	3.7 (12.4)	1.510 (0.014)	7.93 (0.37)
23	4	-0.327 (0.046)	-0.371 (0.026)	0.018 (0.021)	6.2 (7.9)	8.3 (10.7)	7.0 (4.1)	0.496 (0.047)	8.45 (0.16)
24	2	-0.470 (0.035)	-0.501 (0.055)	0.032 (0.011)	9.5 (3.0)	8.9 (1.2)	4.5 (12.2)	0.689 (0.016)	8.16 (0.74)
25	2	-0.618 (0.008)	-0.479 (0.049)	-0.060 (0.028)	-12.5 (4.7)	-2.9 (2.4)	4.1 (7.7)	0.784 (0.022)	7.41 (0.78)
26	2	-0.740 (0.026)	-0.506 (0.037)	-0.085 (0.000)	-7.9 (0.0)	2.9 (5.3)	-0.2 (6.3)	0.900 (0.001)	7.80 (0.18)
27	2	-0.832 (0.008)	-0.400 (0.018)	-0.048 (0.064)	14.0 (4.4)	7.2 (1.8)	-6.1 (7.4)	0.926 (0.018)	8.80 (0.38)
28	2	-1.033 (0.038)	-0.460 (0.006)	-0.030 (0.004)	19.8 (5.8)	9.0 (4.6)	-8.7 (3.3)	1.131 (0.033)	7.53 (0.89)
29	2	-0.822 (0.008)	-0.293 (0.010)	-0.075 (0.066)	7.5 (10.1)	12.2 (0.1)	1.4 (9.6)	0.876 (0.016)	8.17 (1.06)
30	2	-0.484 (0.003)	-0.067 (0.054)	0.006 (0.016)	1.5 (5.1)	1.2 (3.3)	4.9 (3.0)	0.490 (0.005)	8.21 (0.42)
31	2	-1.076 (0.017)	-0.155 (0.014)	0.046 (0.028)	-1.6 (10.7)	5.0 (0.3)	1.2 (5.1)	1.089 (0.016)	6.95 (0.18)
32	2	-0.266 (0.034)	0.147 (0.035)	0.087 (0.023)	1.5 (6.8)	0.1 (3.9)	2.6 (5.9)	0.316 (0.051)	8.12 (0.69)
33	2	-1.192 (0.003)	0.156 (0.006)	-0.024 (0.025)	2.7 (7.5)	-0.7 (5.0)	-2.7 (1.8)	1.202 (0.004)	6.83 (0.01)
34	2	-0.711 (0.056)	0.192 (0.020)	-0.122 (0.013)	-11.2 (3.5)	-8.1 (5.6)	6.9 (2.1)	0.746 (0.061)	7.66 (0.28)
35	5	-0.138 (0.008)	0.333 (0.036)	0.045 (0.053)	6.3 (6.9)	-10.9 (3.6)	-2.0 (2.4)	0.367 (0.031)	8.03 (0.33)

Table C.2: continued

Group number	No. of members	X_{mean} kpc	Y_{mean} kpc	Z_{mean} kpc	U_{mean} km/s	V_{mean} km/s	W_{mean} km/s	d_{mean} kpc	$\log t_{mean}$ dex
36	2	-0.316 (0.067)	0.762 (0.011)	0.029 (0.012)	7.5 (2.4)	-10.9 (1.5)	-3.9 (0.6)	0.826 (0.037)	8.41 (0.49)
37	2	-0.472 (0.004)	1.514 (0.018)	0.053 (0.006)	-19.6 (3.8)	-14.5 (2.9)	2.0 (2.1)	1.587 (0.018)	7.12 (0.18)
38	4	-0.267 (0.044)	1.093 (0.030)	0.026 (0.011)	-8.2 (2.8)	-19.1 (6.3)	10.7 (9.1)	1.126 (0.020)	7.14 (0.15)
39	2	0.162 (0.040)	0.794 (0.040)	0.072 (0.025)	-5.9 (0.1)	-1.5 (4.3)	3.9 (5.0)	0.815 (0.029)	7.18 (0.69)
40	3	0.106 (0.057)	0.571 (0.024)	-0.023 (0.031)	-0.8 (7.9)	-3.4 (5.9)	4.7 (1.6)	0.583 (0.029)	8.42 (0.61)
41	2	-0.357 (0.027)	-0.509 (0.062)	-0.047 (0.005)	7.4 (9.9)	12.1 (8.0)	2.2 (1.1)	0.625 (0.035)	7.82 (0.52)
42	2	-0.760 (0.026)	0.014 (0.009)	-0.142 (0.052)	35.7 (14.1)	-7.3 (0.9)	8.9 (0.3)	0.775 (0.035)	8.30 (0.04)

* Averaged metallicities could not be provided for the OC groupings in Tab. C.2, because only about 30% of the clusters, which belong to a groupings, were equipped with $[M/H]$ information. This can be seen in seen in Tab. C.1.

Bibliography for the Appendix

Ann, H. B., Lee, S. H., Sung, H., et al. 2002, *Astron. J.*, 123, 905

Binney, J. & Merrifield, M. 1998, Galactic Astronomy

Boeche, C., Siebert, A., Williams, M., et al. 2011, *Astron. J.*, 142, 193

Cameron, L. M. 1985, *Astron. Astrophys.*, 147, 47

Clariá, J. J., Lapasset, E., & Minniti, D. 1989, *Astron Astrophys. Suppl.*, 78, 363

Clariá, J. J., Lapasset, E., & Bosio, M. A. 1991, *Monthly Notices Roy. Astron. Soc.*, 249, 193

Clariá, J. J., Piatti, A. E., & Osborn, W. 1996, *Publ. Astron. Soc. Pacific*, 108, 672

Clariá, J. J., Piatti, A. E., Lapasset, E., & Mermilliod, J.-C. 2003a, *Astron. Astrophys.*, 399, 543

Clariá, J. J., Lapasset, E., Piatti, A. E., & Ahumada, A. V. 2003b, *Astron. Astrophys.*, 409, 541

Conrad, C., Scholz, R.-D., Kharchenko, N. V., et al. 2014, *Astron. Astrophys.*, 562, A54

Dias, W. S., Alessi, B. S., Moitinho, A., & Lépine, J. R. D. 2002, *Astron. Astrophys.*, 389, 871

Friel, E. D., Janes, K. A., Tavarez, M., et al. 2002, *Astron. J.*, 124, 2693

Gonzalez, G. & Wallerstein, G. 2000, *Astron. J.*, 119, 1839

Gratton, R. 2000, in Astronomical Society of the Pacific Conference Series, Vol. 198, Stellar Clusters and Associations: Convection, Rotation, and Dynamos, ed. R. Pallavicini, G. Micela, & S. Sciortino, 225

Kharchenko, N. V., Scholz, R.-D., Piskunov, A. E., Röser, S., & Schilbach, E. 2007, Astronomische Nachrichten, 328, 889

Luck, R. E. 1994, *Astrophys. J. Suppl.*, 91, 309

Lynga, G. 1981, Astronomical Data Center Bulletin, 1, 90

Lynga, G. & Wramdemark, S. 1984, *Astron. Astrophys.*, 132, 58

Margheim, S. J., King, J. R., Deliyannis, C. P., & Platais, I. 2000, in Bulletin of the American Astronomical Society, Vol. 32, American Astronomical Society Meeting Abstracts #196, 742

Nissen, P. E. 1980, in IAU Symposium, Vol. 85, Star Clusters, ed. J. E. Hesser, 51–64

Palous, J. & Hauck, B. 1986, *Astron. Astrophys.*, 162, 54

Parisi, M. C., Clariá, J. J., Piatti, A. E., & Geisler, D. 2005, *Monthly Notices Roy. Astron. Soc.*, 363, 1247

Paunzen, E., Maitzen, H. M., Rakos, K. D., & Schombert, J. 2003, *Astron. Astrophys.*, 403, 937

Piatti, A. E., Claria, J. J., & Abadi, M. G. 1995, *Astron. J.*, 110, 2813

Piskunov, A. E., Kharchenko, N. V., Röser, S., Schilbach, E., & Scholz, R.-D. 2006, *Astron. Astrophys.*, 445, 545

Twarog, B. A., Ashman, K. M., & Anthony-Twarog, B. J. 1997, *Astron. J.*, 114, 2556

Erklärung

Hiermit erkläre ich, Dipl.-Phys. Claudia Conrad, dass ich diese Dissertationsschrift in eigener Arbeit, unter Betreuung der angegebenen Personen, und mit den in dieser Dissertationsschrift angegebenen Mitteln erstellt habe.

Des Weiteren erkläre ich, dass diese Dissertationsschrift nur an der Mathematisch-Naturwissenschaftlichen Fakultät der Universität Potsdam zur Begutachtung eingereicht wurde, und an keiner anderen Universität oder Hochschule in Deutschland, Europa oder weltweit vorgelegt wurde.

_____ Potsdam, den 15.06.2015

Dipl.-Phys. Claudia Conrad